UNIVERSITY OF CALIFORNIA,
IRVINE

Leakage, Pressure and Flow Dynamics of the Natural Gas System for Renewable Gas Use

DISSERTATION

submitted in partial satisfaction of the requirements
for the degree of

DOCTOR OF PHILOSOPHY

in Mechanical & Aerospace Engineering

by

Zahra Heydarzadeh

Dissertation Committee:
Professor Jack Brouwer, Ph.D., Chair
Professor Iryna Zenyuk, Ph.D.
Professor Bihter Padak, Ph.D.

2020

DEDICATION

For Hamid

TABLE OF CONTENTS

Page

LIST OF FIGURES v

LIST OF TABLES xi

ACRONYMS xii

ACKNOWLEDGEMENTS xiv

VITA xvi

ABSTRACT OF THE DISSERTATION xviii

1 Introduction 1

1.1 Motivation 1

1.2 Research Goal and Objectives 8

1.3 Approach 9

1.4 Structure of this Dissertation 10

2 Analysis of Methane Emissions Sources from the Natural Gas System 12

2.1 Abstract 12

2.2 Literature Review 12

2.3 Methodology 18

2.4 Results and Discussion 21

2.5 Summary 44

3 Marginal Methodology to Estimate Methane Emissions 45

3.1 Abstract 45

3.2 Literature Review 45

3.3 Methodology 50

3.4 Results and Discussion 52

3.5 Summary 63

4 Analysis of Southern California Gas System for 100% Renewable Energy Penetration 65

4.1 Abstract 65
4.2 Literature Review 65
4.3 Methodology 69
4.3.1 Fuel Cell and Electrolyzer Model 71
4.3.2 Pipeline Model 71
4.3.3 Underground Storage Model 76
4.4 Results and Discussion 78
4.4.1 Model Input 78
4.4.2 Model Results 83
4.4.3 Preliminary Cost Analysis 98
4.5 Summary 100
5 Blending Hydrogen into the Southern California Natural Gas Network 101
5.1 Abstract 101
5.2 Literature Review 101
5.3 Methodology 105
5.3.1 Model Validation 106
5.3.2 Model Development 111
5.4 Results and Discussion 116
5.4.1 Model Input 118
5.4.2 Model Results 122
5.5 Summary 153
6 Conclusions & Future Work 154
6.1 Conclusions 154
6.2 Future Work 157
REFERENCES 159

LIST OF FIGURES

Page

Figure 1.1. Hydrogen blending limits in various countries by volume (taken from [22]) 6

Figure 1.2. Hydrogen blending limits in different sectors by volume (taken from [23]) 6

Figure 2.1. Overview of 2016 U.S. GHG emissions (left), and methane emissions by sector (right) (taken from [5]) 13

Figure 2.2. Change in Emissions and throughput from 1990 to 2016 based on the data [31] 13

Figure 2.3. Total methane emissions percentage from the natural gas system by sector for the 2016 base year (data adapted from [31]) 20

Figure 2.4. The distribution of emissions percentage from each component of the natural gas system for the 2016 base year (data adapted from [31]) 20

Figure 2.5. Theoretical exhaust rate: (a) Intermittent-vent; (b) Continuous-vent (adopted from [55]) 22

Figure 2.6. Fuel-Specific methane emission vs. site throughput for 4SLB engines (taken from [47]) 24

Figure 2.7. Typical Rod Packing System (taken from [60]) 27

Figure 2.8. Centrifugal compressors, wet seal (top), dry seal (bottom)- (taken from [61]) 28

Figure 2.9. Gas wells production rate vs age based on measurements data from [66] 30

Figure 2.10. One solution to mitigate blowdown emissions during shut down (taken from [68]) 32

Figure 2.11. Schematic of gas emissions from the storage well (taken from [69]). 34

Figure 2.12. Methane emissions from the liquid storage tank (taken from [71]) 35

Figure 2.13. Dehydrator unit (taken from [74]) 39

Figure 2.14. The effect of glycol recirculation rate on methane emissions rate (taken from [76]) 39

Figure 2.15. Cut-away Schematic of Diaphragm Pumps (taken from [79]) 41

Figure 2.16. Cut-away Schematic of Piston Pumps (taken from [79]) 42

Figure 3.1. (a) Site-level methane emissions rate vs NG production (b) site-level production-normalized methane emissions vs NG production (adapted from [88]) (measurement data are from eight basins: Marcellus, Denver-Julesburg (DJB), Barnett, Uinta, EagleFord, Uinta, EagleFord, Pinedale, Upper Green River, Fayetteville. Production decile # shows ten different bins number. These bins were categorized based on NG production rate) 49

Figure 3.2. Percent of emissions change against the percent of throughput change vs emissions for the 2016 base year (solid lines are considering all 129 components and dashed lines are only marginally assessed components)..... 56

Figure 3.3. The distribution of emissions percentage from each sector of the natural gas system vs. throughput percentage change compared to the 2016 base year 57

Figure 3.4. The distribution of emissions from each sector of the natural gas system vs. throughput compared to the 2016 base year 58

Figure 3.5. Emissions estimate vs. throughput 60

Figure 3.6. Normalized emissions vs throughput 61

Figure 4.1. Electricity storage technologies (taken from [23])..... 66

Figure 4.2. Different PtG and Hydrogen Integration Pathways (adapted from [100])..... 67

Figure 4.3. Hydrogen underground Storage Worldwide (taken from [104])..... 68

Figure 4.4. Schematic of the Simulated Model..... 70

Figure 4.5. Mesh grid of the solution in x-t plane 74

Figure 4.6. Inlet pressure comparison..... 76

Figure 4.7. Outlet mass flow rate comparison 76

Figure 4.8. Three zones covered by CAISO in California (taken from [126])..... 79

Figure 4.9. Renewable and demand power information (data taken from [126])..... 79

Figure 4.10. SoCalGas underground storage fields (taken from [127]) 80

Figure 4.11. Storage field capacity& compressibility change vs hydrogen concentration (%).... 81

Figure 4.12. Hydrogen storage capacity (kt) 81

Figure 4.13. SoCalGas natural gas service territory (adapted from [128])..... 82

Figure 4.14. Simulated network map..... 82

Figure 4.15. Annual hydrogen produced vs solar scaling factor 85

Figure 4.16. Hydrogen production rate vs solar scaling factor..... 85

Figure 4.17. Storage inventory vs solar scaling factor..... 86

Figure 4.18. Hydrogen stored in balanced storage (solar scaling factor 13 & 50% storage capacity) - scenario 1..... 87

Figure 4.19. Annual pipelines pressure fluctuation for 100% hydrogen delivery - scenario 1 88

Figure 4.20. Annual pipelines pressure fluctuation for 80% of peak hydrogen delivery - scenario 1 89

Figure 4.21. Hydrogen stored in balanced storage (solar scaling factor 17 & 65% storage capacity) - scenario 2..... 90

Figure 4.22. Annual pipelines pressure fluctuation for 100% hydrogen delivery - scenario 2 91

Figure 4.23. Annual pipelines pressure fluctuation for 60% peak hydrogen delivery - scenario 2 92

Figure 4.24. Hydrogen stored in balanced storage (solar scaling factor 15 & 55% storage capacity) - scenario 3..... 93

Figure 4.25. Annual pipelines pressure fluctuation for 100% hydrogen delivery - scenario 3 94

Figure 4.26. Annual pipelines pressure fluctuation for 70% hydrogen delivery - scenario 3 95

Figure 4.27. SoCalGas pipeline network - Pipeline extensions (pipe 16 & 17 - highlighted in red dashed lines) proposed to accommodate all hydrogen produced at the solar sites..... 96

Figure 4.28. Annual pipelines pressure fluctuation for 100% hydrogen delivery - scenario 1-modified..... 97

Figure 4.29. Cost estimate for three studied scenarios 99

Figure 4.30. Approx. land required to provide enough solar power capacity for scenario 1- solar capacity factor of 13 100

Figure 5.1. Schematic of validated paper [140]..... 107

Figure 5.2. Topology of the network created in SAInt for the NG Network Case; network nodes information (top), network pipe information (bottom)..... 108

Figure 5.3. Topology of the network created in SAInt for the NG + H_2 Network Case; network nodes information (top), network pipe information (bottom) 109

Figure 5.4. Pressure of each node in the network created in SAInt for two case studies 110
Figure 5.5. Flow rate for all 14 pipelines in the NG network 110
Figure 5.6. Flow rate for all 14 pipelines in the NG + H_2 network 111
Figure 5.7. Model flow diagram for the case of injecting hydrogen at the receipt point 114
Figure 5.8. Model flow diagram for the case of injecting hydrogen NOT at the receipt point .. 115
Figure 5.9. SoCalGas company system map (taken from [128]) 117
Figure 5.10. The simulated SoCalGas company network 117
Figure 5.11. The total supply and demand daily flow rate 118
Figure 5.12. the daily maximum injection and withdrawal rate limitation 121
Figure 5.13. Pressure fluctuation at the receipt points 123
Figure 5.14. Kramer receipt point pressure and flow rate (100% NG) 123
Figure 5.15. Pressure fluctuation at the demand points 124
Figure 5.16.Compressor stations pressure ratio for simulated network 124
Figure 5.17. End of month storage inventory 125
Figure 5.18. Aliso Canyon end of month and the minimum allowable inventory 126
Figure 5.19. Honor Rancho end of month and the minimum allowable inventory 126
Figure 5.20. La Goleta end of month and the minimum allowable inventory 127
Figure 5.21. Playa del Rey end of month and the minimum allowable inventory 127
Figure 5.22. Hydrogen to natural gas percentage (top) and percent increase of flow rate (bottom) at the demand nodes – scenario 1 131
Figure 5.23. Total hydrogen carrying capacity and cumulative net injection/withdraw - scenario 1 131
Figure 5.24. Storage field's inventory, pressure, and hydrogen concentration - scenario 1 132
Figure 5.25. Hydrogen to natural gas percentage (top) and percent increase of flow rate (bottom) at the demand nodes – scenario 2 134
Figure 5.26. Total hydrogen carrying capacity and cumulative net injection/withdraw - scenario 2 134

Figure 5.27. Storage field's inventory, pressure, and hydrogen concentration - scenario 2 135

Figure 5.28. Hydrogen to natural gas percentage (top) and percent increase of flow rate (bottom) at the demand nodes – scenario 3 137

Figure 5.29. Total hydrogen carrying capacity and cumulative net injection/withdraw - scenario 3 137

Figure 5.30. Storage field's inventory, pressure, and hydrogen concentration - scenario 3 138

Figure 5.31. Hydrogen to natural gas percentage (top) and percent increase of flow rate (bottom) at the demand nodes – scenario 4 140

Figure 5.32. Total hydrogen carrying capacity and cumulative net injection/withdraw - scenario 4 140

Figure 5.33. Storage field's inventory, pressure, and hydrogen concentration - scenario 4 141

Figure 5.34. Mass of hydrogen produced at each node - scenario 4..... 142

Figure 5.35. Hydrogen to natural gas percentage (top) and percent increase of flow rate (bottom) at the two supply nodes – scenario 4M..... 143

Figure 5.36. End of year hydrogen concentration in storage facilities - 2% hydrogen injection scenarios 144

Figure 5.37. Hydrogen carrying capacity - 2% hydrogen injection scenarios..... 144

Figure 5.38. Hydrogen percentage distribution in the SoCalGas pipeline network – scenario 1145

Figure 5.39. Hydrogen percentage distribution in the SoCalGas pipeline network – scenario 2145

Figure 5.40. Hydrogen percentage distribution in the SoCalGas pipeline network – scenario 3146

Figure 5.41. Hydrogen percentage distribution in the SoCalGas pipeline network – scenario 4146

Figure 5.42. Hydrogen percentage distribution in the SoCalGas pipeline network – scenario 4M 147

Figure 5.43. Hydrogen to natural gas percentage (top) and percent increase of flow rate (bottom) at the demand nodes – 20% hydrogen injection scenario..... 149

Figure 5.44. Total hydrogen carrying capacity and cumulative net injection/withdraw - 20% hydrogen injection scenario..... 149

Figure 5.45. Storage field's inventory, pressure, and hydrogen concentration - 20% hydrogen injection scenario..... 150

Figure 5.46. Two identified points facing problem (highlighted in blue) - for 20% hydrogen injection scenario 151

Figure 5.47. Pressure and flow rate of Kramer receipt point - 20% hydrogen injection scenario 152

Figure 5.48. Flow rate of Wheeler compressor station - 20% hydrogen injection scenario 152

LIST OF TABLES

Page

Table 2.1. Marginal Assessment Coefficient 43

Table 3.1. Marginally assessed components and their contributions to emissions 55

Table 3.2. Recommended technologies to reduce methane emissions by EPA/STAR [92] 59

Table 3.3. Emissions change vs. throughput change 62

Table 4.1. PEM EC/FC operating conditions 71

Table 4.2. SoCalGas Underground storage facilities - capacity and pressure limit [124] 80

Table 4.3. Southern California pipeline information 83

Table 4.4. Pipeline expansions information 98

Table 4.5. Infrastructure comparison between different studied scenarios 99

Table 5.1. The actual pipeline length and diameter used in the simulated network 120

Table 5.2. Underground storage facilities information 121

Table 5.3. End of month minimum inventory requirement 121

Table 5.4. Network constraints and initial conditions 122

Table 5.5. Molar fraction and caloric value of natural gas and hydrogen 122

Table 5.6. Solar farm and electrolyzer required to achieve 2% & 20% hydrogen injection 153

ACRONYMS

AB	Assembly Bill
AE	Alkaline Electrolysis
AF	Activity Factor
BCF	Billion Cubic Feet
BCFD	Billion Cubic Feet per Day
CA	California
CAES	Compressed Air Energy Storage
CAISO	California Independent System Operator
CCAC	Climate & Clean Air Coalition
CI	Carbon Intensity
CPUC	California Public Utilities Commission
CV	Caloric Value
EC	Electrolyzer
EDF	Environmental Defense Fund
EF	Emission Factor
EIA	Energy Information Administration
EoS	Equation of State
EPA	Environmental Protection Agency
FC	Fuel Cell
GHG	Greenhouse Gas
GHGI	Greenhouse Gas Inventory
GHGRP	Greenhouse Gas Reporting Program
GREET	Greenhouse Gases, Regulated Emissions, and Energy use in Transportation

GRI	Gas Research Institute
HES	Hydrogen Energy Storage
HHV	Higher Heating Value
LHV	Lower Heating Value
MMCFD	Million Cubic Feet per Day
MSA	Meter Set Assembly
NG	Natural Gas
PEM	Proton Exchange Membrane
PHS	Pump Hydroelectric Storage
PtG	Power to Gas
SAInt	Scenario Analysis Interface for Energy System
SB	Senate Bill
SCE	Southern California Edison
SCF	Standard Cubic Feet
SoCalGas	Southern California Gas Company
SOEC	Solid Oxide Electrolysis

ACKNOWLEDGEMENTS

I would like to express my gratitude to my advisor and committee chair, Professor Jack Brouwer. His continued support, mentorship, patience, and giving me room for making mistakes along the way has helped me grow throughout this experience and is greatly appreciated. His tireless work for a cleaner sustainable environment is inspiring and his passion for teaching is contagious and for that I admire him.

My sincere thanks also go to Prof. Scott Samuelsen, for creating an environment of enthusiasm for clean energy. His dedication in this field motivates me every day and I am grateful that I have been given this opportunity to be part of this amazing group of intelligent scientists in Advanced Power and Energy Program.

I would like to thank Professor Iryna Zenyuk for serving on my dissertation committee and also for her guidance and teaching me the fundamentals of the numerical approach. Thank you to Professor Bihter Padak for serving on my dissertation committee and for providing advice on this work.

Thank you to my labmates in Advanced Power and Energy Program (APEP) for all their help and being co-authors in the publications of this dissertation in Chapters 2, 3, and 4: Thank you to Robert Flores for providing the transportation data for the "Dynamic Modeling of California Grid-Scale Hydrogen Energy Storage" paper and being a great mentor during my first two years of TAing his MAE115 class. Thank you to Derek McVay for helping me to start working with the hydrogen energy storage model and co-authoring the "Dynamic Modeling of California Grid-Scale Hydrogen Energy Storage" paper. Thank you to Michael McKinnon for all his assistance with estimating the marginal methane emissions papers. Thank you to Clinton Thai for always being a great cubemate and helping/co-authoring with the marginal emissions papers. Thank you to Luca Mastropasqua for his support and assistance with the cost analysis part of my study.

Thanks to Dr. Jeff Reed, from APEP, for all his support and assistance during the past four years and co-authoring the marginal methane emissions papers.

Additionally, I thank the American Society of Mechanical Engineers (ASME) for permission to include portions of Chapters 1 and 4 of my dissertation, which was originally published in proceedings of the ASME 2020 Power Conference. I also thank The Applied Energy for permission to include portions of Chapters 2 and 3 of my dissertation, which originally was published in Applied Energy Symposium: MIT A+B. Thanks to Elsevier Ltd for permission to include Chapter 3 and portion of Chapter 2 of my dissertation, which originally was published in Journal of Applied Energy. I thank The Electrochemical Society (ECS) for permission to include portion of Chapter 4 of my dissertation, which was originally published in the ECS AiMES2018 Transactions.

Moreover, I would like to thank my supervisor, Ashkan Nasiri, during my internship at Los Angeles Department of Water and Power (LADWP) for giving me the opportunity to learn a lot

about the LA100 project. I also would like to thank my supervisors during my internship at National Renewable Energy Laboratory (NREL), Michael Penev and Chad Hunter, for all their support and guidance.

Lastly, I would like to thank my family: my parents and my sister for their love and supporting me emotionally throughout my academic journey and my life in general. Most of all, I would like to thank my amazing husband, Hamid, for being more than a partner to me but a true mentor who taught me how to tackle difficult situations throughout my Ph.D. studies. I would not have made it through each step of this work without his care and understanding and for that I am eternally grateful. This work is possible because of him and for him.

VITA

Zahra Heydarzadeh

2003-2007 B.S. in Mechanical Engineering,
University of Mohaghegh, Iran

2010-2012 M.S. in Mechanical Engineering
University of Guilan, Iran

2015-2020 Ph.D. in Mechanical Engineering
University of California, Irvine

Fall. 2016 Teaching Assistant, Fundamentals of Engineering Thermodynamics
University of California, Irvine

Sum. 2018 Intern, Power Planning Development and Engineering,
Los Angeles Department of Water and Power (LADWP), Los Angeles

Sum. 2019 Intern, Transportation and Hydrogen Systems
National Renewable Energy Laboratory (NREL), Golden

Sum. 2020 Lecturer, Fundamentals of Engineering Thermodynamics
University of California, Irvine

FIELD OF STUDY

Evaluate various stages of transitioning the current energy portfolio that relies heavily on natural gas to a zero-emission energy portfolio.

PUBLICATIONS

Need for a Marginal Methodology in Assessing Natural Gas System Methane Emissions in Response to Incremental Consumption
Michael Mac Kinnon, Zahra Heydarzadeh, Quy Doan, Cuong Ngo, Jeff Reed & Jacob Brouwer
Journal of the Air & Waste Management Association, Volume 68, P 1139-1147, 2018.

Dynamic Modeling of California Grid-Scale Hydrogen Energy Storage
Z. Heydarzadeh, D. McVay, R. J. Flores, C. Thai, J. Brouwer
AiMES2018-The Electrochemical Society (ECS) Transactions, Volume 86, P 245-258, 2018.

Investigation of Southern California Natural Gas Infrastructure to Transport and Store Hydrogen to Meet Electric Demand based on a 100% Renewable Energy Portfolio
Zahra Heydarzadeh, Jack Brouwer
ASME 2020 Power Conference, POWER2020-16044, V001T08A001, 2020

Comprehensive Study of Major Methane Emissions Sources from Natural Gas System and Their Dependency to Throughput
Zahra Heydarzadeh, Michael Mac Kinnon, Clinton Thai, Jeff Reed & Jacob Brouwer
Applied Energy Symposium: MIT A+B, APEN-MIT-2020-209

Marginal methane emission estimation from the natural gas system
Zahra Heydarzadeh, Michael Mac Kinnon, Clinton Thai, Jeff Reed, Jack Brouwer.
Applied Energy, Volume 277, 1 November 2020, 115572, 2020.

ABSTRACT OF THE DISSERTATION

Leakage, Pressure and Flow Dynamics of the Natural Gas System for Renewable Gas Use

by

Zahra Heydarzadeh

Doctor of Philosophy in Mechanical & Aerospace Engineering

University of California, Irvine, 2020

Professor Jack Brouwer, Chair

Reducing greenhouse gas (GHG) emissions to mitigate the impact of climate change is a critical mission of policy makers in California. In September 2018, Senate Bill 100 (SB100) was ratified, requiring California to obtain 100% of its power from clean sources by 2045. This law also required utilities to generate 60% of their power from renewable sources by 2030.

Transitioning to a zero-emission portfolio requires significant investments and should be accomplished in multiple stages. In each stage, the impact of changes in the system on the emitted GHG should carefully be analyzed. This will ensure the best transition path to achieve the goal of 100% renewable energy penetration in California is chosen.

In this dissertation, first, the impact of change in throughput on the change in methane emissions, which is one of the major sources of GHG emissions, is studied. The analysis identifies major methane emissions sources from the upstream of natural gas system and their dependencies on time, event, and throughput. A new cause-based model is developed using the marginal methodology to estimate the change in methane emissions with the change in

throughput. The impact of the marginal change in methane emissions when the total throughput changes by 5%, 15%, 30%, and 50% in either direction is studied. The effect of system expansion and reduction as well as the technological improvements is also considered.

Next, the capacity of Southern California natural gas infrastructure to support a zero-emission portfolio is studied. A transient model is developed to determine the amount of additional solar farms, pipeline network capacity, and underground storage facilities that are required to achieve 100% renewable energy penetration. Different scenarios are analyzed, and the most cost-effective option is identified.

Finally, the impact of injecting hydrogen in the existing natural gas infrastructure of Southern California is studied. It is shown that with hydrogen mix of 2% vol., all of the network constraints are met while increasing the hydrogen mix to 20% vol. requires some adjustments to the current pipeline network and compressor stations to ensure all the constraints are met. The effect of hydrogen injection location points on the hydrogen carrying capacity is investigated.

1 Introduction

1.1 Motivation

Recently, California (CA) has set an ambitious goal to eliminate the reliance on fossil fuels and move to zero-emission energy sources for its electricity needs. In 2006, California legislation passed Assembly Bill (AB32), global warming solution act of 2006, to reduce Greenhouse Gas (GHG) emissions up to 30% compared to the 1990 levels by 2020, and 80% by 2050. In 2015, California Governor Edmund G. Brown Jr. issued an executive order to reduce the state's greenhouse gas emissions to be 40% less than 1990 levels by 2030, which eventually led to Senate Bill (SB32). In 2015, SB350 passed, setting a goal of achieving 33% of electricity production from renewable resources by 2020, and 50% by 2030. In September 2018, SB100 was ratified, requiring California to obtain 100% of its power from clean sources by 2045. This law also would require utilities to generate 60% of their power from renewable sources by 2030.

Considering California consumes more than 277 billion kilowatt hours (bn kWh) of electricity per year [1], achieving this goal requires significant investment in the infrastructure for the production, transportation, and storage of alternative green sources of energy. In recent years, and to move in the direction of reducing GHG emissions, fossil fuels with high carbon intensity such as coal have been replaced with natural gas with lower carbon per unit of energy.

The concept of transporting energy in the form of gas through a pipeline network has been around for a long time. The first use of natural gas as a source of energy goes back to 1000 B.C. where it is believed that the Oracle at Delphi on Mount Pamassus was powered by natural gas [2]. The first use of a pipeline system to transport natural gas is reported at around 500B.C., when the Chinese used hollow bamboo trees to transport gas [3] and use it to desalinate water and produce drinkable water. History of gas as a form of energy in America goes back to 1626, when French settlers learned how native Americans ignited gas that were seeping near Lake Erie [2]. In the 1800s, first commercial well was constructed, and various municipalities started using "town" gas as a source of light. As more gas pipeline networks were built in the 1900s, the use of gas was

expanded to home heating and cooking [2]. Town gas contained a mix of hydrogen, methane, and a few other gases and was typically manufactured from coal. In the second half of 20th century, large deposits of natural gas were discovered, a large network of natural gas pipelines were developed, and natural gas was transformed to a mainstream source of energy [4].

Despite the positive impact that the transition from coal to natural gas has had on reducing GHG emissions, the methane emissions from natural gas poses significant risk to the environment. Methane, which is the main component of natural, has a greater global warming potential in the short time frame compared to carbon dioxide. According to the Environmental Protection Agency/ GHG Inventory (EPA/GHGI), the global warming potential of methane is 25 times higher than carbon dioxide on a 100-year time frame [5]. Considering the negative impact methane emissions from natural gas has on global warming, there is a need to eventually transition from natural gas to clean and renewable sources of energy such as hydrogen to mitigate the impact of GHG emissions.

Although it is expected that natural gas will be replaced by hydrogen or similar clean and renewable sources of energy in the long term, the reliance on natural gas as a major part of California's energy portfolio will continue in the short and medium terms. Therefore, it is of paramount importance to accurately estimate the marginal change in the methane emissions from natural gas. Most of the existing methods of calculating the change in methane emissions uses linear regression and does not consider the complex behavior of hundreds of components that contribute to methane emissions in a natural gas network infrastructure. As a result, these simple regression models produce materially inaccurate methane emissions change estimation. Accurate calculation of marginal change in methane emissions provides the policy makers with an invaluable tool to examine the impact of marginally reducing or increasing the reliance on natural gas on methane emissions.

Hydrogen is a clean and renewable alternative to natural gas and has been studied extensively in recent years. Recent legislations in California (e.g. SB 1505) highlights the renewed focus of policy makers on the role hydrogen can play in reducing the reliance of the energy supply on fossil fuels [6]. To adopt hydrogen as one of the major sources of green fuel of the future, several obstacles need to be addressed. A robust infrastructure is needed to transport, and store hydrogen generated at the site of wind or solar farms, which are typically far from urban centers.

There are several hydrogen transportation methods in the industry today, including dedicated pipelines, and especially made trucks [7]. There is no one solution fit all for delivery of hydrogen, and each solution requires significant investment. Several studies have discussed the similarities between natural gas and hydrogen and the potential to utilize the existing natural gas infrastructure to transport hydrogen [8] and [9]. Some of these projects are several decades old and go back to the year 1980. Utilizing the existing natural gas infrastructure for storage and transportation of hydrogen can significantly lower the capital investment need and accelerate the adoption of hydrogen.

Apart from considerable investment needed to upgrade the energy transmission and storage infrastructure to transition to a pure hydrogen network, achieving a 100% clean and renewable energy portfolio also requires massive investment in wind and solar energy production and in appliances that operate with hydrogen. Another obstacle in transition from a well adopted source of energy such natural gas to hydrogen is the lack of experience with managing and handling it. The public acceptance of hydrogen and the confidence in its safety is also a key factor in its adoption. This is critical for convincing policy makers to provide the investment and subsidies needed to transition from natural gas to hydrogen.

To reduce the barriers to adoption of hydrogen as a clean and renewable source of energy, several projects have started with slowly phasing in hydrogen and mix it with natural gas. This is similar to mixing ethanol to gasoline. Several benefits are suggested for starting with injecting a small percentage of hydrogen [10]. First, injecting small percentage of hydrogen reduces the amount of adjustments needed to the existing natural gas infrastructure, resulting in lower initial transition cost. Second, mixing hydrogen with natural gas acts as a gateway to reduce barriers to adoption from consumer, government, and policy perspective and facilitate the transition to 100% hydrogen energy transportation and storage systems. Overtime, the goal is to use the natural gas infrastructure to transport 100% hydrogen and retire natural gas to achieve the goal of zero emissions.

It should be noted that, blending hydrogen into the natural gas infrastructure is still in the early stages of research and one of the challenges of employing existing natural gas infrastructure to transport hydrogen is embrittlement and fatigue crack growth rate enhancement features of hydrogen on natural gas pipelines. Hydrogen molecules are significantly smaller than methane

gas, which gives hydrogen a much faster leakage rate, and increases the corrosive effect of hydrogen on metals [11], [12].

As the vast network of natural gas infrastructure developed in the past 50 years is transitioning to transport hydrogen, several technical and feasibility questions need to be carefully addressed. Some of the questions that need to be addressed include: Would the transportation of hydrogen degrade the pipelines? Can Hydrogen be safely used as a source of energy? Can appliances that currently use natural gas be easily converted to use hydrogen? The answer to these questions is subject of several research projects.

Since early 2000, several projects have been conducted to experiment with injecting hydrogen in the gas grid network and utilizing hydrogen as a mean to transport energy. Percent of hydrogen that can safely be blended in various natural gas infrastructures without violating network constraints has been studied in literature [8]. The overall conclusion is that as long as the percent of hydrogen mixed with natural gas is under 15%, the exiting natural gas infrastructure should be able to transport, deliver, and consume the gas mixture without materially increasing the risk to the network, household appliances, or public safety. 15% limit discussed in [8] is not a definitive limit for every natural gas infrastructure. A few different natural gas infrastructures are studied in [13] and it is shown that hydrogen mix limit is greatly dependent on the structure of each natural gas network. To determine the hydrogen mix limit, each network needs to be examined closely and the hydrogen mix limit be calculated on a case by case basis. Some of these projects are smaller in scope and are limited to very small geographic area while others cover a larger network. Except for a few projects in USA [14], Canada [15], and Australia [16], most of these projects are concentered in Europe [17–19].

One of the earlier experimental projects for injecting hydrogen in natural gas network was conducted in Ameland, Netherlands in 2008 [17]. In this experiment, the energy need of an apartment complex with about fourteen homes were supplied by a pipeline that contained up to 20% of hydrogen. No negative effects were observed either in the pipeline network supplying the apartment complex or in the standard appliances used in the households, and the experiment successfully passed all the necessary safety tests.

GRHYD, a bigger project involving hydrogen injection was funded by French government in 2014 and was conducted by ENGIE and a consortium of industrial partners [18]. In this project, Hythane, a new gas composed of hydrogen and natural gas is injected in the gas distribution network of Le Petit village to provide the needed domestic energy of the village and the supply the fueling stations of the busses located in the nearby Dunkirk Urban community. The project experimented with various levels of hydrogen mixture, including 6%, 13%, and 20% to study the impact of increasing hydrogen percentage in the pipeline network and end users. It was shown that the natural gas network could safely function if the blended hydrogen is under 20%.

Recently, a similar project codenamed HyDeploy started in 2019 and is under development at Keele University in the UK [19]. The mission of the project is "*pioneering hydrogen energy ... to help reduce UK CO_2 emissions and reach the Government's net zero target for 2050*". In this project, up to 20% of hydrogen is injected in the gas pipeline network of the university. The campus uses the gas mixture for a variety of uses from heating and cooling residences to more heavy duty uses and can model a town of about 12000 residents. The project has successfully achieved 15% hydrogen content in the natural gas network so far and is on track to reach 20%.

One of the largest hydrogen injection projects that currently is operational is in Energiepark located in Mainz, Germany [20]. The electrolysis used in the project to produce hydrogen has a capacity of 3.75MW, and source of the electricity is a mixture of the local grid and a wind farm located near Mainz. Energiepark project has successfully injected 15% hydrogen in the natural gas network. A detailed review of the projects that studies the impact of injecting hydrogen in various gas networks and their impacts are outlined in [21]. A summary of various hydrogen projects in various countries versus their blending limits is reported by International Energy Agency (IEA) [22] and depicted in Figure 1.1. The impact of injecting hydrogen in various components of the natural gas infrastructure are reported in [23] and shown in Figure 1.2.

The integrity of network of natural gas pipelines converted to carry hydrogen is studied in [24]. As the percent of hydrogen exceeds 17%, the work in [24] suggest that some of the pipelines in the network need to be replaced. Therefore, the work concludes that significant investment in infrastructure is needed to fully transition to hydrogen to transport energy. Blending hydrogen in the natural gas infrastructure has a different impact on each component of the natural gas

infrastructure. The impact of injecting hydrogen in major components of natural gas network has been studied in the literature and is reviewed in the following sections.

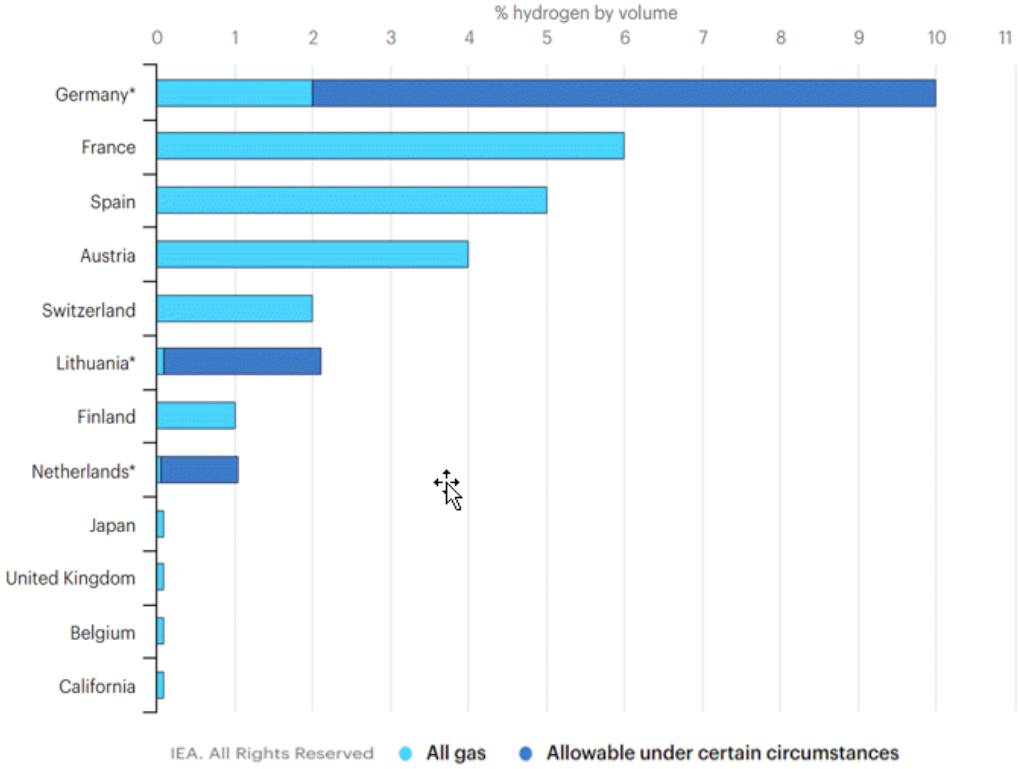

Figure 1.1. Hydrogen blending limits in various countries by volume (taken from [22])

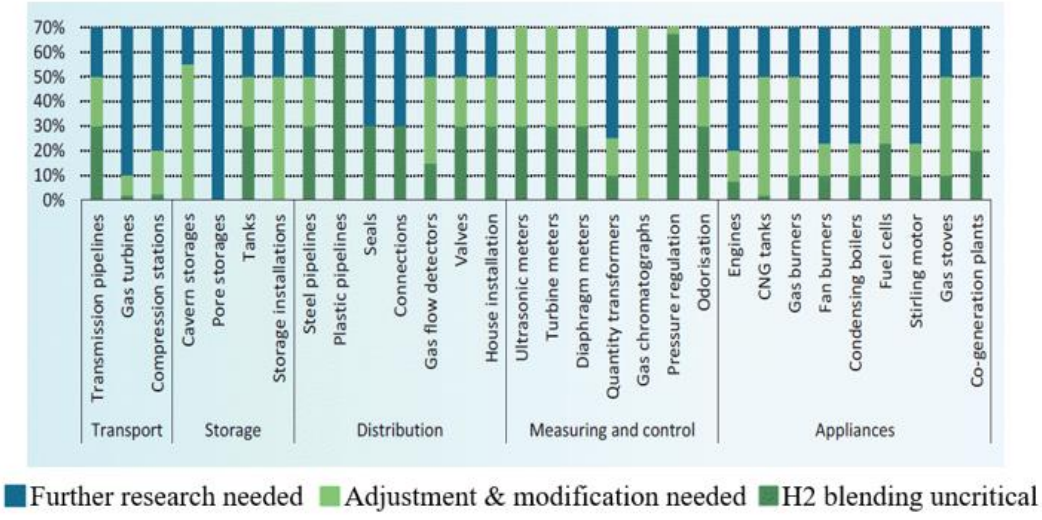

Figure 1.2. Hydrogen blending limits in different sectors by volume (taken from [23])

- **High & Low-pressure pipelines**

One reason that integrity of high-pressure gas transport networks mainly built with high-strength steel can be adversely affected is due to hydrogen embrittlement. Hydrogen has small molecules and therefore it is easier for hydrogen to diffuse into defects and surface flows of the pipeline, eventually leading to crack in the pipeline overtime, resulting in hydrogen leaking out [25]. Decades of experience in transporting hydrogen indicates to reduce the probability of crack and embrittlement, pipelines carrying hydrogen should be made from softer steel [26]. This might indicate that the current natural gas infrastructure is not suitable to carry hydrogen beyond a small mixture and transitioning to new 100% hydrogen carrying network requires significant investment to put in place new pipelines.

As transported hydrogen gets closer to the demand points in urban areas, the pipeline networks transform into a more complex web of low-pressure pipes that carry hydrogen mix to each consumption points. Most of the current pipes in the network were built prior to 1970 and are made of steel and iron [4]. Although the suitability of using these older steel and iron pipeline to carry hydrogen is dependent on their structure, condition, and the type metal used, the studies shows that these pipelines can generally be able to carry low pressure hydrogen safely [27,28]. In recent decades, polyethylene pipelines have started to replace the older steel and iron pipes. Polyethylene is naturally more porous and has a higher probability of leakage when carrying hydrogen. Research conducted in Europe has studied hydrogen leakage from low pressure Polyethylene pipelines carrying hydrogen and it has concluded that hydrogen leakage from the Polyethylene pipelines are small and does not pose a significant risk to safety of the network [29].

- **Compressor stations**

Compressor stations are used to re-pressurize main pipelines that carry hydrogen from their supply point to near the demand network. As hydrogen is mixed with the gas carries in the high-pressure pipeline, volumetric flow rate of the gas mixture increases, and therefore the centrifuges in the compressor require a higher rotational velocity. More research is needed to fully study whether changes to compressor stations is needed as the percent of hydrogen carries in the high-pressure pipelines increases [24].

- **Hydrogen meters**

As natural gas reaches the final consumption points, a meter is typically used to measure the amount of energy a home consumes. As hydrogen is mixed with the natural gas delivered to consumption, the current installed meters are not able to accurately measure the energy consumptions [27]. New meters need to be developed and installed at demand points to accurately and reliably measure the amount of energy each customer uses.

1.2 Research Goal and Objectives

The research in this dissertation focuses on studying the capacity and vulnerabilities of natural gas system (high pressure transmission pipelines, compressor stations, underground storage fields) to transition toward a 100% renewable energy portfolio. Specifically, the overall goal of this research is to help policy makers plan an educated path for transitioning Southern California's energy from natural gas and other forms of fossil fuels to renewable and green sources and means of transportation of energy. The following objectives to achieve this goal are described below:

1. Marginal Methodology to Estimate Methane Emissions from the Natural Gas system
    - Identify major methane emission sources from the upstream of the natural gas system
    - Characterize and estimate emission drivers for those major sources
    - Develop a model to accurately estimate methane emissions change with the change in throughput
2. Power-to-Gas-to-Power Dynamics for Southern California
    - Develop and verify a transient model to simulate the pressure and flow dynamics of natural gas infrastructure (pipelines and underground storage fields)
    - Implement the natural gas system constraints into the model to identify the capacity of renewable energy resources
    - Determine the capacity of southern California natural gas infrastructure to transport and store hydrogen for a 100% renewable energy penetration
3. Blending Hydrogen into the Natural Gas Network of Southern California
    - Develop a model to simulate a mix natural gas and hydrogen system
    - Analyze the impact of injecting hydrogen in the Southern California natural gas infrastructure from various locations
    - Determine the hydrogen carrying capacity at the demand points

1.3 Approach

The following tasks are accomplished in this dissertation to meet the three goals and objective discussed in section 1.2.

Task 1. *Develop a model and provide marginal analysis of the change in methane emissions from the natural gas system*

Chapter 2 and 3 will introduce and develop the marginal methodology to estimate the change in methane emissions with the change in throughput from the upstream of the natural gas infrastructure. The research analyzes various emissions mechanism for different components in the natural gas system as well as categorizing and quantifying the emissions causal factors. The EPA/GHGI methane emissions data is implemented into the developed model to study and provide a more accurate assessment of the impact of change in throughput to change in methane emissions. The results of this work will help policy makers to take the steps needed in a timely manner to mitigate the impact of methane emissions and plan a path to transition to a 100% renewable and clean energy portfolio.

Task 2. *Analyze Southern California's current natural gas infrastructure by creating a power-to-gas-to-Power transient model to achieve 100% renewable energy penetration*

Chapter 4 will develop a transient model to assess resources needed for Southern California to achieve a 100% renewable energy portfolio utilizing the existing natural gas infrastructure. This will include energy production through renewable sources (solar and wind), transportation of hydrogen through existing pipeline networks, and storage of hydrogen using underground depleted oil and gas fields. The needed infrastructure for a zero-emission energy portfolio is compared with the existing infrastructure to determine the changes that needs to be made to the existing infrastructure to achieve 100% renewable energy penetration. It is shown that there is more than one solution to achieve a zero-emission energy portfolio. The comparison between different options and their relative cost impact is presented to help identify the best path to reach the goal of a 100% renewable and clean energy portfolio.

Task 3. *Study the impact of Blending Hydrogen into the Southern California Natural Gas Network*

Chapter 5 will model the natural gas network in Southern California, including high-pressure pipeline network, compressor stations, and underground storage facilities. Various mixes of hydrogen and natural gas is injected in the network, and the impact of injecting hydrogen in the Southern California gas infrastructure is analyzed. This includes the percent of hydrogen that is delivered to demand nodes (referred to as hydrogen carrying capacity) and the change in pressure in various pipelines in the network. These analyses would help policy makers to create a roadmap for mixing hydrogen in the natural gas infrastructure and facilitate the transition to a renewable and clean energy supply.

1.4 Structure of this Dissertation

This dissertation consists of six chapters. Current chapter (chapter 1) provides an introduction and motivation for this research. Chapters two, three, four, and five each outlines literature review, methodology, results and discussion, and a summary. Each of these chapters present the work that is accomplished to meet the goals set in this dissertation. Finally, chapter six summarized the work, and outlines the future work that can be done to build on the work presented in this dissertation.

The results and findings of this dissertation from each chapter are published and submitted to peer-reviewed journals as outlined below.

Chapter 2: A portion of this chapter is a reprint of the material as it appears in the second publication below.

- **Need for a Marginal Methodology in Assessing Natural Gas System Methane Emissions in Response to Incremental Consumption**

  Michael Mac Kinnon, **Zahra Heydarzadeh**, Quy Doan, Cuong Ngo, Jeff Reed & Jacob Brouwer

  Journal of the Air & Waste Management Association, Volume 68, P 1139-1147, 2018.

- **Comprehensive Study of Major Methane Emissions Sources from Natural Gas System and Their Dependency to Throughput**

  Zahra Heydarzadeh, Michael Mac Kinnon, Clinton Thai, Jeff Reed & Jacob Brouwer

  Applied Energy Symposium: MIT A+B, APEN-MIT-209-2020.

Chapter 3: This chapter is a reprint of the material as it appears in the publication below.

Marginal methane emission estimation from the natural gas system

Zahra Heydarzadeh, Michael Mac Kinnon, Clinton Thai, Jeff Reed, Jack Brouwer

Applied Energy, Volume 277, 115572, 2020.

Chapter 4: A portion of this chapter is a reprint of the material as it appears in the publications below.

- **Dynamic Modeling of California Grid-Scale Hydrogen Energy Storage**

  Z. Heydarzadeh, D. McVay, R. J. Flores, C. Thai, J. Brouwer

  AiMES2018-The Electrochemical Society (ECS) Transactions, Volume 86, Number 13, P 245-258, 2018.

- **Investigation of Southern California Natural Gas Infrastructure to Transport and Store Hydrogen to Meet Electric Demand based on a 100% Renewable Energy Portfolio**

  Zahra Heydarzadeh, Jack Brouwer

  ASME 2020 Power Conference, POWER2020-16044, V001T08A001, 2020

- **Pressure and Flow Analysis of Hydrogen Energy Storage System for a 100% Renewable Energy Penetration – A Southern California Case Study**

  Zahra Heydarzadeh, Jack Brouwer

  Applied Energy (to be submitted Dec 2020)

Chapter 5:

- **Impact of Blending Hydrogen into the Natural Gas Network – A Southern California Case Study**

  Zahra Heydarzadeh, Jack Brouwer

  Applied Energy (to be submitted Dec 2020)

2 Analysis of Methane Emissions Sources from the Natural Gas System

2.1 Abstract

This chapter presents a comprehensive study of various sources of methane emissions from upstream of the natural gas system, assess the impact of each source on emissions, and their dependency to throughput, time, and events. The analysis builds upon prior work [30] positing that a cause-based, marginal approach to estimating methane emission impacts of change in natural gas use was more accurate than assuming that methane emissions vary one-for-one with throughput. The results show that there are many components in the natural gas system that emit the same amount of methane to the atmosphere regardless of their operational mode; meaning some emissions sources have no or only partial dependence on throughput. The results of this chapter will be used in the next chapter to build a model using the marginal emission methodology to estimate the change in methane emissions of natural gas systems as system throughput changes.

2.2 Literature Review

According to the Environmental Protection Agency (EPA), 81% of greenhouse gas (GHG) emissions come from CO_2, 6% is comprised of nitrous oxide emissions. Both gases are produced by burning coal, natural gas (NG), and oil. Another 10% of GHG emissions is comprised of methane, which is the primary constituent of natural gas [5] . Figure 2.1 presents an overview of U.S. GHG emissions and the methane contribution in 2016 along with the breakdown of sources of methane emissions.

Figure 2.2 shows U.S. methane emissions from natural gas system versus year and throughput from 1990 to 2016 based on the data presented in [31]. The data in Figure 2.2 show that despite increases in throughput over the last 26 years, total emissions produced has materially decreased. This can be attributed to improvements in various techniques used in methane production and distribution networks. Looking more closely at the data, one can ascertain that although overall

methane emissions have decreased over the last few decades, the emissions have slowly started to increase with throughput in the last 10 years.

It can be argued that technological advances in production and distribution of methane have matured and that the increase in the throughput required to meet demand has outpaced these technological advances, resulting in an increase in the amount of emissions produced.

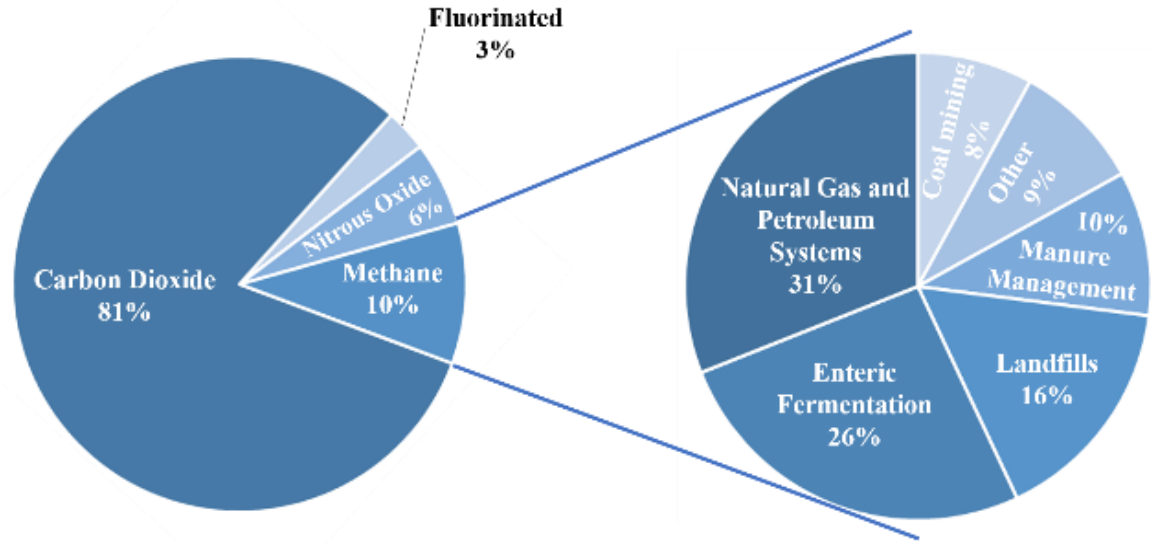

Figure 2.1. Overview of 2016 U.S. GHG emissions (left), and methane emissions by sector (right) (taken from [5])

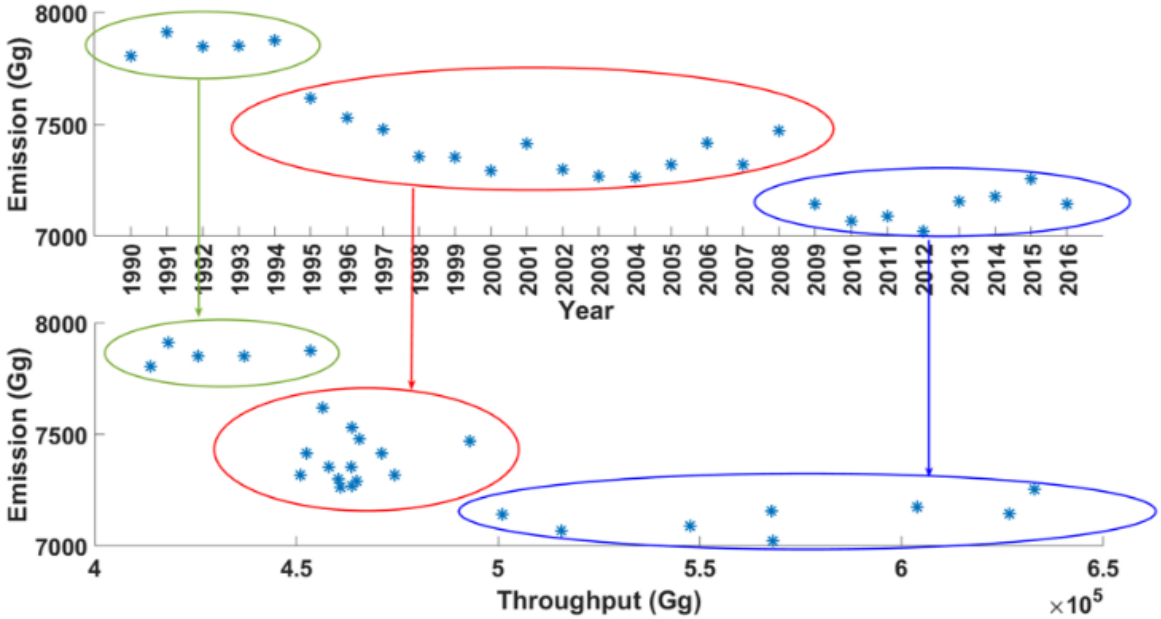

Figure 2.2. Change in Emissions and throughput from 1990 to 2016 based on the data [31]

The amount of methane emissions from U.S. natural gas supply chain was first published in 1996 using 1992 as the base year in a multi-volume set of reports by the Environmental Protection Agency (EPA) and Gas Research Institute (GRI) [32]. Since then, EPA has released two reports annually: The GHG Inventory (GHGI) of U.S. GHG emissions and sinks, and the Greenhouse Gas Reporting Program (GHGRP) [33]. The GHGI annual report publishes U.S. GHG emission estimates from 1990 to two years before the published year while GHGRP collects greenhouse gas information from all facilities with emissions over the threshold rate of 25,000 metric tons of CO_2 equivalent per year. The emission factor (EF) and activity factor (AF) are the main components used by GHGI and GHGRP (developed in 1996 by EPA/GRI) in calculating the annual national emission rates. The emission factor is the methane emission rate per unit of activity factor for each component of the natural gas system while the activity factor assesses the extent to which each component is utilized (active) within the system. For some sources, such as pipelines, the activity factor has units of miles (length) or standard cubic feet (scf) for volume, whereas for others it is the number of active units (number) of an emissions source e.g., compressors, pumps, etc. Total emissions for each source are the product of the activity factor and emission factor (Emissions=AF*EF). Using this formulation for predicting changes in methane emission rates carries the embedded assumption that changes in throughput lead to a proportional change in methane emissions via the emission factors which are all constants. Although throughput is a fully appropriate normalizing factor for reporting methane emissions, incorrect conclusions can be drawn if it is used as a causal factor rather than a normalizing parameter.

Although emission factors have been widely used in the industry for estimating emissions, recent research has identified several inaccuracies that resulted from solely relying upon emission factors to calculate total emissions and impacts of throughput changes as outlined in [34], [35] and [36]. To calculate emissions from a specific source, emission factors are typically calculated over a small population of samples over a short period of time. The derived emission factor is then used to "estimate" the overall emission over a larger area and expanded time horizon. The limitations on the population sample size, and time span used to calculate emission factors limits the accuracy of the emissions that are estimated using emission factors [37]. In addition, it cannot necessarily be assumed that emission factors using throughput as an activity factor are constant with respect to changes in throughput. For example, a simple leak that emits at a constant rate (grams per hour)

will show an emission factor that changes inversely with throughput which is simply stating that a constant leak rate normalized by throughput behaves as 1/x. Other leaks may be pressure dependent and decrease as a function of throughput to behave as –EF/x.

EPA/GRI initially published the emission factors of a large number of components in its 1996 GHGI annual report, and since then, the agency has been regularly updating those estimates. The most recent report on emission factors was published in 2018, outlining emission factors of each component from 1990 to 2016.

Significant efforts have been made to improve the accuracy of estimated emissions. The Barnett Shale coordinated campaign supported by the Environmental Defense Fund (EDF) is one of these major initiatives. The campaign funded 16 research projects to help more accurately estimate the emission of different components at the Barnett Shale field. Several papers published on these studies indicate that there are significant needs to update emission factors to more accurately account for emission of various components. Studies of methane emissions can be categorized into two groups: bottom-up analysis and top-down analysis. In bottom-up analysis, the research aims to estimate emissions for each component and then calculate the total emissions by adding up the emissions from each component. In top-down analysis, overall emissions of the system are measured over a large geographic area and then the result is scaled down to estimate the emissions from system subsets (e.g., a single compressor station). The lack of agreement between the two approaches as summarized in [38] has driven additional research into the reasons for the differences in estimated emissions.

The estimated emissions factors that resulted from Barnett Shale project are compared with the results published by EPA in [38]. The comparison indicates that the emission factors published by EPA are consistently underestimated because some factors that contribute to the inaccuracy include small sample size, and not accounting for super-emitters (meaning that a small number of emission sources are responsible for a large fraction of the leakage [38]). The analysis in [38] shows that the top-down analysis overestimates the emission while the bottom-up analysis underestimates it. The emission of compressor stations is studied in [39] to determine the accuracy of data reported by GHGI. The emission at compressor stations and its associated pneumatic devices and storage components are monitored when the station is both in operation and standby.

The analysis in [39] shows that the emission at compressor stations is linearly correlated to fuel consumption at the station, suggesting they are proportional to throughput only when the station is in operation and nearly zero for components that are not in operation. Similar results are also reported for emissions calculated in AP-42 program [40].

Another top-down analysis reported in [41] estimates the emission of a natural gas basin by monitoring the methane in the atmosphere and correlating it the natural gas production from the site. The analysis shows a relatively wide emission factor range, and the research in [41] is inconclusive about whether emission from basin is a function of gas production rate.

In [42], the component-based methane emissions from use of natural gas in the heavy-duty transportation sector are analyzed. The effects of engine tailpipes, vents, and fuel nozzles upon methane emissions as a percent of throughput are investigated. The analysis of various comments in [42] shows that sources of the emission could be from continuous leaks, or events (such as unloading fuel deliveries). Therefore, the authors of [42] suggest a more holistic approach is required to accurately estimate emissions: "a national inventory would require additional measurements and a better understanding of the current fleet and infrastructure and their operation. Generally, there is a need for more measurements at current and new fueling facilities to provide a larger statistical sample for developing emissions factors" [42].

Top-down analysis reported in [43] shows that estimated emissions are higher than what is the reported in the EPA inventory. The difference in estimated emissions is attributed to the fact that only a few large facilities were used to develop AP-42 emission factors, resulting in an underestimation of emission as a function of throughput. Another explanation for overestimation of emissions in top-down analysis is suggested in [44]. The studies in [44] find that 15-29% of methane in the Barnett Shale area are attributed to landfills instead of natural gas production. This can explain why top-down analysis overestimated the emissions.

The emission from super-emitters in the Barnett Shale region are analyzed in [45].The studies show that the operations and status of the equipment, which include hardware degradation, maintenance malfunctions, dynamic operation, can significantly increase the emissions. For example, the study finds that for compressor stations, the estimated emissions shown in AP-42 is

570 times higher than what is reported in GHGRP, because GHGRP does not account for these factors.

Laser-based sensors are used in [46] to measure the emissions of compressor stations over time. The research in [46] shows that emissions have relatively small dependency upon throughput, but high variability throughout the day. This implies that emissions are not necessarily a linear function of throughput and the emission factors that are derived from data that represent short time durations might be accurate. Emissions at five compressor stations were measured in [47], and researchers were able to quantify what percentage of emissions at each site was due to engines, compressors, valves, or slop tanks. Downwind tracer flux and onsite emission of compressor stations was measured with an infrared camera in [48]. The study shows that site-level emissions verses natural gas throughput has an r-squared of 38%, while the normalized emission is negatively correlated with throughput. This means that emissions as a percentage of throughput decreases as throughput increases. [49], [50], and [51] all use different methods to measure emissions of automobiles in the Barnett Shale area and suggest a distribution of emission factors to estimate total emissions.

In [52], emission and activity factors of more than 1000 facilities as well as 2300 on-site measurements have been used to create a new emission estimate model. The emissions estimated in [52] are similar to the results published by GHGI, except for a few differences. The GHGI model assumes a significantly smaller number of centrifugal compressors and wet seals, which is a reasonable assumption considering the use of these equipment types have been an effective way to reduce emissions in the past decade [53].

All works mentioned above have been studied to investigate the accuracy of measurements/estimates without discussion of causation. But the premise of this paper is to relate the changes in emissions versus throughput based on causal factors. [30] reports that the percentage dependency of emission sources upon natural gas system throughput has never been quantified in detail. Further research is needed to fully characterize the effect of throughput change on total system emissions. As described in [30], a clear understanding of the change in emissions with incremental increase or decrease in consumption of natural gas is essential in determining its environmental impact. They continue that currently most methods and tools rely upon a simple averaging approach and use a pro rata allocation to account for the environmental impact of increased emissions as natural gas consumption changes. For instance, the Greenhouse Gases,

Regulated Emissions, and Energy use in Transportation (GREET) model is a popular Life Cycle analysis (LCA) tool [54] that adds the average historical emissions from various steps and then the total is divided by the total annual throughput to estimate the normalized emissions.

Although the GREET model is the current gold standard to determine emission rates from natural gas, it has significant shortcomings in forecasting emission as throughput in the system changes. In the GREET model it was assumed that the change of methane emissions is directly proportional to the change of throughput such that a given percent change in throughput creates the same percent increase in emissions. In other words, the GREET model assumes that all components of the natural gas system are 100% throughput based using throughput as a single activity factor with total system emissions divided by total system throughput as the emission factor. Once total system emissions are estimated, carbon intensity (CI) models such as GREET attribute GHG emissions to uses pro-rate with throughput. This is an average as opposed to marginal formulation that does not accurately measure the change in GHG emissions associated with changes in end-use consumption. The term "marginal" is used in this manuscript to refer to the term-of-art that describes the technical features associated with understanding the resources that are active in a system “on the margin” – meaning, understanding which resources are most immediately turned up or down with increases or decreases, respectively, in throughput. The goal of this chapter is to expand the characterization of components in the natural gas system. This is the first building block needed to determine the impact of changes in natural gas throughput on the total methane emissions. These results will be used in the next chapter to calculate total system emissions change from the upstream of the natural gas system.

2.3 Methodology

The first step in estimating marginal emissions of the natural gas infrastructure is to identify sources that have material impact on the emissions and for which enough component level data exists.

As discussed in the previous section, the emissions from each component of the natural gas system are attributed to several factors and therefore calculating the total amount of emissions from the natural gas system and their causal dependencies is a very complex process. In order to

simplify, these factors are divided into three categories as suggested in [30]: Throughput-based, time-based, and event-based.

Equation (1) shows how our marginal approach calculates the total emissions for each individual emissions source in terms of its dependency upon time, event and/or throughput as was presented in [30] where E_T, E_E, and E_{TP} are emissions rates driven by time, event, and throughput respectively, and a, b, and c are the marginal emissions coefficients of time, event, and throughput, respectively.

$$E = aE_T \times bE_E \times cE_{TP} \quad (1)$$

Comprehensive literature review is conducted in the next section to assess these marginal emission factor coefficients (a, b, c). The study of throughput, time, and event-based dependency of major emission sources is documented in order to determine each category percentage contribution.

The analysis in this study focuses on the upstream of natural gas infrastructure including the exploration sector, the production sector, the processing sector, the transmission and storage sector, and the distribution sector. Figure 2.3 shows the distribution of each sector to the total methane emissions from the natural gas system for the 2016 base year.

A 2018 EPA/GHGI report [31] identifies 129 methane emissions sources from the U.S. natural gas system. Figure 2.4 shows emissions percentages from each source. The “other” category in Figure 2.4 represents sources in the natural gas system with methane emissions less than 3%.

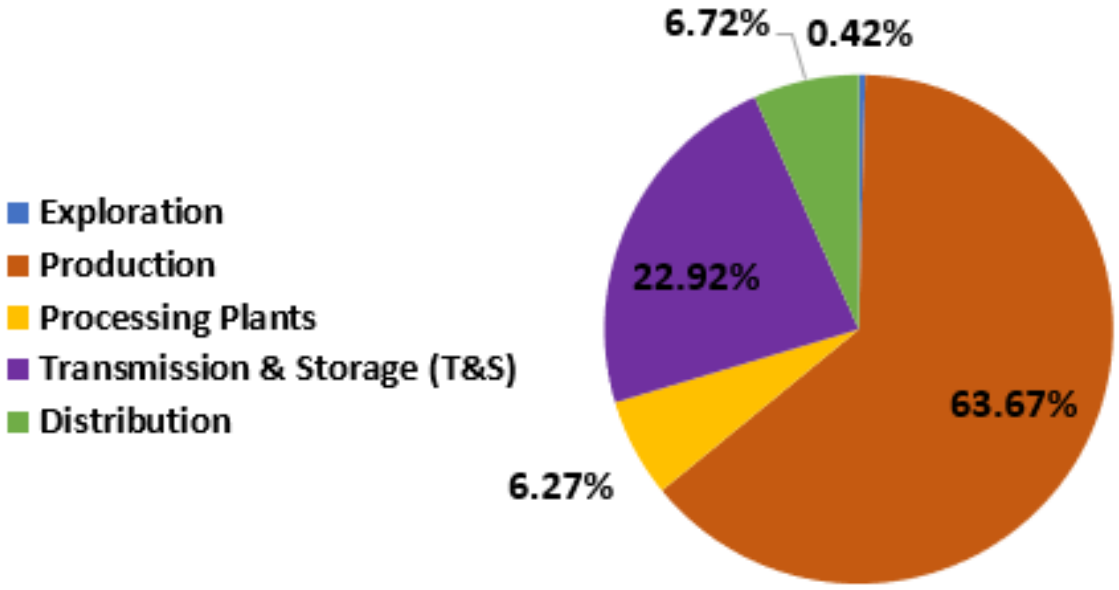

Figure 2.3. Total methane emissions percentage from the natural gas system by sector for the 2016 base year (data adapted from [31])

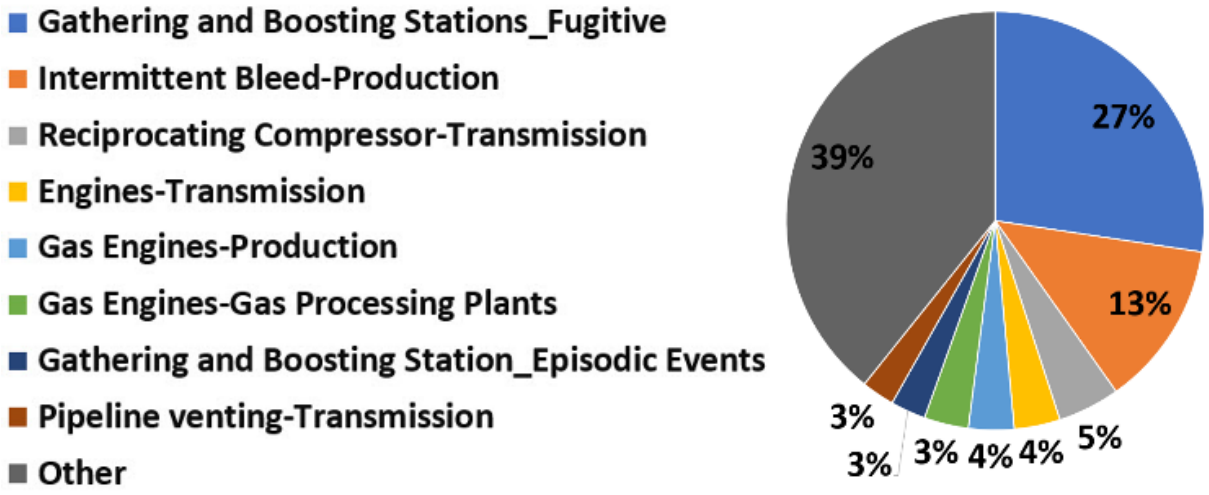

Figure 2.4. The distribution of emissions percentage from each component of the natural gas system for the 2016 base year (data adapted from [31])

2.4 Results and Discussion

Major sources of methane emissions from natural gas systems are outlined in 2018 EPA/GHGI [31]. These sources are carefully studied and categorized as throughput, event, and time dependent as explained in detail in the following sections. The final estimated coefficients are outlined in Table 2.1. Further experimental work is needed to evaluate the dependency of each source on throughput, event, and time. This will help improve the accuracy of the estimated total emissions of the system using the developed model.

- **Pneumatic Controllers**

Some of the major contributors to the total methane emissions from the natural gas system are Pneumatic controllers and therefore are examined closely in this chapter. Pneumatic controllers are divided into two categories based on the type of emissions: intermittent vents, and continuous bleeding. They both can be used in on/off and throttling services. The distinction between intermittent venting and continuous bleeding is that intermittent controllers have a mechanical seal between the supply gas and the actuators but in the continues bleeding controllers there is no barrier between the supply gas and the actuator and gas from the supply gas is continuously venting in order to maintain the pressure.

The intermittent vent controller utilizes gas pressure to open or close a valve. To open the valve, controller reduces pressure by venting off gas to the atmosphere. Effective sealing can keep emissions rate at a very low level even after the actuator is depressurized. Figure 2.5(a) depicts exhausted gas of an intermittent controller [55]. As shown in the figure, to open the valve, gas is released to the atmosphere. The amount of gas released depends on actuation frequency, supply gas pressure, type of process flow, and the condition/age of the equipment.

In a continuous bleed controller, no seal exists between the actuator and the supply gas and instead there is a continuous gas flow through the orifice. To close the valve, the bleed port will partially cover the block resulting in less gas released, which in turn increases the pressure as shown in Figure 2.5(b) [55]. This also causes a sudden drop-in emissions rate for a short period of time. Similarly, the valve can be opened by reducing the built-up pressure, which results in the block uncovering the bleed port. The opening process temporarily increases emissions rate until the system settles in a steady state condition and emissions rate is reduced. The sudden increase

and decrease of emissions rate after opening and closing the valve cancel each other out, resulting in a continuous emissions rate independent of the valve opening/closing process.

The continuous bleed controllers are also categorized as high and low bleed controllers based on the emissions rate (emissions higher than 6 scfh over 50 Mcf considers high bleed devices according to the natural gas STAR program [56]). The devices that need to control process flow very quickly should have a large orifice hole and as a result, the bleed port would be large resulting in higher emissions.

EDF funded study in [57] measures the emissions rate from 377 natural gas powered pneumatic cotrolleres that are mostly located at the natural gas production sites throughout the U.S. It was found that the level controllers used in the seperators and the compressors have the highest emissions rate compared to others (e.g. well head, plunger lift, process heaters, dehydration system, and flare).The study also measured the dependency of emissions rate to the site region and obserevd that Rocky Mountains region has the lowest amount of emissions rate while Gulf Coast has the highest emissions rate. Among the 377 contollers studied, 40 sites with highest emissions rate all had equipment issues. In summary, the study shows that while emissions rate of controlelrs are dependent on the type of service, the process being served, and the location of the site, equiemnt problems are one of the main contributers of emissions rate.

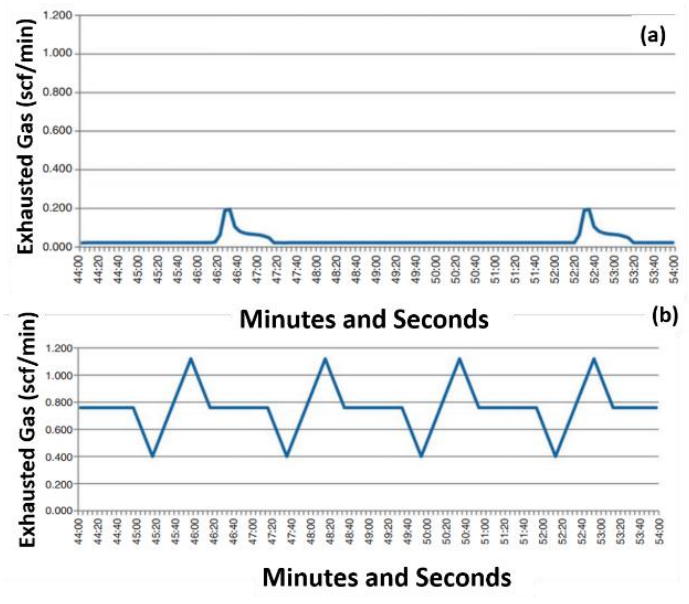

Figure 2.5. Theoretical exhaust rate: (a) Intermittent-vent; (b) Continuous-vent (adopted from [55])

Emissions rate of intermittent controllers are highly dependent on frequnecy of opening and closing the valve, and therefore emissions rate for these types of devices are event based. When intermittent contollers process more gas flow (throughput), the actuation rate will increase, resulting in more venting to the atmosphere and as a result emissions rate is also partitially dependent on throughput as shown in Table 1 (a=0%, b=80%, c=20%). For continous bleeding controllers, the temperarry effect of openig and closing the valves on emissions rate canceled each other out, and therefore emissions rate for these type of contollers are time based (a=100%, b=0%, c=0%).

- **Gas Engine**

Methane emissions from the exhaust of compressor engines are one of the significant sources of emissions resulting from incomplete combustion of natural gas. As part of the EDF funded series of studies Johnson et al. conducted audits of emissions in three compressor stations and two storage facilities [47]. The goal of the study was to compare their measured emission factors with those of AP-42 [40], the 1996 EPA/GRI [53], and Allen et al. [58]. From data collected in this study, it was shown that 46% of overall emissions are from engine exhaust, 5% from crankcase and the rest are from other component leaks and venting. The sites employ a combination of four-stroke lean-burn (4SLB), two-stroke lean-burn (2SLB) engines, and gas turbines. The measured engine exhaust reported in [47] varies significantly compared to calculated results from AP-42. For example, measured emission for G3512 engine is 5.7 (kg/h) while the calculated value is underestimated by 23% at 4.4 (kg/h).

The significant estimation difference of emissions in AP-42 is likely due to the calculation only relying on fuel input as the only parameter. Another major source of emissions that is not considered in AP-42 calculation is the leaks from the engine's crankcase. As shown by Johnson and Covington [47], considering the effect of emission from both exhaust and crankcase significantly reduces the difference between the measured and calculated emissions. Specifically, for sites that employ new 4SLB technology, after adjusting for crankcase emissions, measured emissions were only on average 11.4% lower than AP-42 estimates. [47] proposed a new method for estimating the total site emissions based on correlating the total site emissions and throughput. The measured site emission rate over engine throughput from a limited number of sites that employ 4SLB technology was plotted against total site throughput as shown in Figure 2.6. It was shown

that the total measured emission rate has a high degree of negative correlation with the throughput with an R-squared value of 89%. Stations with higher throughput have lower emissions per engine throughput. Therefore, the measured response can be used to model the emissions based on the station's throughput and can be applied to reliably estimate the total emission of sites that employ 4LSB technology. Based on the results reported in [47], creating a library of measured emission and station throughput for sites that use 4SLB technology can provide an invaluable tool for estimating the total emissions of various sites nationally. Based on this, we suggest that engine emissions are 80% throughput-based due to the burning of natural gas and 10% time-based due to the leaks associated with pressurized operation.

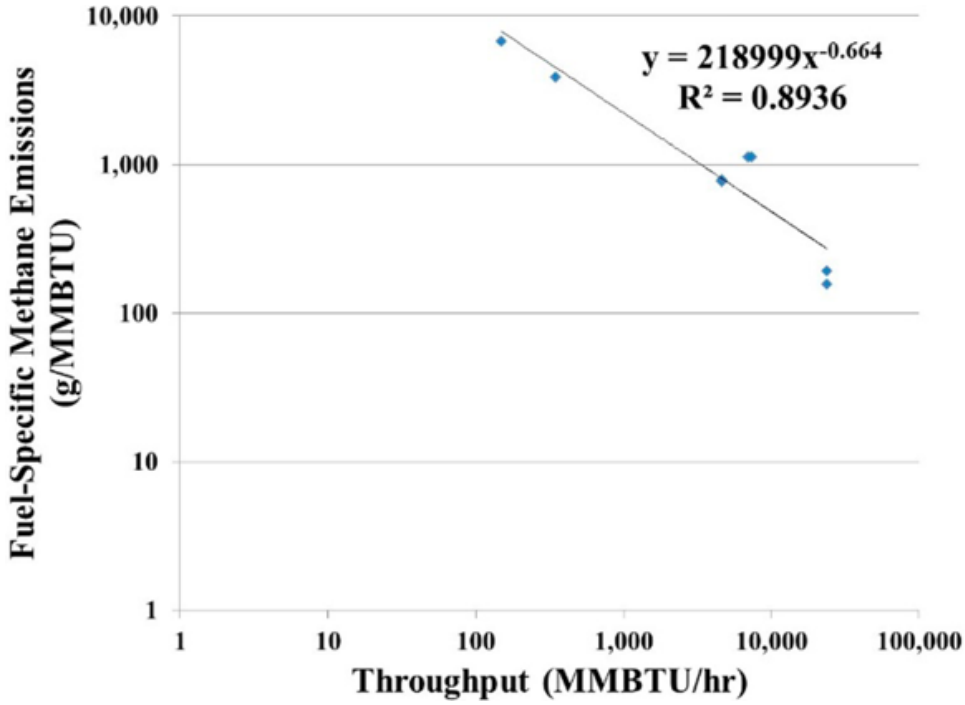

Figure 2.6. Fuel-Specific methane emission vs. site throughput for 4SLB engines (taken from [47])

- **Compressor**

Compressors are mainly used to facilitate the transfer of natural gas from one point to another through pressurizing the gas. Compressors are generally divided into two categories: reciprocating and centrifugal. Reciprocating compressors employ a mechanical piston to pressurize the gas though a compression cylinder. The pistons are typically powered by gas engines themselves. Centrifugal compressors rely on centrifugal force to pressurize the gas. An impeller spinning at high speeds exerts force on a diffuser element that transfers kinetic energy and pressurizes the gas.

In both compressor types, increasing the pressure produces heat and increases the temperature of the gas. To moderate the temperature of the gas and keep the system stable, cooling elements are also added to the compressors.

Emissions from compressors in various states, including when they are pressurized and operating, pressurized but idle, and not pressurized are analyzed in [59]. Typically, two to six compressors are placed at each transmission and processing station. As demand changes, compressors are pressurized or depressurized to meet the demand. Another reason for depressurizing compressors is to perform maintenance, which can occur regularly or irregularly in response to failures.

Depressurized compressors have zero fugitive emissions, and their only emission comes from blowdown valve that vent to atmosphere. With increase in demand, more compressors are pressurized and brought to service, which in turn proportionally increases gas throughput and pressurized fugitive leaks. The total duration that pressurized compressors are in service is proportional to the demand it serves. As reported in [59], reciprocating compressors are in operations 45% of the time, are idle 34%, and are depressurized the rest of time while centrifugal compressors are active 24% of time, are idle 6% of the time, and are depressurized the rest of the time. This statistic is used as a baseline to estimate the total usage of compressors.

Compressors can operate at various speeds, and as compressor speed increase, so does the emission it produces. This is since higher speeds, there are more chances for gas to leak during each piston stoke. In practice, compressors are operated at a fix speed and are either pressurized, and in operation or in idle state as demand changes. Higher throughput is achieved by bringing more compressors online and as a result, station-based compressor-related fugitive emissions are expected to be strongly correlated with the total throughput.

Fugitive emission leaked from pistons and its housing is present and cannot be avoided even in newly and properly installed reciprocating compressors as reported by Natural Gas STAR Partners [60]. As compressors age and the shafts and seals of the compressors wear down from friction and heat, fugitive emissions increase. Considering the complexity of calculating various factors affecting emission overtime due to pressurized leak, leak per stroke, and frequency of

pressurization, most analysis in literature only measures emissions over a short period of time and assumes continuous constant leakage.

It can be concluded that for component-based emissions from reciprocation compressors the amount of gas escaping from the system through the gaps is strongly function of the gas pressure, the compressor speed and therefore increasing throughput will increase the emissions from one specific reciprocating compressor but since compressors usually operate at constant speed at the compressor station it can be thought that the degree of dependency of emission to the throughput is week (10%). At the same time the gaps between various packing cups and rod even in newly installed system indicates that there is a constant leakage that accumulates over time as a result it is believed that big part of emissions from reciprocating compressors are time based (90%). Figure 2.7 shows a schematic of the reciprocating compressors [60].

Another type of compressor used to pressurize natural gas is centrifugal compressor. The structure of a centrifugal compressor is shown in Figure 2.8 [61]. The compressor in Fig. 3 operates by creating suction pressure through a rotating shaft. The process gas will move rapidly outward from the force of the rotating shaft, which increases the pressure of the gas. The emission created between the housing and rotating parts are reduced by utilizing sealing that attempts to cover the voids between the moving parts. Two different types of seals used are wet and dry seals. Wet seals block the voids by circulating oil at high pressure around the surface of the shaft and sealant rings [62]. This prevents the gas from leaking. The sealing oil overtime traps gas and needs to be cleaned to maintain its lubricative properties. The process of purging oil from the trapped gas, called degassing, produces gas which usually vent to the atmosphere and is the primary source of emission in wet seal centrifugal compressors [62].

Dry seal centrifugal compressors employ a ring press around the shaft to seal the voids in the rotating shaft. The ring relies on the pressure difference and springs to prevent the process gas from escaping. Dry seals can be more efficient in preventing emissions at a lower cost compared to wet seals [61]. Similar to reciprocating compressors, it could be challenging to estimate emissions associated with impeller speed, and frequency of pressurization.

In terms of causal based emissions analysis for centrifugal compressors it can be said that the small percentage of the leakage from the wet seal is related to fugitive emissions at the seal face

and this can be thought as time-based emissions since even newly installed wet seal compressors leak (20%). Whereas most of the gas leakage happens at the vent from degassing unit which is directly proportional to the throughput meaning higher throughput require more oil circulation as a result more oil should be cleaned up therefore higher gas vent to the atmosphere. Therefore, this source of emission is throughput based (80%).

The main difference between wet and dry seal centrifugal compressors is that emission caused by degassing process is only present in wet seal centrifugal compressors. Consequently, new technologies offered in dry seal centrifugal compressors offer some of the lowest emissions in the industry [61]. Therefore, replacing the older wet seal centrifugal compressors with newer dry seal centrifugal compressors can significantly reduce the amount of emissions. Another proposed solution for reducing emission from centrifugal compressors is to efficiently capture the leaked natural gas and the redirect the gas to fuel another process on the site [58]. Other research by EPA indicates that maintaining the compressors properly and replacing seals and rod shafts every few years is an effective way to limit leakage and reduce emissions [60].

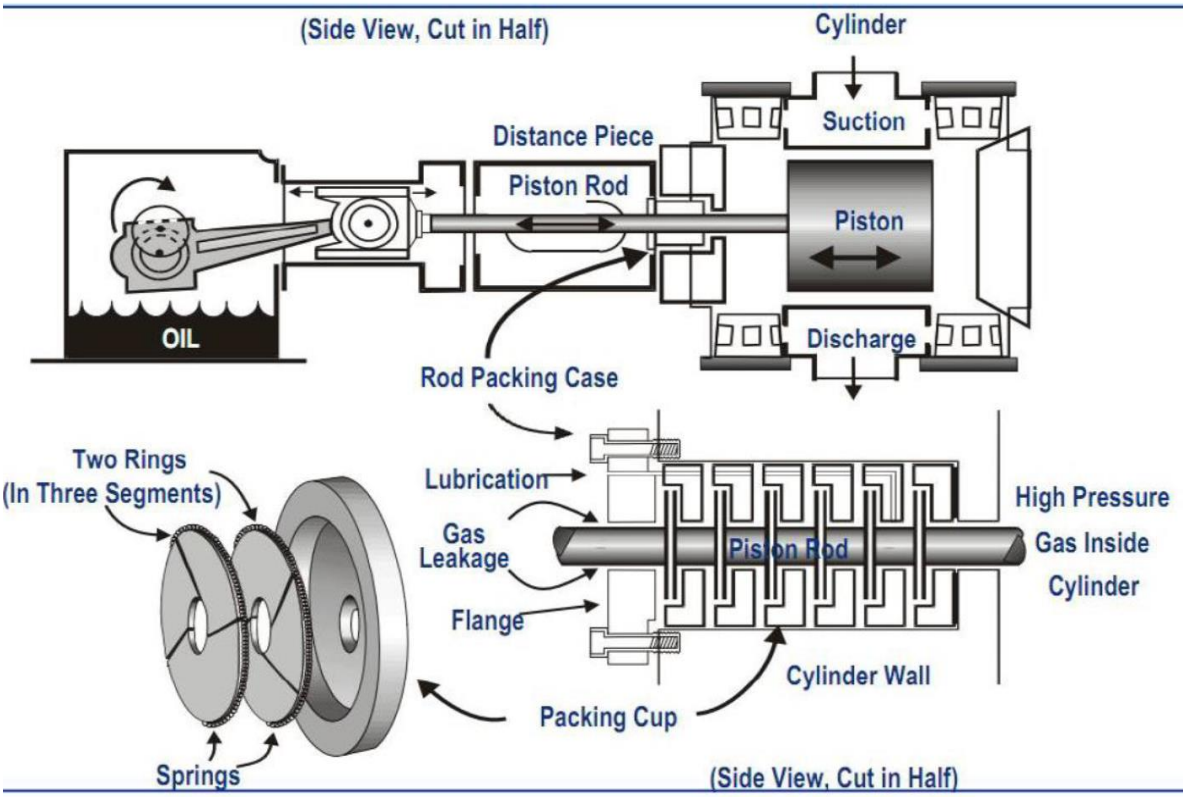

Figure 2.7. Typical Rod Packing System (taken from [60])

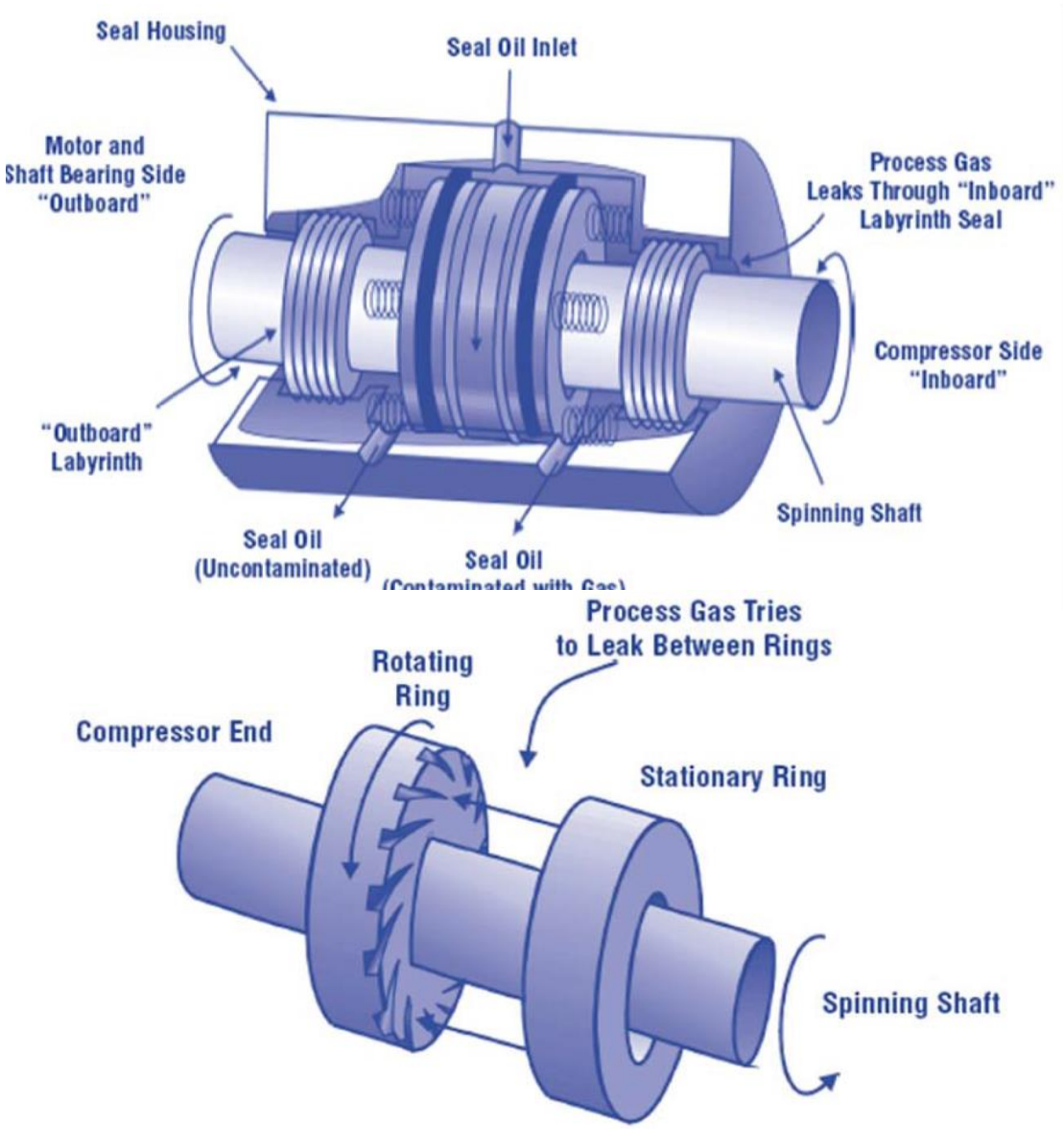

Figure 2.8. Centrifugal compressors, wet seal (top), dry seal (bottom)- (taken from [61])

- **Liquid Unloading**

A process of removing liquid (oil, water, and condensate) accumulated in a gas well to the surface is called liquid unloading. The reasons liquid is accumulated in the gas well include either reduction of the reservoir pressure or the velocity of the gas. It also might be because of variation in the Gas to Liquid Ratio (GLR) [63]. The accumulation of the liquid in the wellbore can reduce the gas production from the gas well. There are different technologies for removal of liquids from the wellbore such as installation of a pump or velocity tubing. But these methods do not result any

emissions to the atmosphere. Liquid unloading with and without plunger lift is other method which leads to the emissions by changing the direction of the flow from separators to the storage tank. Liquid unloading without plunger lift occur when an operator changes the flow's direction from a separator usually operating at high pressure to the storage tank typically operating at the atmospheric pressure to increase the pressure difference between the bottom of the well and the surface. This high-pressure difference let more gas with high velocity flow toward the surface while entraining liquids. Unloading using a plunger lift removes liquid by releasing plunger which is held at the top of the well to the bottom of the wellbore when the well is closed. By opening the well, this allows plunger to use the well's own energy to lift the liquids to the surface. In this case there are two conditions; if plunger could reach to the top of the well then liquids and gas flow through the separators and there are no emissions but if plunger stopes somewhere and could not return to the top of the well then the controller sends a signal and redirect the flow toward the atmospheric pressure tank instead of the separator where emissions occur. The methane emission source is gas vent to the atmosphere from the storage tank. The process of unloading with or without plunger lift can be done either manually by operators or automatically [63], [64], and [65].

Allen et al. [66] measured methane emissions from 107 wells sampled from four different natural gas production regions including Rocky Mountain, Mid Continent, Gulf Coast, and Appalachian. 32 gas wells without plunger lift all manually triggered and 74 well with plunger lift both automatically and manually triggered. It was found that unloading with plunger lift results in lower emissions per event compered to unloading without plunger lift. The frequency of the event in an unloading with plunger lift is higher (>200 events per year) compared to without plunger lift (<10 events per year). In [66] the statistical analysis between gas well characteristics (age, depth, and static shut-in pressure, surface flow line pressure, volume, and gas production SCF per day) and measurements data (event duration, event per year, annual emissions, emissions per event) was done. The goal was to identify the relationship between well characteristics and annual emissions and explain the high variability of the frequency of unloading events. It was found that the correlation between the annual emissions and the event frequencies are significant and there is a positive correlation between the event frequencies and the age of wells, suggesting that gas wells with older age have more unloading. There is also a negative correlation between the annual emissions and the depth of the gas, suggesting gas wells with higher depth have lower annual

emissions. It can be concluded that the younger wells have higher depth and lower number of events resulting in lower total annual emissions.

The relationship between the gas well age and the gas production rate (scf/day) was conducted using measurements data [66]. As it was shown in Figure 2.9, there is a positive correlation between them, meaning that older gas wells have less gas production rate.

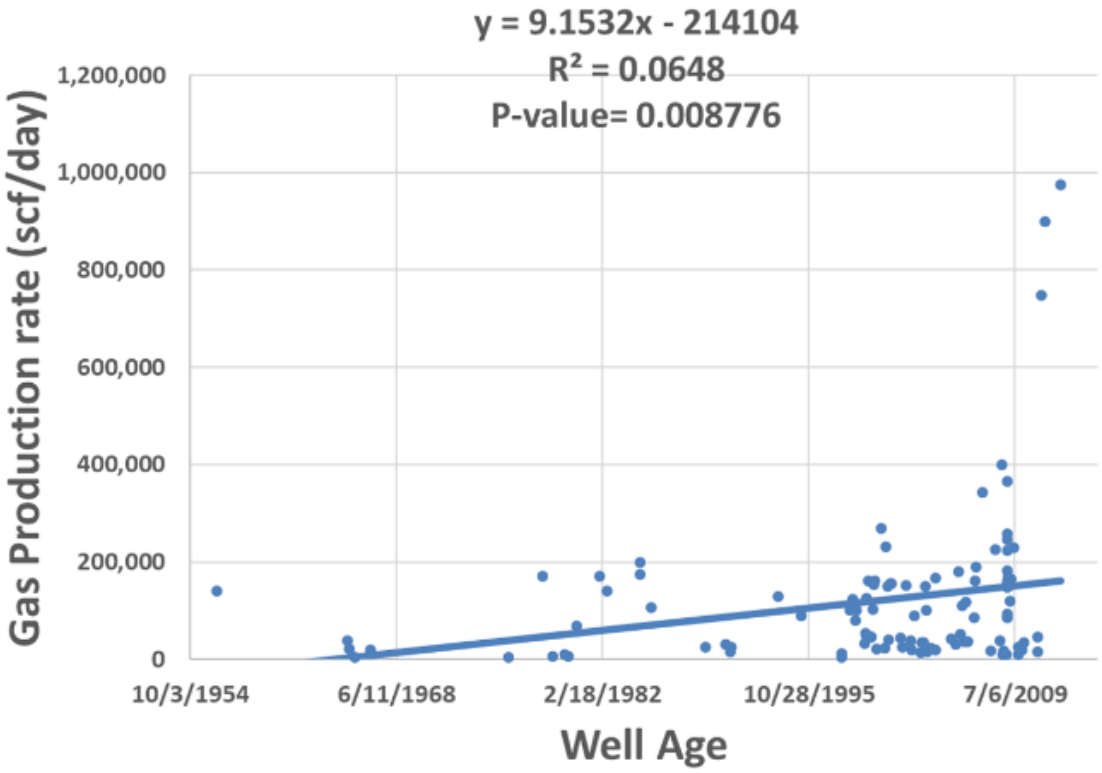

Figure 2.9. Gas wells production rate vs age based on measurements data from [66]

In order to show the dependency of emissions on unloading event and throughput, a statistical analysis has been done using measurement data from [66]. Since EPA/GHGI reports two separate sources for unloading, with and without plunger, the data was divided by these two categories. For unloading with plunger, the correlation between: 1) well methane production (scf/day) and annual methane emission (scf); 2) well methane production (scf/day) and normalized emission (annual methane emission/annual methane production); 3) annual unloading event and annual methane emission; 4) unloading event and emission per event were calculated. Data also is categorized based on well characteristics: 1) well with only manual plunger; 2) wells with only automatic plunger; 3) all conventional wells; 4) all unconventional wells; 5) all tight reservoirs; and 6) all

shale gas, to show the dependency of well-specific characteristic to the throughput and unloading events. It was found that there is not any significant relationship between well methane production and methane emissions and between well production and normalized emissions. Although, there is a significant relationship between annual methane emissions and unloading events (all with p-value less than 0.05) and overall dependency of annual emissions to events is around 13.83% for plunger wells. Among 7 different group of wells, the group with the highest percentage of manual loading (100%) have highest dependency to the event frequencies while wells with automatic plunger do not have any correlation to the event frequencies. The combination of well formation, conventional/unconventional, age and many other factors determine the total dependency to the unloading events. According to measurement data [66] and the nature of the unloading event it can be thought that unloading emissions are mainly event based (80%) and a small portion is throughput based (20%), since more extraction from well causes more gas to flow through the wellbore and lead to unloading events.

It should be noted that the measurements data from [66] only sampled 107 wells out of 60158 throughout the whole U.S., but it is still the only broad and large set of measured data for unloading among the literatures.

- **Blowdown**

Blowdowns are on-off devices that can quickly depressurize a system to atmospheric pressure. Blowdowns are used both in an emergency when the system needs to depressurize quickly and in regular repair and maintenance in the system. Blowdowns are used in compressors, gas wellbores, pipelines, vessels, and some other small volume sources. In the production process, blowdown valves are routed to a flare to reduce emissions. Some compressors route most of the blow down natural gas to a nearby low-pressure reservoir such as a fuel saver to prevent the gas from leaking to atmosphere and reduce emission [67].

The EPA has measured and recorded the frequency and volume of emissions from blowdown events. Blowdown valves are mainly used for gas unloading in the production sector and in compressors in the transmission sector [67]. In the production sector, gas wellbore blowdowns are utilized to relieve pressure by lifting out water that prevents gas flow [68]. According to data recorded by EPA, approximately 65% to 70% of operators maintain their pressure while the

compressor is idle while the rest will use the blowdowns to depressurize the compressor to atmospheric pressure [67]. In some processing plants, blowdown lines are routed to a flare to limit emissions. This option is almost never available in the transmission sector. One solution to reduce emission in the transmission sector during shut down is to keep compressors mostly pressurized [68]. This approach reduces the amount of gas released to atmosphere in the blowdown process. The drawback of mainlining the pressurized compressor is that this will cause emission from compressor rod packing and closed blowdown valves. As shown in Figure 2.10, emissions from maintaining pressurized compressor is far smaller than the emission caused by a blowdown [68].

Blowdowns mainly occur during emergency and maintenance and by definition, emissions caused by blowdowns are event based (80%). Increasing throughput and usage could increase the need for regular maintenance. As a result, it can be argued that emissions from blowdowns can have a small throughput-based cause (20%). Despite this reasoning, some of observations at gas wells and compressor sites show no instances of blowdowns for an extended period, suggesting that blowdowns should only be considered an event-based source of emissions.

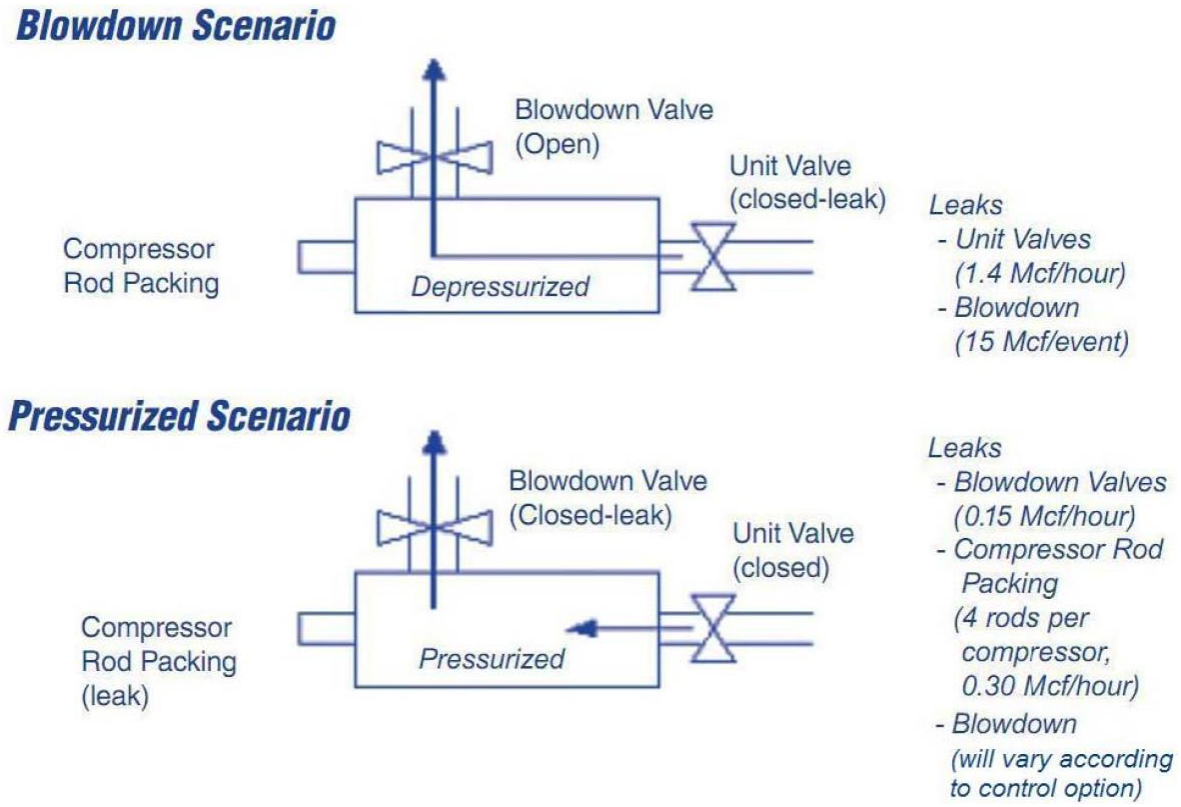

Figure 2.10. One solution to mitigate blowdown emissions during shut down (taken from [68])

- **Storage Wellhead and Wellbore**

Natural gas can be stored in three types of the geographical reservoirs: depleted oil and gas fields, depleted aquifers, and salt caverns. Approximately 79% of U.S. underground natural gas storages are depleted oil and gas fields [69]. The natural gas underground storage primarily consists of three sections; the wellhead which is a series of valves, pipes and some other components to monitor and control the gas flow injection and withdrawal, the wellbore which connect the wellhead to the storage field and is a series of concentric pipes extending from the surface to all the way down to the storage formation [69].

The sources of natural gas emissions from storage wells usually are; failure in the wellhead sealing and some components, leakage in the production casing, and leaks around the surface casing or subsurface lithology [69]. The schematic of storage well with three leakage pathways are depicted in Figure 2.11, [69].

The failure of mechanical seals in which separate each layer of different casing can cause the gas from the production casing leaks through an open annulus valve. If annulus valve is closed then gas pressure can build up in the annulus and therefore, in this case it may cause more failures and issues. In order to prevent this condition some operators keep the annulus valves open during normal operation to let the gas exit through the annulus valve. The second source of the leakage occurs within the wellbore due to the fracture in the production casing wall and letting gas inside the case escape and finds its way up to the surface to emit. The last source of emissions occurs when the pressure of the surface casing surpasses the yield strength of the surrounding lithology. This causes the gas to change its direction and instead of moving upward through the wellbore find a least resistance way to escape. As a result, gas can travel to another storage field or could move up to the surface where emits to the atmosphere [69].

In terms of causal based analysis of the methane emissions from storage wells it can be concluded that the methane emissions due to the failure of mechanical seals can be categorized as equipment leaks. Thus, as long as the wellhead is pressurized there is a continuous leakage of methane to the atmosphere therefore, theses emissions are time based (30%). Methane emissions due to the two other sources from storage wells are mainly event- based (70%) since many factors

can cause the fracture in the production casing such as earth movement or some heavy production operations close to the storage site and etc. [69].

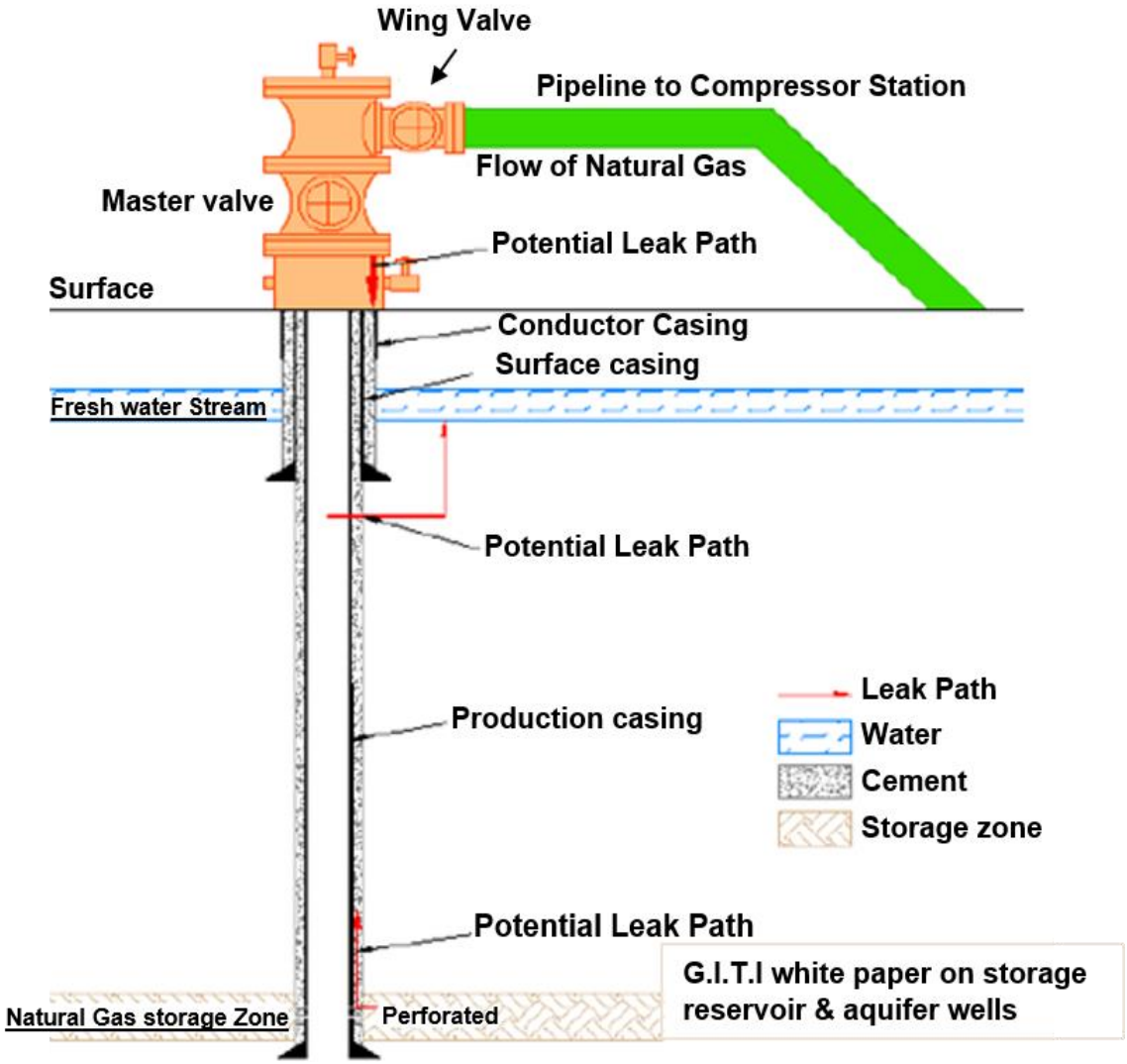

Figure 2.11. Schematic of gas emissions from the storage well (taken from [69]).

- **Storage Tank**

Storage tank in the natural gas industry is used to store water, condensate, all the impurities and slugs forming in the gas pipeline or gas well pad. The natural gas needs to be cleaned before entering to the compressor stations or after extracting from the well. The scrubber separates all the solids and liquids parts from the natural gas stream and sends them to the atmospheric pressure tank by the means of the scrubber dump valve.

High pressure liquids with dissolved natural gases at the exit of the separator enter to the atmospheric pressure tank. The pressure difference between the separator and the atmospheric pressure tank causes vaporization of the dissolved gas and venting to the atmosphere. This type of the emissions from the storage tank is called flash losses. There are two other types of the emissions from the storage tank; working losses and standing losses [70]. Working losses occur when the liquid level in the tank increases because of the continuous flow of liquids from the scrubber to the tank and causes the vapors at the top of the tank vent out to the atmosphere. Standing losses occur because of the surrounding change of the temperature and the pressure in which cause the vaporization of the dissolved gas and venting to the atmosphere through the tank roof [70]. Figure 2.12 exhibits the methane emissions from the storage tank captured by IR camera [71].

Figure 2.12. Methane emissions from the liquid storage tank (taken from [71])

The amount of emissions from the storage tank depends on the pressure difference between the tank and the separator and the liquid flow rate. Depending where or what segment (production, processing, and transmission) the storage tank is located the amount of emissions would be different for the same amount of the throughput. It can be concluded that higher pressure difference between tank and the separator results the higher emissions. But, regardless of the pressure difference for a specific facility with a certain pressure range it is clear that the main cause of the emissions is the throughput (90%). The more throughputs to the facility create more flash and

working losses from the liquid tanks. At the same time depending on the seasonal and daily change of the temperature and the pressure, some portion of the emissions can be considered as event based (10%).

It should be noted that sometimes because of the malfunction of the scrubber dump valve the high-pressure natural gas can leak through the valve and vent to the atmosphere. As a result, the calculated or lab analysis amount of emissions would be less than the actual amount of gas released to the atmosphere [70]. In order to prevent the emissions underestimation from condensate tank, the emissions from malfunctioning separator dump valves are measured as a separate source of emissions under condensate tank vents in EPA/GHGI report [31].

- **Equipment Leaks**

There are several components in a compressor that cause emissions if they are installed improperly or malfunction. These components are involved in the process of the gas at the compressor. Some of these components as listed by Climate & Clean Air Coalition (CCAC) are valves, connectors, flanges, open-ended lines, and scrubber dump valves [72]. The leaks can occur due to improper installation, manufacturing defect, corrosion, excessive temperature, vibration, and other factors resulting in tear and wear. Although each component plays a small role in adding to the total emission of the compressor, they collectively create a significant amount of emission. Some in the literature suggest that emission caused by component leaks are random and only frequent inspection and utilizing early detection equipment can reduce them [72].

The leaks from the equipment in the transmission sector are categorized into two separate areas: compressor related, and non-compressor related. This is due to the fact that leakage properties are categorically different for components in close contact to composers because of vibration [73]. The average CH_4 emission factors measured is in Kg/component (kg CH_4/heater, kg CH_4/separator, etc.) by EPA/GHGI.

All these components have continued leakage over time and therefore a big portion of the emission is considered time-based (90%). Furthermore, gas leakage increases as the gas flowing through them increases, and as a result, another portion of the leakage from the equipment is considered to be throughput based (10%).

- **Dehydrator and Gas-Assisted Glycol Pumps**

The natural gas needs to be pipeline-quality standard ready before delivering for sale. The reason is that the natural gas after production from reservoir contains water which can cause corrosion, hydrates formation and etc. Therefore, to prevent this the water content of the gas is set 7 lb/MMscf and less according to Gas Processors Association. The dehydration unit is used to remove the water from the gas and make it ready for the pipelines. The dehydrators usually use liquid triethylene glycol (TEG) to remove the water from the wet natural gas because of its properties which can absorb the water from the natural gas. Figure 2.13 shows the schematic of the dehydrator unit [74].

The dehydrator unit needs a pump to pressurize the glycol from the regenerator pressure to the contractor pressure. In the contactor two streams (wet natural gas and dry glycol) flow counterclockwise. At one exit dry natural gas and the other one wet glycol (glycol + water absorbed) leave the contractor. Most of the time some gas and other hydrocarbons entrain in the wet glycol and flow toward the pump. After passing a pump the stream flow into the regenerator where water and other hydrocarbons heats up and vent to the atmosphere (the source of methane emission).

There are usually two common types of pumps used in the dehydrator unit to circulate glycol; gas-assisted pumps and electric pumps [74]. Gas- assisted pumps are used in areas with no access to the electricity and by design need extra high pressure wet natural gas in addition to gas entrained in the wet glycol to drive low pressure dry glycol. Thereby, passing three times of wet natural gas compared to an electric pumps toward a regenerator and as a result will be discussed in this chapter [74]. Gas-assisted glycol pumps in which Kimray is a leading manufacturer for that in the natural gas industry are being studied in volume 15 of the multi-series study by EPA/GRI in 1996 [75].

Since EPA/GRI 1996 report use two different approaches to calculate emission and activity factor for dehydrators and gas-assisted glycol pumps, EPA/GHGI reports dehydrators and Kimray pumps as two separate methane emissions sources even though in both dehydrators and gas-assisted pumps methane is vented to the atmosphere through the regenerator venting line [75].

The parameters affecting the amount of emissions from a dehydrator unit were studied using ASPEN/SP model by EPA/GRI 1996 report [76]. It was found that when glycol to gas ratio is held

constant the glycol circulation rate is proportional to the gas flow rate meaning increasing in the gas throughput yield more glycol circulation rate. As a result of that the amount of emissions are linearly proportional to the glycol circulation rate as it is shown in Figure 2.14 which make the dehydrators a throughput-based emission source. The effect of other parameters was also investigated such as methane composition in the wet natural gas flowing through the contactor, the flash tank pressure, gas pressure and temperature and it was found that the methane composition and the flash tank pressure both have a linear correlation with the methane emissions rate [76].

It should be noted that the effect of gas-assisted pumps is neglected in the modeling. Although the emission factor calculation methodology is different between the dehydrators and gas-assisted pumps but a dehydration unit with a gas-assisted pump vent methane and other hydrocarbons from the same venting line and there is no methane emission point from the pump itself. Hence, the gas-assisted glycol circulation pumps are also mainly throughput based (100%) meaning the cause of the methane emissions is the throughput not the event or time-based causal factors.

That being said, there are many wells in the natural gas production segment that their glycol circulation rate is higher than it should be [77]. The reason for that is, for these units the glycol circulation rate is designed for the highest gas production rate from the well but the well gas production rate decline as they age. As a result, these dehydration units have to circulate more glycol than necessary and emit more methane to the atmosphere. Therefore, it can be concluded that for some of dehydration units installed in the gas well to remove water from the produced wet natural gas, regardless of throughput the amount of emissions is constant because their circulation rate is fixed for the maximum gas flow rate from the well [77].

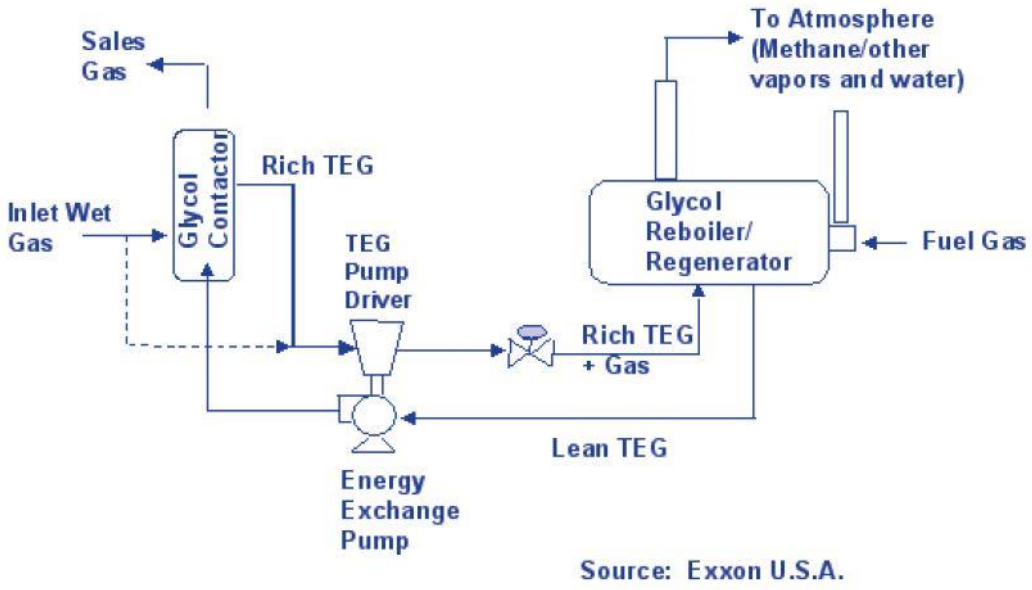

Figure 2.13. Dehydrator unit (taken from [74])

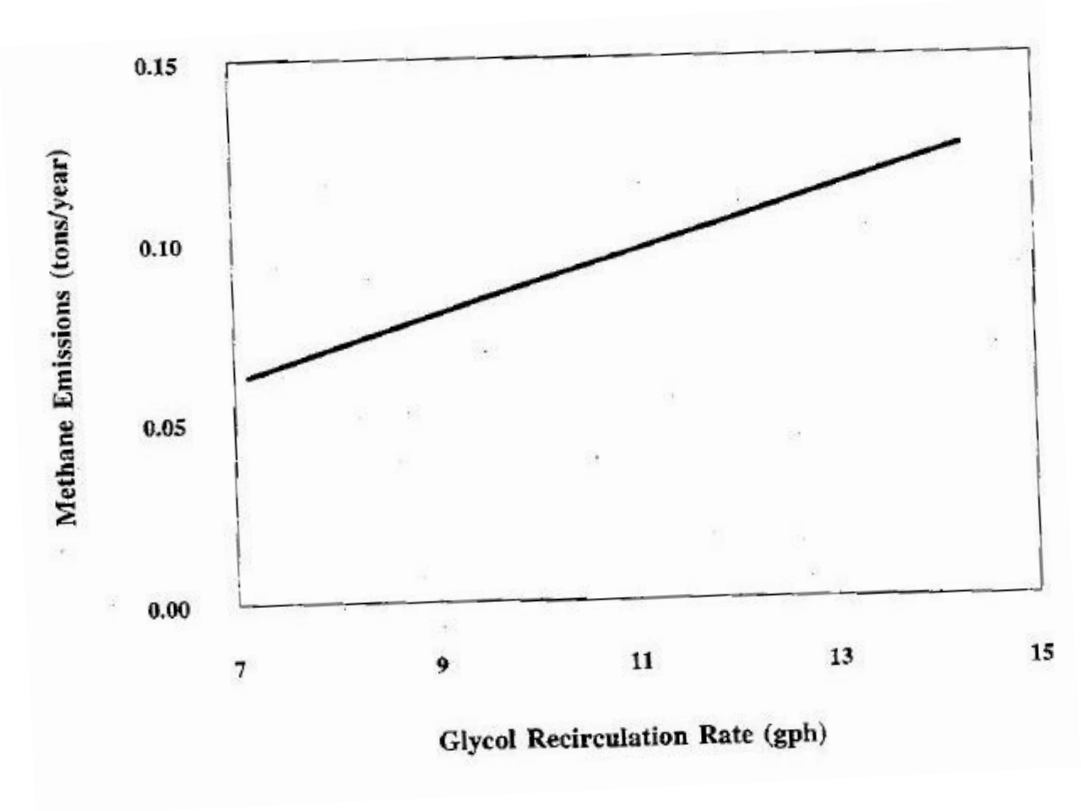

Figure 2.14. The effect of glycol recirculation rate on methane emissions rate (taken from [76])

- **Chemical Injection Pumps**

Chemical injection pumps are small pumps commonly in production segment of the natural gas system used to inject small amount of chemicals usually biocides, demulsifies, etc. into gas wells and pipeline to prevent corrosion and protect equipment [78]. In this chapter, only the natural gas-powered pumps are investigated in terms of causal based methane emissions factors (beside gas-driven pumps there are electric pumps, solar powered pumps, and air-driven pumps). Gas-driven pumps use the pressure of the natural gas to drive the small amount of the chemical from low pressure to the high pressure point in areas where electricity is not available easily [78].

There are two types of the gas-driven pumps in the natural gas industry; piston pumps, and diaphragm pumps as it is shown in Figure 2.15 and Figure 2.16. EPA/GRI study [78] uses two different equations to calculate Emission factors for piston and diaphragm pumps as shown in equation (2) and (3).

$$EF_{diaphragm\ pump} = Gas\ Usage\ (^{scf}/_{stroke}) \times Frequency\ (^{stroke}/_{day}) \times Opertion\ time\ \times \%\ Methane \quad (2)$$

$$EF_{piston\ pump} = Gas\ Usage\ \left(^{acf}/_{stroke}\right) \times Density\ \left(^{scf}/_{acf}\right) Frequency\ \left(^{stroke}/_{day}\right) \times Opertion\ time \times \%\ Methan \quad (3)$$

For these pumps, the natural gas usage ($^{scf}/_{gal}$), the stroke length, and the plunger/piston diameter are provided by the manufacturers. EPA/GRI developed an equation to calculate the gas usage ($^{scf}/_{stroke}$) using manufacturer data. From the manufacturer model for a given diameter and the stroke length, the natural gas usage ($^{scf}/_{gal}$) has a certain range.

To assess the cause of emissions from these pumps based on above information, it is clear that the reason methane is vented to the atmosphere from a pump is related to the pump frequency rate

(actuation rate). The more chemical is injected the greater the actuation rate. Thus, higher throughput to either the well or the pipeline always causes more pump actuation. It is obvious that as the pump size gets bigger the amount of gas emissions also gets bigger but the cause of the emissions from a pump is completely throughput based.

The difference between the diaphragm and the piston pumps emission factor is that for the piston pumps, the supply gas pressure can affect the gas usage. However, the cause of emissions from piston pumps is still throughput of natural gas being processed by pumps. In other words, for a given piston pumps operating in the high-pressure region, the only thing that can change the emissions rate would be the throughput change but comparing this pump to the same pump operating in the low-pressure region, high pressure pumps consumes more amount of gas.

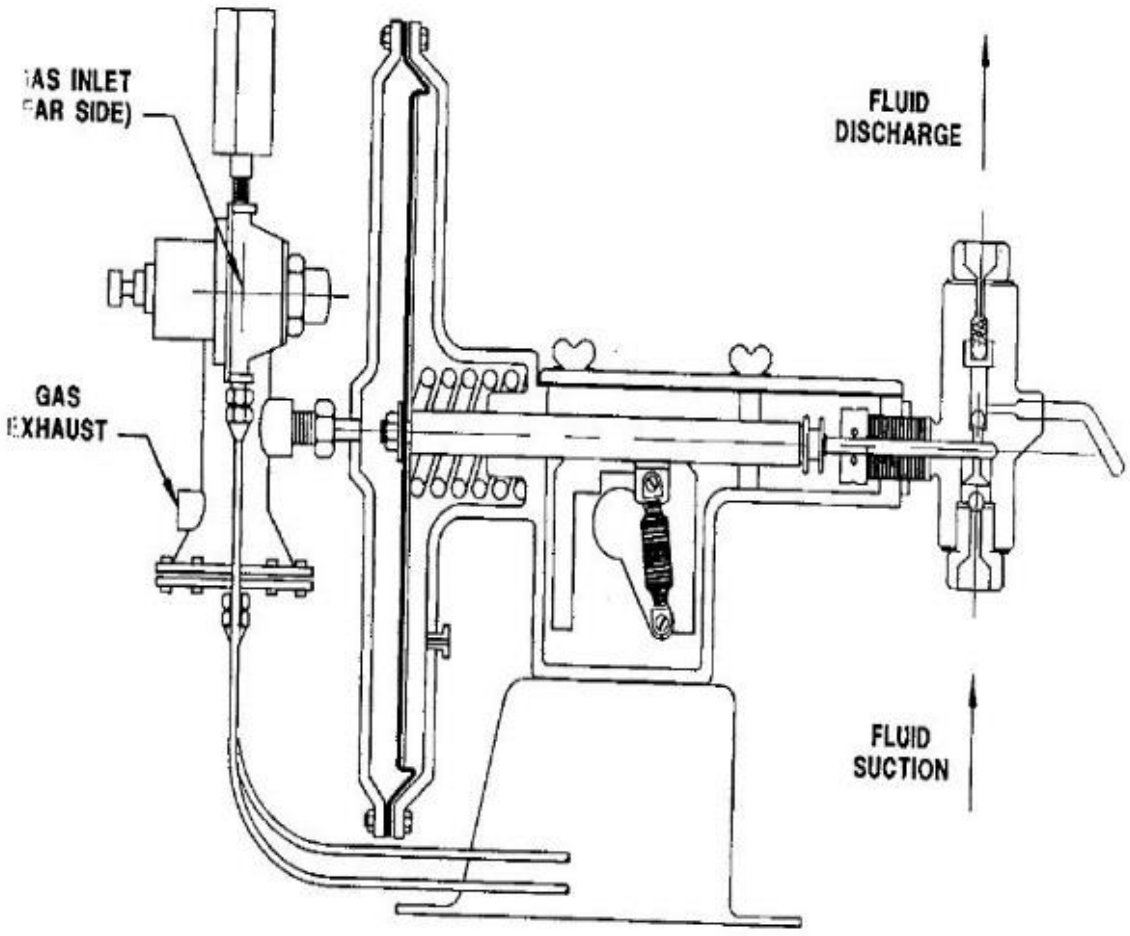

Figure 2.15. Cut-away Schematic of Diaphragm Pumps (taken from [79])

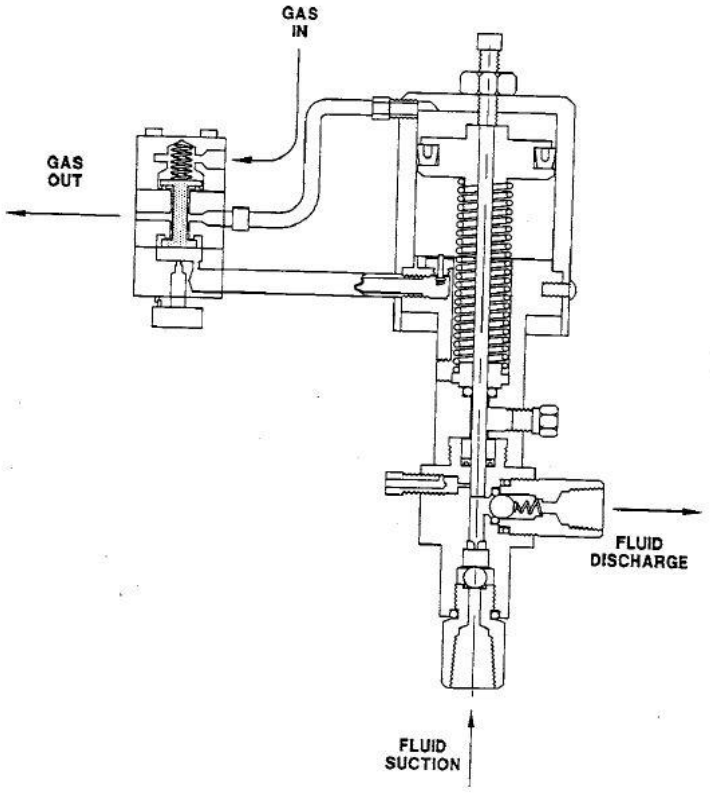

Figure 2.16. Cut-away Schematic of Piston Pumps (taken from [79])

It's worth mentioning that based on a study done by natural gas STAR partner companies replacing natural-gas powered chemical injection pumps with compressed air, electric pumps (solar-charged direct current and standard alternating current) have relatively quick payback (instrument air pumps) and can be more reliable (electric driven pumps) and also more precise (solar-charged pumps) [79].

The final estimated coefficients for the investigated sources are presented in Table 2.1. The data in Table 2.1 shows that some methane emission sources may emit the same amount of gas regardless of their throughput and others show only partial dependence upon throughput. These coefficients (*a*, *b*, *c*) are then used in the next chapter to build a model using the marginal emission methodology to estimate the change in methane emissions of natural gas systems as system throughput changes. The partial dependency or complete independency of these sources to throughput indicates that system emissions do not proportionally change with the change in throughput. As outlined in Table 2.1, emission sources have dependency upon more than one casual based factor, and can have dependency to throughput, time, and/or events at the same time.

Table 2.1. Marginal Assessment Coefficient

	Time Based (*a*)	**Event Based (*b*)**	**Throughput Based (*c*)**
Liquid Unloading	0%	80%	20%
Continuous Pneumatic	100%	0%	0%
Intermittent Pneumatic	0%	80%	20%
Dehydrator vents	0%	0%	100%
Blowdown vents	0%	80%	20%
Reciprocating compressors rod packing	90%	0%	10%
Centrifugal Compressors (Wet Seal)	20%	0%	80%
Centrifugal Compressors (Dry Seal)	90%	0%	10%
Storage tank	0%	10%	90%
Storage wellhead	30%	70%	0%
Gas engine	20%	0%	80%
Equipment leaks	90%	0%	10%

2.5 Summary

In this chapter, the marginal emission coefficients are determined through a comprehensive study of the literature and an engineering assessment of the mechanisms for the tripartite distribution (event based, time based, throughput based). Results from this work suggest that major emission sources within the natural gas system do not show emissions change one-for-one with changes in throughput. For some components, increasing or decreasing throughput will not change the emissions at all. The results of this chapter will be used in the next chapter to calculate the change in emissions of the natural gas system as throughput changes.

3 Marginal Methodology to Estimate Methane Emissions

3.1 Abstract

A new cause-based approach was used to estimate the change in methane emissions from the natural gas system resulting from a change in throughput. The analysis shows that a cause-based, marginal approach to estimating marginal change in methane emission results in more accurate estimates compared with the traditional average method from natural gas system. The goal of this chapter is to determine the relationship between methane emissions and changes in throughput both over short time horizons where the gas infrastructure is fixed and over time periods where system expansion (or retirement) and technological improvements via component replacement occur. The results show that methane emissions change with throughput but the relative change in emissions is less than the relative change in throughput. The amount of methane emissions from several components in the natural gas system are not dependent on their throughput (or are only partially dependent). As a result, reducing natural gas consumption in the future will not yield a directly proportional reduction in the methane emissions. It is believed that the results of this study will help energy policymakers to understand better the effect of policies aimed at reducing natural gas use on greenhouse gas (GHG) emissions and where such policies should be applied (e.g. system operator or end user).

3.2 Literature Review

As stated in in the previous chapter, the simple pro rata approach used in GREET models inaccurately overestimates/underestimates the effect of increased/decreased natural gas consumption by including the fixed and non-incremental portion of the emissions in the calculations. This potential misestimation of emissions can lead to policy making decisions that might not result in the most optimized GHG footprint.

Public policy could have a major impact on the direction of technological integration (e.g., increasing renewable generation, transitioning to lower carbon fuels, or implementing carbon credits). More accurate information on estimating emissions changes with throughput is crucial to accurately assessing tradeoffs and priorities in setting energy policies. The marginal methodology for estimating methane emissions changes is especially important as natural gas throughput will be flat or declining in most policy scenarios in some states, e.g., in California due to renewable energy outgrowing other sources of energy. Therefore, it is essential to accurately estimate the marginal reduction in GHG produced from natural gas infrastructure as fixed sources of emissions will continue producing the same level of emissions irrespective of the level of natural gas consumption.

Mac Kinnon et al. [30] point out that relying upon employing average emissions as opposed to marginal emissions in assessing the effect of changes in natural gas consumption is analogous to estimating the emissions impact of using electricity as a vehicle fuel. Foley [80] investigated the impact of the incremental increase in electricity demand to fuel electric cars using PLEXOS (a power system modeling). Foley concluded that charging mostly done in off peak hours at night, does not proportionally require an increase in electrical generators. [81] argues that an average method to estimate emissions change with the change of electricity demand is not accurate since all the system components do not respond proportionally to the change of demand. Therefore, a marginal approach is the correct way to estimate the increase in electric generators needed to meet this increase in demand. A number of previous works also have studied the impact of the location and time of use on the marginal GHG emissions estimation in the electricity sector [82], [83]. [84] quantifies the difference between average and marginal emission factors in transportation system operations and shows that marginal emission factors are lower than average emission factors. A similar approach is needed to study the impact of changes in emissions as demand for natural gas changes. An experimental example of a residential meter set assembly (MSA) presented in [30], shows that the MSA's primary emission source is the continuous leak, a function of primarily pressure, at the threaded connections [85]. In the mentioned study, throughput is increased for three MSA and a reduction in emissions is observed. As concluded in [30], all of the components used in the natural gas system can be categorized into three types: time-based, random-event-based

and throughput-based emissions sources to marginally assess the change of methane emissions with changes of natural gas throughput.

The marginal method for estimating emissions focuses upon the change of methane emissions as natural gas consumption, or throughput, changes. The present analysis addresses the change in emissions as throughput varies on the natural gas system both with and without changes to the system facilities. This can be understood as a marginal analysis approach addressing different time frames. For natural gas consumption, the incremental GHG emission for each unit of consumption is the short-term marginal emissions at the time the gas is consumed. For practical purposes such as GHG regulations, temporal and spatial averaging is needed but incorporating a marginal approach will lead to more accurate reflection of the changes in emissions resulting from changes in consumption of natural gas for various uses.

Previously, the impact of natural gas system expansion on methane emission was studied in [86] and summarized in [87]. [86] which is an engineering estimation of methane emissions changes with system expansion to meet increasing throughput, concluded that the natural gas system emissions increase with the increase of the throughput but the percent increase in emissions would be smaller than the percent increase in the system throughput. That analysis is a medium-term marginal approach (the timescale considers system expansion) whereas the current work also incorporates a marginal approach to assessing how emissions from an existing component or facility change as throughput changes. This addition is important in considering scenarios where the existing gas system has significant capacity for increased throughput or where efficiency and fuel switching offset increased use in other applications.

Only a few studies have been published that relate emissions changes to the throughput. In some recent experimental work detailed below, the relationship between site-level methane emissions and the natural gas production has been quantified to better understand the relationship between natural gas production and the resulting methane emissions. It was shown that measured site-level methane emissions decrease as throughput increases meaning that there is a negative correlation between throughput and the emissions. These results confirm that some components in the natural gas systems have leak rates that are not 100% throughput based, and as a result, emissions will not change in proportion to changes in throughput.

Site-level methane emissions measurement data from more than 1000 NG production sites in eight different basins were used by Omara et al. [88] to better understand the relationship between site-level methane emissions and NG production as well as developing a new national methane emission estimate from NG production sites. The measured data sets were obtained from onsite and downwind ground-based site level techniques to quantify methane emissions rate from routine operations components and intentional venting sources (malfunctioning equipment) and were taken to exclude emissions from completion flowback and liquid unloading.

Omara et al. [88] state that the results from different studies suggest that the site- and basin-level methane emissions have a great deal of variation and may be the result of the many factors affecting the emissions such as NG production rate, well formation, age, etc. To do the statistical analysis some sites were removed and a total of 1009 measurement data sets were investigated. The data were grouped into 10 bins based upon their production rate. It was found that sites with higher production rates have higher emissions rates. In fact, 50% of the emissions come from the top 5% of the sites as is illustrated in Figure 3.1(a). Although, the correlation between the normalized emissions (emission over production) and NG production is negative, which suggests that low production sites have higher normalized emissions or lose more of their NG production in other words, it reflects (again) that a significant portion of emissions are independent of throughput. Figure 3.1(b) shows production-normalized methane emissions and NG production. Omara et al. reported that sites with high emissions rate and high NG production rate are younger sites, which most likely are equipped with advanced components and will be inspected more often than older sites. Overall, based on Figure 3.1, Omara et al., concluded that "On average, low NG producing sites emit a larger fraction of their CH_4 production than high NG producing sites and up to 74% of the variability is explained by variability in NG production rates" [88]. Note that the "fit all data" light blue curve from Figure 3.1(a) shows that for five orders of magnitude increase in throughput there is only one order of magnitude increase in emissions suggesting a 20% throughput dependence.

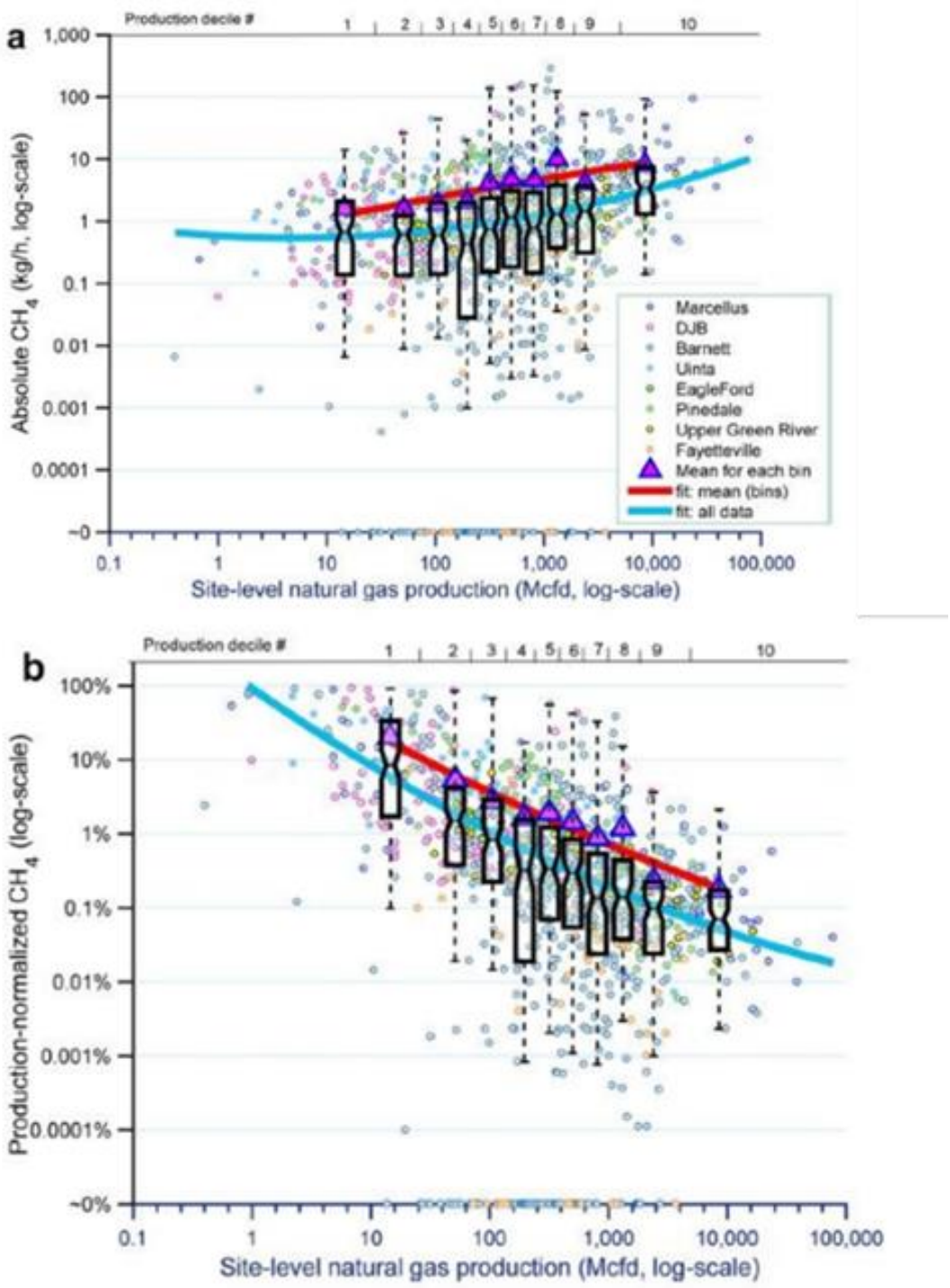

Figure 3.1. (a) Site-level methane emissions rate vs NG production (b) site-level production-normalized methane emissions vs NG production (adapted from [88]) (measurement data are from eight basins: Marcellus, Denver-Julesburg (DJB), Barnett, Uinta, EagleFord, Uinta, EagleFord, Pinedale, Upper Green River, Fayetteville. Production decile # shows ten different bins number. These bins were categorized based on NG production rate)

Brantley et al. [89] explain that the reason for a weak correlation is indication of the effect of intentional venting or operator errors, which can considerably enhance the emissions rate from the site in comparison with routine operation. The production-normalized emissions versus gas production with the negative correlation was observed, which shows low producing sites emit the highest fractions of their production. The single regression correlation between site age and emissions was strong with the R^2=0.2 as opposed to multivariate regression with no correlation. [89] compared their results with two other onsite measurement studies by Allen et al. and the Eastern Research Group (ERG), respectively [58] and [90]. Contrary to the data shown in [89], condensate tank emissions are not included in ERG's data set due to the absence of condensate production. The measurement data provided by Allen et al. [58] provides emissions from some of the condensate tanks.

Emissions from 114 gathering and 16 processing sites were measured in [91]. Facilities were categorized into five types: I) Compression (C); II) Compression and Dehydration (C/D); III) Compression, Dehydration, and Treatment (C/D/T); and IV) Dehydration (D); and Dehydration and Treatment (D/T). Weighted Average Facility Level Emission Rate (WAFLER) versus reported natural gas throughput were plotted. It was shown that sites with higher throughput have higher emissions rates (R-squared=0.38). As opposed, throughput normalized weighted average facility level emission rate (tnWAFLER) has a negative correlation with the reported natural gas throughput. The reason high throughput sites have lower tnWAFLER is indication of throughput independency of some emissions sources as stated by [91].

In this chapter, the goal is to build a model using EPA/GHGI 2018 data provided in [31] to determine the impact of changes in natural gas throughput upon total methane emissions. In particular, of 129 sources of emissions identified by EPA/GHGI 2018, we focus upon the 47 most important sources that have a major impact on total methane emissions and study event-based, time-based, and throughput-based dependency of the emission sources as introduced in [30].

3.3 Methodology

To calculate emissions changes related to changes in throughput, the dependency of emission factor and activity factor to throughput was analyzed. The chapter studies two scenarios to estimate methane emissions change with the change in throughput:

- Scenario I: the effect of technological improvement was neglected meaning an analysis for a fixed date (instant in time). In this scenario, the timescale does not consider system expansion/reduction.
- Scenario II: technological improvement was applied for a future instant in time.

For scenario I, it was assumed that the system has enough capacity to accommodate extra throughput and therefore, activity factor remains constant and only the emission factor coefficient impacts marginal emissions rate. For scenario II, the natural gas system requires expansion to accommodate additional throughput and as a result, the activity factor coefficient changes as well. The data that show how much the natural gas system capacity changes with the change of throughput was taken from the Columbia gas report [86]. The report outlines the system emissions estimation for the expansions of 5%, 15%, and 30% based on facilities and equipment reflective of the time of the study in 1992. As was mentioned in [86], each sector has a different capacity to accommodate gas and by increasing throughput each sector needs to expand their number of components or length, or volume, etc. Three different load profiles (Uniform, Winter, and Summer) were studied in [86] to estimate the system expansions and emissions. [86] provides an engineering estimation of system expansion for the following components: wellhead, pipeline, gas cleaning, compression, and metering components in the production sector; net plant in the processing sector; pipeline, compression, and metering in the transmission sector; and city gate meters, district regulation, main pipeline, service lines, and customer metering in the distribution sector.

The data provided in [86] only focused on emissions estimation for increased throughput. The effect of reduction in emissions as throughput decreases is assessed with the assumption that most components are not retired and remain in the system for a significant amount of time. For example, less throughput results in some closure of exploration and low producing wells but it does not usually lead to significant compressor station changes.

In effect, the difference between Scenario I and Scenario II reflects the likely step change in components and technology and their associated emissions that can occur over time (e.g., like the differences between and transition from conventional gas extraction to shale gas extraction by hydraulic fracturing).

Equation (4) shows how the devised marginal approach calculates total emissions for scenario I, where *c* is the marginal emissions coefficient of throughput from Table 2.1.

$$E = EF_{2016} \times AF_{2016}\,(1 + c \times \%\ of\ throughput\ change) \tag{4}$$

The equations (5) and (6) are developed to marginally determine the emissions of assessed sources when throughput increases and decreases, respectively for scenario II). Where *c* is the marginal emissions coefficient of throughput, α is the system expansion coefficient from [86] and β is the system reduction coefficient that was determined and only applied on some components in the exploration and production sector. It is worth mentioning that the interdependency between time, event, and throughput is very complex, and needs extensive experimentation, and is outside the scope of the current work conducted in this research. Thus, for the purposes of this study the time and event coefficients (*a* and *b*) are assumed to not depend upon throughput resulting in equations (5) and (6) that assess throughput dependency.

$$E_{Increase} = EF_{2016} \times AF_{2016}\,(1 + c \times \%\ of\ throughput\ increase + \alpha \times \%\ of\ component\ expansion) \tag{5}$$

$$E_{Decrease} = EF_{2016} \times AF_{2016}\,(1 + c \times \%\ of\ throughput\ decrease + \beta \times \%\ of\ component\ reduction) \tag{6}$$

It is expected that this approach provides a more accurate method compared to the GREET constant-emission-factor method to calculate the change in emission of the system as throughput changes.

3.4 Results and Discussion

Ten individual major methane emissions sources from upstream of the natural gas system were evaluated in the previous chapter and their marginal emissions coefficients (*a, b, c*) were estimated. The coefficients for the ten sources studied are presented in Table 2.1. In this chapter, a cause-based marginal method for estimating the change in emissions from various elements of the natural gas system as a function of throughput is employed, (see [30]), using 2018 EPA/GHGI report data [31].

The data can be categorized into 2 types: I) marginal- emission-based sources; II) average-emission-based sources. After carefully analyzing the 129 emissions sources identified by EPA/GHGI, marginal analysis was applied to all those with material impact on the total emissions and for which adequate component level data exist. This constituted 47 out of the 129 sources, contributing to 50.7% of total emissions. The remainder of the 82 emissions sources where marginal analysis was not applied to are divided into two categories.

The first category consists of emissions sources that are station based. The marginal analysis presented in this paper uses a bottom up component level approach to estimate the change in methane emissions with throughput. Since component level data does not exist for this category, marginal method cannot be used to assess the change in methane emissions. This category contains 11 sources, contributing to 35.2% of total methane emissions of which 30.1% is related to only two emissions sources from gathering and boosting stations in the production sector (27.4% from fugitive emissions and 2.7% from episodic events). Considering the importance of emissions from gathering and boosting stations, future research and measurement campaigns are needed to better evaluate methane emissions from this sector of the natural gas system.

The second category of emissions sources are related to operations such as different types of well drilling or emissions sources where component level data to correlate methane emissions to throughput does not exist (e.g. emissions from shallow and deep-water gas platforms or emissions from LNG stations). These sources combined contribute to 14.1% of methane emissions, most of which contribute to less than 1% of the total methane emissions.

For sources that were not assessed relative to marginal emissions (82 out of 129), the traditional method was used to calculate emissions (Emission=AF*EF). Activity factor was predicted using linear regression with the throughput from 1990 to 2016 and the emission factors were assumed to be constant and based upon the year 2016. 36 out of 82 sources have a strong correlation between activity factor and throughput from 1990 to 2016, 6 out of 82 have a strong correlation between activity factor and the throughput from 2010 to 2016, and 40 out of 82 of the emissions sources are considered as a constant emissions sources. The criteria used to predict activity factor were r-squared above 50% and P-value below 0.05. For those sources with r-squared below 50% and P-value above 0.05 the regression on the activity factor was applied from 2010 to 2016. The remaining sources with no significant activity factor correlation with throughput were assumed to

have constant emissions with any change in throughput. It was noticed that the activity factor stayed almost constant from 2010 to 2016 for the constant emissions category.

Table 3.1 outlines all marginally assessed components and their contribution to the total and sector emissions. Note that each component in this table can represent several of the 129 emissions sources shown in Figure 2.4.

In the production sector, out of 63.67% of the total emissions as previously shown in Figure 2.3, 27.36% is attributed to gathering and boosting and is not marginally assessed as discussed before. From the remaining 36.31%, 29.61% is marginally assessed. Among the marginally assessed sources of emissions from the production sector, Pneumatic devices-intermittent bleed is the highest single emission source at 12.83%. The second highest emissions source belongs to the equipment leaks (6.06%) and the gas engines have the third highest emission sources (3.44%).

In the processing sector, out of 6.27% of the total emissions shown in Figure 2.3, 5.42% were marginally assessed. The gas engines have the highest emissions in the processing sector (3.39%).

In the transmission and storage (T&S) sector, out of 22.92% of the total emissions shown in Figure 2.3, 15.65% were marginally assessed, where reciprocating compressors are the main contributors (6.27%).

Table 3.1. Marginally assessed components and their contributions to emissions

Production Sector			
Marginally Assessed Components	# of Emissions Sources in EPA/GHGI	Emission Contribution to the total emissions (%)	Emission Contribution to the sector (%)
Pneumatic Devices (Intermittent Bleed)	1	12.83	20.14
Other-Equipment Leak	6	6.06	9.52
Gas Engines	1	3.44	5.40
Other-Chemical Injection Pumps	2	2.61	4.09
Other-Pneumatic Devices (High/Low Bleed)	2	1.91	3.01
Other-Liquid Unloading w/wo Plunger Lifts	2	1.86	2.92
Other-Tanks w/o control	3	0.40	0.62
Other-Dehydrator Vents	1	0.32	0.51
Other-Blowdowns/Venting	6	0.19	0.30
Production Total	24	29.61	46.51
Processing Sector			
Gas Engines	1	3.39	54.13
Other-Reciprocating Compressors	1	0.88	14.03
Other-Blowdowns/Venting	1	0.51	8.13
Other-Centrifugal Compressors (wet seals)	1	0.29	4.55
Other-Dehydrators	1	0.21	3.40
Other-Centrifugal Compressors (dry seals)	1	0.14	2.26
Processing Total	6	5.42	86.50
Transmission & Storage Sector (T&S)			
Reciprocating Compressor -T&S	2	6.27	27.35
Engines -T&S	2	3.84	16.77
Pipeline venting - T&S	1	2.56	11.18
Other-Centrifugal Compressor (dry seals)	1	0.86	3.77
Other-Centrifugal Compressor (wet seals)	1	0.77	3.34
Other-Wells (Storage)	1	0.49	2.12
Other-Pneumatic Devices (High/Low)- T&S	4	0.43	1.89
Other-Pneumatic Devices (Intermittent)-T&S	2	0.29	1.26
Other-Dehydrator Vents -T&S	2	0.09	0.39
Other-Pipeline Leaks - T&S	1	0.05	0.20
T&S Total	17	15.65	68.26
Total	47	50.68	-

For Scenario I, the methane emissions change for the average, lower, and upper estimate is presented in Figure 3.2. As the throughput increases the methane emissions increase but the increase of emissions is less than the increase in throughput which reflects the phenomenon that some sources in the natural gas system are only partially dependent upon or even independent of throughput. Figure 3.2 presents the throughput dependence of both the 47 components that are marginally assessed in our model (dashed lines) and those of all 129 components that include the remainder that are assumed to be 100% throughput based (solid lines). For a 50% decrease in throughput total emissions change 33.79% and 9.23% for all 129 components and only marginally assessed components, respectively. This explains that almost one third of the total emissions are affected by marginally assessed components. It should be noted that there are still some additional components that can be marginally assessed that have not yet been included in this study.

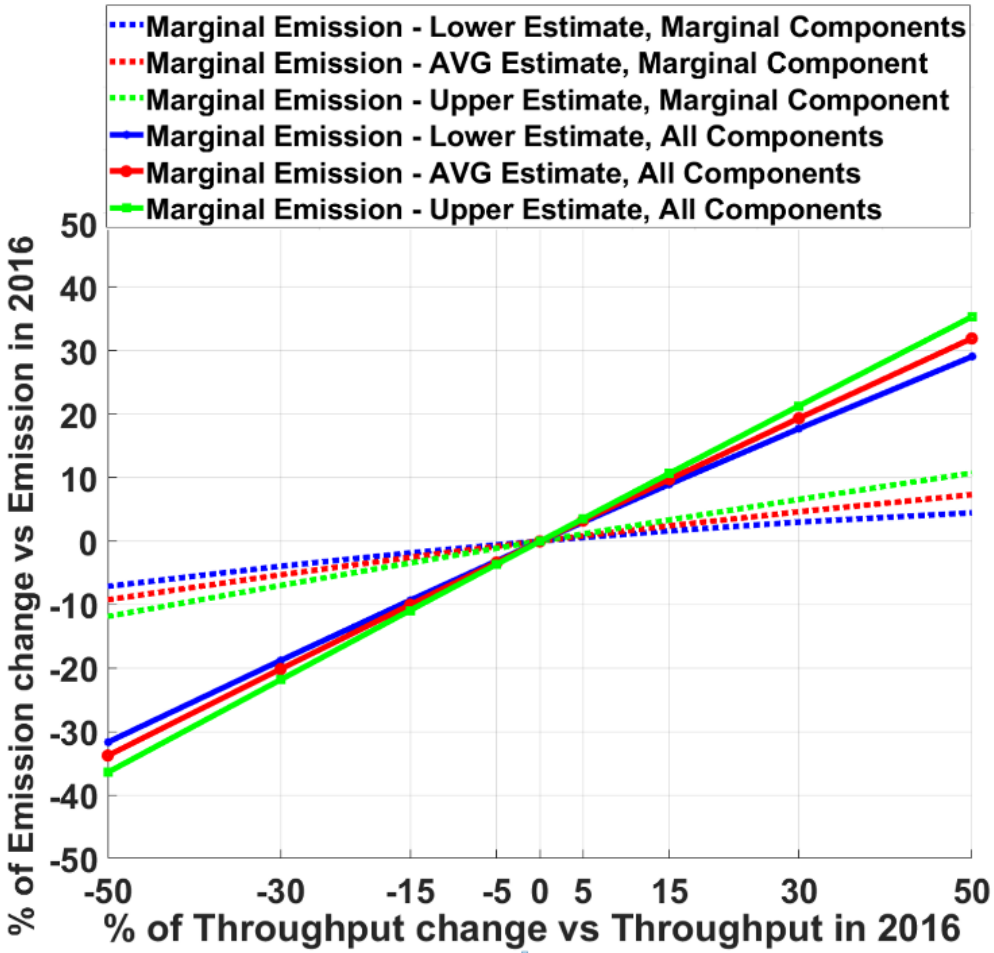

Figure 3.2. Percent of emissions change against the percent of throughput change vs emissions for the 2016 base year (solid lines are considering all 129 components and dashed lines are only marginally assessed components)

The distribution of each sector to the total emissions from the natural gas system as a percentage of total emissions versus throughput percentage change, and emissions against throughput are presented in Figure 3.3 and Figure 3.4 respectively. The increasing share of total emissions attributable to production as throughput increases is a result of the fact that the production sector has the highest dependency upon throughput. As discussed in the previous chapter, key production sector components such as dehydrators, chemical injection and glycol pumps, and storage tanks have a high degree of dependency on throughput. Another reason is the effect of the gathering and boosting stations which are included in the production sector and were assumed to produce emissions in direct proportion to throughput, although these system elements were not analyzed with respect to marginal emissions (due to the fact that gathering and boosting station data is facility based not component based as explained earlier).

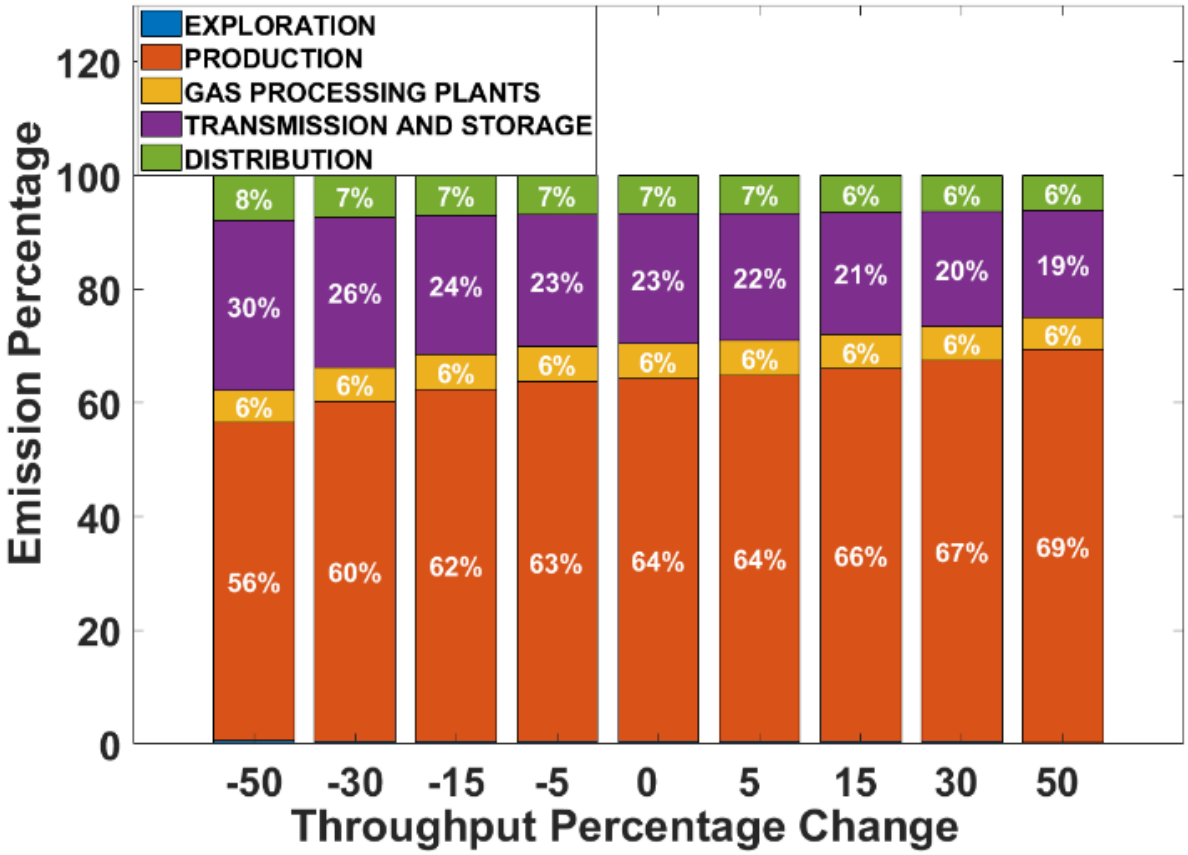

Figure 3.3. The distribution of emissions percentage from each sector of the natural gas system vs. throughput percentage change compared to the 2016 base year

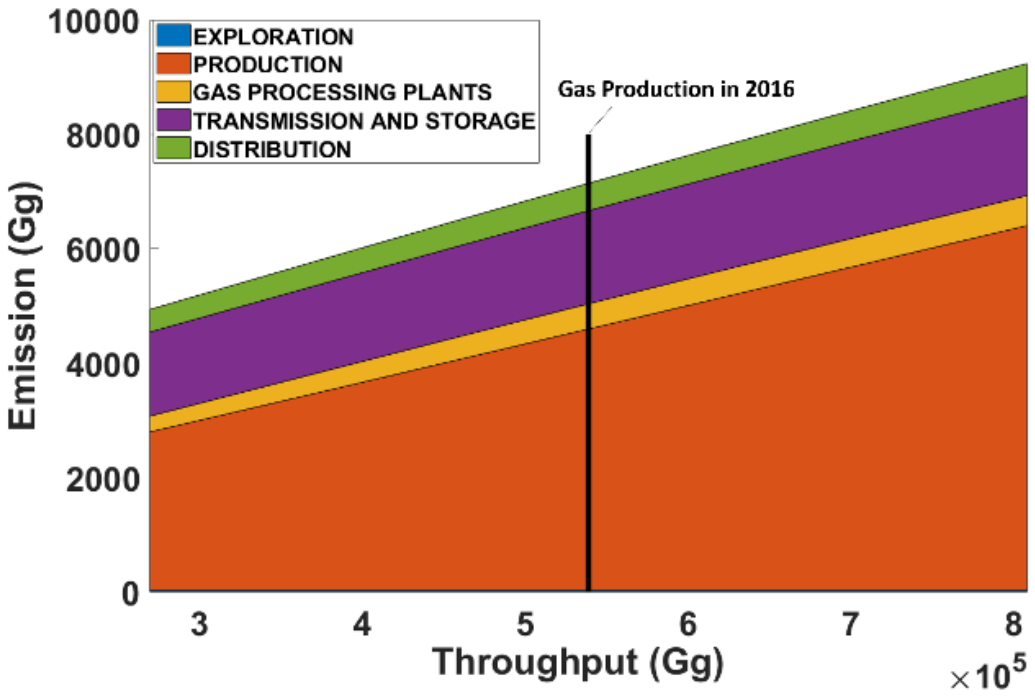

Figure 3.4. The distribution of emissions from each sector of the natural gas system vs. throughput compared to the 2016 base year

For scenario II, sources that were considered to be replaced with the low or no emission sources per natural gas STAR program‘s recommendations are listed in Table 3.2, [92]. 25% of high bleed pneumatic controllers will be replaced by low bleed controllers, 25% wet seal centrifugal compressors will be replaced with the dry seal compressors, 50% of the liquid unloading wells without a plunger will be replaced with those with a plunger, 25% of the natural gas-driven chemical injection pumps and glycol pumps will be replaced with the air-driven pumps, and that 25% of the compressor gas engines will be replaced with an electric motor. Note that most of the STAR program actions are taken on a time-based replacement schedule in addition to application to new facilities.

As noted above, although the overall marginal emissions framework allows for system expansion or retirement, the analysis in this section addresses changes in emissions for a given set of gas infrastructure reflecting a short time horizon.

Table 3.2. Recommended technologies to reduce methane emissions by EPA/STAR [92]

Recommended technologies to reduce methane emissions	Sector Applied
Replacing Wet Seals with Dry Seals in Centrifugal Compressors	Production, Gathering and Processing, Transmission.
Convert Natural Gas-Driven Chemical Pumps	Production, Gathering and Processing, Transmission.
Convert Pneumatics to Mechanical Controls	Production, Gathering and Processing, Transmission.
Replacing Gas-Assisted Glycol Pumps with Electric Pumps	Production, Gathering and Processing.
Install Electric Compressors	Production, Gathering and Processing, Transmission
Installing Plunger Lift Systems in Gas Wells	Production

The comparison of emissions versus throughput between the two scenarios is shown in Figure 3.5. Figure 3.5 presents historical data of total gas system emissions as a function of throughput compared to the instantaneous marginal emissions estimates of the current model for Scenario I and Scenario II. Please note that while the historical data can be correlated to throughput, the changes in emissions result from technology evolution over time in addition to throughput. The current marginal emissions model does not account for technology evolution over time, but rather, estimates marginal emissions changes that occur at an instant in time with changes in gas throughput. The fact that the magnitude and slope of emissions in a small period of time (see several blue x data points in Figure 3.5) in which technology improvements may not significantly contribute to changes in emissions (like an instant in time) well match the marginal emissions model is encouraging.

The two cases reflect short-run marginal emissions at different points in time. The red line of Figure 3.5 is for the year 2016 while the green line represents a future year in which a certain number of technology improvements have been made. The period of time between 1990 – 2009 (historical data shown as gray dots in Figure 3.5) was a period of significant changes applied to the natural gas system according to technology improvements recommended by the STAR Program (see Table 3.2) [92]. Other technology improvements in this same period have been associated with hydraulic fracturing and horizontal drilling practices, for example, that led to significantly increased production per well and lower marginal emissions in this same timeframe.

The historical data from the period of 2009 – 2016 (shown in blue crosses in Figure 3.5) is a period in which emissions begin to increase with throughput due to a combination of lesser technology improvements (the low hanging fruit technology improvements were primarily accomplished in the previous period) and the marginal dependence of emissions upon throughput. With this understanding, our marginal emissions model appears to be very reasonably showing a dependence that is consistent with the historical data. Note that the slope of emissions dependence upon throughput of the historical data is much lower than the marginal emissions slope that our model predicts because the data are influenced by both technology improvement and marginal emissions dependence of the system.

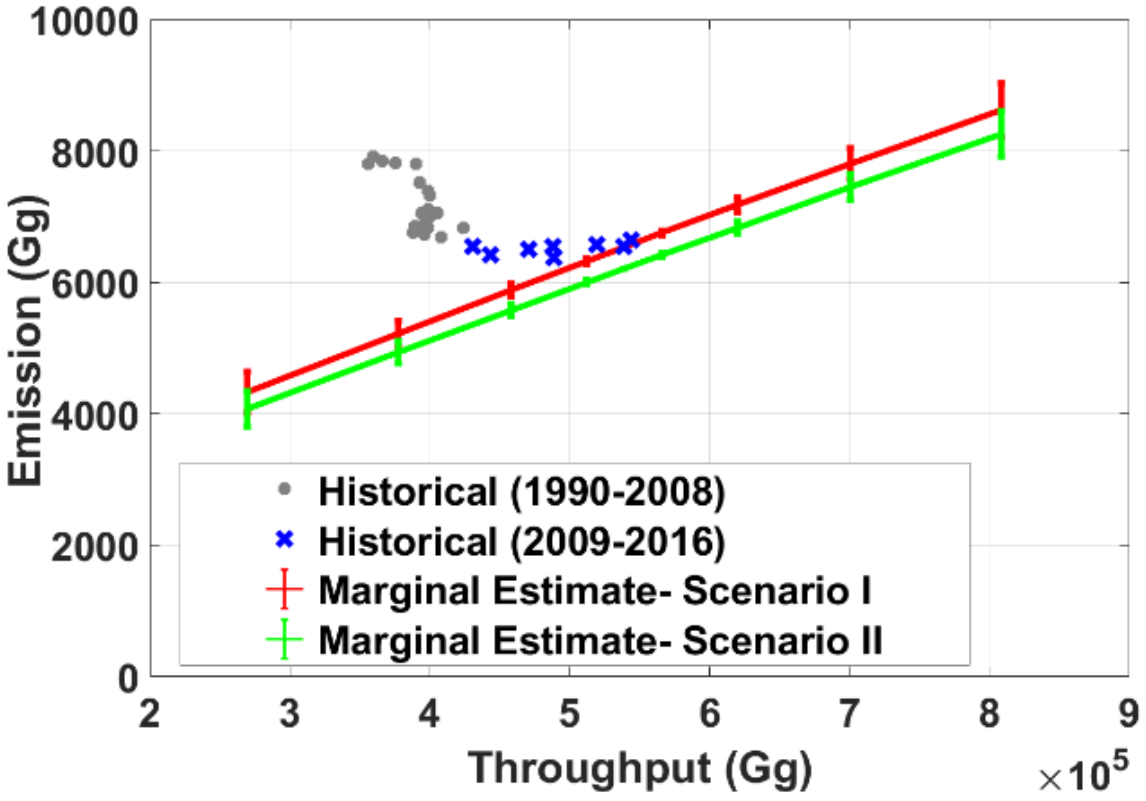

Figure 3.5. Emissions estimate vs. throughput

For Scenario II where the effect of the technology is applied, the emissions show greater dependence upon throughput compared to Scenario I (without technology improvement). The total emissions reductions that are reported in 2018 EPA/GHGI as part of the gas STAR program and the regulatory reductions was assumed to be the same as the 2016 base year. Normalized emissions versus throughput for the two scenarios are shown in Figure 3.6. As can be seen, normalized emissions decrease as throughput increases and increase as throughput decreases for both scenarios. This is a result of sources that are either fully or partially independent upon throughput.

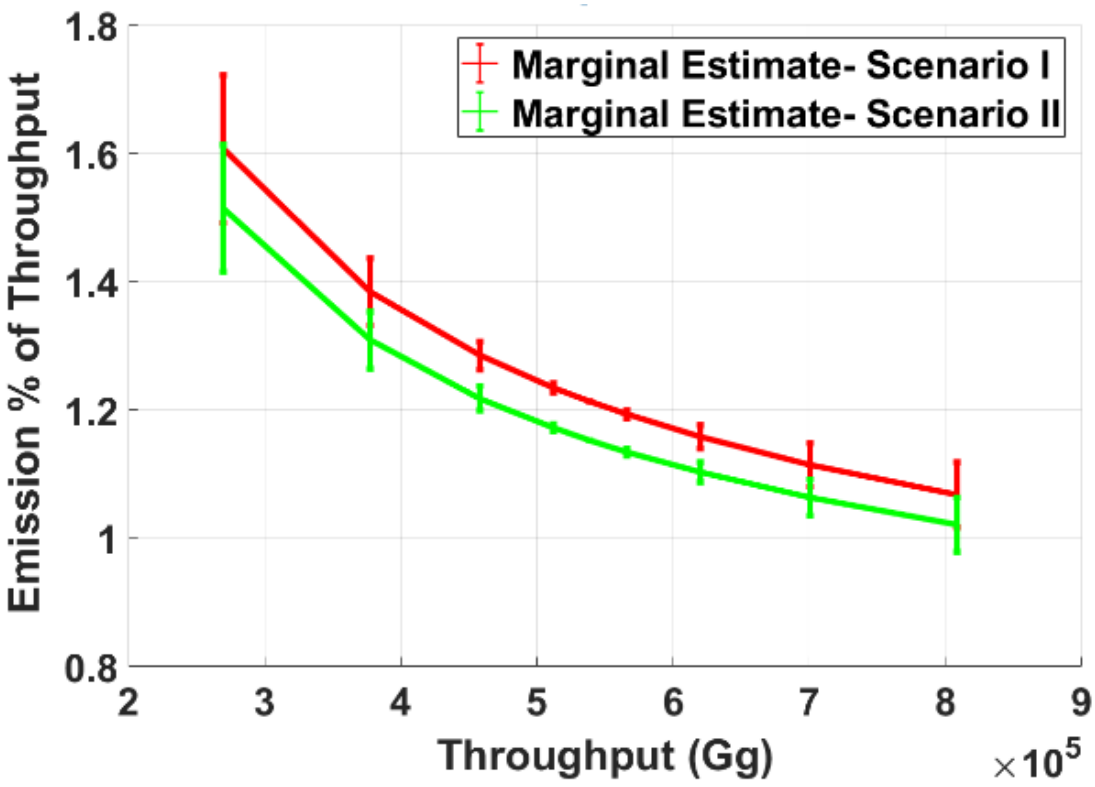

Figure 3.6. Normalized emissions vs throughput

Table 3.3 summarizes the results for Scenario I and Scenario II with all 129 components and only marginally assessed components respectively for throughput changes of 5%, 15%, 30%, and 50%. As expected, emissions increase with the increase of throughput, but the percentage of increase is less than throughput increase, and emissions decrease as throughput decreases but emissions percent decrease is less than throughput decrease. The percentage decrease of emissions is much less than that of throughput where only marginally assessed components are considered.

Table 3.3. Emissions change vs. throughput change

	System Throughput Change			
	-5 & 5 %	**-15 & 15 %**	**-30 & 30 %**	**-50 & 50 %**
Scenario I: The effect of technological improvement is neglected				
Emissions 2016 base year (%) All 129 Components	-3.36 & 3.22	-10.02 & 9.73	-20.16 & 19.36	-33.79 & 31.92
Total emissions/ throughput (%) All 129 Components Base year = 1.21%	1.23 & 1.19	1.28 & 1.15	1.38 & 1.11	1.60 & 1.06
Emissions over 2016 base year (%) Marginally Assessed Components	-0.83 & 0.81	-2.56 & 2.39	-5.30 & 4.62	-9.23 & 7.32
Total emissions/ throughput (%) Marginally Assessed Components	0.69 & 0.64	0.74 & 0.60	0.86 & 0.55	1.11 & 0.50
Scenario II: The effect of technological improvement is applied				
Emissions over 2016 base year (%) All 129 Components	-6.4 & 0.03	-12.9 & 6.45	-22.92 & 15.96	-36.24 & 28.41
Total emissions/ throughput (%) All 129 Components Base year = 1.21%	1.19 & 1.15	1.24 & 1.12	1.33 & 1.08	1.54 & 1.03
Emissions over 2016 base year (%) Marginally Assessed Components	-0.54 & 0.51	-1.75 & 1.45	-3.82 & 2.62	-7.14 & 3.81
Total emissions/ throughput (%) Marginally Assessed Components	0.69 & 0.64	0.76 & 0.59	0.88 & 0.53	1.16 & 0.47

3.5 Summary

In this chapter the behavior of methane emissions relative to changes in throughput was evaluated using a novel marginal method. The result of the comprehensive literature survey conducted in chapter 2 was utilized to develop a cause-based marginal methane estimation model that relied on a combination of factors, including event, time, and throughput to calculate the change in emissions. It was shown that for some components of the natural gas system, increasing or decreasing throughput will not change the emissions at all or has very little impact. The overall analysis for the system showed that emissions only decreases 34% relative to 50% decrease in throughput.

Marginal methane emissions were estimated for two distinct scenarios, (1) the assumption that technological improvements are neglected and current technological status for natural gas system components remains equivalent to the base year; and (2) technological improvements (such as those assumed in the EPA STAR program) are applied to the base year emissions sources resulting in lower overall gas system emissions. Emissions from the natural gas supply chain will increase with the increase of the natural gas production, but the percent of increase in emissions is less than the throughput increase. Emissions will decrease with the decrease of throughput, but the percent of decrease is less than the throughput decrease. Additionally, normalized emissions will decrease with increased throughput as emissions from some sources are fully or partially independent of throughput. Of the129 emission sources identified within the EPA/GHGI, only 47 were assessed as part of the present work due to data availability. Treating the remaining sources using the traditional approach therefore underestimates the difference between a marginal and average methodology. Only 6 methods out of many recommendations were used to reduce methane emissions for the technological effect scenario from EPA/STAR program which also can be the reason why emissions change versus the change in the throughput is high.

The results have importance within the context of carbon emissions mitigation due to (1) the need for establishing accurate GHG inventories and (2) understanding the cause and effect for attaining emissions reductions. Generally, for the natural gas system current assessment methods allocate direct emissions of methane on a proportional basis to throughout, i.e., as more or less gas is consumed direct emissions either increase or decrease proportionately. For example, commonly utilized carbon intensity models GREET use a one-factor method for allocating attributable

methane emissions from the natural gas system to the carbon intensity of transportation fuels involving natural gas at any point in their life cycle. However, the results here demonstrate that doing so may overestimate emissions increases from the increased production and use of natural gas derived fuels (or conversely overestimate reductions from decreases) as only a fraction of the total emission sources behave in a proportionate manner, and therefore marginal emissions will not be one-to-one proportional to changes in throughput. This is particularly important from a regulatory and policy perspective, as carbon intensity is often used as an important determinant within technological decision making, e.g., qualification of transportation fuels under California's Low Carbon Fuel Standard pursuant to Assembly Bill 32 [93].

The work presented in this paper is a first step in introducing marginal methane emissions estimation from natural gas systems. Further research is needed to fully account for other factors that affect change in methane emissions, including effect of pressure, age, and geology. Considering these factors provides a more comprehensive model to estimate methane marginal emissions from natural gas infrastructure more accurately.

4 Analysis of Southern California Gas System for 100% Renewable Energy Penetration

4.1 Abstract

In this chapter, I utilize Southern California (SoCal) natural gas transmission pipelines and underground storage resources for transporting and storing hydrogen gas for a 100% renewable energy penetration. The goal is to determine to what extent natural gas infrastructure can be used to deliver and store hydrogen to meet SoCal electric demand for a 100% renewable energy portfolio. Hydrogen is produced from solar power generation using electrolysis next to the gas transmission pipelines whenever it is available in quantities greater than the electricity demand.

Three scenarios, each using a different solar scale factor and storage capacity, are studied to identify the optimum scale factor and storage capacity that results in 100% renewable energy penetration. The constraints each scenario has on the network pipelines are also investigated and remedies are suggested to increase the network capacity to meet the demand. It is found that adding 300 kt hydrogen storage capacity to the existing Southern California gas network can reduce the required solar production capacity by 32 GW. Another benefit of the added storage is lowering the required pipeline network capacity by ~20% to achieve 100% renewable energy.

4.2 Literature Review

Recently, California (CA) has set an ambitious goal to eliminate the reliance on fossil fuels and move to zero-emission energy sources for its electricity needs. In September 2018, California senate passed SB100, which requires the Golden State to obtain 100% of its power from clean sources by 2045.

One of the biggest challenges in moving toward 100% renewable energy portfolio is the integration of the renewable sources to the grid. The variability of renewable energy sources, specifically for large scale integration into the electricity sector, has brought increased attention to the requirements for energy storage systems. To mitigate the intermittency and uncontrollability

of renewable energy, many different energy storage technologies, such as pump hydroelectric storage (PHS), compressed air energy storage (CAES), batteries, flow batteries, hydrogen energy storage, capacitors, and flywheels are variously being deployed and/or considered for deployment. Some of these energy storage systems (e.g., batteries, flywheels) are best suited for short-term storage and highly dynamic operation, while others (e.g., hydroelectric storages, flow batteries, hydrogen energy storage (HES)) can accomplish massive and seasonal storage of renewable electricity because of independent power and energy scaling that can lead to large energy capacity and low self-discharge capabilities [94], and [95]. The integration of high levels of renewable power will require the features of both of these categories of energy storage systems. Figure 4.1 shows different electricity storage technologies [23].

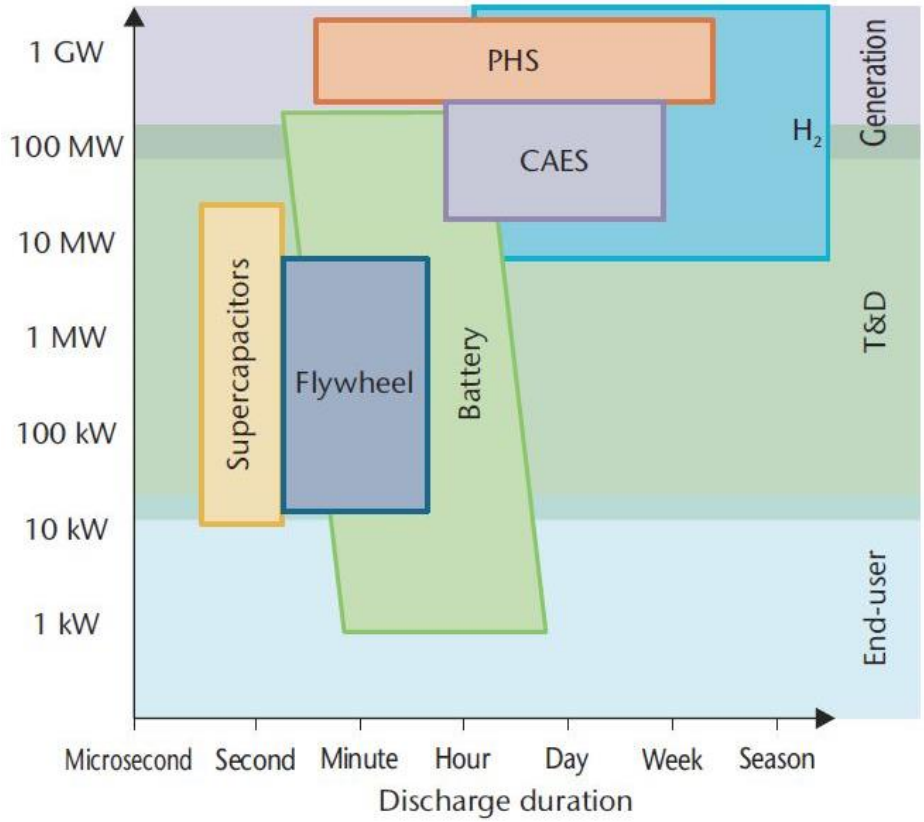

Figure 4.1. Electricity storage technologies (taken from [23])

HES systems generate hydrogen gas from water using electrolysis as the main conversion technology which can be dynamically powered to complement renewable intermittency. HES can become cost effective by using inexpensive or otherwise curtailed renewable energy, storing the

hydrogen, and subsequently using the hydrogen for various purposes (e.g., to produce electricity via a fuel cell for power generation or transportation applications).

Several projects, including some in Europe, have utilized the off-peak intermittent renewable electricity from wind or solar that would have otherwise been curtailed to produce hydrogen [96]. The transformation of excess renewable power to gas, which is referred to as "Power to Gas" (PtG) is a very economically attractive solution as the excess renewable energy from wind and solar farms cannot readily used in the markets, and as a result is very low cost. In other words, hydrogen is used as a storage method to store the excess renewable power. Technological and economical overview of PtG is discussed in depth by various authors [97], [98], and [99]. Figure 4.2 illustrates different hydrogen integration pathways [100]. The highlighted pathway in red is the focus of this chapter which will be explained in detail in the next section.

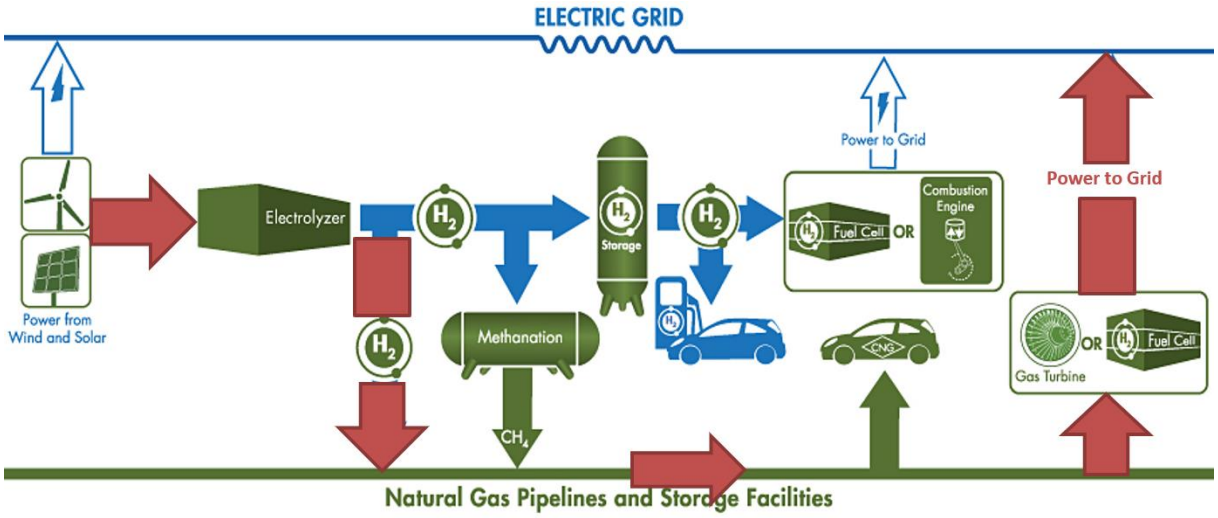

Figure 4.2. Different PtG and Hydrogen Integration Pathways (adapted from [100])

In order to increase the renewable energy penetration in California with high level of renewable energy generation, power to gas technology has been shown to be promising [101]. California is also interested in using hydrogen to fuel its transportation sector [102] and [103] which produces the largest percentage of greenhouse gases.

A robust transportation infrastructure is needed to transport and store hydrogen that is produced at the site of wind or solar farms using the excess power which is far from urban centers in CA. In California, today hydrogen is transported through specialty pipelines that are specifically designed from carbon steels that are well-suited to long term exposure to pure hydrogen.

The idea of storing hydrogen into the existing underground storage has been around since 1970. In fact, hydrogen has been stored in the underground storage reservoirs in some countries and is currently stored in salt cavern in the U.S. Panfilov summarized all the projects that use underground reservoir to store hydrogen worldwide [104] as presented in Figure 4.3.

	Type	% H_2	*P*, *T*	Depth (m)
Bad Lauchstädt, Germany	Salt cavern		150 bar	820
Kiel, Germany	Salt cavern	60–64	80–100 bar	1330
Teesside, UK	Salt cavern	95	50 bar	400
Texas: Air Liquid, USA	Salt cavern	95		
Texas: ConocoPhillips, USA	Salt cavern	95		850
Texas: Praxair, USA	Salt cavern			
Beynes, France	Aquifer	50		430
Ketzin, Germany	Aquifer	62		200–250
Lobodice, Czech	Aquifer	50	90 bar, 34 °C	430
Diadema, Argentina	Natural Gas	10	10 bar, 50 °C	600

Figure 4.3. Hydrogen underground Storage Worldwide (taken from [104])

To store such large scale of hydrogen produced from excess renewable energy resources, natural gas underground geological reservoirs in the form of salt caverns, depleted oil and gas fields, and aquifers are the only options available to date [104]. In one hand, storage of hydrogen in the salt caverns has some advantages compared to the porous media (aquifer and depleted oil and gas reservoir: a) the impermeability of the cavern's wall to any gas; b) prevention of the transformation of hydrogen into other gases because bacteria cannot survive in that condition [104]; c) the lower cushion gas requirement (20-35%) [99]; d) the higher withdraw and injection rate [104]. However, salt caverns have smaller volume hence can store less gas and there are limited geological areas that are suitable for salt caverns formation [104]. On the other hand, the high-volume capacity of depleted oil/aquifer reservoirs, their experience and history storing natural gas make them suitable to store the large amounts of hydrogen. However, the gas reaction with the microorganism existed in the underground and the high diffusivity of hydrogen into water-bearing units can pose some issues [104].

All four underground storage facilities in Southern California are depleted oil and gas fields. The depleted oil and gas storage facilities located in the porous rock structures require 50-65% of

total gas as a cushion gas (base gas) which is the required gas in the gas wells at the minimum pressure to retain sufficient pressure during the entire injecting and withdrawing processes [99]. The amount of gas that is available to the market is called the working gas.

There are various types of electrolyzers with features that depend upon their electrolyte type: Proton exchange membrane (PEM) electrolysis using solid polymer electrolyte membranes, Solid oxide electrolysis (SOE) using a solid metal oxide electrolyte, Alkaline electrolysis (AE) utilizing aqueous alkaline electrolyte solution [99]. In this study PEM fuel cell/electrolyzer was used in the modeling. PEM electrolyzers can operate under pressurized conditions (even creating higher hydrogen pressure through electrochemical pumping) and both PEM and alkaline electrolyzers can operate in a highly dynamic fashion.

The goal of this chapter is to analyze and identify optimum infrastructure requirements to achieve a 100% renewable energy portfolio, including renewable energy production, energy transportation, and storage utilizing hydrogen. Comparing the infrastructure requirement to existing infrastructure provides an estimate of resources needed to achieve this goal. It is worth mentioning that the purpose of the study is not to determine the optimum mix of solar and wind generation in the southern California region for a 100% renewable energy penetration but to investigate the capabilities and vulnerabilities (pressure and flow dynamics) of southern California natural gas infrastructure to transport and storage hydrogen. Simply put, this study will answer the question of “Do we have enough gas underground storage facilities and transmission pipelines to store and deliver hydrogen for the extreme case of meeting all the electric demand by use of hydrogen energy storage system in the existing natural gas infrastructure alone?”.

4.3 Methodology

In the current work, the large-scale implementation of renewable energy resources was studied using the Hydrogen Energy Storage (HES) system. For the extreme case of 100% renewable energy penetration, the goal is to meet the entire electric demand of Southern California (SoCal) region by utilizing the existing natural gas infrastructure owned by SoCalGas to transport and store hydrogen. HES system was modeled in MATLAB to investigate the capability and capacity of SoCalGas natural gas infrastructure for a 100% renewable energy portfolio. when the renewable energy generation is greater than the electric demand in SoCal region the excess power is directed

to the proton exchange membrane electrolyzer to produce hydrogen. Hydrogen then needs to be pressurized before injection into the transmission pipelines in a two-stage compressor. Through a network of pipelines hydrogen is delivered to the underground storage facilities. When the electric demand is higher than the renewable energy generation, hydrogen is dispatched from the storage facilities. In order to depressurize the withdrawn hydrogen from the storage facilities, hydrogen is directed to a turbine to expand before directing to the proton exchange membrane fuel cell to generate electricity. Figure 4.4 shows a schematic of the simulated HES system.

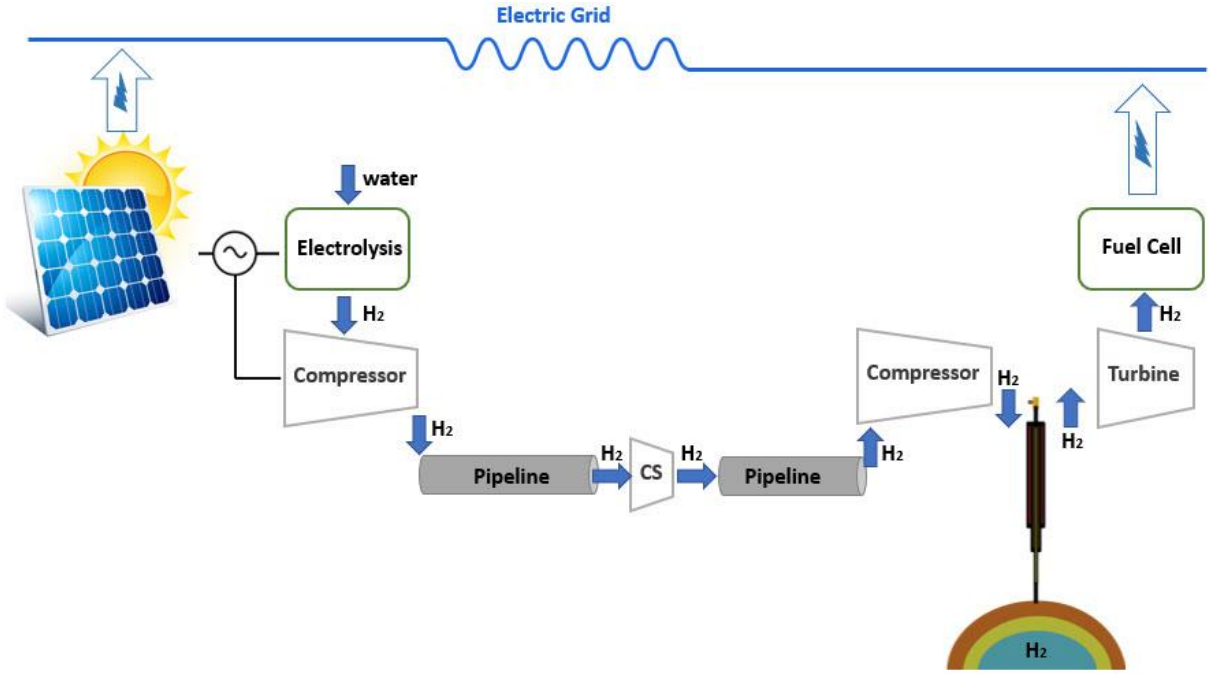

Figure 4.4. Schematic of the Simulated Model

Note that the analysis herein assumes that: a) natural gas infrastructure maybe used as part of HES system that operate in the same pressure range with appropriate retrofits; b) Sufficient and adequate equipment are accessible/available to produce hydrogen from electrolyzer and generate electricity from fuel cell. Power to Power technology (store otherwise curtailed renewable energy in the form of hydrogen and then later generate electricity through fuel cell when the demand is higher than the renewable power generation) is still at its early stages and future research and development will answer what modifications or retrofits may be required for natural gas infrastructure to adapt hydrogen. This is a different topic and is not in the scope of this study.

4.3.1 Fuel Cell and Electrolyzer Model

The models used to estimate the hydrogen production from excess electricity using an electrolyzer and electricity production from hydrogen stored in underground storage using fuel cells are discussed here. Equation (7) shows how hydrogen production in PEM electrolyzer and hydrogen consumption in PEM fuel cell using Faraday's Law is calculated.

$$\dot{N} = \frac{P}{zFE} \tag{7}$$

Where F – Faraday's constant (F = 96485 *Coulombs/mole*); z – number of mole of hydrogen (z = 2); P – power (*J/s*); E – electrolysis voltage (*J/Coulombs*); $\dot{N}$ – hydrogen production/consumption rate (*mole/s*).

Hydrogen is produced in PEM electrolysis (EC) with the efficiency of 66% (HHV) which operates at 55°C and 13 bar [95]. Hydrogen is consumed in PEM fuel cell (FC) to generate electricity with the efficiency of 64%. Table 4.1 summarizes the PEM FC/EC operating conditions.

Table 4.1. PEM EC/FC operating conditions

PEM fuel cell system efficiency (LHV), [105]	64%
PEM electrolyzer system efficiency (HHV), [106]	66%
Electrolyzer H_2 outlet pressure (bar), [95]	13.1
Electrolyzer H_2 operating temperature (°C), [95]	55

4.3.2 Pipeline Model

Significant research has been done to study hydraulic properties of pipelines that carry natural gas. These studies can be categorized into two groups. First group studies the behavior of the gas pipelines in a steady state condition while the second group analyzed the gas flow and pressure of the pipes in the transient state.

While steady state models are simpler and can quickly calculate gas flow and pressure in a pipe and are often used for optimization problem where a model needs to be solved iteratively [107] and [108], more complex transient models are necessary to answer some of the more complex questions and analyze networks where pipeline dynamics are slower, and steady state conditions are not reached quickly ([109], [110], [111], and [112]). At its core, transient models solve a set

of nonlinear Partial Differential Equations (PDEs) and therefore much of the work published on transient models address the details of numerical methods used to solve these PDEs and how they compare with other numerical methods ([113], [114], [115], and [116]). A detailed analysis that studies the suitability of using more complex transient methods versus simpler steady state models is outlined in [117].

Among the numerical methods used for transient analysis, [118] provided a unique approach of using a typical electrical model that includes inductors, capacitors, and resistors to model to simulate the properties of a gas pipeline. The advantage of this method is that the significant tools and research done on electrical networks can then be used to study the properties of gas pipelines.

Choosing the right dynamic versus steady state model is important to ensure the results can realistically represent the stated model. [119] studies in which scenarios using a steady state model to simulate the properties of a pipeline provides inaccurate results. The work shows that the cause of inaccuracy can be attributed to attempting to solve problems that are dynamic in nature with steady state models.

As stated in this section, a rich body of work exists in literature that models the properties of gas pipelines, both in transient and steady state conditions. In this chapter, we utilize the model based on the work developed by [120] and [121] to analyze the transient properties of natural gas pipeline carrying hydrogen. The choice of transient model used in [121] enable us to monitor the gas pressure at the inlet of the pipeline while the mass flow rate at the inlet is known and to make sure it does not exceed the maximum allowable amount at any given time. This is a crucial requirement to ensure the safety and health of the gas system studied.

- **Numerical Approach**

In order to analyze the flow characteristics at the inlet of the pipeline a series of equations (continuity, momentum, energy) need to be solved. One dimensional, transient, and compressible flow is modeled with the following assumptions:

- Isothermal flow: The change of temperature is negligible throughout the pipeline
- Constant compressibility factor
- The convective inertia term in the momentum equation is negligible
- Horizontal pipe ($\theta=0$)

By assuming isothermal flow, the energy equation drops, and momentum and continuity equations are solved in terms of mass flow rate $\dot{m} = \rho u A$ where $\rho, u \; and \; A$ are the density of the gas, velocity and the cross-sectional area of the pipe, respectively. The compressibility factor (Z) is a function of temperature and pressure but for the transient isothermal analysis it is adequate to take Z at the average system pressure and temperature [122]. According to [122] the effect of the convective inertia term in the momentum equation (second term in Equation(9)) is much smaller than the others, and as a result it could be negligible. The continuity equation, momentum equation, compressibility factor (ideal gas law), and friction factor are expressed in the following forms (Equations (8)-(11)), respectively [122] and [123]:

$$\frac{\partial \rho}{\partial t} + \frac{\partial (\rho u)}{\partial x} = 0 \tag{8}$$

$$\frac{\partial (\rho u)}{\partial t} + \frac{\partial (\rho u^2)}{\partial x} + \frac{\partial P}{\partial x} = -\frac{f \rho u |u|}{8} \pi D - \rho g sin\theta \tag{9}$$

$$\frac{P}{\rho} = \frac{ZRT}{M} = c^2 \tag{10}$$

$$\frac{1}{\sqrt{f}} = -2\log\left(\frac{\varepsilon}{3.7D} + \frac{2.51}{Re\, f^{0.5}}\right) \tag{11}$$

Where $\rho, u, p, f, Z, T, R, M, Re, D, \varepsilon,$ and c are the density of the gas, velocity, pressure, friction factor, compressibility, temperature, molar mass, Reynolds number, diameter of the pipe, the roughness of the pipe, and speed of sound in hydrogen, respectively. The friction factor is from the Coplebrook friction factor equation, which is an experimentally derived equation commonly used in the natural gas industry [123]. In Equation (9), as it was mentioned before, θ is zero for the horizontal pipeline. The simplified version of the continuity and momentum equations are reduced in terms of $\dot{m}$ and P and presented in Equation (12) and (13) [122] and [123]:

$$\frac{\partial P}{\partial t} + \frac{ZRT}{MA}\frac{\partial \dot{m}}{\partial x} = 0 \tag{12}$$

$$\frac{\partial \dot{m}}{\partial t} + A\frac{\partial P}{\partial x} = -\frac{fZRT\dot{m}|\dot{m}|}{2\, D\, A\, p} \tag{13}$$

To numerically solve Equation (13), its nonlinear term is linearized using the Taylor expansion method. A fully implicit finite difference method is used to solve the above equations which is

time independent and conditionally stable, and also making it easier to take larger time steps compared to the time dependent explicit method [122]. [120] investigated different discretization methods and concluded that a cell-centered method (flow values are calculated at the center of two grid points) is unconditionally stable to solve the isothermal flow. The partial time derivative, the spatial derivatives, and the individual terms are given in Equations (14)-(16), respectively [122], [123] and [120]:

$$\frac{\partial Y}{\partial t} = \frac{(Y_{i+1}^{n+1} + Y_i^{n+1} - Y_{i+1}^{n} - Y_i^{n})}{2\,\Delta t} + O(\Delta t) \tag{14}$$

$$\frac{\partial Y}{\partial x} = \frac{(Y_{i+1}^{n+1} - Y_i^{n+1})}{\Delta x} + O(\,\Delta x^2) \tag{15}$$

$$Y = \frac{(Y_{i+1}^{n+1} - Y_i^{n+1})}{2} + O(\,\Delta x^2) \tag{16}$$

The implicit finite difference method for discretizing time and the cell-centered method for discretizing each pipe section described above are used to discretize partial derivatives of pressure (p) and mass flow rate ($\dot{m}$) in Equations (12) and (13). The pipeline is divided into N sections as it is shown in Figure 4.5, similar to what was shown in [122] and [123]. Each discretized section of the pipeline has length Δx, where $\Delta x = \frac{pipeline\ length}{N}$. This results in N+1 nodes for the pipeline, and each node is characterized by its mass flow ($\dot{m}_i$) and its pressure (p_i), where $i = 1, \cdots, N+1$. The discretization process explained above yields 2N+2 variables and 2N equations at any given time interval Δt.

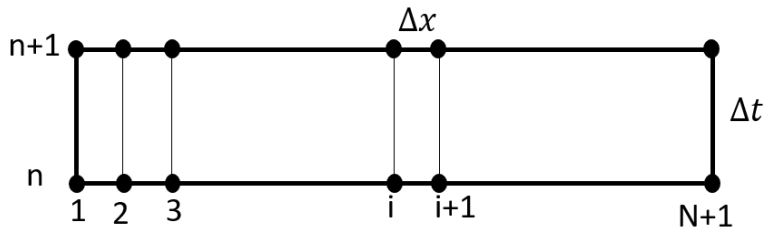

Figure 4.5. Mesh grid of the solution in x-t plane

Next, the boundary conditions at both end of the pipe is applied to reduce the number of variables to 2*N* and create a set of 2*N* equations and 2*N* variables that can be readily solved at a given Δt. The choice of boundary conditions is decided based on the information that is available

about the pipeline. In this chapter, our goal is to determine the inlet pressure fluctuations of the pipeline by injecting a given hydrogen mass flow rate at the inlet. Therefore, the pressure at the exit of the pipeline is maintained constant psi: $p(L,t) = contsant\ (psi)$ and mass flow rate at the inlet of the pipe is equal to the hydrogen produced from the PEMEC: $\dot{m}(0,t) = f(t)$, where $f(t)$ is the mass flow profile. With the boundary conditions applied, for a given time step t^n, the following set of linear equations are formed:

$$Mv = b;\ where \quad v = \begin{bmatrix} p_1 \\ \vdots \\ p_N \\ \dot{m}_2 \\ \vdots \\ \dot{m}_{N+1} \end{bmatrix} \tag{17}$$

The above system is solved in MATLAB using LU factorization to efficiently calculate the inverse of matrix M for each time step. To start the transient analysis at time step 1, the initial conditions is set at $t = 0$. Equation (13) in steady state condition ($\frac{\partial p}{\partial t} = 0$ and $\frac{\partial \dot{m}}{\partial t}$=0) is used to calculate initial pressures at each section of the pipeline based on a steady mass flow rate, $\dot{m}(t = 0)$. The pressure drop at section i of the pipeline can then be calculated using Equation (18).

$$p_{i+1}^2 - p_i^2 = \Delta x\ \frac{fZRT\dot{m}(t=0)|\dot{m}(t=0)|}{pA^2} \tag{18}$$

- **Pipeline Model Validation**

The pipeline numerical model developed in this chapter is validated by comparing its result with the work presented by Helgaker et al. [121]. The paper presented simulation result of pressure and mass flow rate fluctuations of a 650 km pipeline, which was also verified by experimental data. The pipeline had a diameter of 1m, outlet pressure was set at 10MPa, and $\Delta t = 60s$. The comparison between the results shown in [121], and our model is depicted in Figure 4.6 and Figure 4.7. The close agreement between the results shown validates the model developed.

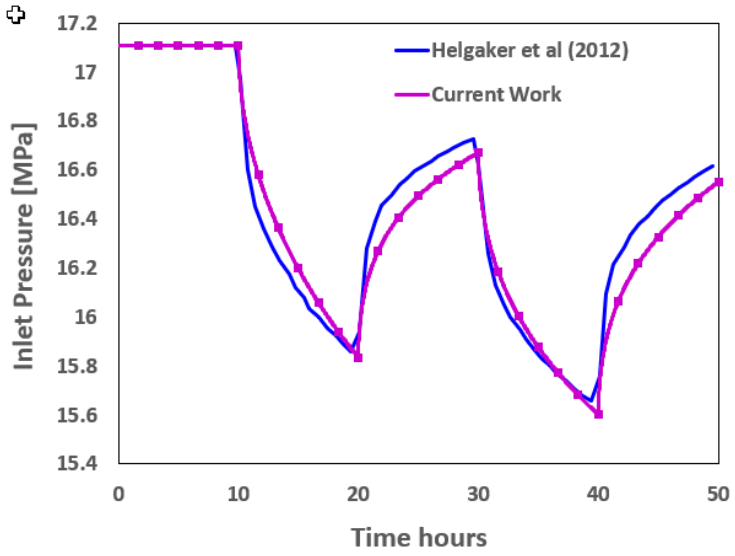

Figure 4.6. Inlet pressure comparison

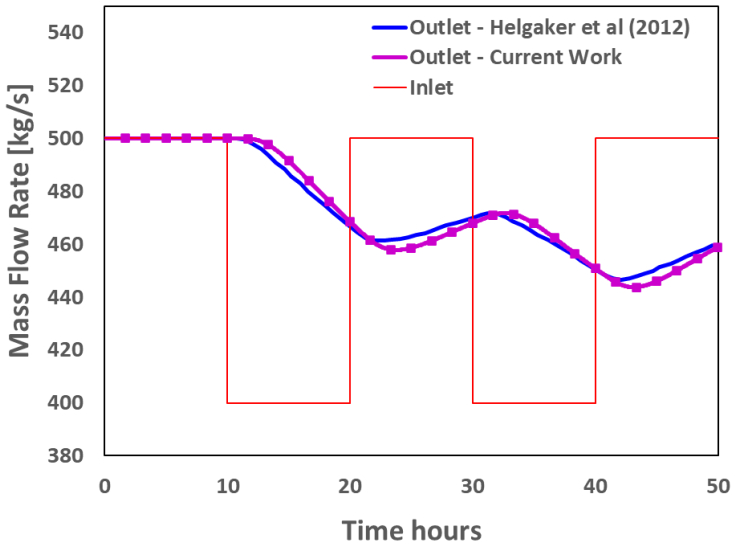

Figure 4.7. Outlet mass flow rate comparison

4.3.3 Underground Storage Model

The characteristics of the underground storage facility was modeled based on the actual information for each storage field in Southern California region obtained from U.S Energy Information Administration (EIA) [124]. For each of the four storage fields in southern California, the maximum amount of working hydrogen that can be stored and the corresponding pressure is calculated.

The data about Southern California storage fields in [124] pertains to natural gas. Working volume ($V_{working}$) and the cushion gas volume ($V_{cushion}$) provided by EIA for each underground storage is used to calculate working gas mole ($N_{working}$) and cushion gas mole ($N_{cushion}$) using Equations (19) and (20), where P_S – standard pressure (14.7 psi); T_S - standard temperature (288 K); R – universal gas constant (8.314 kJ/kmole. K). Working gas and cushion gas moles are then used to calculate the pore volume of each storage facility using Equations (21) and (22), where P_{max} – maximum storage operation pressure (kPa); T_{max} (K) – maximum storage temperature; Z_{NG} (T, P, X) – the compressibility factor of natural gas which is a function of temperature, pressure, and component composition (X). The storage temperature was assumed to be constant at 298 K.

As it was explained previously, cushion gas is the minimum amount of gas in the storage that cannot be withdrawn from the storage and is needed to maintain the adequate pressure for the storage operations. The working gas is the maximum amount of gas that can be stored in the underground storage. Volumes calculated previously are then used to calculate the maximum amount of hydrogen that can be stored at each storage facility using Equation (23) and its corresponding pressure calculated from Equation (24). The compressibility factor used in Equations (22) and (24) to calculate the amount of natural gas and hydrogen that can be stored in a given storage facility were obtained from [125], where the compressibility factor was calculated using GERG-2008 Equation of State (EoS).

$$N_{working,NG} = \frac{P_S\, V_{working}}{RT_S} \tag{19}$$

$$N_{cushion,NG} = \frac{P_S\, V_{cushion}}{R\, T_S} \tag{20}$$

$$N_{max} = N_{cushion} + N_{working} \tag{21}$$

$$V_{res} = \frac{Z_{NG}\, R\, T_{max}\, N_{max}}{P_{max}} \tag{22}$$

$$N_{working,\,H_2} = \frac{P_{max} V_{res}}{Z_{H_2} R\, T_{max}} \tag{23}$$

$$P_{res} = \frac{Z_{H_2}\, R\, T_{res}\, N_{res}}{V_{res}} \tag{24}$$

4.4 Results and Discussion

This section utilizes the model developed in the chapter to analyze three different scenarios for achieving 100% renewable energy penetration in Southern California using existing natural gas infrastructure. The analysis scales up the current solar energy production in Southern California to achieve 100% renewable energy production and uses the existing natural pipeline networks and underground storage system to transport and store hydrogen. The simulation results highlight the extra pipeline capacity and storage system needed for each scenario and provides a preliminary cost comparison to achieve 100% renewable energy production. Finally, a modest pipeline network expansion is suggested that will enable Southern California to achieve 100% renewable energy penetration. The analysis is done over an entire year to consider the seasonal impact of change in demand on the amount of production, transport, and storage facilities that is needed. The inputs needed to analyze each scenario are:

- The hourly demand & renewable power (wind & solar) of Southern California region
- Available underground natural gas storage facilities in the region
- Current natural gas pipeline network infrastructure

4.4.1 Model Input

- **The hourly demand & renewable power of Southern California region**

SoCal region hourly renewable power generation data and Southern California Edison (SCE) service territory hourly demand data was obtained from the California Independent System Operator (CAISO) [126] (see Figure 4.9) for the entire year as an input to the model. CAISO reports renewable power generation real data on an hourly basis for three zones; NP15, ZP26, and SP15 as presented in Figure 4.8. Wind and solar data from zone SP15 which is a SoCal region was used as potential new renewable power sources in the studied scenario. Total SCE hourly demand data was also needed to be scaled up to match the entire SoCal region electricity demand since SCE is not the only power provider in the SoCal region. It is also worth noting that, the hourly data from other power utility companies in the SoCal region was not publicly available.

Figure 4.8. Three zones covered by CAISO in California (taken from [126])

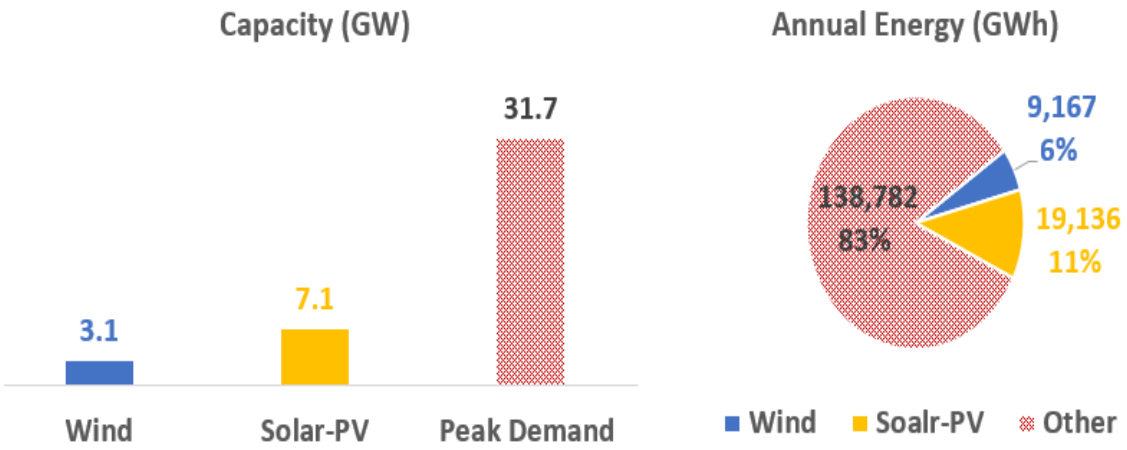

Figure 4.9. Renewable and demand power information (data taken from [126])

- **Available underground natural gas storage facilities in the region**

Four available underground natural gas storage facilities in Southern California shown in Figure 4.10, namely Aliso Canyon, Honor Rancho, La Goleta, and Playa del Rey, are included in the model. The data related for each storage facility are obtained from EIA [124] and are outlined in Table 4.2.

Table 4.2. SoCalGas Underground storage facilities - capacity and pressure limit [124]

Storage Field	Aliso Canyon	Honor Rancho	La Goleta	Playa del Rey
P_min (psig)	1614	1722	1173	1163
P_max (psig)	2926	4400	2050	1700
Inventory (BCF)	86.2	27	21.5	2.4
Cushion gas (BCF)	81.53	21.00	24.59	4.46
Max Withdrawal Rate (BCFD)	1.86	1.00	0.42	0.40
Max Injection Rate (BCFD)	0.60	0.30	0.14	0.08

Figure 4.10. SoCalGas underground storage fields (taken from [127])

Hydrogen has higher compressibility factor compared with natural gas. Transforming the four natural gas storage facilities described above to store hydrogen reduces their overall capacity. The storage model described earlier are used to calculate the capacity reduction as % of hydrogen stored in each facility (see Figure 4.11) and reaches 74% of its original capacity when hydrogen concentration reaches 100%. The overall hydrogen storage capacity of each facility is outlined in Figure 4.12.

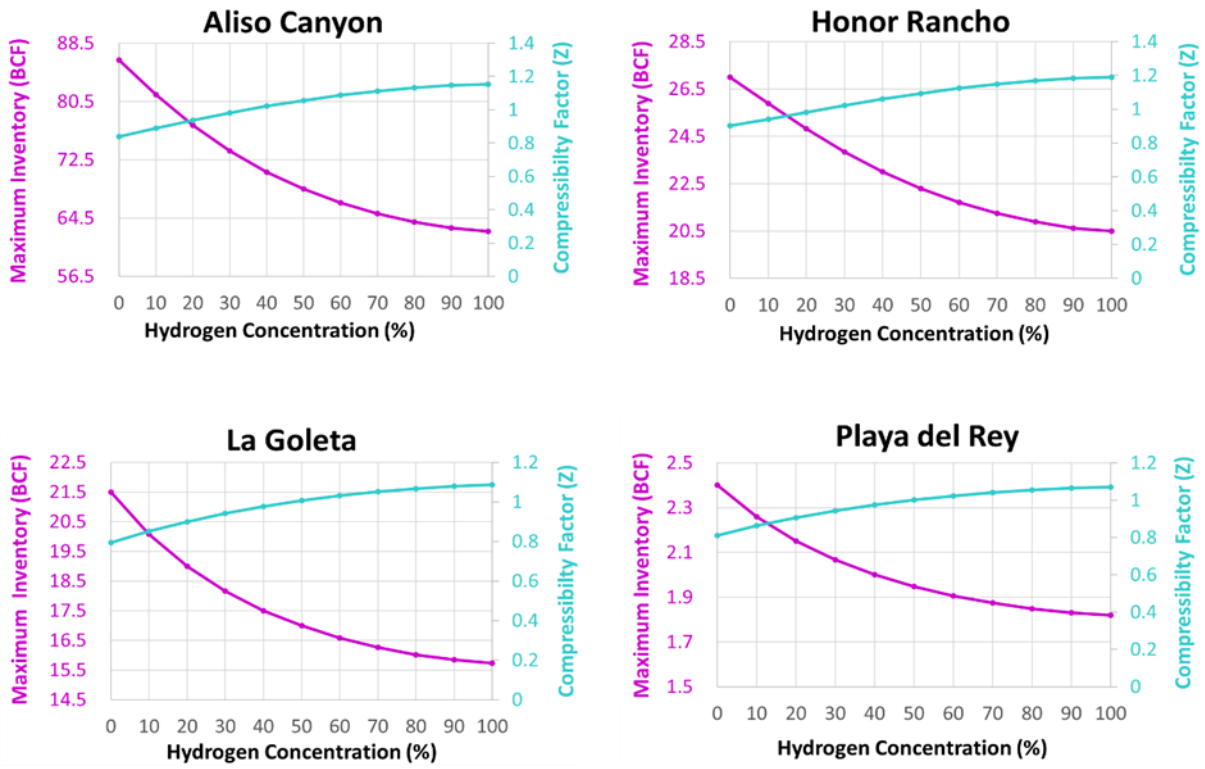

Figure 4.11. Storage field capacity& compressibility change vs hydrogen concentration (%)

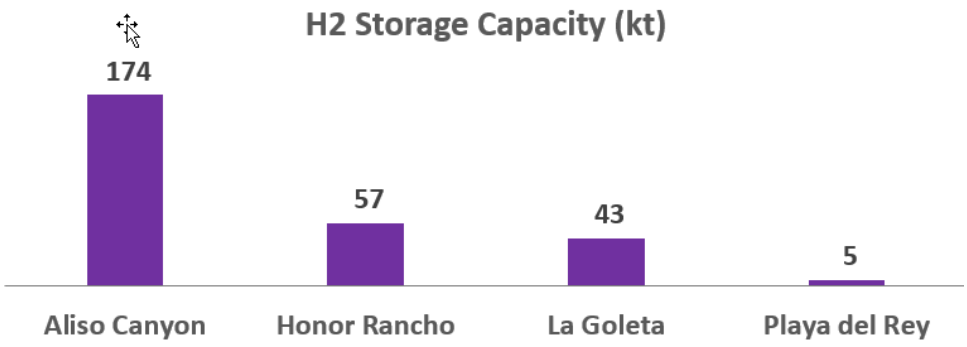

Figure 4.12. Hydrogen storage capacity (kt)

- **Current natural gas pipeline network infrastructure**

SoCalGas transmission pipeline network shown in Figure 4.13 is adopted from [128]. Figure 4.14 shows the SoCalGas transmission pipeline network topology used in our model based on the information provided in Figure 4.14. Detail information from the fifteen pipelines included in our model (see Figure 4.14) are taken from [129] and [130], and are outlined in Table 4.3.

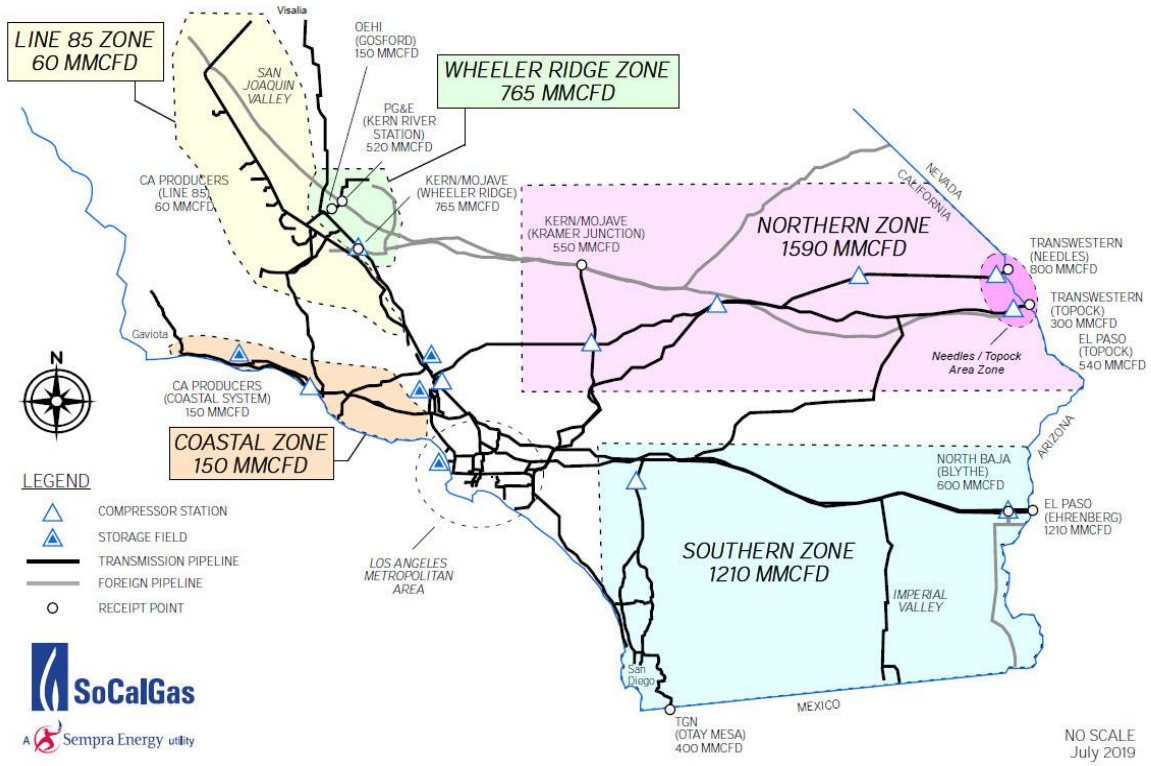

Figure 4.13. SoCalGas natural gas service territory (adapted from [128])

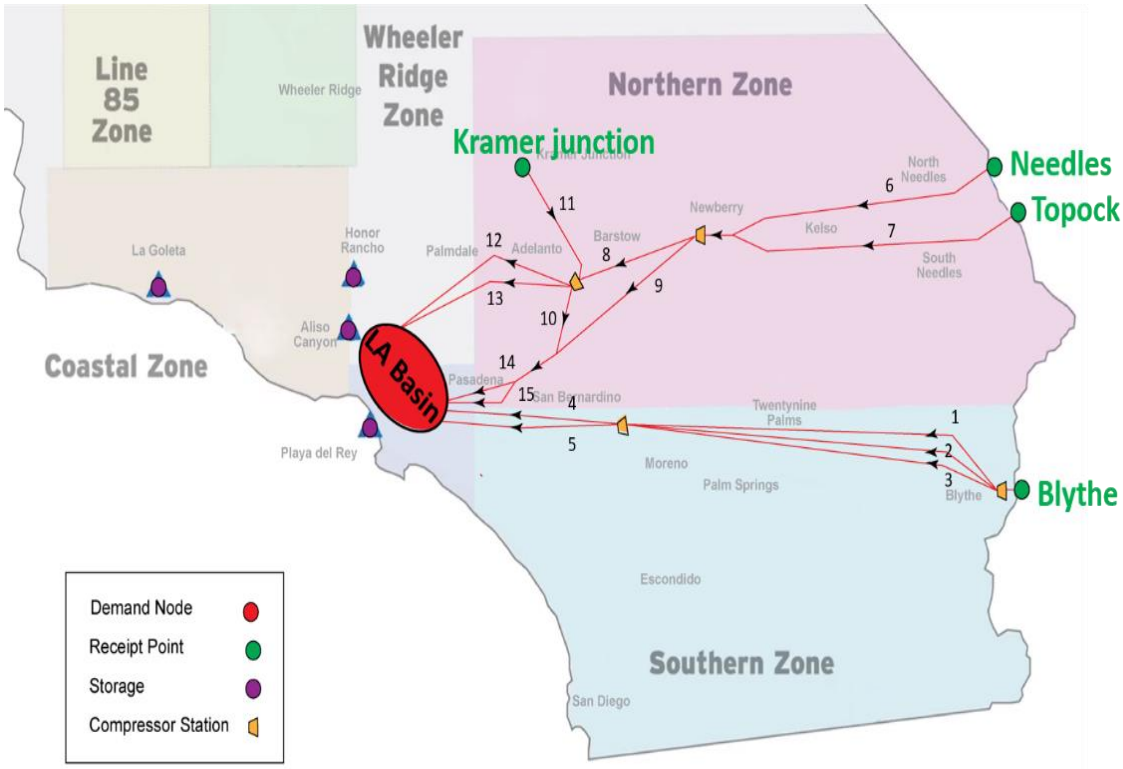

Figure 4.14. Simulated network map

Table 4.3. Southern California pipeline information

Pipeline #	Diameter (inch)	Length (mile)	Max Pressure (psi-g)
1	30	151	1,000
2	36	151	1,100
3	30	151	1,000
4	30	60	1,000
5	30	68	1,000
6	34	115	1,100
7	30	124	1,000
8	30	54	1,000
9	36	62	1,100
10	36	16	1,100
11	24	32	950
12	30	65	1,000
13	30	65	1,000
14	36	48	1,100
15	36	55	1,100

4.4.2 Model Results

To achieve 100% renewable energy penetration in Southern California and meet the current demand, the existing hourly solar energy production provided in [126] is scaled up, while the amount of wind generation is assumed to be the same. It is estimated that 11.79% of in-state renewable generation comes from solar and 6.24% comes from wind [1]. Since southern California has the potential of generating more solar energy and since solar is currently typically cheaper than wind, a scaled solar generation for the SoCal region is used in the model. That said, this scenario should not be considered a realistic scenario, but rather, one intentionally conceived to introduce the maximum need for dynamically supporting the electric grid with the goal of determining the capacity (pressure and flow dynamics) of the SoCal natural gas infrastructure to transport and store hydrogen.

Not considering the efficiency of converting electricity to hydrogen when there is excess power and converting hydrogen to electricity during power deficit, the initial calculated solar installation scaling factor of 6.77 is needed to match the demand. To determine the minimum solar installation scale factor that is needed that takes into account the seasonal nature of demand and the inefficiencies of the fuel cells and electrolyzers, a transient model was developed in MATLAB that simulated the Southern California pipeline network explained in this chapter.

The model calculates total cumulative hourly hydrogen production minus consumption each hour for an entire year for various solar installation scale factors. The result of this analysis is depicted in Figure 4.15.

To meet the energy demand of Sothern California using 100% renewable energy and employing hydrogen to store and transport hydrogen, the total net hydrogen production should be greater than zero. Meeting this requirement ensures that enough hydrogen is available to compensate power deficit and stored hydrogen is not depleted over a few years.

The analysis in Figure 4.15 shows that a minimum solar installation scale factor of 13 meets the above requirement. Cumulative hydrogen production range in Figure 4.16 also confirms that solar installation scale factors of 13 provides smaller range variations. Despite a lower solar installation scale factors, as shown in Figure 4.17, balancing the hydrogen storage level for this scenario with the current level of available storage in Southern California is not feasible. New hydrogen storage facility is needed to balance the stored hydrogen at the beginning and end of the year. To balance the stored hydrogen at the beginning and end of the year, the solar installation scale factor is increased. The simulation results show that at solar installation scale factor of 17.5, the existing Southern California underground storage infrastructure can be successfully balanced. To show the sensitivity of each factor, a third scenario with solar installation scale factor of 15 is also simulated, and the extra storage needed to balance the stored hydrogen at the beginning and end of the year is evaluated.

In-depth analysis of following scansions that was discussed above is provided in the next section:

- Scenario 1: Solar scaling factor 13, No power curtailment required
- Scenario 2: Solar scaling factor 17.5, No extra hydrogen storage needed
- Scenario 3: Solar scaling factor 15, a mix of extra hydrogen storage and power curtailment

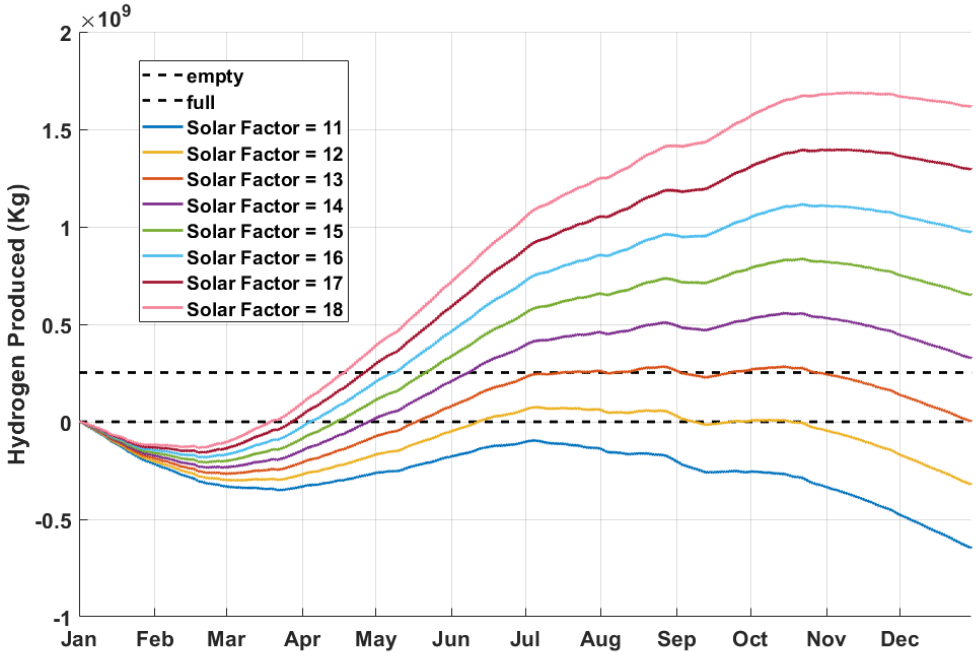

Figure 4.15. Annual hydrogen produced vs solar scaling factor

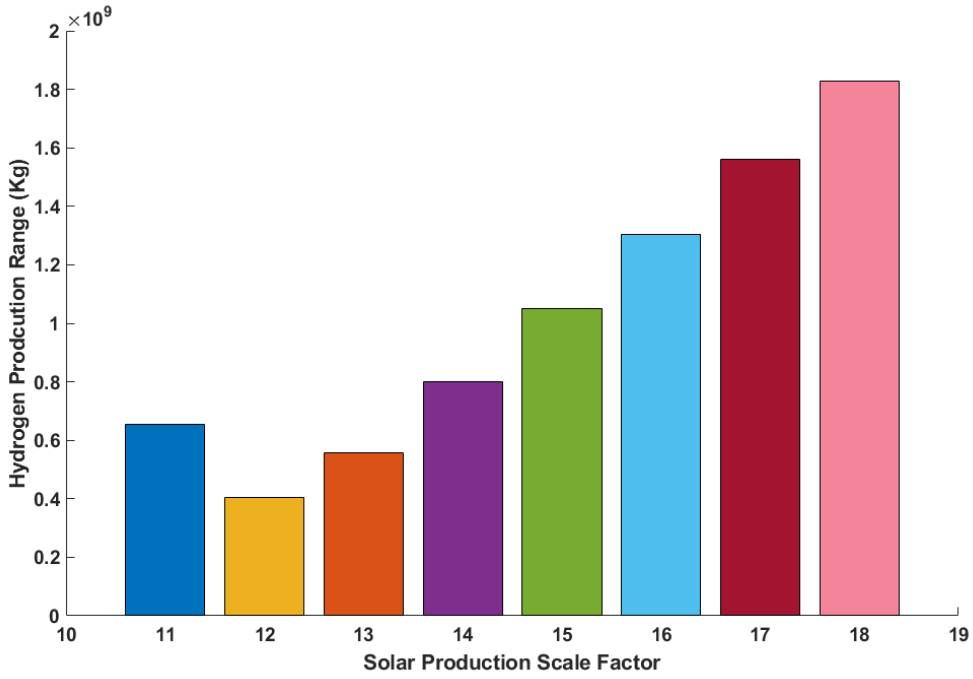

Figure 4.16. Hydrogen production rate vs solar scaling factor

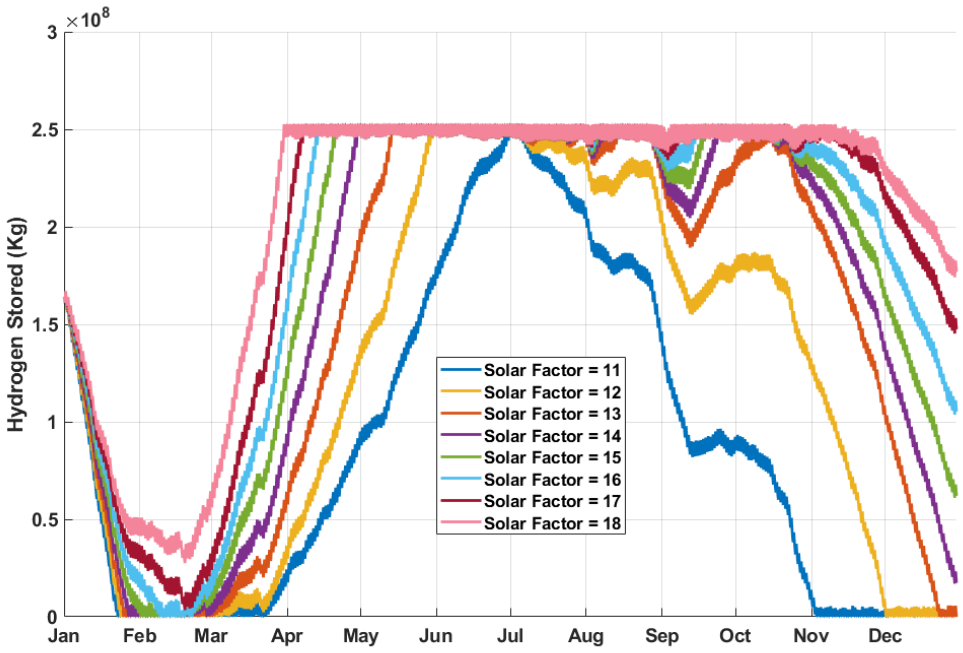

Figure 4.17. Storage inventory vs solar scaling factor

- **Scenario 1: Solar scaling factor 13, No power curtailment required**

In the first scenario analyzed, solar scaling factor of 13 is chosen to ensure total net hydrogen produced for the entire year is not negative. This is based on the data that is outlined in Figure 4.15, where solar scaling factor of 13 is the lowest scaling factor for which cumulative hydrogen produced at the end of the year is positive. As mentioned earlier, meeting this condition is a requirement to ensure the hydrogen storage facilities are not depleted after a few years.

The simulation results of hydrogen stored in the current storage facilities in Figure 4.17 shows that for the solar scaling factor of 13, current storage facilities are not sufficient. Therefore, expansion of underground storage is necessary to balance the beginning and end inventories. The model calculates the lowest extra storage needed to be around 331kt of hydrogen, which translates to a 120% increase in the current hydrogen storage capacity in Southern California. Next, the model calculates the storage fill level at the beginning of the year to balance the beginning and end inventories. Figure 4.18 shows the simulation result of the balanced stored hydrogen for solar scaling factor of 13. In this scenario, the model indicates that storage fill level should be at 50% capacity at the beginning of the year to ensure beginning and end inventories are balanced. Moreover, Figure 4.18 shows that for solar scaling factor of 13, no curtailment of renewable energy

produced in solar and wind farms are necessary, resulting in the most efficient use of those resources.

The last step in analyzing the network infrastructure is to evaluate its capacity to carry the produced hydrogen to Southern California storage facilities outlined in Table 4.2. The hydrogen produced from the excess power when demand is less than supply is transported through pipelines depicted in Figure 4.14. The transient simulation results of the pipeline network using hourly data for the entire year for major pipelines in the network is shown in Figure 4.19. The analysis indicates that pipelines 1, 3, 4, 5, 7, and 11 are above capacity. The model then scales down and balances the transported hydrogen, and the simulation results show that after balancing the distributed hydrogen at the pipeline inlets, (pipe1=11.6%%, pipe 2=20.8%, pipe3=11.6%, pipe6=23.3%, pipe 7=15.8%, pipe11=16.6%,) , the pipeline network can only carry 80% of the peak demand. Figure 4.20 shows that the inlet pressures of the main pipelines meet the network constraints when the transported hydrogen is balanced and scaled down at 80%.

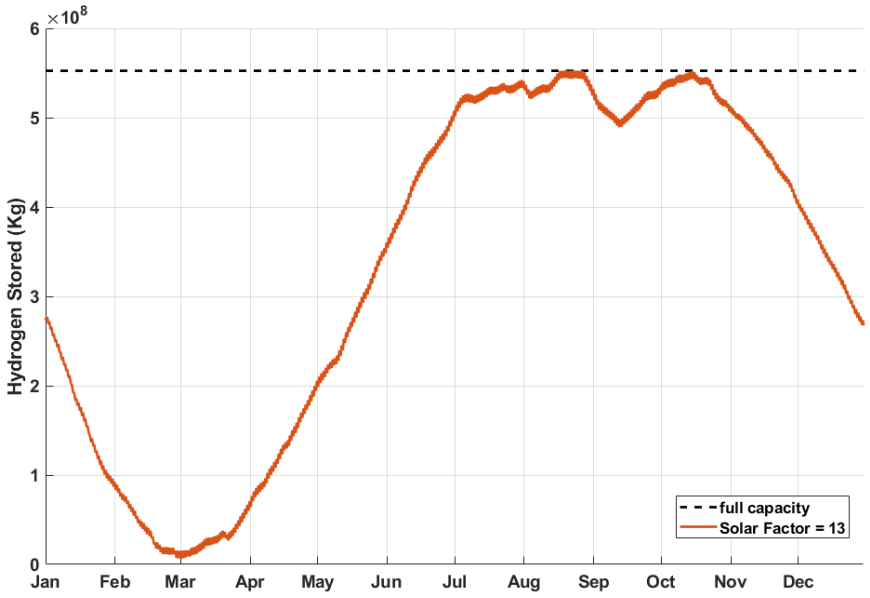

Figure 4.18. Hydrogen stored in balanced storage (solar scaling factor 13 & 50% storage capacity) - scenario 1

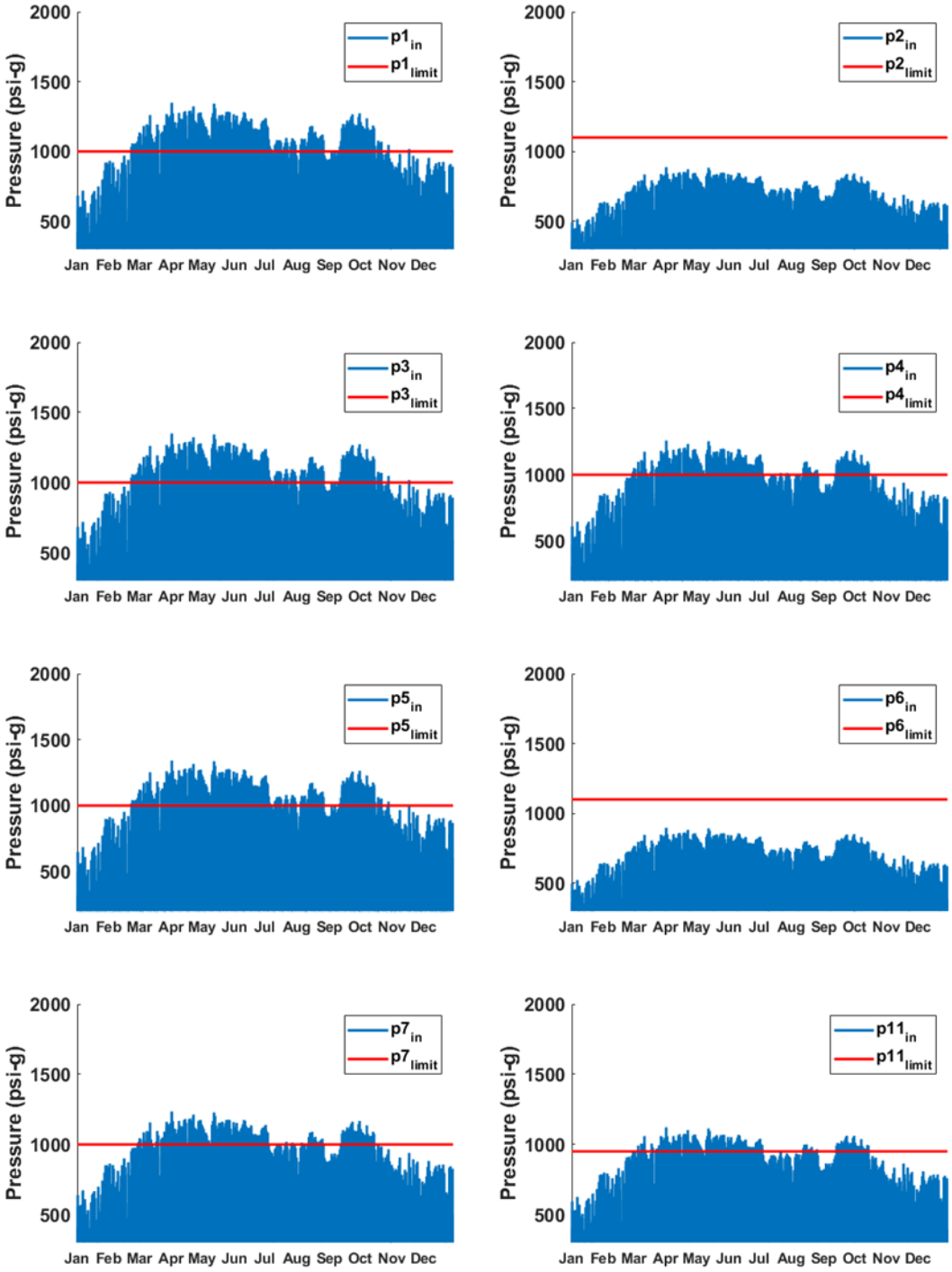

Figure 4.19. Annual pipelines pressure fluctuation for 100% hydrogen delivery - scenario 1

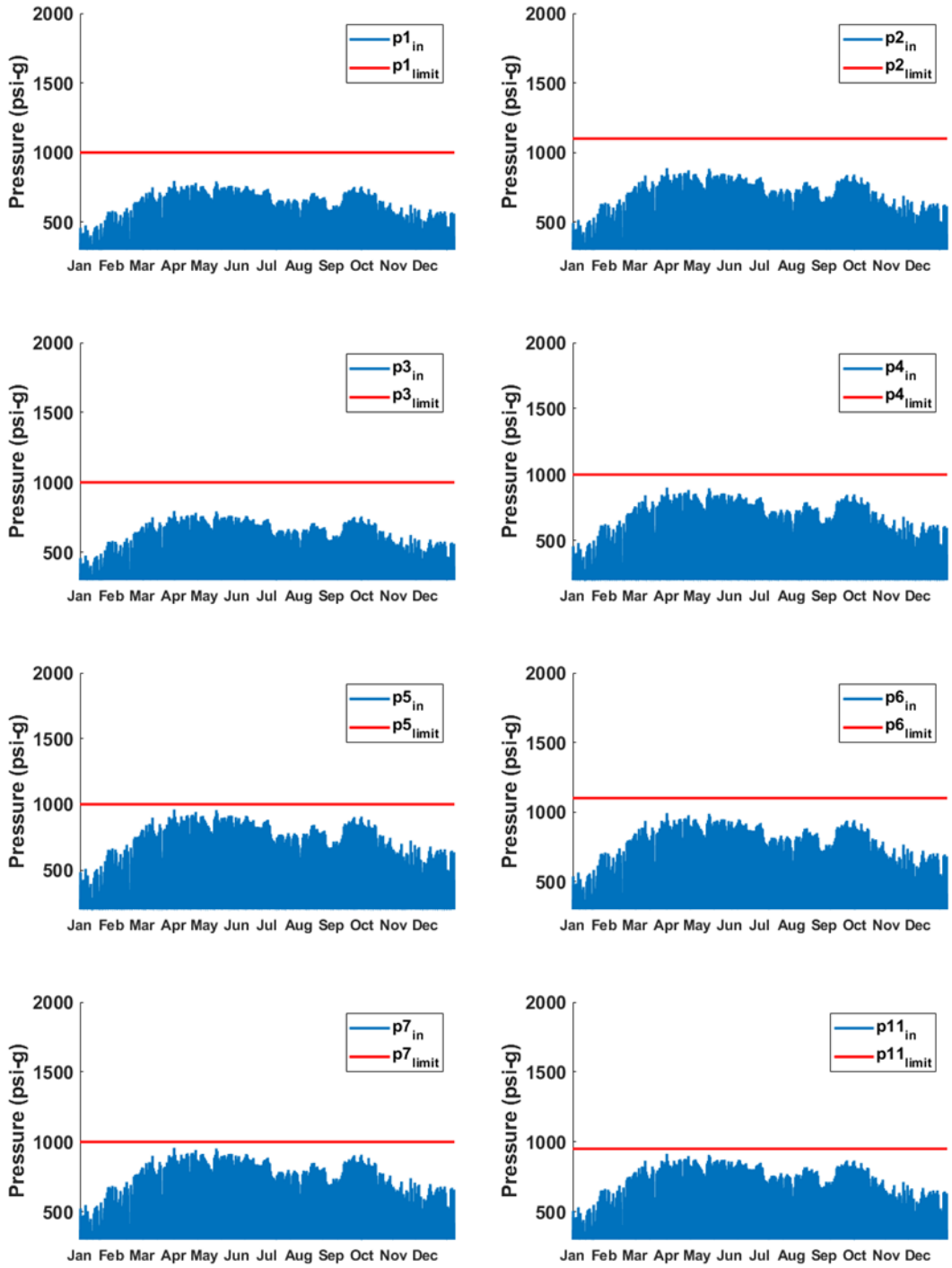

Figure 4.20. Annual pipelines pressure fluctuation for 80% of peak hydrogen delivery - scenario 1

- **Scenario 2: Solar scaling factor 17, No added storage needed**

Achieving 100% renewable energy penetration with a lower solar scaling factor (scenario 1) has several advantages, including smaller capital investment in solar farms and lower capacity requirement for the hydrogen pipeline network. The drawback of scenario 1 is the need to expand hydrogen storage capacity to balance the beginning and end inventories. In scenario 2, we assume increasing the hydrogen storage capacity is not an option and we are limited to the existing ~279 kt of underground storage in Southern California. In this scenario, solar scaling factor is increased to compensate for the limitation placed on hydrogen storage capacity. The model simulated the network with this added constraint and found that the system can achieve 100% renewable energy penetration with a solar scaling factor of 17.5. For this scenario, storage fill level of 65% ensures that the beginning and end inventories of hydrogen storage facilities are balanced. Figure 4.21 shows the simulation result of the balanced stored hydrogen for solar scaling factor of 17.5 and storage fill level of 65%. Similar to the analysis for scenario 1, the capacity of Southern California pipeline network to transport hydrogen produced from excess renewable energy is analyzed and the inlet pressures are depicted in Figure 4.22. The inlet hydrogens are then scaled down and it is observed that the current pipeline network in Southern California can only carry 60% of the peak demand while meeting the network constraint requirements (see Figure 4.23).

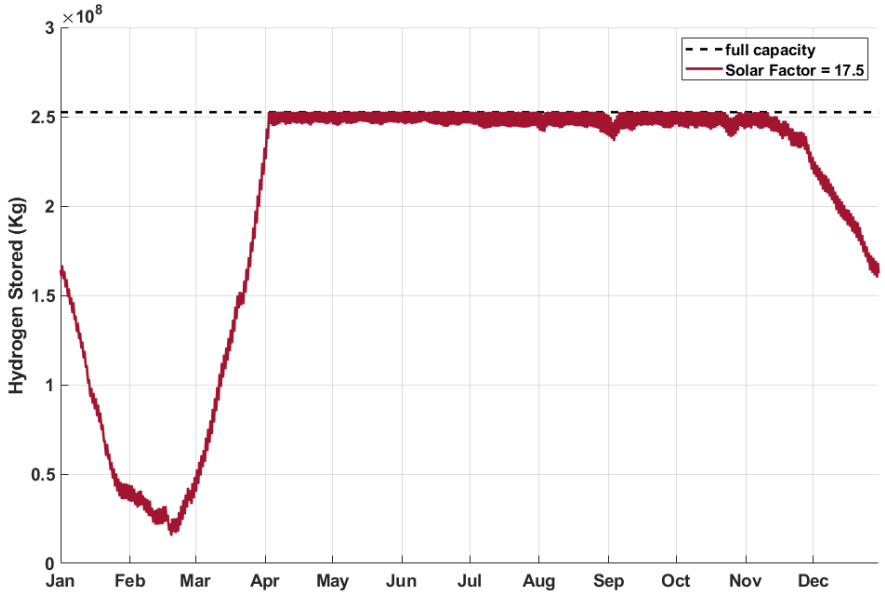

Figure 4.21. Hydrogen stored in balanced storage (solar scaling factor 17 & 65% storage capacity) - scenario 2

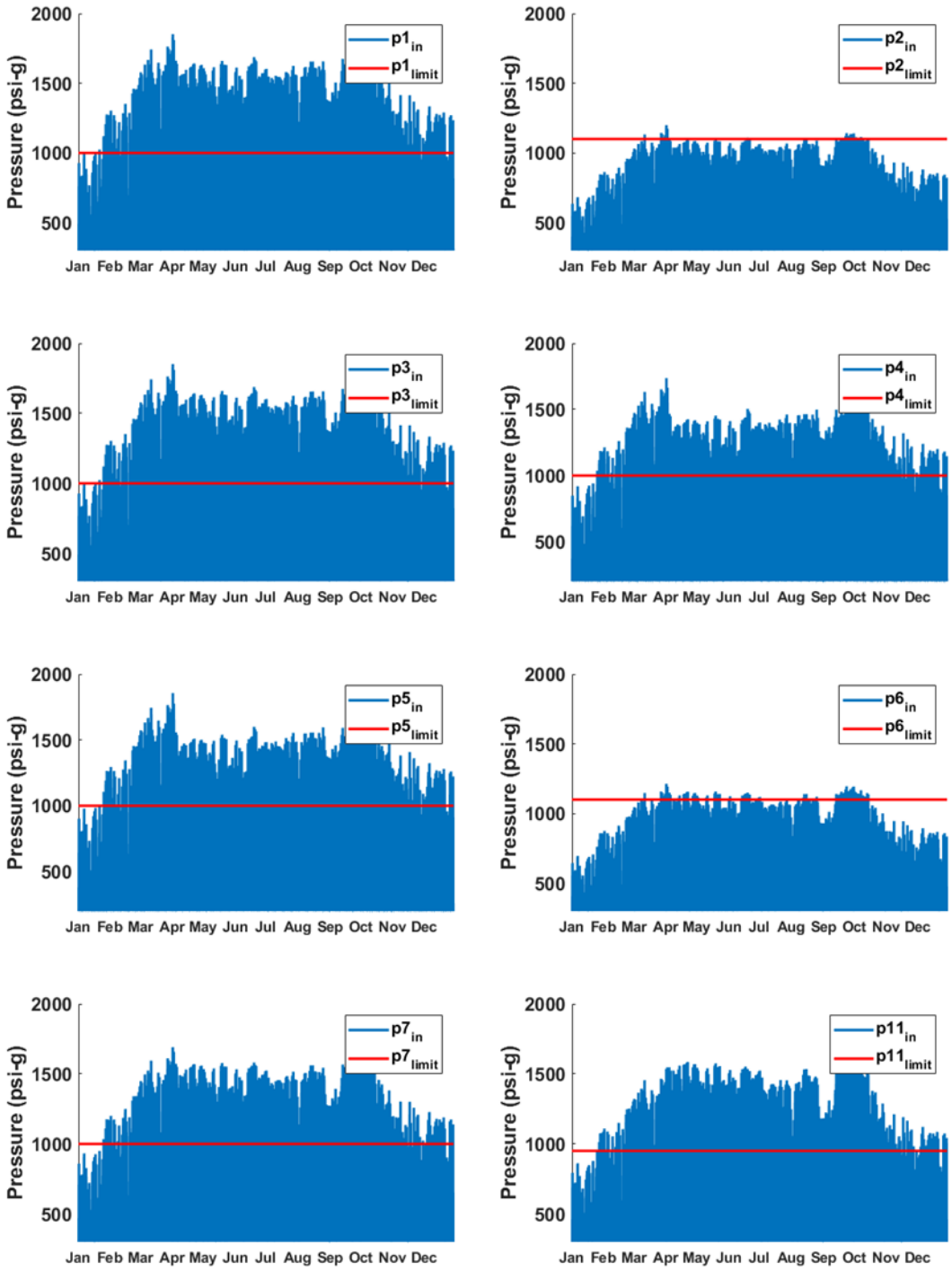

Figure 4.22. Annual pipelines pressure fluctuation for 100% hydrogen delivery - scenario 2

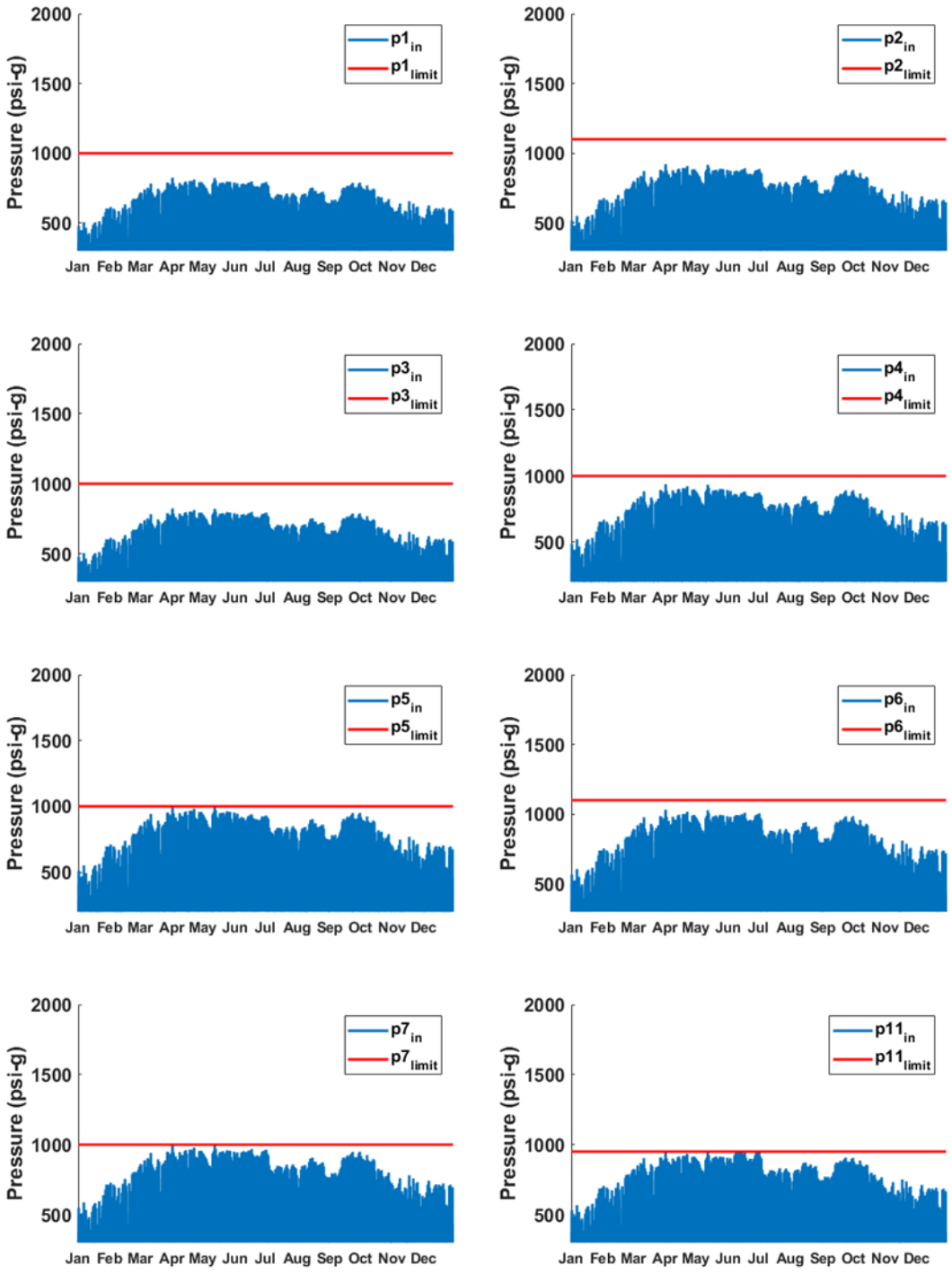

Figure 4.23. Annual pipelines pressure fluctuation for 60% peak hydrogen delivery - scenario 2

- **Scenario 3: Solar scaling factor 15, a mix of expanded storage & power curtailment**

The major drawbacks of scenario 2 is the added cost to expand renewable energy production 35% more than scenario 1, significant curtailment of produced energy, and the added capacity constrained on the hydrogen pipeline network. In the third scenario, we combine scenario 1 and 2. We increase our hydrogen storage capacity by 165kt (50% of the proposed expansion in scenario 1). With the added storage capacity, our model calculates that a solar scaling factor of 15 and a storage fill level of 55%. is enough to balance the beginning and end inventories (see Figure 4.24) and achieve 100% renewable energy penetration.

Similar to the analysis for previous two scenarios, the capacity of Southern California pipeline network to transport hydrogen produced from excess renewable energy at solar scaling factor of 15 is analyzed and the inlet pressures are shown in Figure 4.25. Same process is used to balance and scale down the hydrogen flow rates at the inlets to meet the network constraint requirements as depicted in Figure 4.26. The analysis shows that hydrogen flow rates need to be scaled down at 70%.

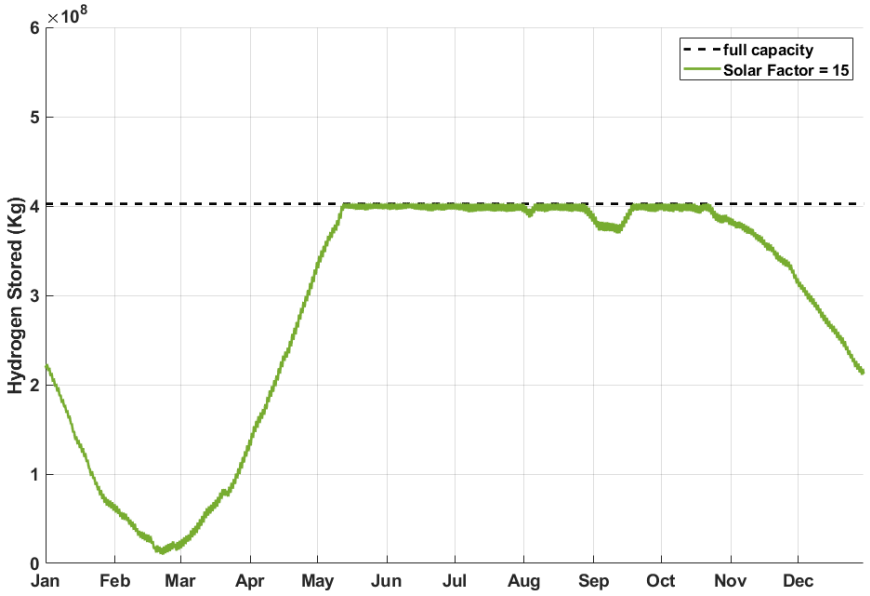

Figure 4.24. Hydrogen stored in balanced storage (solar scaling factor 15 & 55% storage capacity) - scenario 3

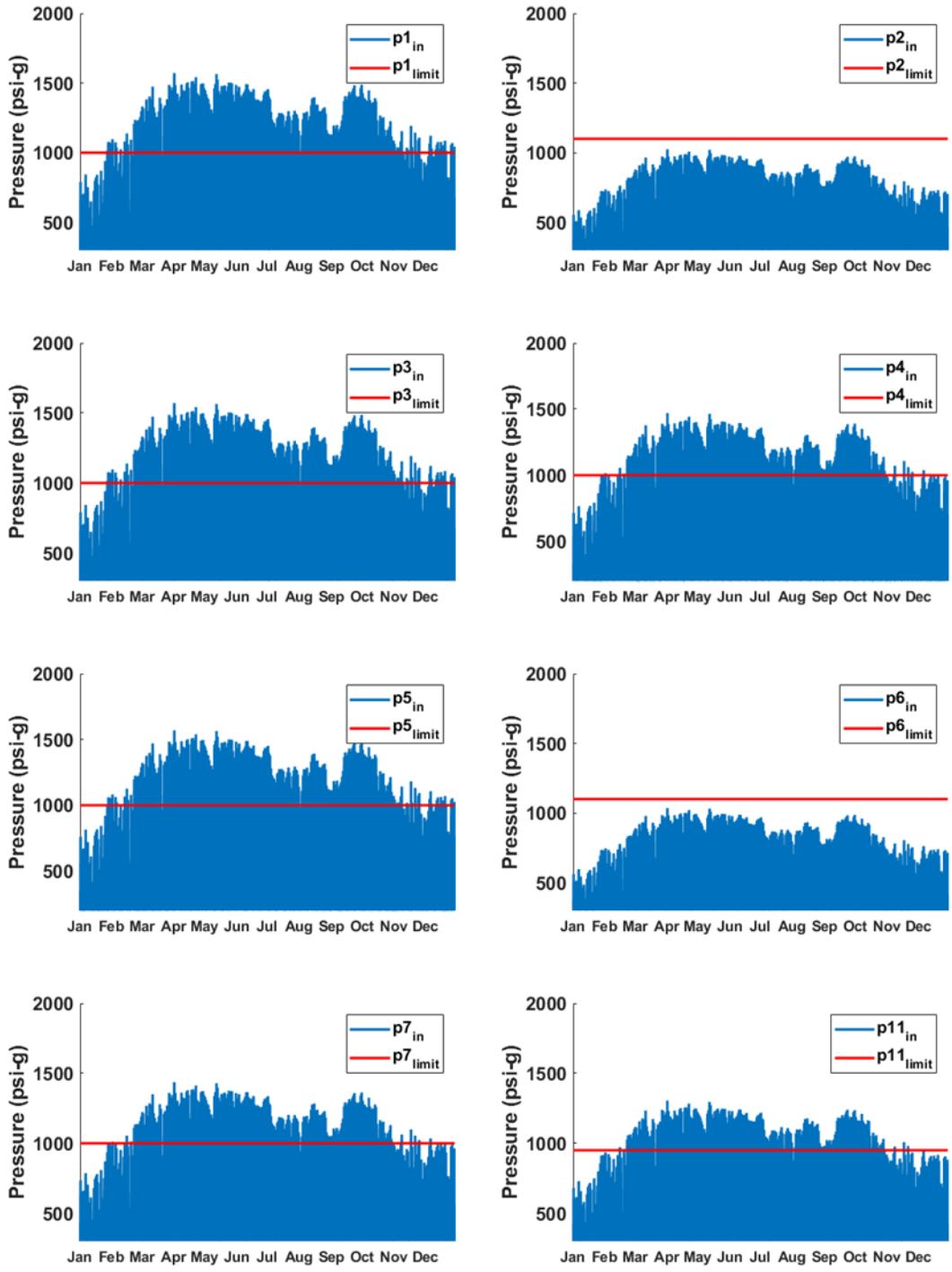

Figure 4.25. Annual pipelines pressure fluctuation for 100% hydrogen delivery - scenario 3

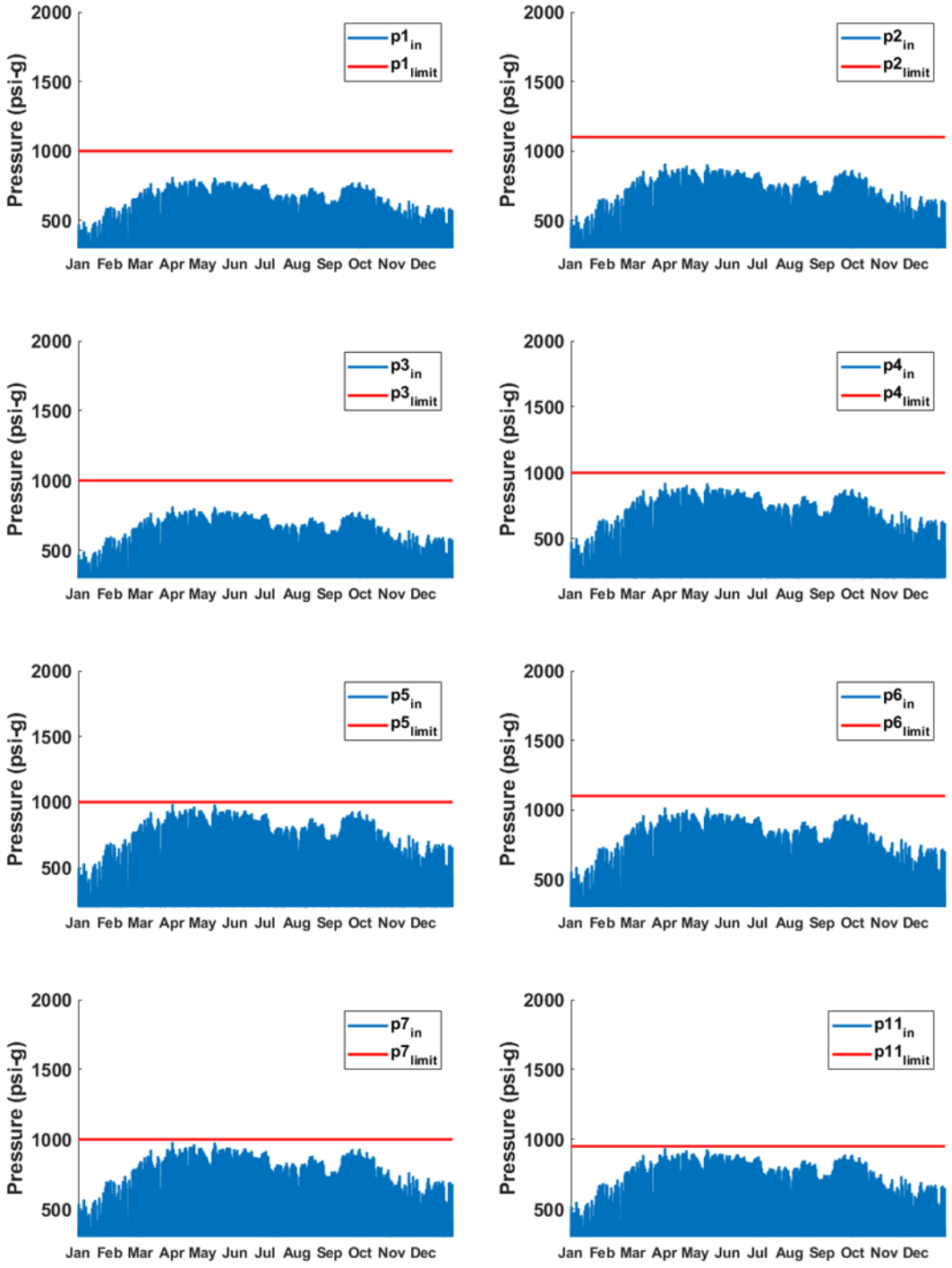

Figure 4.26. Annual pipelines pressure fluctuation for 70% hydrogen delivery - scenario 3

- **Addressing Southern California Networking Capacity Limitations**

Through all the three different scenarios discussed in the previous sections, it was noted that the Southern California network pipeline does not have enough capacity to transport the hydrogen necessary to achieve 100% renewable energy penetration. As discussed above, with solar scaling factors of 13, 15, and 17.5, the current Southern California pipeline network can only transport 80%, 70%, and 60% of the peak hydrogen demands, respectively.

Increasing the pipeline network capacity requires installation of new pipelines, which is a very expensive process and requires significant regulatory approvals. Therefore, proposals for adding pipelines to the existing network should be done selectively and addition of pipelines should be kept to a minimum. Studying Southern California pipeline networks in Figure 4.14 and pipeline pressure distributions at the inlets for scenarios 1, 2, and 3, it is concluded that adding two pipelines, one from Kramer junction to intersection of pipelines (8,10,11,12,13) and one from the intersection of pipelines (1,2,3,4,5) to the intersection of pipelines (9,10,14,15) as shown in Figure 4.27 can redistribute hydrogen mass flow rates, which increases the hydrogen transport capacity of the network. Figure 4.28 shows the pressure distribution of the proposed network for solar scaling factors of 13.

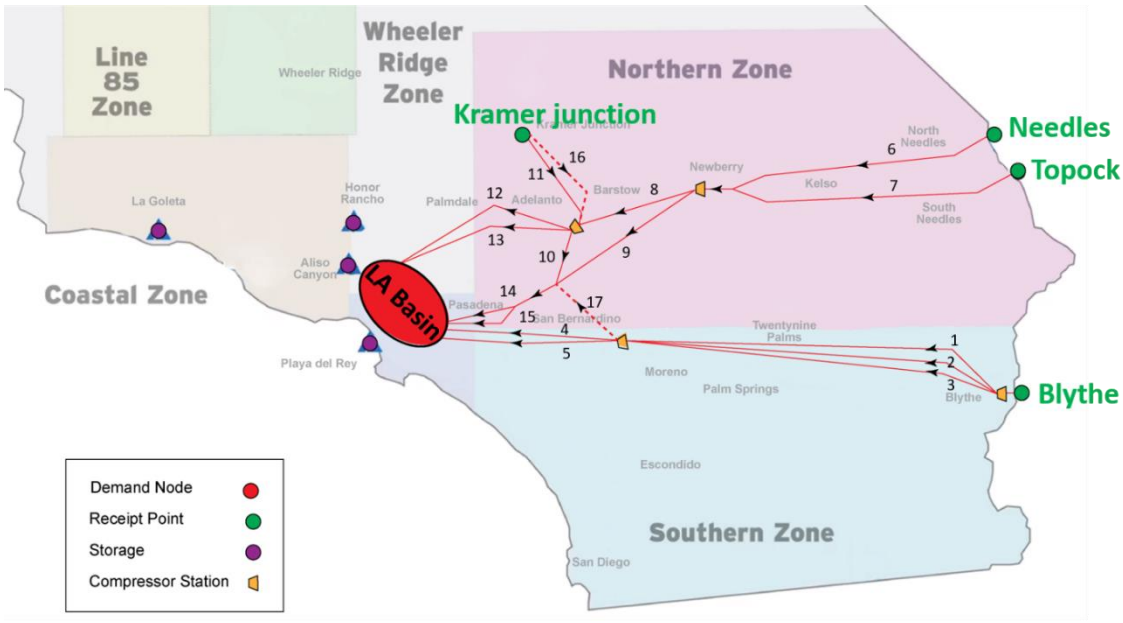

Figure 4.27. SoCalGas pipeline network - Pipeline extensions (pipe 16 & 17 - highlighted in red dashed lines) proposed to accommodate all hydrogen produced at the solar sites

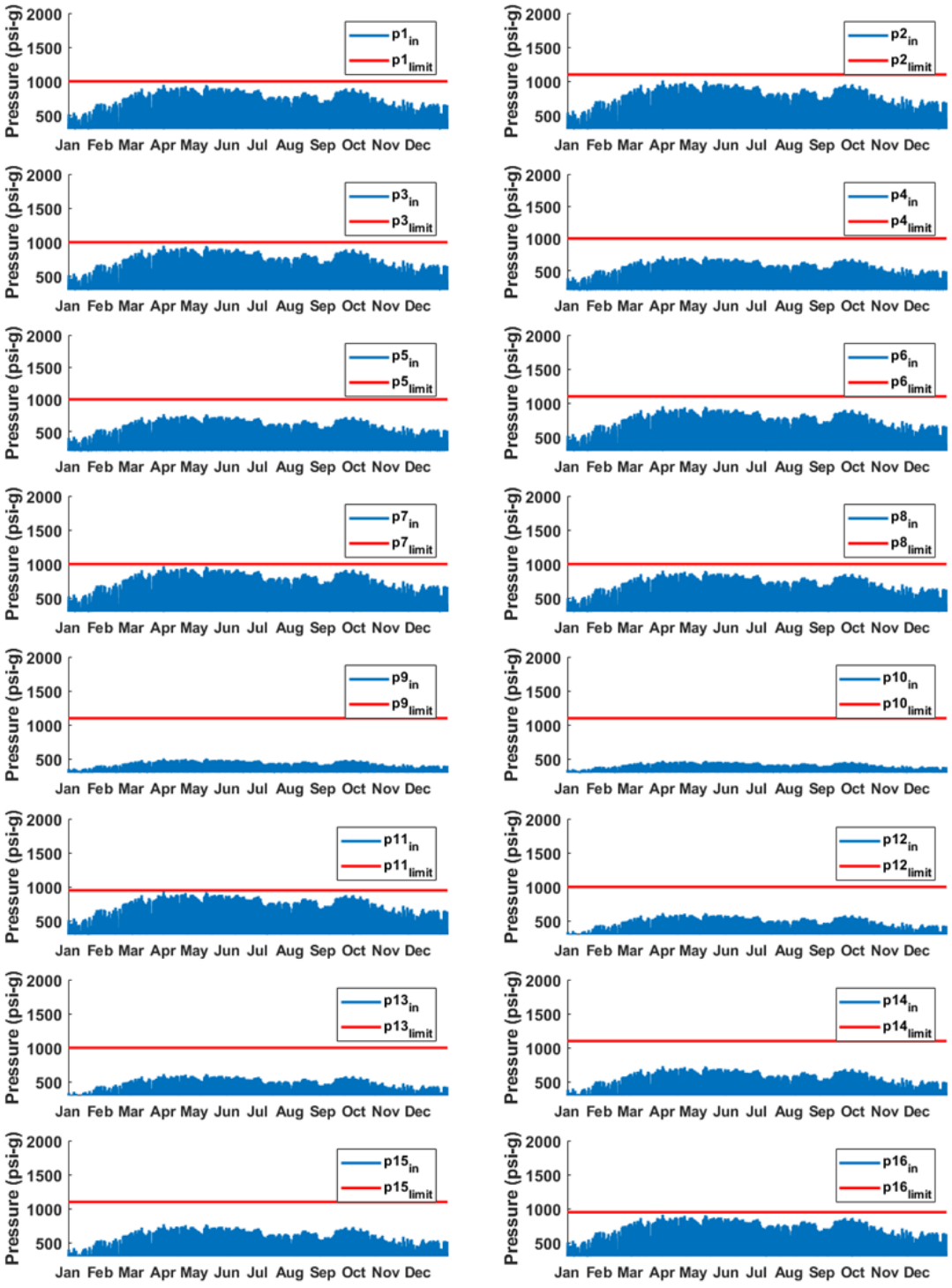

Figure 4.28. Annual pipelines pressure fluctuation for 100% hydrogen delivery - scenario 1- modified

The detail information about the added pipelines are provided in Table 4.4. The hydrogen pressure disrubution of the modified pipeline network in Figure 4.28 for solar scaling factors of 13 shows that the addition of the two pipelines can enable the current Southern California pipeline network support 100% renewable energy penetration. For solar scaling factors of 15, and 17.5, the pipeline network capacity for 100% renewable energy penetration also increases by 20%, reaching 90%, and 80% respectively.

Table 4.4. Pipeline expansions information

Pipeline #	Diameter (inch)	Length (mile)	Max Pressure (psi-g)
Kramer junction to intersection of pipelines (8,10,11,12,13)	24	32	950
2 intersection of pipelines (1,2,3,4,5) to the intersection of pipelines (9,10,14,15)	30	20	1,000

4.4.3 Preliminary Cost Analysis

In this section, a preliminary cost comparison between the three scenarios studied in this chapter is provided. The cost of moving to 100% renewable energy in Southern California provided in this section is a rough estimate and should only be relied on as relative measure between different scenarios. The cost analysis is based on the following capital cost assumptions:

- Underground hydrogen storage cost per Kg: $10, [131]
- Solar Energy Production (One Axis) per Watt DC: $1.03, [132]
- Electrolyzer capital cost per kW: $340, [131]
- Fuel cell capital cost per kW: $434, [131]

In addition to providing additional capital cost of renewable energy production and hydrogen storage facilities to reach 100% renewable penetration for each scenario, land-use requirement for solar PV installation is also calculated. The land use assumes that solar PV installation is fixed and the average power capacity per square miles is 85MW based on the analysis provided in [133]. The comparison between the infrastructure needed for the three scenarios studied in this chapter is outlined in Table 4.5, and used to calculate the capital investment needed for each scenario to reach 100% renewable energy penetration. A summary of additional capital investment costs for each scenario is provided in Figure 4.29 and shows that an additional capital investment of $131B-

$172B, depending on the choice of solar scaling factors is required to reach 100% renewable energy . This cost analysis does not factor in the additional cost needed to expand the pipeline capacity, and only estimates the additional cost of solar farms, fuel cells, electrolyzers, and underground storage facility. The analysis also highlights that using solar scaling factors of 13 compared with solar scaling factors of 17.5, which requires an increase in the storage capacity, can reduce the additional capital investment needed to reach 100% renewable energy penetration by $41B. The approximate land use required to provide enough solar power capacity at each gas receipt points is shown in Figure 4.30.

Table 4.5. Infrastructure comparison between different studied scenarios

	Scenario 1	Scenario 2	Scenario 3
	No Curtailment	Mix	No Added Storage
Solar Scale Factor	13	15	17.5
Added Solar Capacity (GW)	85	99	117
Extra land for solar (sq. mile)	999	1165	1374
Added Storage (Kt)	331	165	0
Solar Utilization Factor	100%	85%	72%
Pipeline Capacity	80%	70%	60%

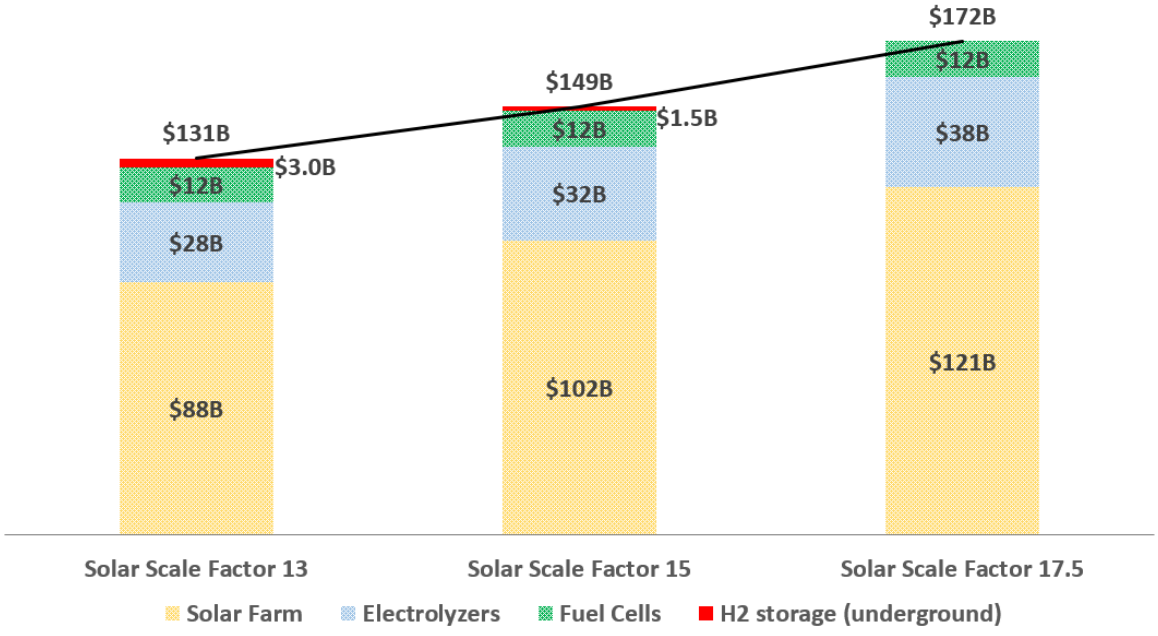

Figure 4.29. Cost estimate for three studied scenarios

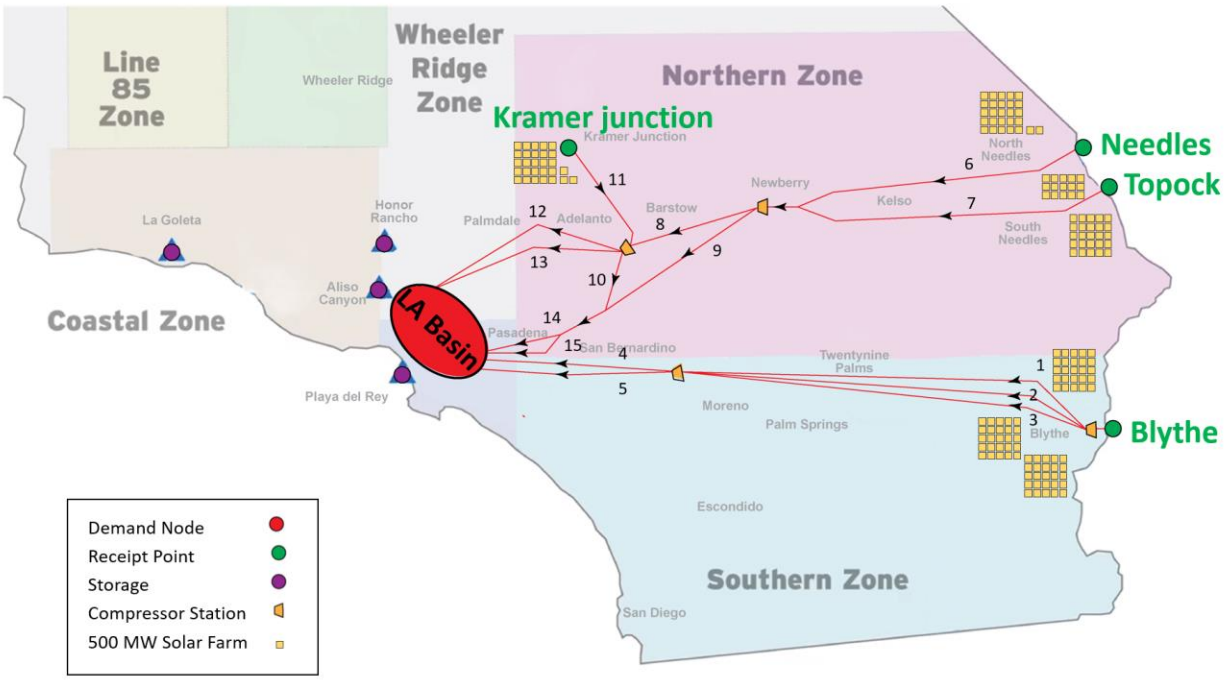

Figure 4.30. Approx. land required to provide enough solar power capacity for scenario 1- solar capacity factor of 13

4.5 Summary

In this chapter, the infrastructure of Southern California for transition to 100% renewable energy penetration was evaluated. The analysis focused on examining the amount additional renewable energy, the capacity of pipeline network, and the size underground storage that is required to meet the energy demand of Southern California over an entire year.

To accomplish this goal, a transient model was developed in MATLAB to analyze the power-to-power system. The model produces hydrogen from the excess power when demand is less than supplied power through an electrolyzer and transport the produced hydrogen to underground storage facilities using a high-pressure transmission pipeline network. The model also produces electricity using the hydrogen stored in the underground facilities through a fuel cell when demand is higher than generated power.

Several scenarios were analyzed, and the seasonal hydrogen levels in storage facilities, hydrogen pressure across pipeline network, and amount of additional renewable energy required were calculated. An optimum solution with solar scale factor of 13 was proposed with additional preliminary cost of $131B to achieve 100% renewable energy penetration in Southern California.

5 Blending Hydrogen into the Southern California Natural Gas Network

5.1 Abstract

In this chapter, the Southern California Gas network is modeled to study the impact of hydrogen injection on the operating condition and balance of the network and delivery of hydrogen-mixed gas to end customers. A realistic model of Southern California natural gas infrastructure was developed to study the impact of mixing hydrogen in the system. Southern California gas network is analyzed for scenarios where injected hydrogen is 0%, 2%, and 20%.

It is observed that the current natural gas infrastructure in Southern California can support 2% vol. hydrogen, meeting all the pipeline network pressure and compressor capacity constraints. The impact of injected 2% vol. hydrogen in various locations of the network is investigated. For the case when 2% vol. hydrogen is injected in almost all the receipt points, the hydrogen carrying capacity reaches 1.92% at the end of the year.

When percent of hydrogen injected at the receipt points is increased to 20%, the simulation model shows that one the pipelines in the network exceed the pressure limits, and one of the compressor stations exceed capacity. As a result, increasing the injected hydrogen percentage to 20% vol. requires some changes to the network.

5.2 Literature Review

Natural gas has played an increasingly important role in supplying the energy required to meet the world's energy needs. It is estimated by the International Energy Agency that natural gas constitutes 25% of world energy supply by 2040 [134]. To address the impact of climate change, several initiatives are underway across the globe to mandate a transition from fossil fuels to renewable energy.

One approach to reducing the carbon footprint of energy supply is to rely on renewable sources of energy to produce hydrogen. The produced hydrogen is then injected in the natural gas system, and the mixed gas is transported and delivered to consumers. Mixing of hydrogen from renewable sources help reduce the overall carbon footprint of the supplied energy. Overtime, the percent of hydrogen mixed in the natural gas network can be increased with the goal of substituting natural gas with hydrogen entirely in the long term.

As discussed in Chapter 1, several studies on the injection of hydrogen in the natural gas infrastructure indicates if the hydrogen mix is kept under 15%, most natural gas infrastructures and consumer appliances should be able to function with little to no modifications. 15% hydrogen mix is only an approximation, and detail and case by case analysis is needed for each natural gas infrastructure to determine the acceptable levels of hydrogen that can be safely mixed in an existing network without the need to make major changes to the system. Increasing the hydrogen mix above certain limits require major changes the gas pipelines and end consumer appliances, and therefore require a long-term plan and significant capital investment. Injecting hydrogen produced from several distributed renewable sources into a web of natural gas network results in a complex network that needs to be carefully molded and analyzed. Several studies have been conducted in the past few years to investigate the economic benefit, usefulness, and feasibility of injecting hydrogen in the natural gas infrastructure. Some of the notable works are reviewed below.

One of the earlier studies was done by Dickenson et al. [135] in 2010 to identify optimal location of injecting hydrogen in Southern Australia, and the capital and operational cost associated with it. The analysis by Dickenson did not offer a detail hydrogen injection model and instead only offered a system level analysis. Several other studies focused on assessing the economic viability of injecting hydrogen produced from renewable energy in the natural gas infrastructure. The overall assessment of various research work done on the economic assessment of injecting hydrogen concludes that government support and taxation policy is needed to create a profitable business case. For example, De Bucy's research [136] focusing on the European region concluded that "*Power-to-gas for grid injection will likely not meet viability without strong financial support, due to its high CAPEX and the low market value of the produced gas*". Schiebahn et al. [99] studied the economic benefits of injecting 5% hydrogen in the natural gas infrastructure in Germany and concluded that cost of the hydrogen used in the natural gas

infrastructure is significantly higher than the gas price. Even studies that tried to focus on more favorable business cases and included other benefits of injecting hydrogen in the natural gas infrastructure such as grid balancing still showed that mixing of hydrogen in the natural gas infrastructure is not economical [137]. As Guandalini et al. discussed in [138], government support in the form of carbon tax, and other subsidies are needed to create viable business opportunities for use of hydrogen and to promote the transition from natural gas to hydrogen. Recent legislations in California (e.g. SB 1505) [6] highlights the renewed focus of policy makers on the role hydrogen can play in reducing the reliant of California energy supply on fossil fuels. It is expected that government policies in California will favor the use of hydrogen and therefore it is important to model and characterize the impact of injecting hydrogen in the natural gas infrastructure.

The models that have been used in many of the studies reviewed above had limited ability to consider the intermittency of renewable energy, and the amount of storage needed to supply enough energy to satisfy the energy needs of the system. A review of various models and research projects that studies the injections of hydrogen into gas networks is outlined by Quarton et al. in [21]. Some of the simulation models have been created to study the characteristics of hydrogen and natural gas mixture in the pipeline network [139] and [140], where gas pressure in all the pipelines in the network and the corresponding gas flow rate are calculated. The studies use different approaches to study the impact of injecting hydrogen in the gas network in steady state and transient states. Gas flow equations are used to model the pressure drop in the pipelines. Each pipeline is characterized by the properties of the gas mixture flowing in the pipeline and the physical properties of the pipeline such as its material, and its dimensions. Kirchhoff's law is then applied at each node to ensure net flow at each node is equal to zero. Zeng et al. [141] modeled an integrated natural gas and electrical power network where energy can be converted from gas network to electrical grid and vice versa using Kirchhoff's law and energy flow equations explained above.

Pellegrino et al. [139] created a steady state simulation model to study the injection of hydrogen into an Italian natural gas network, and the model showed that up to 10% hydrogen can be blended in the network without violating any of the network constrains. Abeysekera et al. [140] created a steady state model to study a gas network with multiple hydrogen injection points and showed that by properly managing the location of injection points and amount of gas injected, network

constraints can properly be met. Similar models have been developed by Hafsi et al. [142] and Tabkhi et al. [143] studied natural gas networks injected with hydrogen. Tabkhi used a model that considered that impact of mixture of natural gas and hydrogen in the pipelines going through several compressors to compensate for the pressure drop in the pipeline and represent a more realistic network.

To better understand natural gas network behavior when it is injected with hydrogen, a detailed model of the system representing the actual natural gas network under study is desired. A few models ([144], [145], and [146]) have been developed that provide a more refined temporal resolution to accurately capture the demand and supply dynamics in the system. The refined nature of the time steps increases the complexity of simulation calculation and as a result it becomes computationally intensive to simulate the problem for longer time periods (more than a few days). Piecemeal simulation of a longer time horizon is suggested to simulate the gas network under hydrogen injection.

With rapid advancement of computational power, more realistic models representing the actual network that has high temporal resolution and at the same time covers a long enough time period (typically one year or higher) can adequately characterize the properties of a complex network. A model with a more refined temporal resolution provides the ability to better capture the supply and demand dynamics in the network. Covering a long enough time horizon in the model ensures that the network can be optimized for intersessional variabilities and determine investment needed in the pipeline network and storage systems to meet all the network constraints throughout the year.

In this chapter, we outline a detailed mix gas network model for Southern California that is developed in Python and utilizes SAInt [147] software API to perform semi steady state simulation of the network, when natural gas is mixed with hydrogen injection. The steady state model is called through the API is a simplified version of the dynamic model that was developed in Chapter 4. The model analyzes complex natural gas network of Southern California each day for the entire year. The refined resolution of the model combined with the time horizon of one year makes it possible to adequately study the behavior of the network under hydrogen injection. The model can determine if all the network and storage constraints are met when hydrogen is injected in the network. These constraints include ensuring that maximum allowable pressure in none of the pipelines in the network are violated, compressor stations are withing their working limit, and none

of the storage units are outside their allowable range. The model is used to study the impact of injecting different hydrogen mixtures at different locations.

5.3 Methodology

A combination of SAInt (Scenario Analysis Interface for Energy system) software and Python is used to model Southern California's gas pipeline network and storage facilities. SAInt is a simulation tool that uses a quasi-dynamic model to couple gas and electricity transmission networks [147]. For the purpose of this study, SoCalGas company's pipeline network is created in SAInt. In the network modeled in SAInt, two main components were used: pipelines and compressor stations. SAInt models pipeline by numerically solving continuity and momentum equations (Equation (8) and (9)) for two cases; the slow transient equation (STE) and the fast transient equation (FTE). In the STE case, the inertia term from the momentum equation (the first term in Equation (9)) was assumed to be negligible due to the fact that the change in boundary conditions are slow (which is the common operation condition in the gas system). In the FTE case, the change of the boundary conditions are rapid and therefore the effect of the inertia term was applied and approximated using an implicit time integration method (the common case when the sudden change occur in the system i.e. closure of valve and compressor station). The details of the SAInt pipeline modeling is explained in [119]. The inertia term in the momentum equation first was described in chapter four in Equation (9) as follows:

$$\underline{\frac{\partial(\rho u)}{\partial t}} + \frac{\partial(\rho u^2)}{\partial x} + \frac{\partial P}{\partial x} = -\frac{f \rho u |u|}{8} \pi D - \rho g sin\theta$$

Inertia term

Compressor stations modeled in SAInt calculates the actual power required for compression by considering the mechanical efficiency of the rotating shaft drivers (i.e. the efficiency of gas turbine is assumed to be η_m = 0.28 - 0.38 and electric η_m = 0.7 - 0.92). The equation used in SAInt to calculate the required compression power is presented by the following Equation (25), [119]:

$$Comression\ Power = \frac{\rho Q}{\eta_m \eta_s} \left[\left(\frac{k}{k-1}\right) \frac{Z \bar{R}\, T}{M} \left((r_P)^{\frac{k-1}{k}} - 1\right)\right] \quad (25)$$

Where ρ - density; Q - the volumetric flow rate; η_m - the rotating shaft driver efficiency; η_s – isentropic efficiency of compressor; k - specific heat ratio; Z – compressibility factor; M molecular weight; r_P pressure ratio; $\bar{R}$ – universal gas constant; T – temperature.

Utilizing a commercial API such as SAInt to analyze the SoCalGas network has several advantages. The model developed in SAInt can be easily scaled up to include several pipelines and present a more realistic representation of the actual network with minimum impact on the development and simulation time. As the number of pipelines increases and the network becomes more complex, the benefit of using a simulation tool becomes more evident. Furthermore, SAInt provides the quality tracking for the network which was not studied in the chapter 4. This is very important when analyzing the capacity of the gas system for injecting hydrogen to any node in the network. In the following subsection, SAInt network model will be validated with a paper published in the Applied Energy journal to verify the accuracy of the results.

5.3.1 Model Validation

In this section, SAInt network model is validated with a paper, [140], published in Applied Energy. [140] developed a steady state model to analyze the impact of hydrogen and biogas injection on the pressure and gas quality of the network. Figure 5.1 shows the gas network created by [140] to utilize the developed steady state model. The initial network consists of 14 pipes and 11 nodes. Two case studies from [140] were selected to validate the results with SAInt. The first case (NG Network) has only one natural gas supply node at node 1 and the rest are the demand nodes. The second case (NG+H_2 Network) has two supply nodes: natural gas at node 1 and hydrogen at node 12 (total 12 nodes and 14 pipelines). For the boundary conditions, pressure at node 1 assumed to be constant at 75 mbar and the volume flow rate (m^3/h) at the demand nodes were given. The goal is to evaluate the change of pressure and flow rate in the pipelines and at the supply and demand nodes in the network.

The two case studies created in SAInt is depicted in Figure 5.2 and Figure 5.3 for the NG and NG+ H_2 network, respectively. The top section of both Figure 5.2 and Figure 5.3 shows the results obtained from SAInt for the network nodes which includes node numbers, caloric value (CV) in MJ/sm^3 , flow rate (Q) in sm^3/h, and pressure (bar-g). And the bottom section provides the results for all 14 pips which includes pipes number and flow rate (Q) in sm^3/h.

The change of pressure for each node in the network for both case studies is shown in Figure 5.4. As it can be seen in this figure, there is close agreement between results obtained from SAInt and [140]. Natural gas at node 1 is supplied to the network and as it flows through the pipelines its pressure decreases from 75 mbar-g to 23 mbar-g at node 11 for the NG network and to 27 mbar-g for NG + H_2 network. The reason node 11 pressure is higher in the second case study compared to the first case study is due to the assumption that the flow rate of demand nodes remains constant. Figure 5.5 and Figure 5.6 compares the results from SAInt and [140] for case 1 and case 2, respectively. The small deviation in flow rate between SAInt and Abeysekera et al. is attributed to difference in friction factor calculation. In SAInt, different equations for friction factor calculations are available (e.g., AGA, Colebrook, and modified Colebrook). The Colebrook equation applied to calculate the friction factor of the network is presented in Equation (11) of chapter 4 (see below).

$$\frac{1}{\sqrt{f}} = -2\log\left(\frac{\varepsilon}{3.7D} + \frac{2.51}{Re\, f^{0.5}}\right)$$

Abeysekera et al. [140] used Equation (26) and Equation (27) to compute the friction factor for the low (<0.75 bar-g) and medium (0.75-7 bar-g) pressure networks, respectively. Where f is the friction factor, D is the diameter of the pipe, Re is the Reynolds number, and E is the efficiency factor for the pipe.

$$f = 0.0044\,(1 + \frac{12}{0.276D}) \tag{26}$$

$$\frac{1}{\sqrt{f}} = 5.338\,(Re)^{0.076}E \tag{27}$$

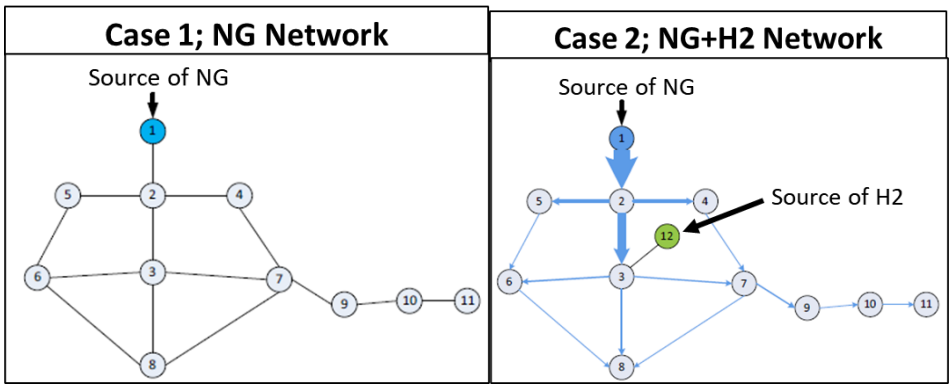

Figure 5.1. Schematic of validated paper [140]

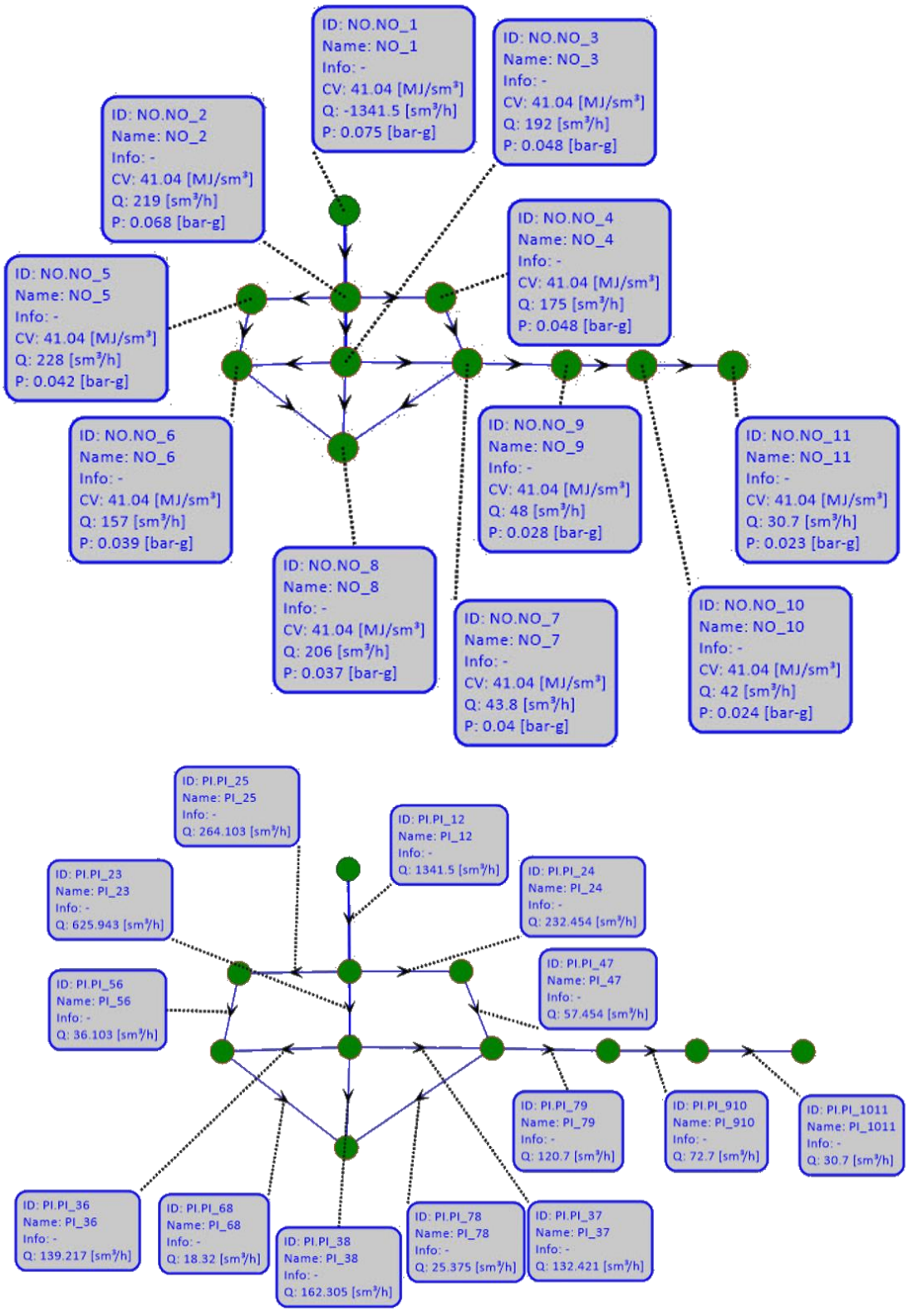

Figure 5.2. Topology of the network created in SAInt for the NG Network Case; network nodes information (top), network pipe information (bottom)

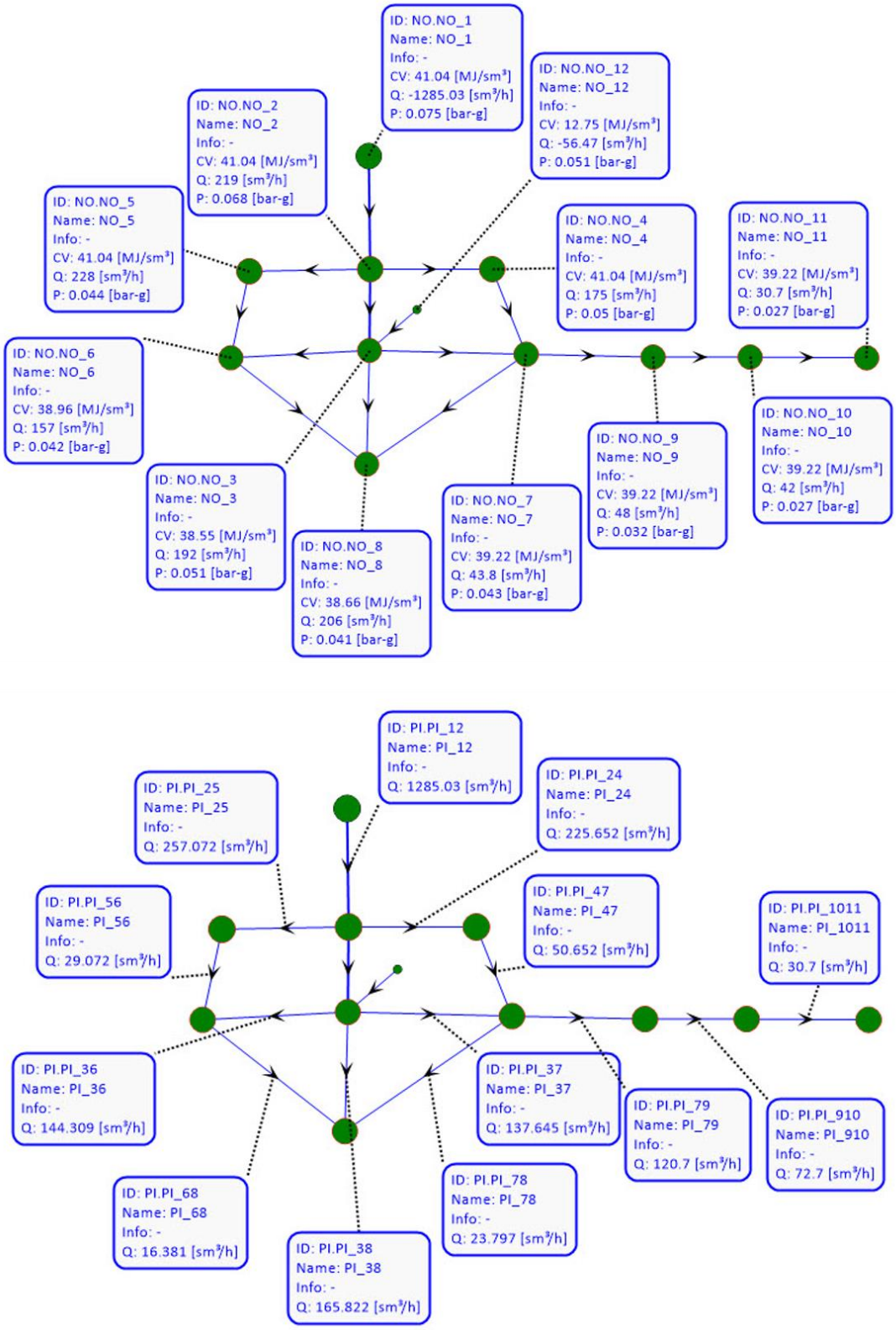

Figure 5.3. Topology of the network created in SAInt for the NG + H_2 Network Case; network nodes information (top), network pipe information (bottom)

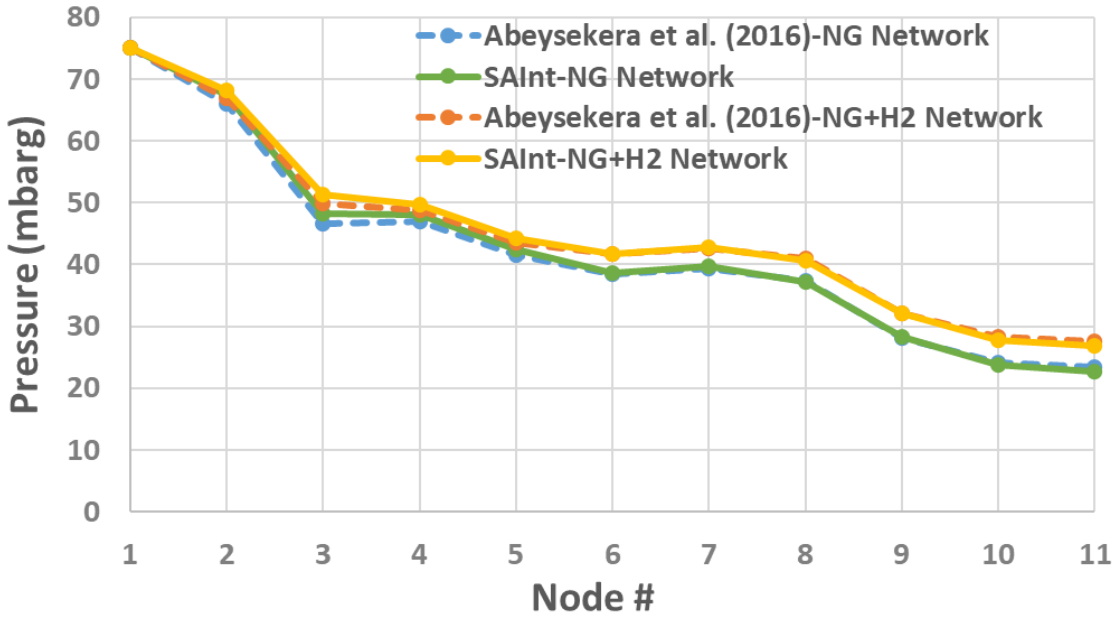

Figure 5.4. Pressure of each node in the network created in SAInt for two case studies

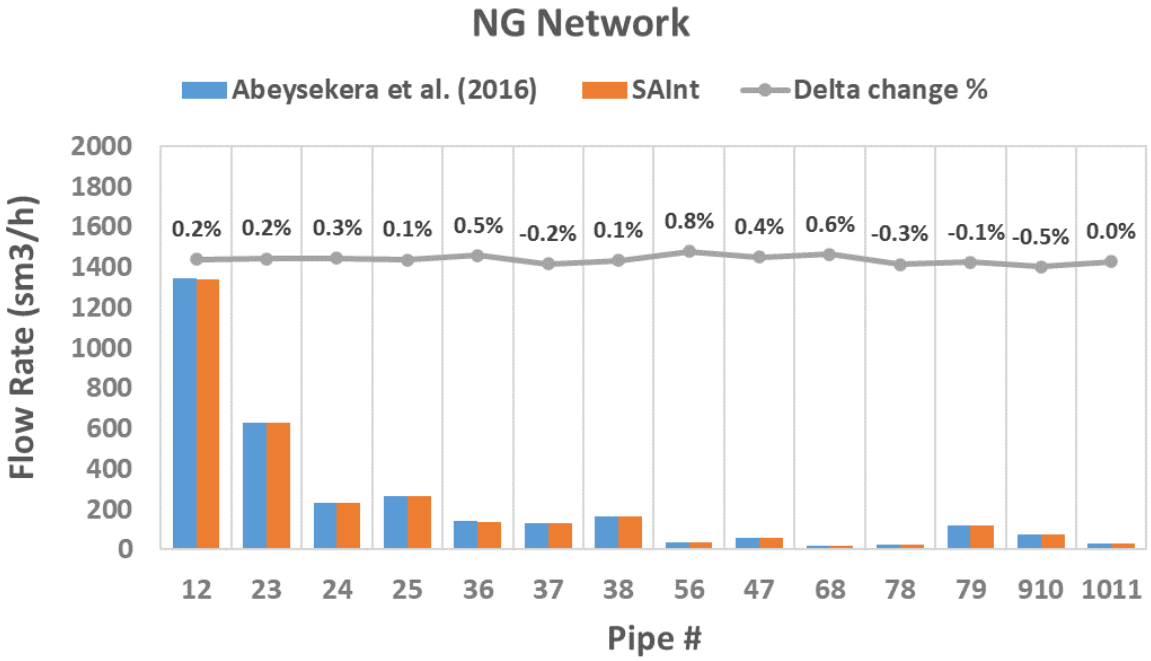

Figure 5.5. Flow rate for all 14 pipelines in the NG network

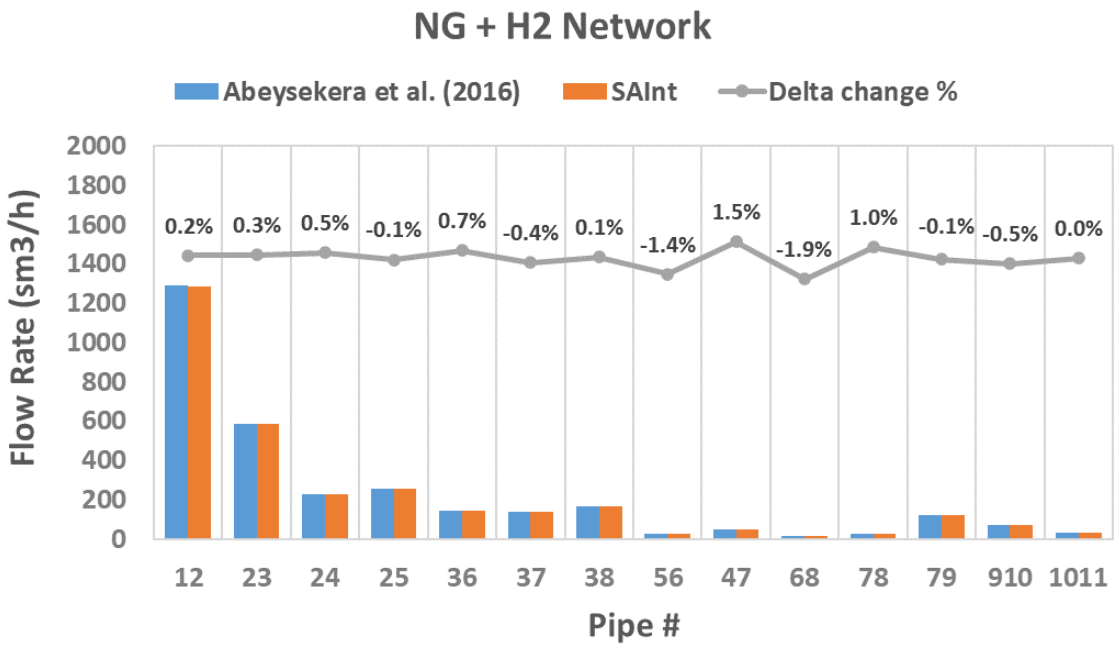

Figure 5.6. Flow rate for all 14 pipelines in the NG + H_2 network

5.3.2 Model Development

The SoCalGas natural gas system is modeled and analyzed in Python. The program calls SAInt API to simulate Southern California's realistic gas transportation pipeline network, consisting of 62 pipes. The python program performs the following functions:

- Utilizes the API of SAInt software to perform network analysis and calculate the gas flow, gas concentration, pressure, caloric value, and wobbe index at all nodes.
- Employs an iterative process to ensure the energy delivered at the demand nodes are identical to the energy demand of the network before hydrogen is injected.
- Couples the storage model with the network to calculate hydrogen and natural gas concentrations, compressibility factors, pressure, mole number, and amount of inventory in each storage at each time step both in the withdraw and injection modes.

Figure 5.7 shows the model flow diagram for analyzing the impact of hydrogen injection to the natural gas network when the hydrogen is injected at the receipt point. The analysis starts by loading the pre-defined network topology and setting the initial supply and demand values, and network and storage constraints. Network constraints include pipeline and compressor inlet and

outlet pressure while storage constraints include minimum and maximum allowable pressure, max withdrawal and injection rates, and winter minimum end of month inventory level.

If total network demand is higher than the supply, the system requires to withdraw gas from underground storage and therefore the percent of hydrogen in storage needs to be loaded in the system. The program calls the SAInt API to analyze the network and calculate the gas flow, gas concentration, pressure, caloric value, and wobbe index at all nodes. The results are used to update the hydrogen and natural gas concentrations, compressibility factors, pressure, mole number, and amount of inventory in each storage.

To update characteristics of each storage, a more detail storage model is employed. The model assumes the hydrogen injected in the storage is well mixed with the natural gas instantly in each time step. The storage model used in the program is based on the underground storage model outlined in the previous chapter with the impact of compressibility factor and component composition added to the model. The relationship between reservoir pressure (P_{res}), temperature (T_{res}), universal gas constant (R), total mole number (N), storage pore volume (V_{res}), and the compressibility factor (Z_{mix}) is provided in Equation (28).

$$P_{res} = \frac{Z_{mix}\, R\, T_{res}\, N_{res}}{V_{res}} \tag{28}$$

The values of R, T_{res}, N_{res}, and V_{res} are given or can be readily calculated as explained in the previous chapter. To calculate P_{res}, it is necessary to estimate the value of Z_{mix}; however, Z_{mix} is a function of pressure, gas composition and temperature and its value cannot be easily calculated without knowing the value of pressure. To overcome this challenge, the P_{res}/Z_{mix} ratio is first calculated from Equation (28). Next, an open source compressibility factor model provided in [125] is used to calculate the values of P_{res}/Z_{mix} for a given pressure and component concentration. Using the model, a table is created to look up P_{res} of a reservoir for a given P_{res}/Z_{mix}, and hydrogen concentration. Finally, the table is embedded in the program and is called to calculate P_{res} of each of the underground storage fields. The lookup table uses the data provided by the U.S. National Institute of Standard and Technology (NIST) [125] to solve the GERG-2008 Equation of State (EoS). The equation uses 21 natural gas components and covers the entire phases, including gas phase, liquid phase, supercritical region, and vapor−liquid equilibrium states. GERG-2008 Equation validity range is between 90K to 450K of temperature and pressure of up to 35MPA. The

range can be extended to 700K and 70MPa. This data is adopted in the ISO 20765-2 as outlined in [148]. The range covers the operating temperature and pressure needed for the developed model. Two cubic EoSs and three non-cubic models (including GERG-2008) are compared in [149]. It is concluded that GERG- 2008 provides more accurate results over a wide pressure and temperature range and is well suited for use in mixed gas scenarios, which is the use case of the model discussed in this chapter.

After the storage values are updated, the program calculates the energy delivered to the demand nodes using the hydrogen concentration at those nodes. The delivered energy is then compared with the delivered energy in the previous step to determine if the analysis has converged. After convergence is achieved, the final characteristics of the network is recorded for that time step and the hydrogen carrying capacity is calculated.

For the scenario where the hydrogen injection points are not at the receipt points, an extra block is added to program as shown in Figure 5.8. The added block creates a constraint to ensure the hydrogen concentration at the injection points does not exceed a specific value and a conditional block optimizes the network until hydrogen concentration at the injection point approaches the given value.

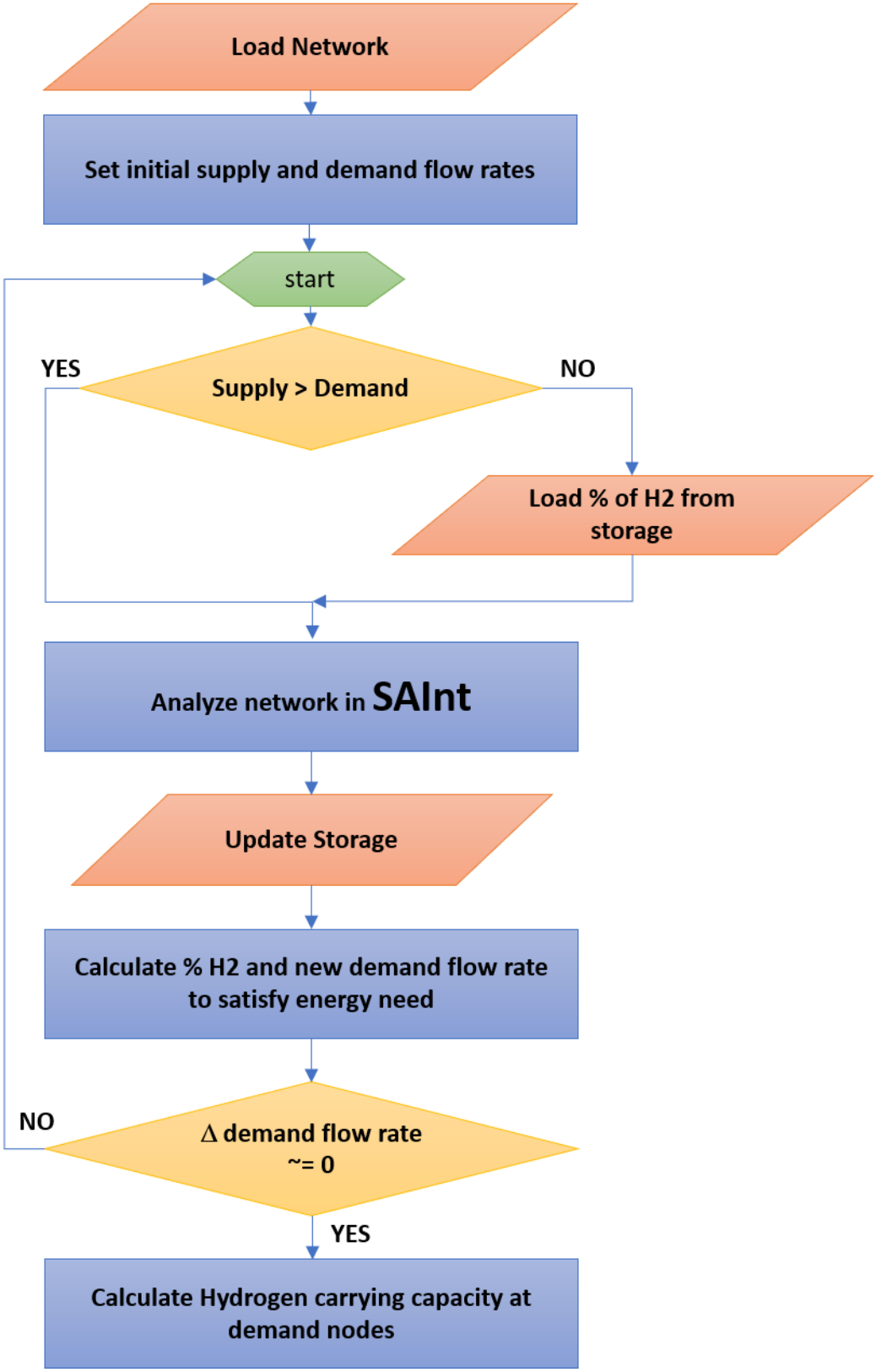

Figure 5.7. Model flow diagram for the case of injecting hydrogen at the receipt point

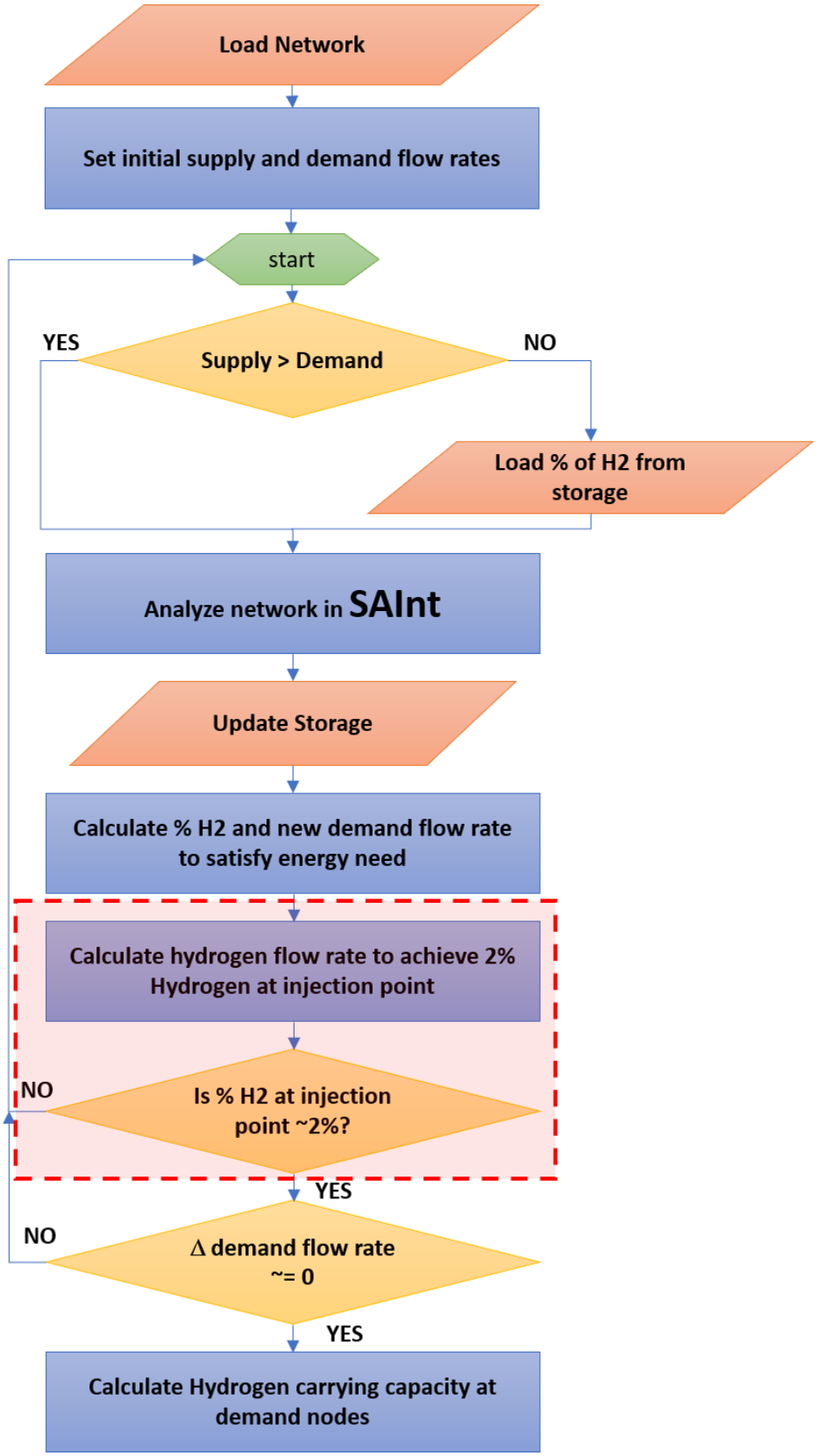

Figure 5.8. Model flow diagram for the case of injecting hydrogen NOT at the receipt point

5.4 Results and Discussion

The model developed in the previous section is used to simulate the Southern California Gas company (SoCalGas) natural gas network which includes the high-pressure transmission and distribution pipelines, compressor stations, and the underground storage facility. The entire SoCalGas company natural gas network that is analyzed is depicted in Figure 5.9. The simulated network created in SAInt is shown in Figure 5.10. The network consists of 11 supply nodes (receipt points), nine demand nodes, ten compressor stations, sixty-two pipelines, and four underground storage facilities.

SoCalGas network receipt points shown as green circles in Figure 5.10 are: California production (CP) in Line 85, North Coastal, Other; Ehrenberg/Blythe; Topock; Needles; Kramer junction; Wheeler Ridge (Kern/Mojave); Wheeler Ridge (OEHI); Wheeler Ridge (PG&E); San Diego (TGN- Otay Mesa).

The four depleted oil and gas underground storage facilities are presented with purple circles in Figure 5.10. Ranked from highest capacity are Aliso Canyon; Honor Rancho; La Goleta; Playa del Rey.

The nine demand nodes shown with red circles in Figure 5.10 are: Imperial Valley; San Diego; Los Angeles (LA) Basin; Palmdale; Ventura; Santa Barbara; S Fresno; N Fresno; Porterville . All ten compressor stations presented in Figure 5.10 are represented with yellow trapezium.

Two different analyses will be studied: the short-term plan and the long-term plan. For the short-term plan, 2% vol. hydrogen that is produced locally from solar farms or other renewable sources is injected at various locations of pipeline network. Various scenarios are examined, including when hydrogen injection locations are at the receipt points, which are far from the urban areas (customer demands), or when the injection points are closer to the demand nodes in the developer zones. For the long-term plan, the % of injected hydrogen is increased to 20% vol. The simulation results are used to analyze the capacity and vulnerability of the SoCalGas natural gas network for short and long-term plans and identify if any changes to the pipeline network is needed to ensure all the network constraints are met.

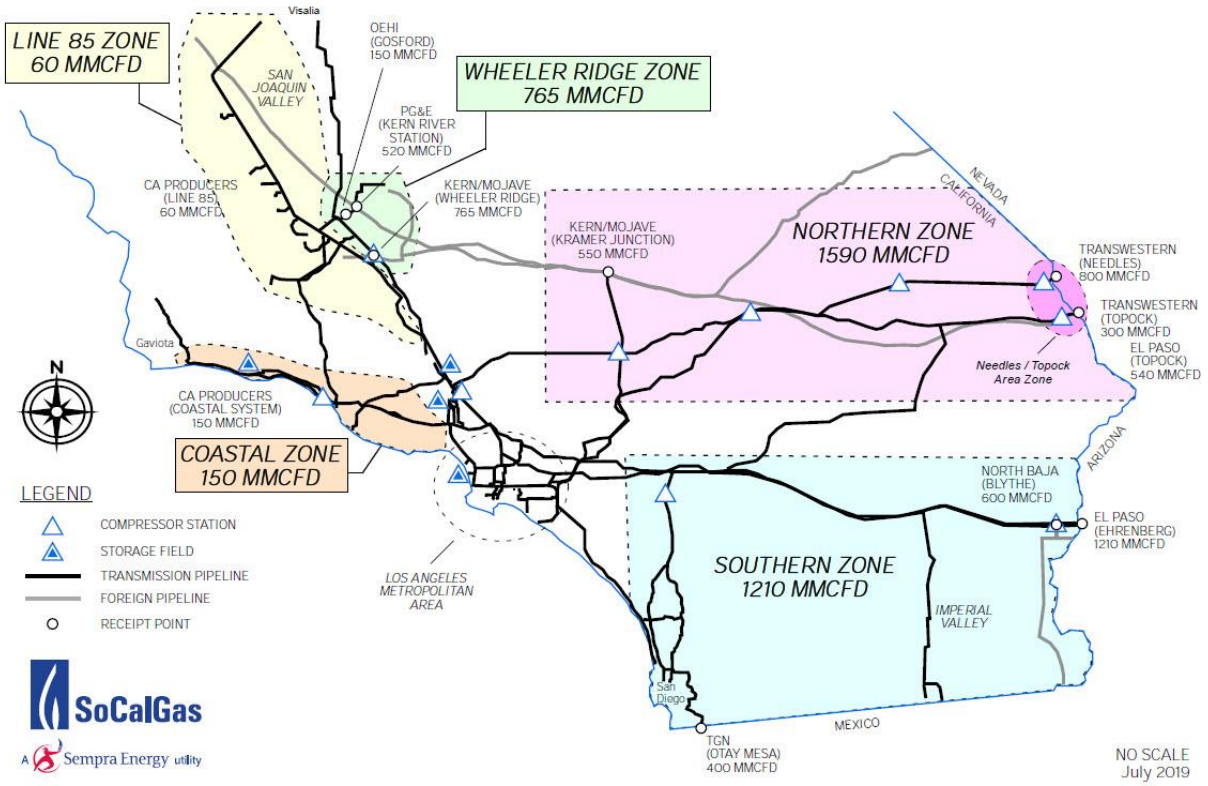

Figure 5.9. SoCalGas company system map (taken from [128])

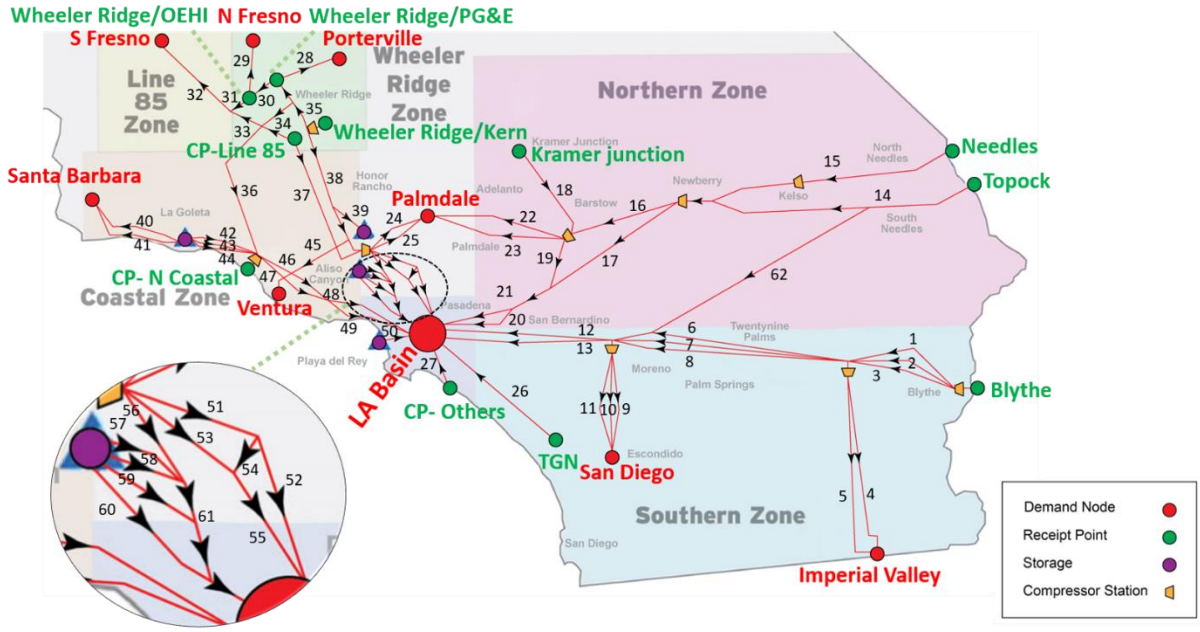

Figure 5.10. The simulated SoCalGas company network

5.4.1 Model Input

SoCalGas ENVOY [128] was used to gather the daily supply flow rate for each receipt points and the total daily demand flow rate for the whole network for 2019. The total daily supply and demand flow rate per million cubic feet (MMCFD) for SoCalGas company network is shown in Figure 5.11. Starting from January until mid-March and starting from November until the end of the year, the natural gas demand is higher than the natural gas supply. During this time period, natural gas is supplied to the customer using all four underground storage facilities that are close to urban areas. The daily demand flow rate for each node was estimated based on the energy usage reported in [150]. LA Basin is the main demand node in Southern California and is connected to the neighboring states (Nevada and Arizona) through major natural gas transmission pipelines. It is estimated that LA Basin consumes 60% of total demand in Southern California.

SoCalGas company natural gas network in 2019 receives 2.81% of its annual total gas from California production (CP) in Line 85, North Coastal, and Other receipt points; 29.6% from the Ehrenberg/Blythe points, 5.27% from Topock points, 6.01% from Needles point, 24.8% from Kramer junction point, 22.20% from Wheeler Ridge (Kern/Mojave) point, 1.16% from Wheeler Ridge (OEHI) point, 6.87% from Wheeler Ridge (PG&E) point, and 1.29% from San Diego (TGN-Otay Mesa).

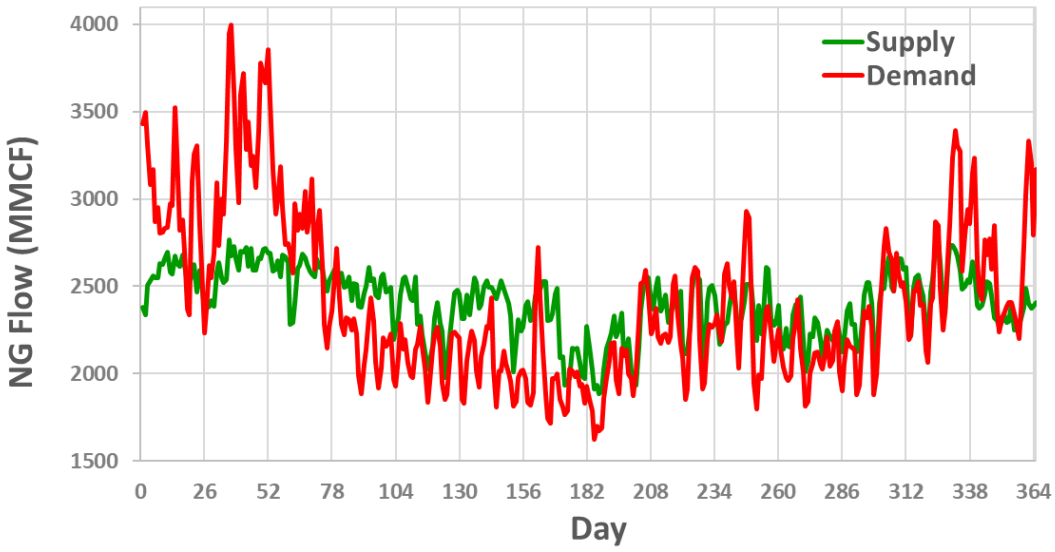

Figure 5.11. The total supply and demand daily flow rate

The actual diameter and length of 62 pipelines used in the simulated network shown in Figure 5.10 was taken from Arc GIS Hub [129] and are detailed in Table 5.1. Minimum and maximum pressure of underground storage facilities (psi-g), working and cushion gas capacity (BCF), and the maximum injection and withdraw rate billion cubic feet per day (BCFD) is taken from [124] and [151] and shown in Table 5.2. It should be noted that maximum allowable operating pressure of Aliso Canyon storage facility was reduced to 2926 (psi-g) from 3600 (psi-g) after a leak incident on October 23, 2015, which decreased its capacity to 68.8 billion cubic feet (BCF) from 86 (BCF) [152]. The new operating pressure and inventory was taken into account in the simulated network.

In order to model a more accurate representation of the storage facilities, the minimum end-of-month inventory requirement set by SoCalGas company ([153], [154]) for five months during the withdrawal season from each storage facilities was also taken into the account (see Table 5.3). Another constraints added to the simulated network model was to limit the daily maximum injection and withdrawal rate from the storage facilities as it can be seen from Figure 5.12. As it is shown in the figure, when the system is in injection mode, the daily maximum injection rate is reduced proportionally when the storage facility is at 80% inventory. Similarly, when the system is in withdrawal mode, the maximum daily withdrawal rate is reduced proportionally when the storage is at 50% inventory. These assumptions are the typical operating conditions for depleted oil and gas facilities [119].

The fill level for each storage facility at the beginning of the first day of the year was based on the total inventory at the last day of December 2018 (69.2 BCF). The inventory level for each storage was calculated relative to their capacity, considering their minimum end-of-month inventory requirements as shown in Table 5.3.

The maximum pipeline operating pressure is between 550- 1300 (psi-g) for the receipt points and the minimum operating pressure at the demand nodes is assumed to be 200 (psi-g) as shown in Table 5.4. The compressor station minimum inlet and maximum outlet pressure are set to 300 (psi-g) and 850 (psi-g), respectively as outlined in Table 5.4.

The mole fraction and caloric values in Mega Joule per meter cube (MJ/m^3) for natural gas and hydrogen is presented in Table 5.5.

Table 5.1. The actual pipeline length and diameter used in the simulated network

Pipe #	Pipe Length (mile)	Pipe Diameter (inch)	Pipe #	Pipe Length (mile)	Pipe Diameter (inch)
1	52	36	32	90	30
2	52	30	33	13.3	30
3	52	30	34	10	30
4	82	20	35	16.28	30
5	75.5	20	36	79	20
6	103.44	30	37	60	30
7	99.38	36	38	47	34
8	103	30	39	10	34
9	34.46	16	40	24.07	16
10	35.72	16	41	20.36	16
11	34.39	24	42	39.4	22
12	60.38	30	43	38	16
13	68.57	30	44	35.8	16
14	124.57	30	45	46.45	34
15	115.33	34	46	54.03	22
16	53.45	30	47	57.42	18
17	62	36	48	3.91	22
18	31.67	24	49	5.25	18
19	15.44	36	50	10	30
20	60.38	30	51	4.97	22
21	48.17	36	52	17.91	30
22	38	30	53	24.64	30
23	38	30	54	3.87	22
24	26.69	30	55	9.38	30
25	26.69	30	56	8	36
26	75.5	30	57	3.2	30
27	10	30	58	4.7	30
28	7	30	59	5.39	30
29	59.3	30	60	4.18	36
30	7	30	61	10	36
31	15.7	30	62	116.74	16

Table 5.2. Underground storage facilities information

	Aliso Canyon	Honor Rancho	La Goleta	Playa del Rey
P_ min (psi-g)	1614	1722	1173	1163
P_ max (psi-g)	2926	4400	2050	1700
Inventory (BCF)	68.8	27	21.5	2.4
Cushion gas (BCF)	81.53	21.00	24.59	4.46
Max Withdrawal Rate (BCFD)	1.86	1.00	0.42	0.40
Max Injection Rate (BCFD)	0.60	0.30	0.14	0.08

Table 5.3. End of month minimum inventory requirement

Month to End Minimum Inventory by Field (BCF)					
Storage Field	Jan	Feb	Mar	Nov	Dec
Honor Rancho	12.6	7.5	5	13.9	13.2
La Goleta	7.7	7.6	7.5	8	7.9
Playa del Rey	1.5	1.1	0.7	1.9	1.9
Non-Aliso total	21.8	16.2	13.2	23.8	23
Aliso Canyon	4.4	3.8	2.1	5.7	5.1
Total	26.2	20	15.3	29.5	28.1

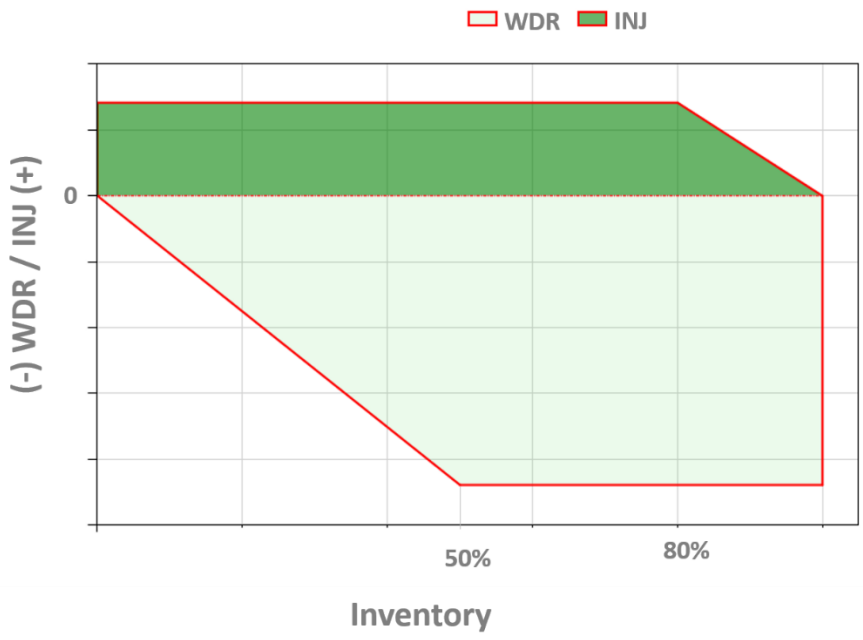

Figure 5.12. the daily maximum injection and withdrawal rate limitation

Table 5.4. Network constraints and initial conditions

Model Initial & Boundary Conditions	
Pipelines Maximum allowable Pressure at the receipt points (psi-g)	550-1300
Pipelines Minimum allowable Pressure at the demand nodes (psi-g)	200
Compressors Minimum Inlet Pressure (psi-g)	300
Compressors Maximum Exit Pressure (psi-g)	850
Aliso Canyon First Day Inventory (BCF)	33.6
Honor Rancho First Day Inventory (BCF)	22
La Goleta First Day Inventory	11.4
Playa del Rey First Day Inventory (BCF)	2.2

Table 5.5. Molar fraction and caloric value of natural gas and hydrogen

	CH_4	C_2H_6	C_3H_8	C_4H_{10}	CO_2	N_2	H_2	Caloric Value (MJ/m^3)
Natural Gas (%)	94	4.1	0.3	0.1	1	0.5	-	40.632
Hydrogen (%)	-	-	-	-	-	-	100	12.752

5.4.2 Model Results

- **Model Validation for 100% Natural Gas Case**

Before injecting hydrogen into the network, the accuracy of the model is verified to ensure the simulated network can satisfy all the network constraints. Figure 5.13 shows the pressure fluctuation for all the receipt points when 100% of the gas injected in the pipeline network is natural gas. Transmission pipeline's maximum allowable operating pressure is a function of pipe's diameter, wall thickness, and the design characteristics of the pipeline. Pipeline maximum allowable operating pressure in the SoCalGas network was estimated to vary from 550─1300 (psi-g) for pipelines diameter range from 16─36 (in). As it can be seen in Figure 5.13, the maximum pressure in the network is 933 (psi-g) at the Kramer receipt point. Figure 5.14 shows gas flow rates at the Kramer receipt point. The on-system operating capacity at the Kramer receipt point is 750 (MMCFD). The maximum allowable operation pressure is estimated to be 950 (psi-g) for this point. As it is depicted in Figure 5.14, Kramer point is at its capacity for two to three months during 2019 year.

Figure 5.15 shows the pressure fluctuation at all the demand nodes. The minimum pressure at the demand nodes at the city gates were constrained to be 200 (psi-g) The maximum allowable

pressure at the demand nodes also was constrained at 800 (psi-g), since the maximum discharge pressure of compressor stations were constrained to 850 (psi-g).

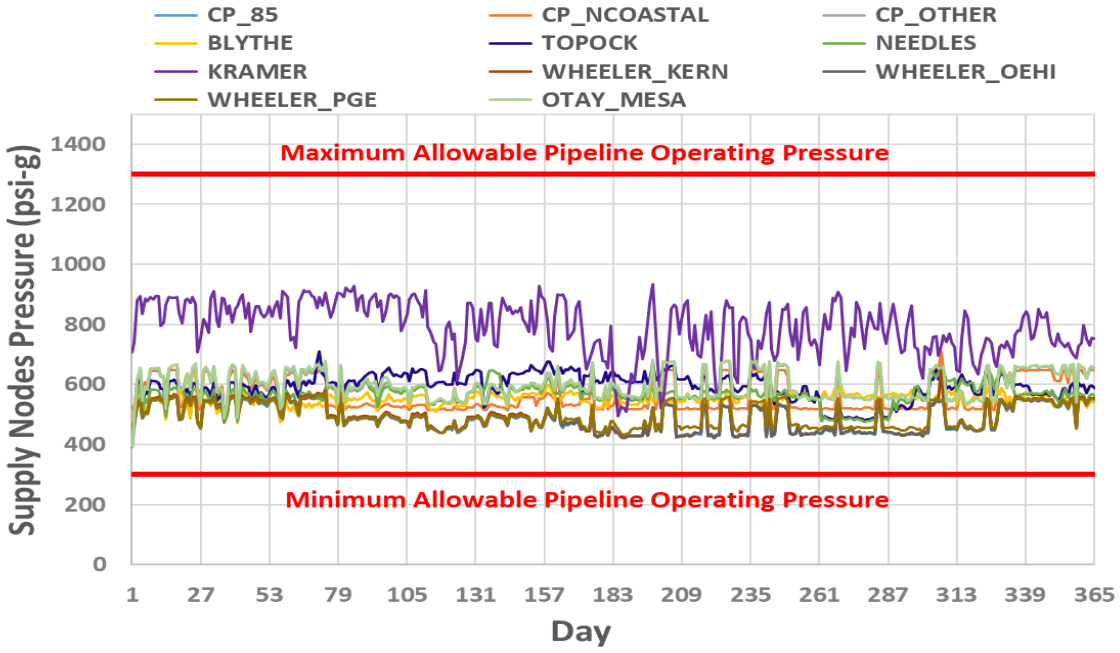

Figure 5.13. Pressure fluctuation at the receipt points

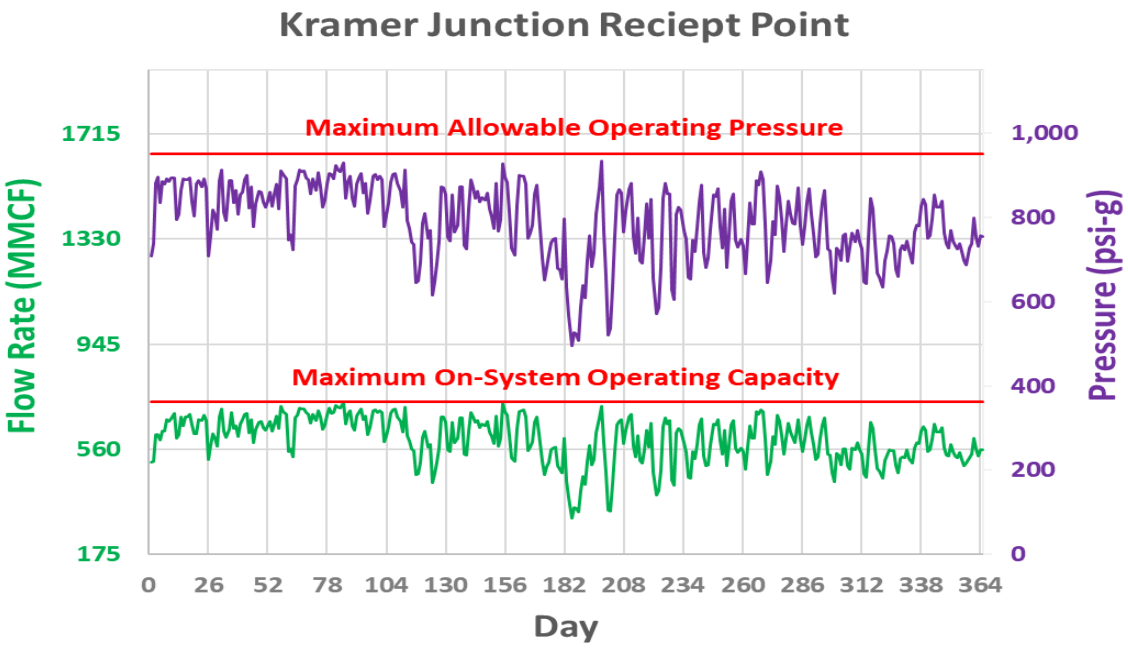

Figure 5.14. Kramer receipt point pressure and flow rate (100% NG)

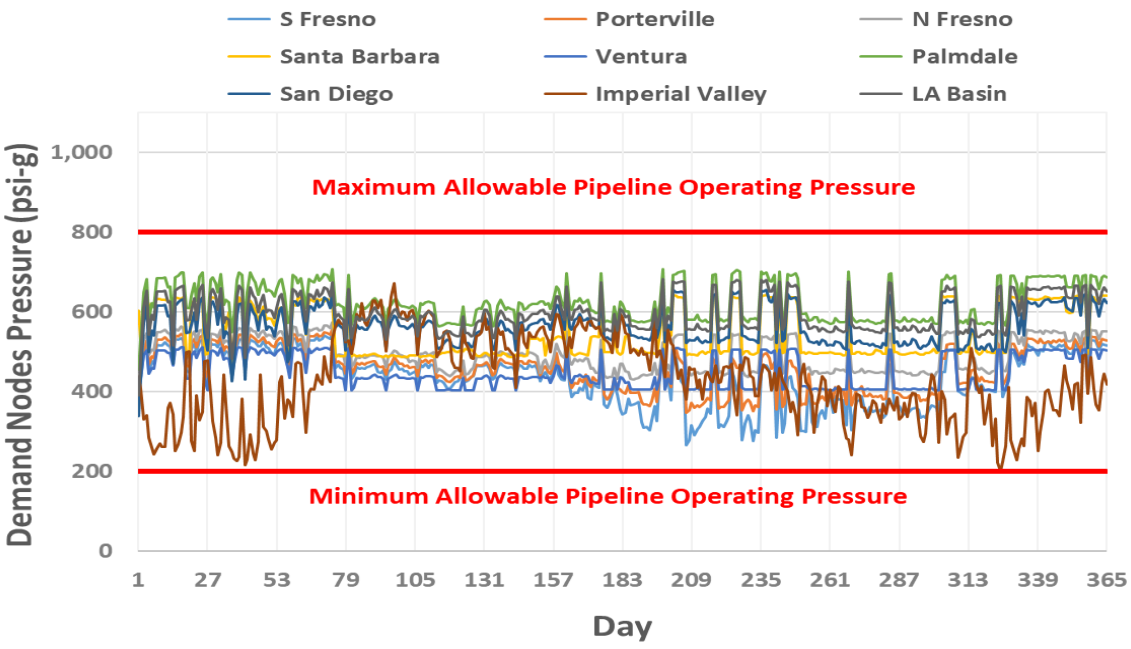

Figure 5.15. Pressure fluctuation at the demand points

For the simulated network, the flow rates at the receipt and demand points are given as an input and the model set the pressure ratios of compressor stations to ensure all the pressure constraints in the network are met. The calculated pressure ratios of compressor stations is shown in Figure 5.16.

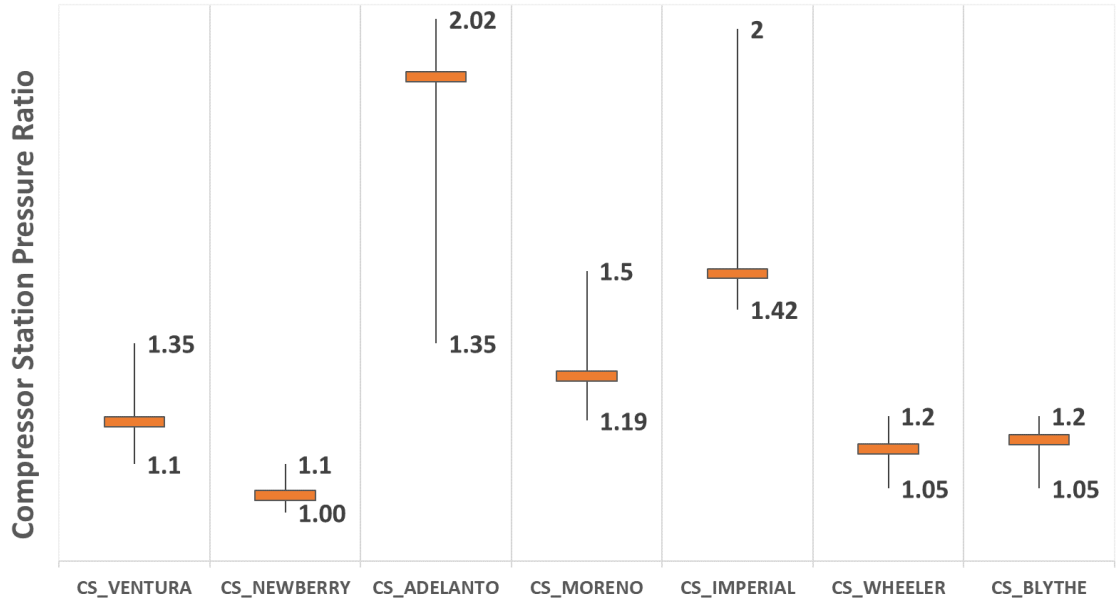

Figure 5.16.Compressor stations pressure ratio for simulated network

The operation condition of all four storage facilities also need to be analyzed in order to make sure the minimum requirements are met. Figure 5.17 shows the total SoCalGas end of month inventory of storage facilities. The 2018 end of year inventory is 69.2 (BCF) based on the data provided by SoCalGas ENVOY [128]. As it can be seen from Figure 5.17, starting from January until mid-March, storage facilities are in the withdrawal mode since the natural gas demand is higher than the supply during the winter month. Starting from April until end of October, storage fields are in the injection mode and their fill level start to rise. From November until the end of year when Southern California start to get cold, natural gas demand is higher than the supply, and hence, natural gas is dispatched from the storage. At the end of 2019, the storage fill level reaches 67.82 (BCF), which is 1.38 (BCF) less than end of 2018. The reason for this is the restriction on the Aliso Canyon filed after the 2015 leak incident. While Aliso Canyon maximum available capacity was reduced to 68.8 (BCF) from 86 (BCF) after the incident, to ensure public safety, its maximum authorized capacity indicated by the California Public Utilities Commission (CPUC) was reduced even further to 34 (BCF). In the simulated model this restriction was added to the storage constraints at the Aliso Canyon storage facility.

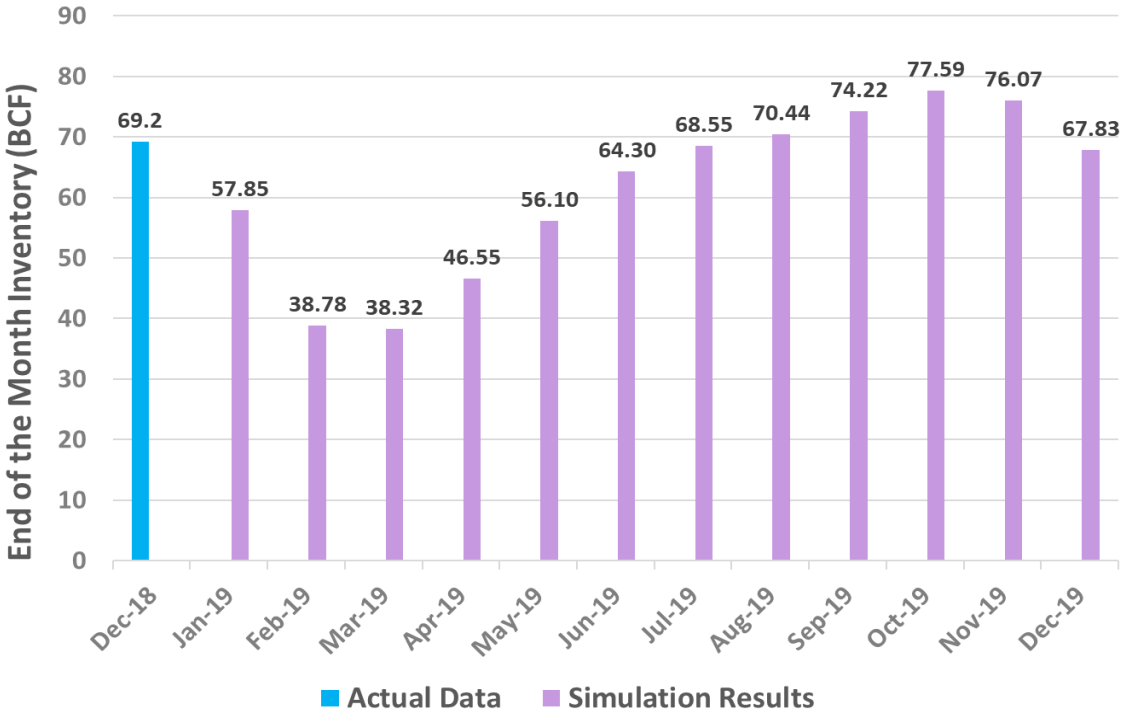

Figure 5.17. End of month storage inventory

Figure 5.18 and Figure 5.19 show the end of month inventory for the whole year and the minimum allowable inventory for five months when temperature in Southern California is below the average for Aliso Canyon and Honor Ranch. As shown in Figure 5.18 and Figure 5.19, both storage facilities meet the minimum end of month inventory requirement and Aliso Canyon inventory does not go above 34 (BCF) limit set by CPUC.

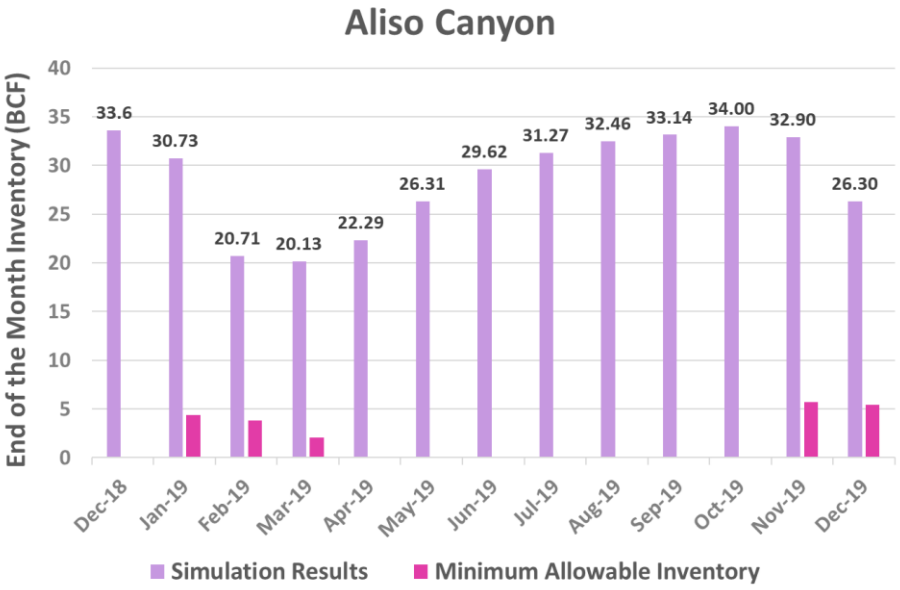

Figure 5.18. Aliso Canyon end of month and the minimum allowable inventory

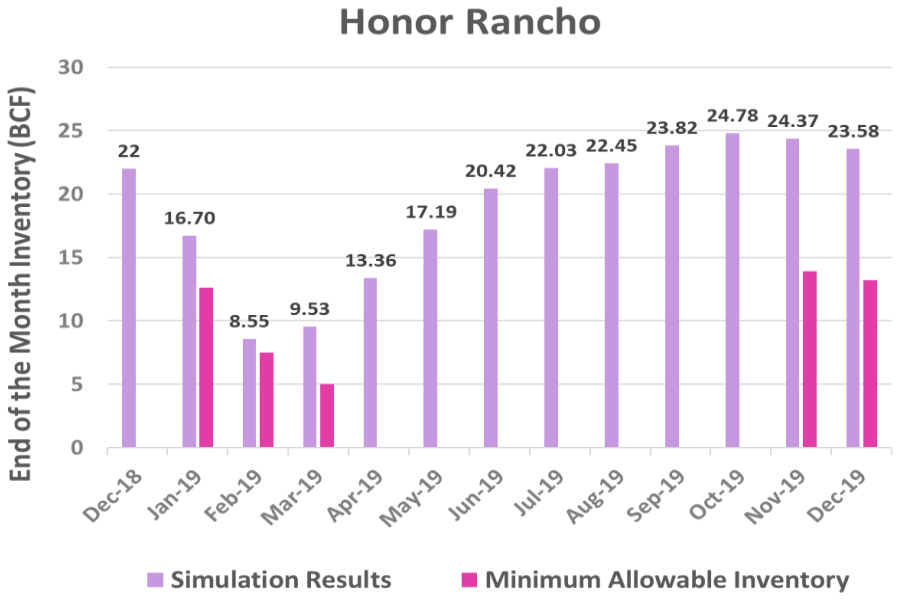

Figure 5.19. Honor Rancho end of month and the minimum allowable inventory

End of month inventory and the minimum end of month inventory requirememts is shown in Figure 5.20 and Figure 5.21. Playa del Rey maximum capacity is 2.4 (BCF) and as it is depicted in Figure 5.21, Playa del Rey reaches its maximum capcity at the end of July and can not accomodtae more gas for the rest of the season. Although Playa del Rey has the smallest capacity among the four storage fields, due to its location in LA Basin area, it plays an important role in balancing supply and demand.

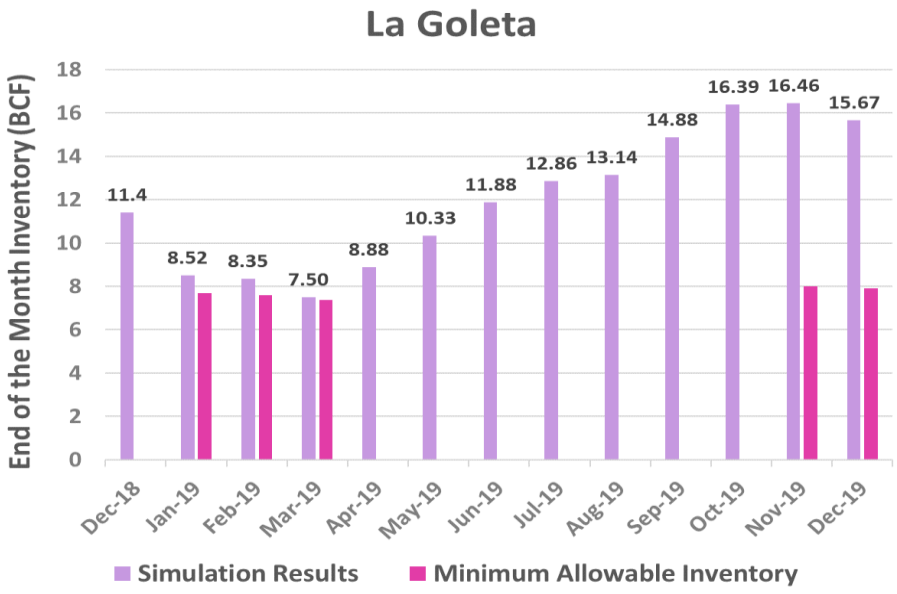

Figure 5.20. La Goleta end of month and the minimum allowable inventory

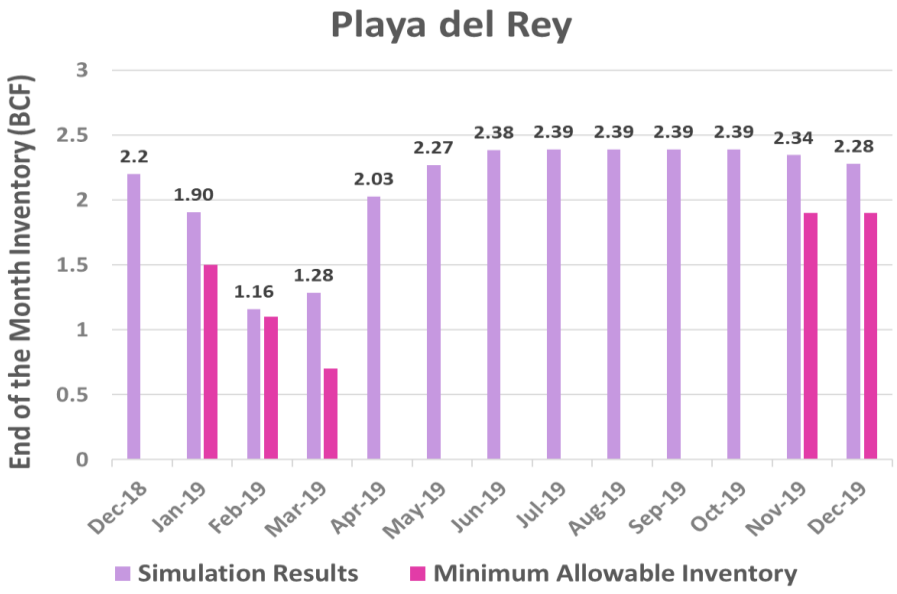

Figure 5.21. Playa del Rey end of month and the minimum allowable inventory

The above analysis confirms the modeled Southern California pipeline network can meet the energy demand when the gas in the pipeline is 100% natural gas. Next, the impact of mixing hydrogen with natural gas and injecting the mixed gas in the same pipeline with the same constraints is evaluated.

For the short-term plan, 2% vol. hydrogen is injected into the natural gas network. For this case, a few different scenarios are analyzed. First, 2% vol. hydrogen is injected at all the receipt points. To maintain constant supply of energy compared to the original system with 100% natural gas, the receipt point mix gas flow rate is increased by 1.39% while natural gas flow rate is declined 0.64%. This change in flow rates are outlined in Equation (29) and (30) with the assumption that the same amount of energy as the case with 100% natural gas is delivered to the network.

$$C_{v,NG} = 40.632\ \frac{MJ}{m^3}\ , C_{v,0.98\ NG+0.02\ H_2} = 40.075\ \frac{MJ}{m^3} \tag{29}$$

$$E_{NG} = E_{0.98\ NG+0.02\ H_2}$$

$$Q_{NG} * C_{v,NG} = Q_{\ 0.98\ NG+0.02\ H_2} * C_{v,0.98\ NG+0.02\ H_2}$$

$$\frac{Q_{\ 0.98\ NG+0.02\ H_2}}{Q_{NG}} = \frac{C_{v,NG}}{C_{v,0.98\ NG+0.02\ H_2}} = 1.0139$$

$$0.98 * Q_{\ 0.98\ NG+0.02\ H_2} = 0.98 * 1.0139 * Q_{NG} = 0.9936\ Q_{NG} \tag{30}$$

$$\frac{Q_{NG,old} - Q_{NG,new}}{Q_{NG,old}} = 0.0064\ or\ 0.64\%$$

Where C_V – natural gas caloric value; $C_{V,\ 0.98\ NG\ +\ 0.02\ H2}$ – the caloric value of the mixture of 98% natural gas + 2% hydrogen; Q_{NG} – volumetric flow rate of natural gas; $Q_{0.98\ NG\ +\ 0.02\ H2}$ – volumetric flow rate of the mixture of 98% natural gas + 2% hydrogen. Other hydrogen injection points in developer zones are also analyzed to calculate the parentage of hydrogen that is delivered to the demand nodes (referred to as hydrogen carrying capacity).

For the long-term plan, 20% vol. hydrogen is injected at all the main receipt points of the natural gas pipeline network in order to evaluate the capacity of the SoCalGas network for handling higher percent of hydrogen and determine whether any of the constraints for the pressure and flow dynamics in the pipelines and storage facilities are violated. Injecting 20% vol. hydrogen in the receipt points requires 15.91% mass flow rate increase of the mixed gas to ensure the same energy

is supplied to the network while Natural gas flow rate at the receipt point is decreased by 7.27% (Similar calculation as shown in Equation (29), $C_{V,0.8\ NG\ +\ 0.2\ H2}$ = 35.056 $\frac{MJ}{m^3}$; caloric value of the mixture of 80% NG +20% H_2).

- **Model Case Studies**

In order to analyze the impact of hydrogen into the SoCalGas pipeline and storage facilities five scenarios are analyzed:

- Scenario 1: Hydrogen is injected into five receipt points at 2% vol. (96% of Supply)
    - Blythe
    - Topock
    - Needles
    - Kramer Junction
    - Wheeler Ridge (Kern/Mojave, OHEI, PG&E)
- Scenario 2: Hydrogen is injected into three receipt points at 2% vol. (41% of Supply)
    - Blythe
    - Topock
    - Needles
- Scenario 3: Hydrogen is injected into two receipt points at 2% (55% of Supply)
    - Blythe
    - Kramer Junction
- Scenario 4: Hydrogen is injected into two receipt points at 2% vol. and Aliso Canyon Field
    - Blythe
    - Kramer Junction
    - Aliso Canyon Storage
- Scenario 5: Hydrogen is injected into five receipt points at 20% (96% of Supply)
    - Blythe
    - Topock
    - Needles
    - Kramer Junction
    - Wheeler Ridge (Kern/Mojave, OHEI, PG&E)

- **Scenario 1: Hydrogen is injected into five receipt points at 2% vol.**

In the first scenario, 2% vol. hydrogen is injected to five receipt points that supply 96% of the gas in the network. Three California production nodes and one receipt point that brings natural gas from Mexico (TGN- Otay Mesa) were not injected with hydrogen to simplify the analysis (4% of the total annual supply). Since hydrogen is injected into the receipt points 2% by volume, demand nodes receive between 0-2% hydrogen by volume depending on their location. Hydrogen to natural gas percentage and percent increase of mass flow rate at the demand nodes is depicted in Figure 5.22 (top and bottom, respectively). As can be seen from the figure, six nodes (Porterville, N and S Fresno, Palmdale, San Diego, and Imperial Valley) received 2% vol. hydrogen as they are directly connected to the receipt points in which supply 2% hydrogen.

Figure 5.23 shows hydrogen carrying capacity as well as the net injection/withdraw from the storage facilities. During the first three months of the year when the gas demand is higher than supply, gas is withdrawn from the storage fields and as a result less hydrogen is distributed to the network since only natural gas is withdrawn from the storage and is mixed to the network. Once the gas supply (which has 2%vol. hydrogen) is higher than the demand, the net injection/withdraw start rising due to the increase effect of hydrogen concentration the receipt points.

Figure 5.24 presents how each storage field is depleted and filled during the entire year as well as how the pressure in the storage follows the inventory. Hydrogen concentration in the storage field changes as storage level changes. Playa del Rey is the first facility that reaches its maximum capacity beginning of June (day 183) since it has the lowest capacity among all four fields (2.4 BCF). This facility is in the LA Basin region and plays an important role in balancing the supply and demand in the LA Basin area. The figure shows that when storage is in the withdrawal mode, the hydrogen concentration does not change and stays flat. Aliso Canyon starts at 33.6 (BCF) at the beginning of the year and reaches 26.3 (BCF) at the end of the year. Honor Rancho fill level at the beginning of the year was 22 (BCF) and reaches 23.11 (BCF) at the end of the year. La Goleta fill level fluctuates between 11.4 (BCF) and 16.78 (BCF) from January 1st to December 31st, 2019.

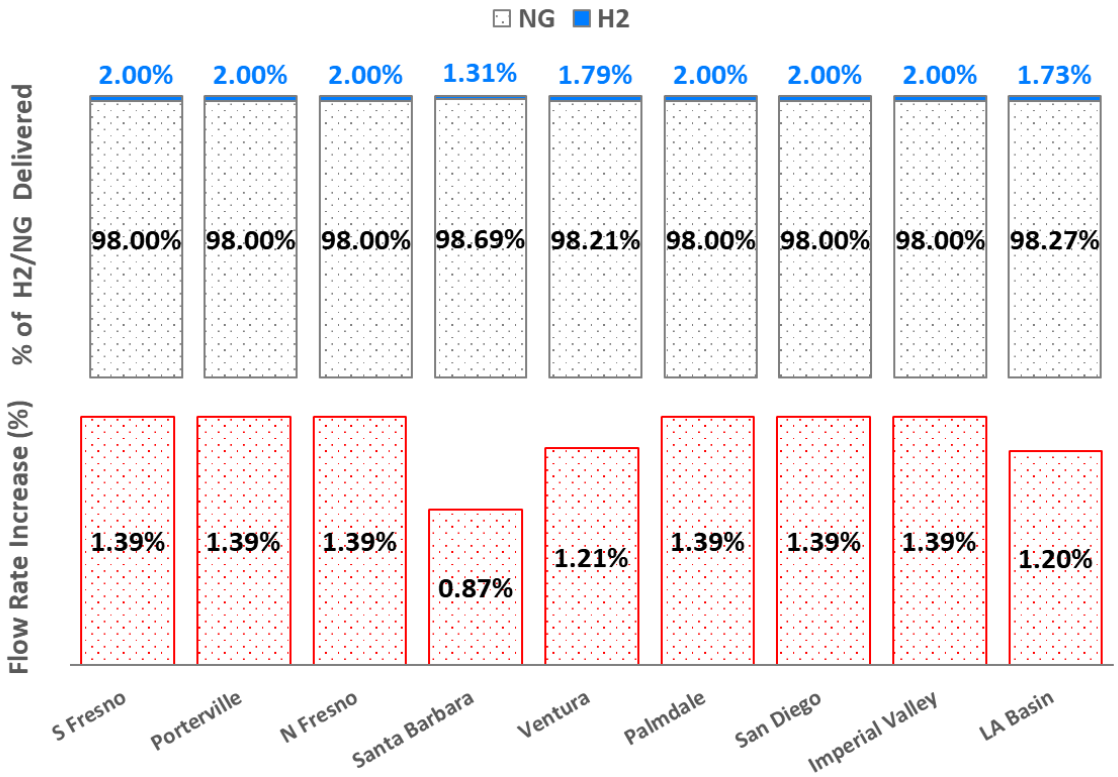

Figure 5.22. Hydrogen to natural gas percentage (top) and percent increase of flow rate (bottom) at the demand nodes – scenario 1

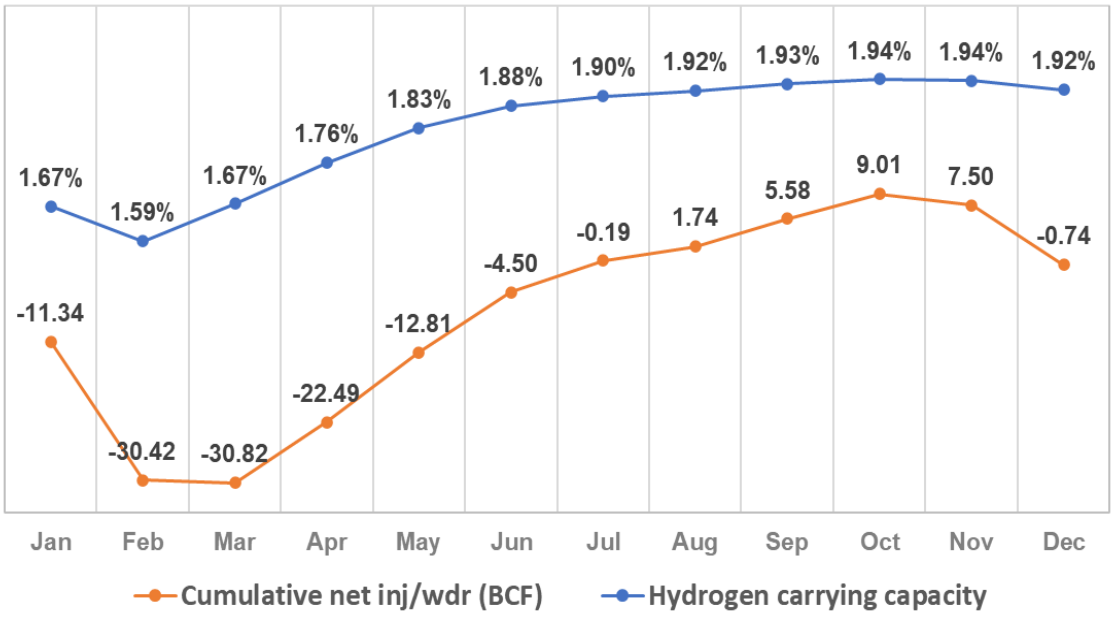

Figure 5.23. Total hydrogen carrying capacity and cumulative net injection/withdraw - scenario 1

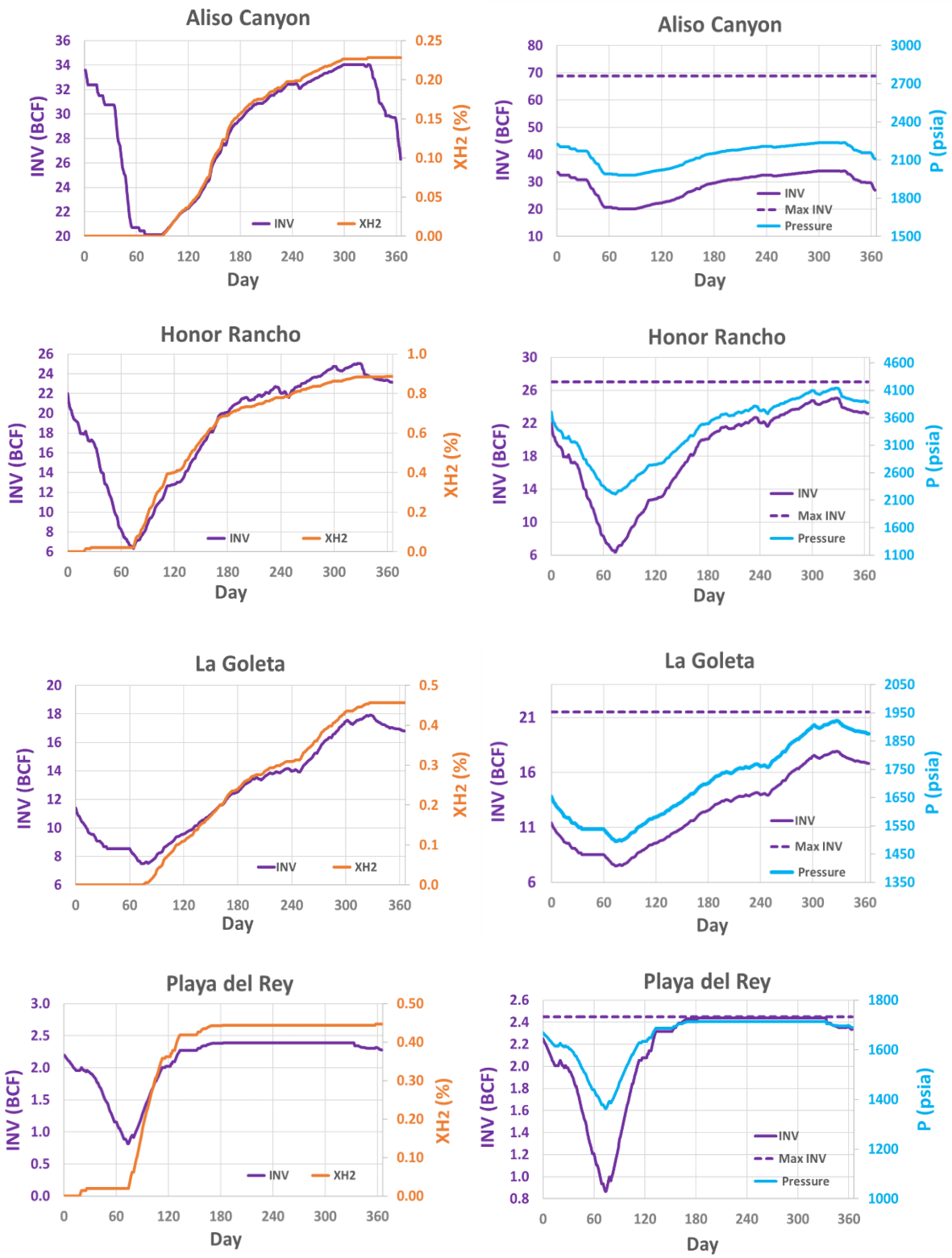

Figure 5.24. Storage field's inventory, pressure, and hydrogen concentration - scenario 1

- **Scenario 2: Hydrogen is injected into three receipt points at 2% vol.**

In scenario 2, 2% vol. hydrogen is injected at Needles, Topock, and Blythe receipt points, impacting 41% of total supply. Hydrogen/natural gas concentration and the flow rate percent change of the simulated network is presented in Figure 5.25.

As it is shown in the Figure 5.25, hydrogen/natural gas mixture does not reach the north part of the map (Porterville, N Fresno, S Fresno) and Ventura demand nodes and only a small portion of hydrogen/natural gas reaches to Santa Barbara. Since San Diego and Imperial Valley receipt points are receiving gas from Blythe, Topock, and Needles and no other pipelines are feeding these two demand nodes, their hydrogen concentration is the same as these supply points (2%). LA Basin and Palmdale are two demand nodes that receives mixed gas that contains 0.76% and 0.21% hydrogen, respectively. Since the gas stream from Kramer and Needles/Topock mixes before reaching to Palmdale, its hydrogen percentage is below 2% vol. LA Basin also receives gas from several parts of the network and as a result receive mix of hydrogen and natural gas.

Figure 5.26 shows how the cumulative net injected/withdrawn hydrogen and percent of hydrogen received at the demand point (referred to as hydrogen carrying capacity) changes during an entire year. Figure 5.26 shows that the hydrogen carrying capacity is around 0.71% at its lowest in February and increases slowly from February and reaches its maximum of 0.82% in November and stabilizes at that level.

Figure 5.27 presents the dynamics of storage facilities throughout the year as their operation condition changes from injection to withdraw mode. Aliso Canyon inventory reaches 26.3 (BCF) at the end of the year from 33.6 (BCF), which is similar to the scenario where 100% of the gas in the pipeline network was natural gas. Hydrogen concentration increases to nearly 0.02%, which is a very small amount compared to scenario 1, where hydrogen concentration reached 0.23%. Honor Rancho inventory level reaches 22.6 (BCF) and hydrogen concentration does not change and remains at near zero. La Goleta fill level and the concentration of hydrogen is 16.7 (BCF) and 0.02% at the end of year, respectively. The inventory of Playa del Rey reaches 2.28 (BCF) at the end of year while hydrogen concentration reaches 0.20%.

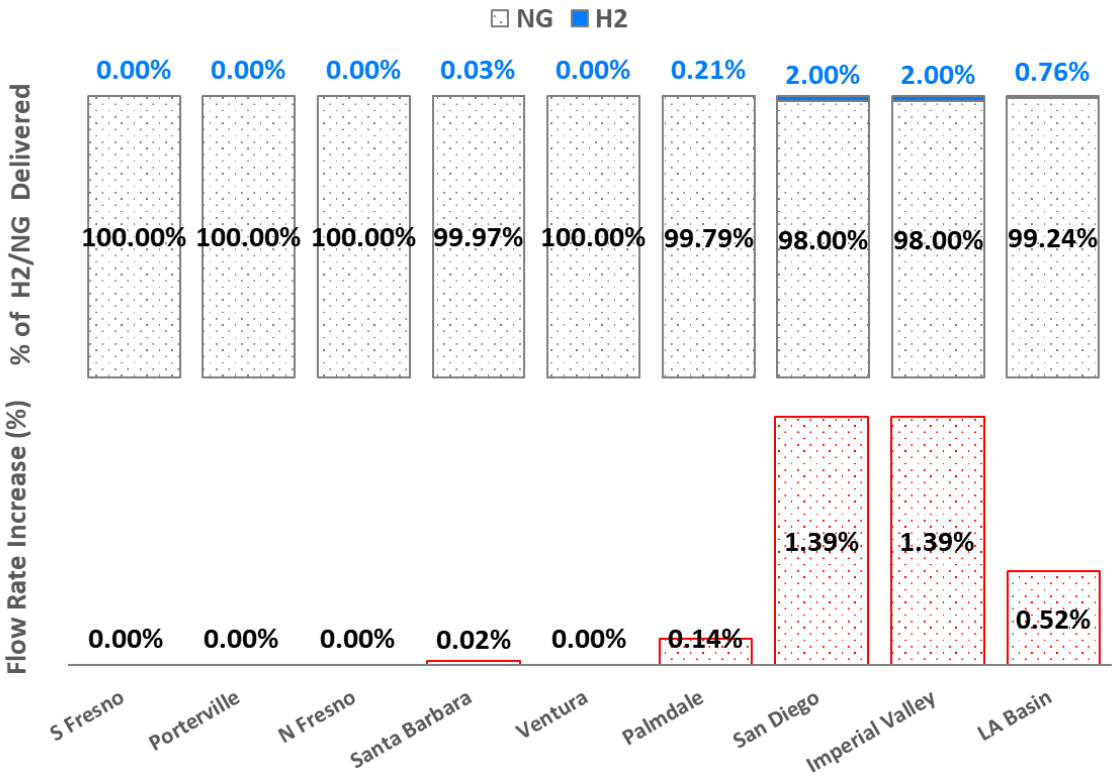

Figure 5.25. Hydrogen to natural gas percentage (top) and percent increase of flow rate (bottom) at the demand nodes – scenario 2

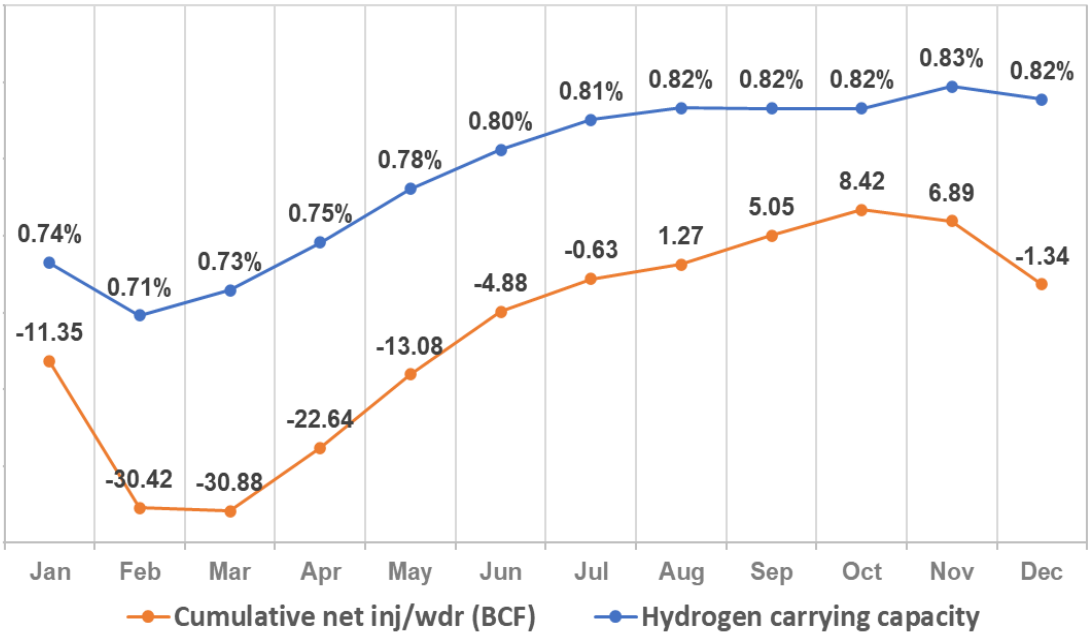

Figure 5.26. Total hydrogen carrying capacity and cumulative net injection/withdraw - scenario 2

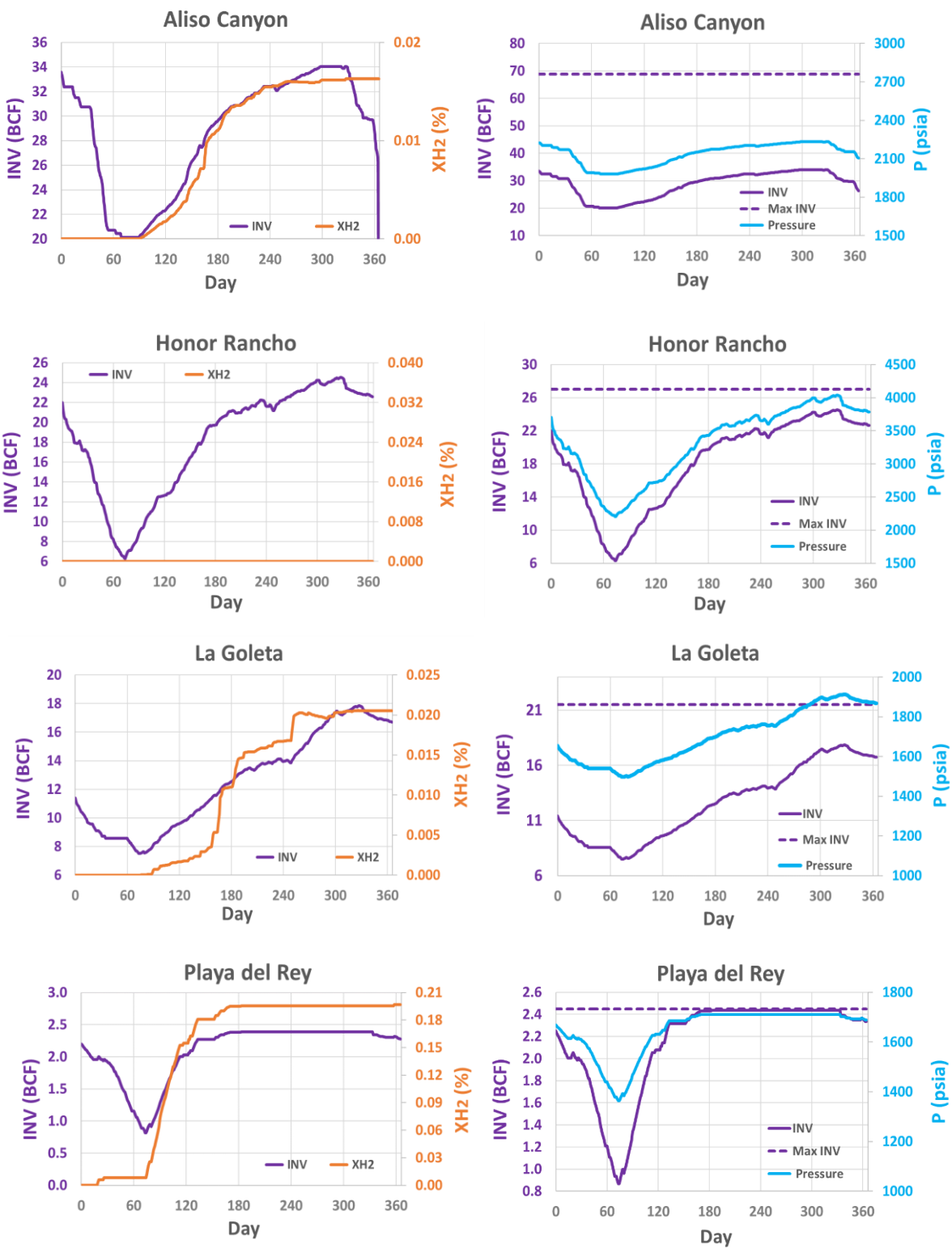

Figure 5.27. Storage field's inventory, pressure, and hydrogen concentration - scenario 2

- **Scenario 3: Hydrogen is injected into two receipt points at 2% vol.**

In scenario 3, 2% vol. hydrogen is injected into the network from two receipt points. These two receipt points are Blythe and Kramer, which in total provides 55% of gas supplied to the SoCalGas system. Figure 5.28 depicts the impact of injecting hydrogen at these two receipt points on the percent of hydrogen that is received at the demand nodes.

As it is illustrated in Figure 5.28, the effect of hydrogen injection from these two locations has more impact on LA Basin, Palmdale, San Diego, and Santa Barbara demand nodes in comparison with scenario 2. As previously was explained, Imperial Valley demand node is only connected to Blythe, which in this case supplies gas with 2% hydrogen. Therefore, the amount of hydrogen in this node is the same as Blythe receipt point. Figure 5.28 shows that for Imperial Valley demand node, where % of delivered hydrogen is 2%, mass flow rate increases by 1.39%.

Compared with scenario 2, in this scenario, hydrogen carrying capacity at the LA Basin, Palmdale, and Santa Barbara increases from 0.76%, 0.21%, and 0.03% to 1.08%, 1.80%, and 0.19%, respectively. Similarly, as the percent of hydrogen in the gas mix received at the demand nodes increases, higher mass flow rate is needed to meet the energy demand of each node. Mass flow rates of each demand node for LA Basin, Palmdale, and Santa Barbara compared to mass flow rate of the same nodes in Scenario 2 shows that higher mass flow rates are needed in scenario 3 (Compare Figure 5.28 with Figure 5.25). Hydrogen carrying capacity of scenario 3 increases from 0.82% to 1.09% compared to Scenario 2 as shown in Figure 5.29. The increase in the hydrogen capacity is scenario 3 is attributed to the choice inject point locations and the amount of total hydrogen injected in the natural gas pipeline network.

Figure 5.30 shows the concentration of hydrogen for various storage facilities throughout the year. Hydrogen concentration of Honor Rancho is zero at the end of year as most of the gas stored in the Honor Rancho comes from the Wheeler Ridge/Kern. La Goleta stores more hydrogen compared to Scenario 2 and by the end of year, hydrogen concentration reaches 0.11% (compared with 0.02% in Scenario 2). Playa del Rey hydrogen concentration is increased to 0.20% (compared to 0.29% in Scenario2). Similar to Playa del Rey and La Goleta, Aliso Canyon store more hydrogen, and its concentration rises from 0.02% in Scenario 2 to 0.13% in Scenario 3.

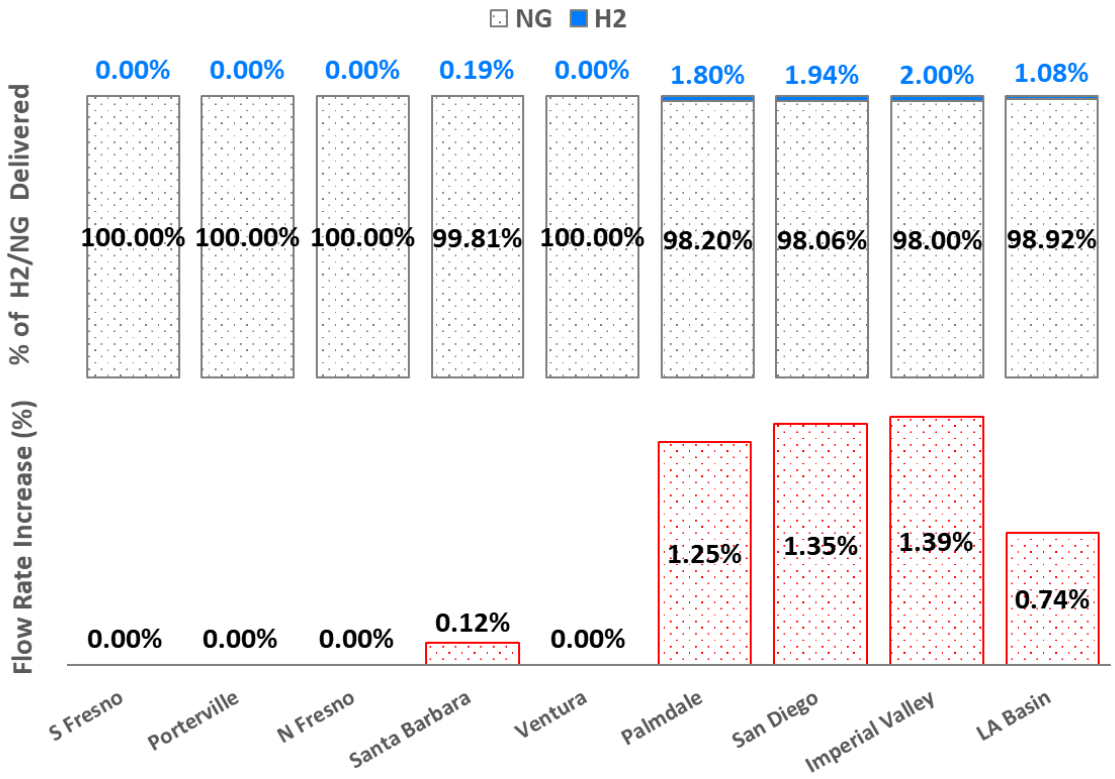

Figure 5.28. Hydrogen to natural gas percentage (top) and percent increase of flow rate (bottom) at the demand nodes – scenario 3

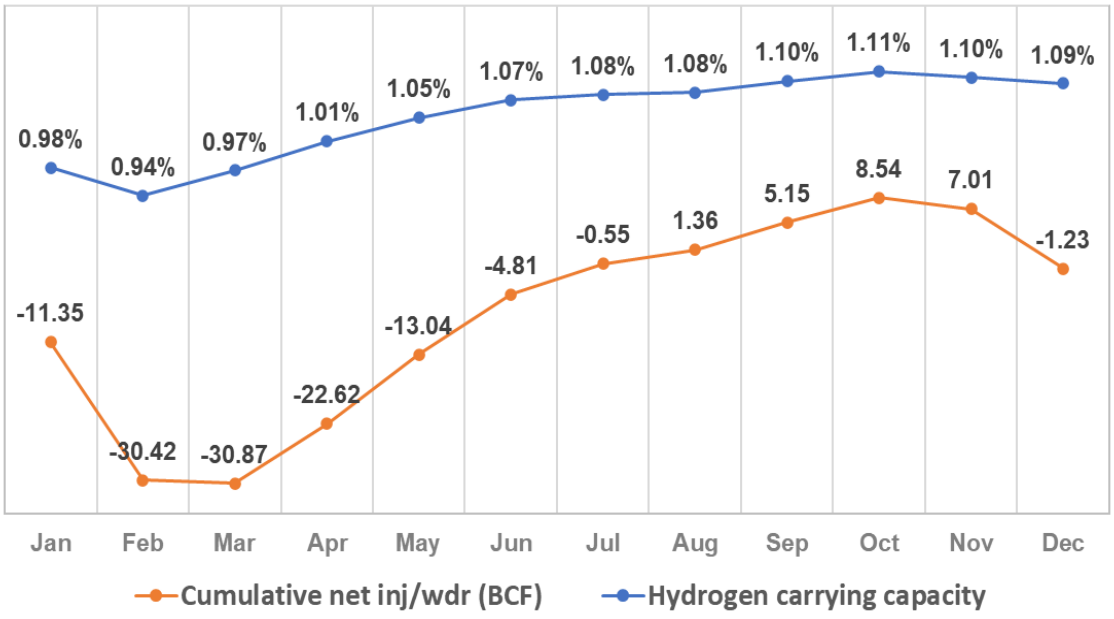

Figure 5.29. Total hydrogen carrying capacity and cumulative net injection/withdraw - scenario 3

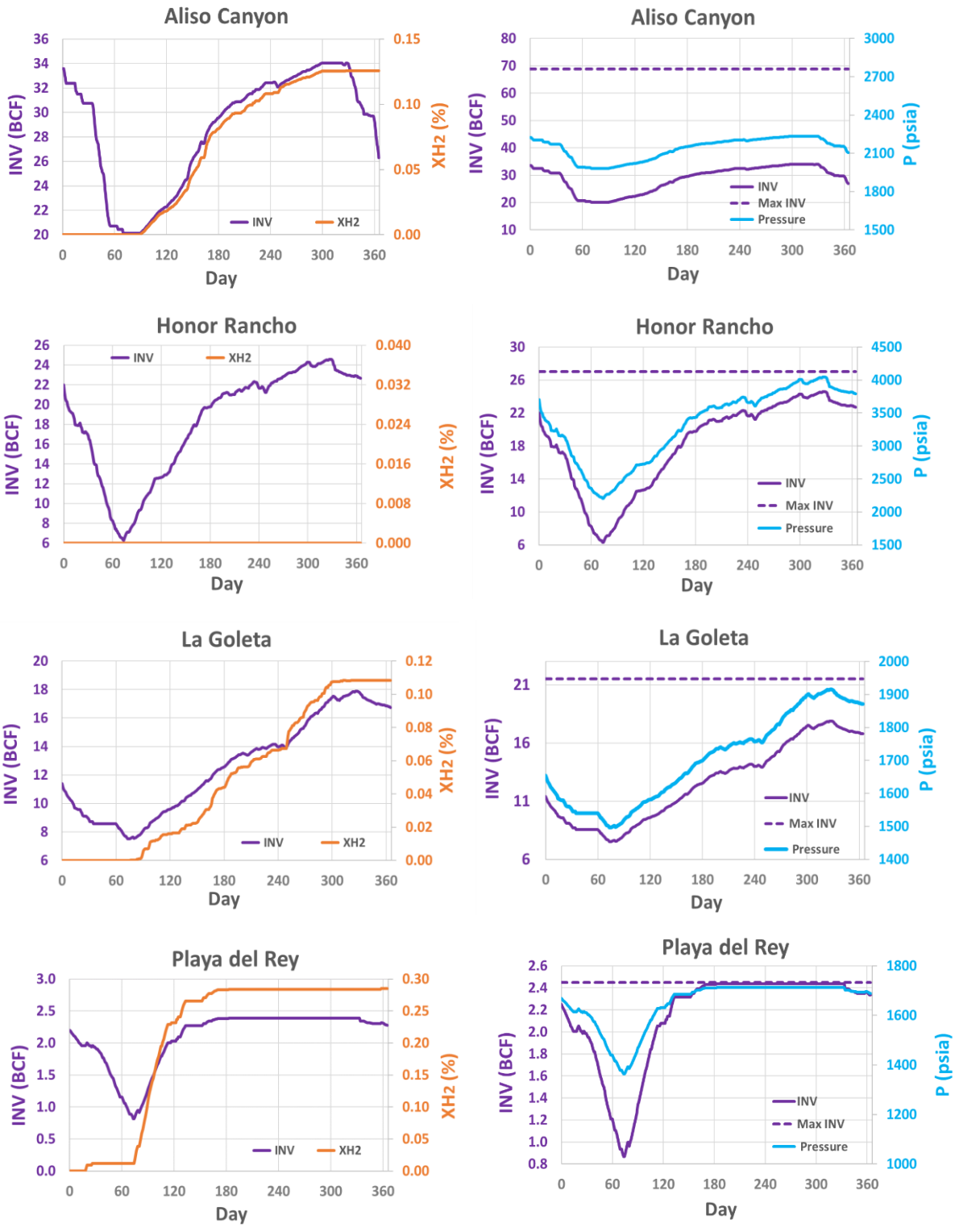

Figure 5.30. Storage field's inventory, pressure, and hydrogen concentration - scenario 3

- **Scenario 4: Hydrogen is injected into two receipt points and Aliso Canyon field**

In scenario 4, Hydrogen is injected into the network from Blythe, Kramer, and the Aliso Canyon storage field. The scenario is similar to the Scenario 3, with one more hydrogen injection point added directly to one storage facility.

The main difference in the model used for this scenario compared to previous scenarios is that that the amount of hydrogen injected to the storage filed needs to be calculated in the model. In each time step, amount of hydrogen injected at the storage distribution node is calculated to ensure amount hydrogen at the node is 2%. Implementing this condition requires adding a new iterative procedure to the Python model of the system. The flow diagram in Figure 5.8 shows the changes that was made to the initial flow to accommodate the injection of hydrogen directly to storage fields.

If the supply is higher than the demand and the storage is in the injection mode, then hydrogen produced near the storage field is mixed with other flow streams injected to the storage field. If the storage is in the withdraw mode, i.e. supply is less than demand, produced hydrogen near the storage field is mixed with the gas that is withdrawn from the storage and other pipeline with incoming streams. The mixed gas is then distributed to the network to meet the demand. The analysis shows that the impact of hydrogen injection in Aliso Canyon filed has more impact on Santa Barbara and LA Basin demand nodes. As it is shown in Figure 5.31, hydrogen concentration for Santa Barbara and LA reaches 0.29% and 1.23%. Hydrogen carrying capacity of the network in scenario 4 reaches 1.21% compared to 1.09% in scenario 3. This is mainly attributed to the higher hydrogen concentration received in LA Basin (see Figure 5.32).

Figure 5.33 shows the fill level in each storage facility throughout the year. It should be noted that compared to scenario 3, Aliso Canyon Inventory does not change and remains at 26.26 BCF while hydrogen concentration reaches 0.25% compared to 0.13% (this is because of the constraint that was applied to Aliso Canyon). Hydrogen concentration does not change in Honor Rancho the same way it did in scenario 2 and 3. Compared to scenario 3, hydrogen concentration at La Goleta increases to 0.16% from 0.11% and at Playa del Rey, it increases to 0.30% from 0.29%.

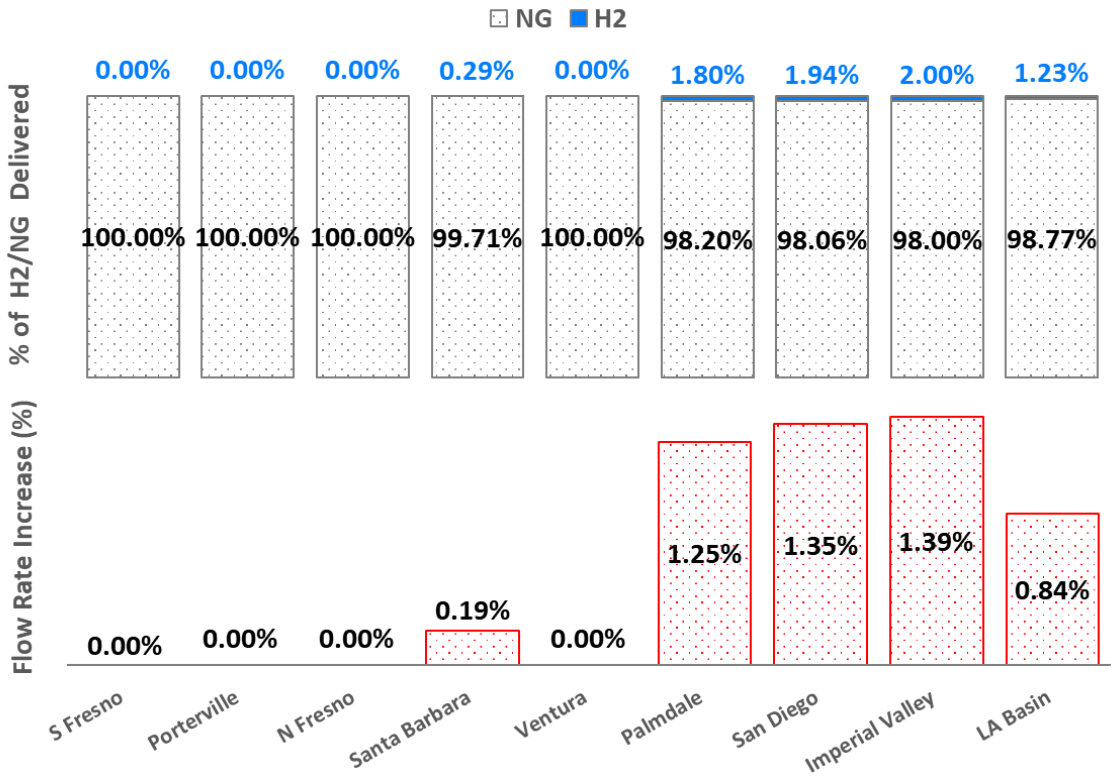

Figure 5.31. Hydrogen to natural gas percentage (top) and percent increase of flow rate (bottom) at the demand nodes – scenario 4

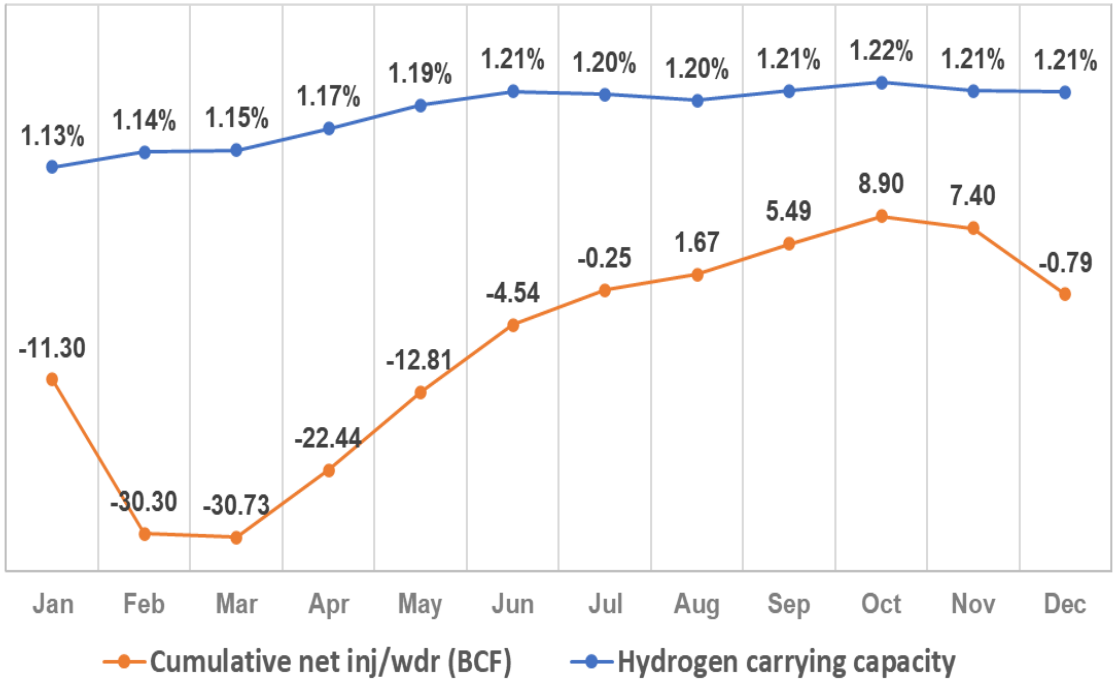

Figure 5.32. Total hydrogen carrying capacity and cumulative net injection/withdraw - scenario 4

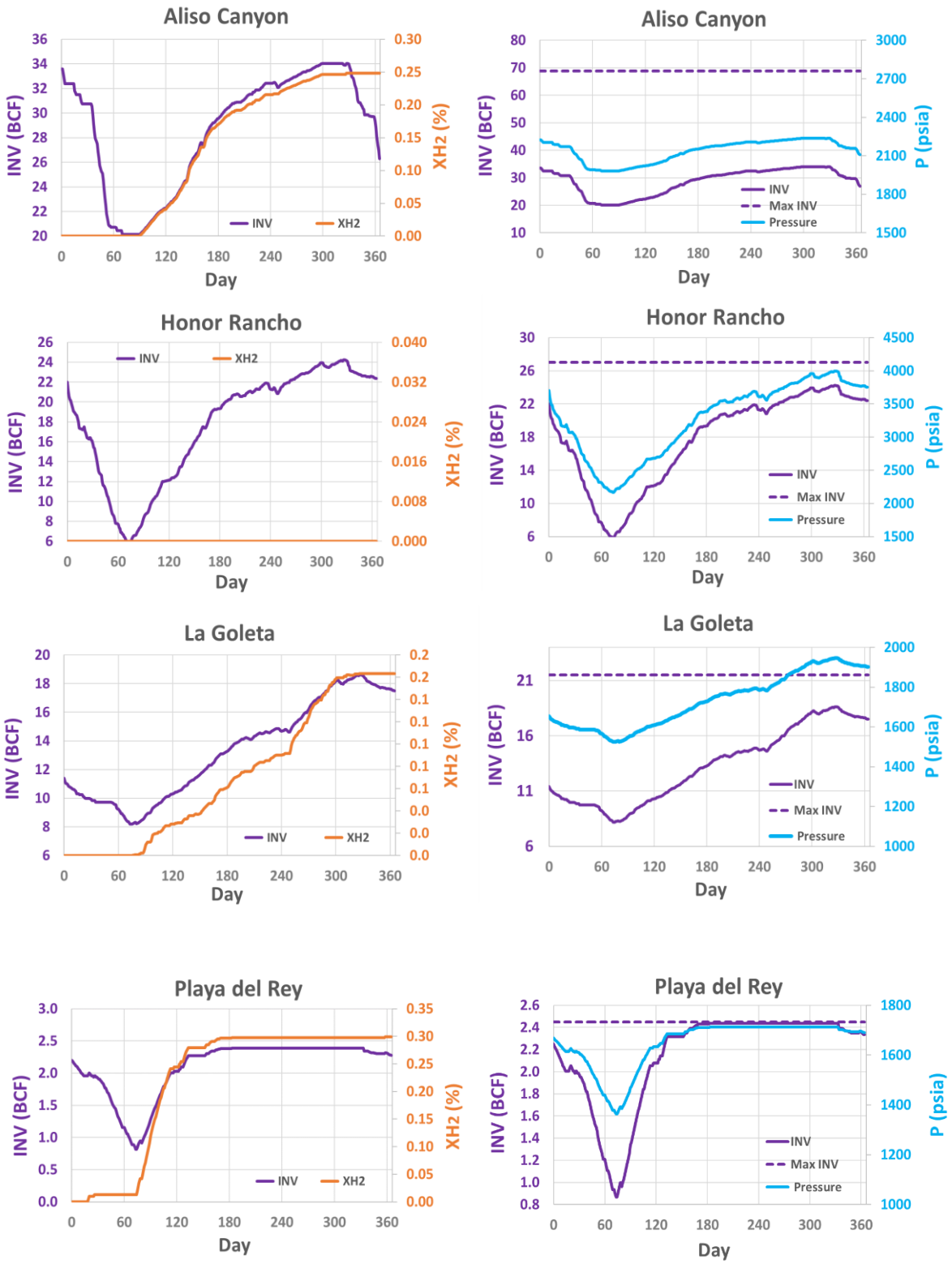

Figure 5.33. Storage field's inventory, pressure, and hydrogen concentration - scenario 4

Figure 5.34 compares the amount of hydrogen produced at three nodes in this scenario 4. Hydrogen produces in this scenario is 10.54% higher than scenario 3. The total amount of hydrogen produced at the storage field is 2.6 kt. As it can be seen from Figure 5.34, in the first three months when the gas demand is higher than the supply, and gas is dispatched from Aliso Canyon (with zero hydrogen concentration), more hydrogen should be produced in order to maintain 2% hydrogen injection into the network.

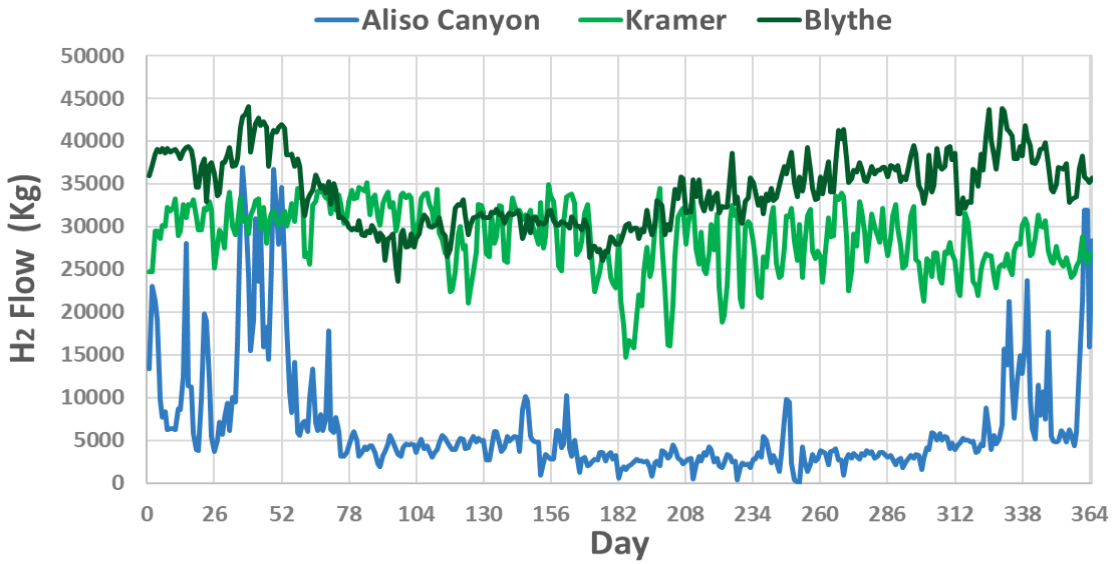

Figure 5.34. Mass of hydrogen produced at each node - scenario 4

To further study the effect of the location of hydrogen injection on the network and specifically hydrogen carrying capacity, scenario 4 modified (scenario - 4M) was defined. In this scenario, the amount of hydrogen injection in the network is the same as scenario 3. As a result, as hydrogen is injected in Aliso Canyon 2% by volume, the amount of hydrogen in Kramer and Blythe is reduced in each time step (daily) in order to keep the amount of hydrogen constant as shown in Figure 5.35. Hydrogen carrying capacity turned out to be the same as scenario 3 (1.09%) which shows that the effect of hydrogen injection location in this scenario is negligible. This can be explained since hydrogen concentration in Aliso Canyon and La Goleta storage fields which are closer to the hydrogen injection point is increased compared to scenario 3 from 0.13% and 0.11% to 0.25% and 0.16%, respectively.

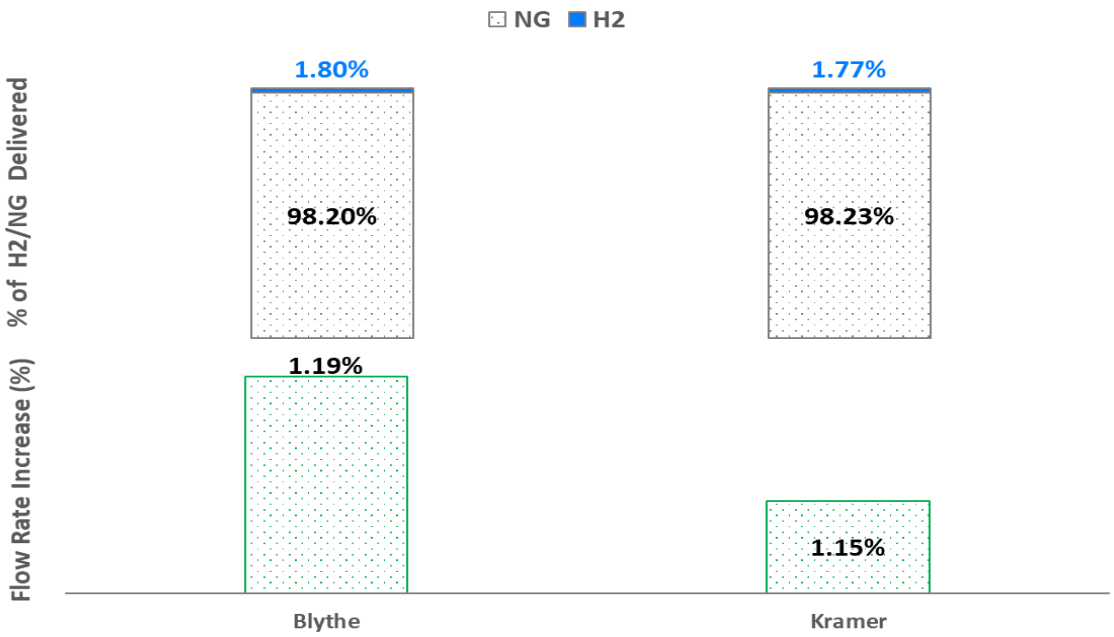

Figure 5.35. Hydrogen to natural gas percentage (top) and percent increase of flow rate (bottom) at the two supply nodes – scenario 4M

The comparison between four scenarios discussed above, where 2% hydrogen was injected to various locations in the network are shown in Figure 5.36 and Figure 5.37. Figure 5.36 compares how hydrogen concentration changes in each storage facilities for each scenario. Hydrogen concentration in Honor Rancho does not change in scenarios 2, 3, and 4 where hydrogen is injected to the system from the east side of the network (Blythe, Needles, Topock, Kramer). This can be explained by the fact that this field is supplied only from Wheeler ridge receipt point located at the north part of the network.

Hydrogen carrying capacity (defined as total amount of hydrogen injected in a period divided by the total amount of gas demanded by all loads in system in that same period) for all scenarios is combined in Figure 5.37. Hydrogen carrying capacity reaches to 1.92% at the end of year for scenario 1 where hydrogen is injected in all receipt points. Hydrogen carrying capacity for scenarios 2, 3, and 4 reaches 0.82%, 1.09%, and 1.21%, respectively.

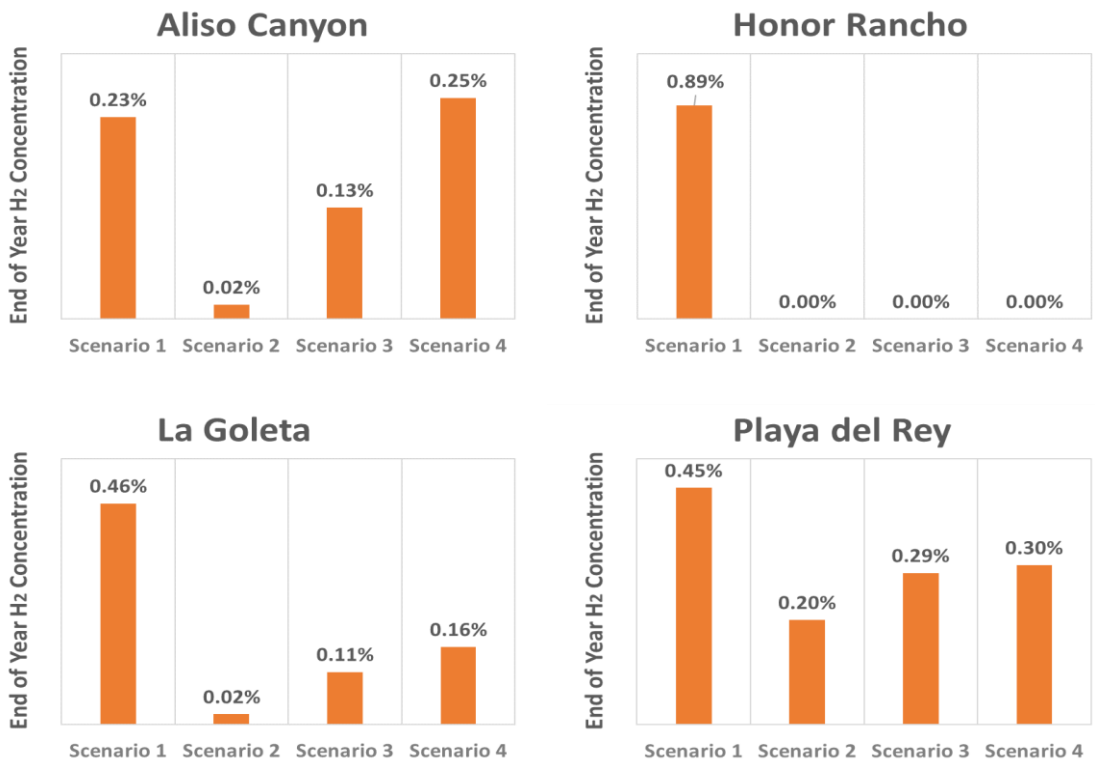

Figure 5.36. End of year hydrogen concentration in storage facilities - 2% hydrogen injection scenarios

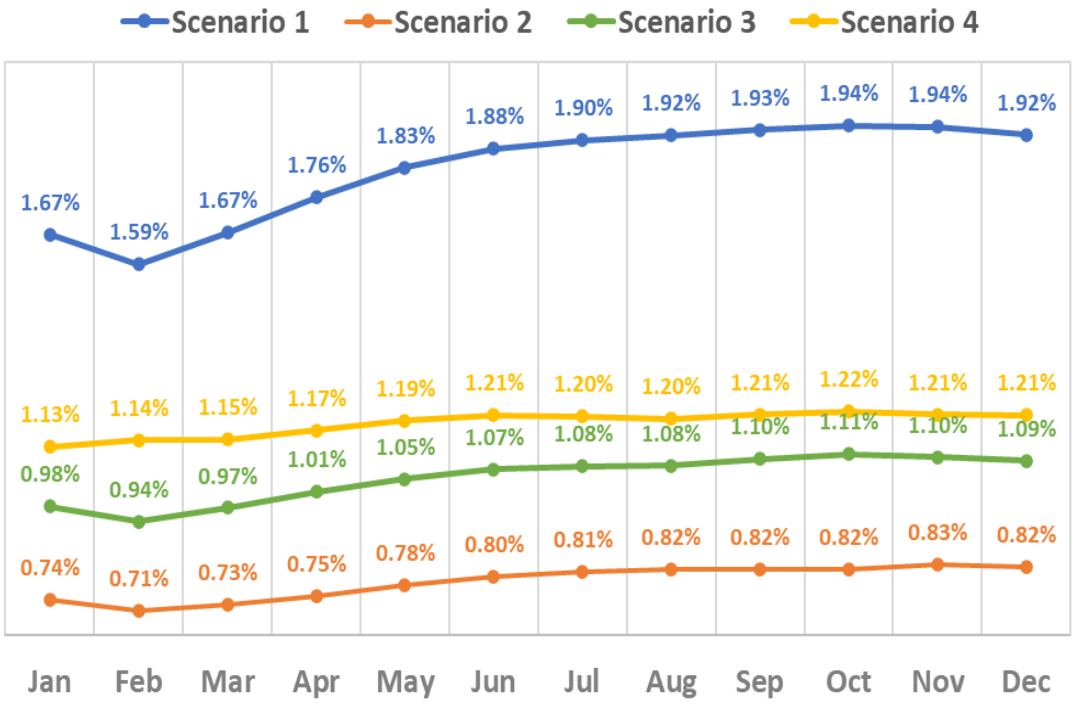

Figure 5.37. Hydrogen carrying capacity - 2% hydrogen injection scenarios

Hydrogen percentage distribution for scenarios 1-4 in SoCalGas pipeline network are shown in Figure 5.38 through Figure 5.42.

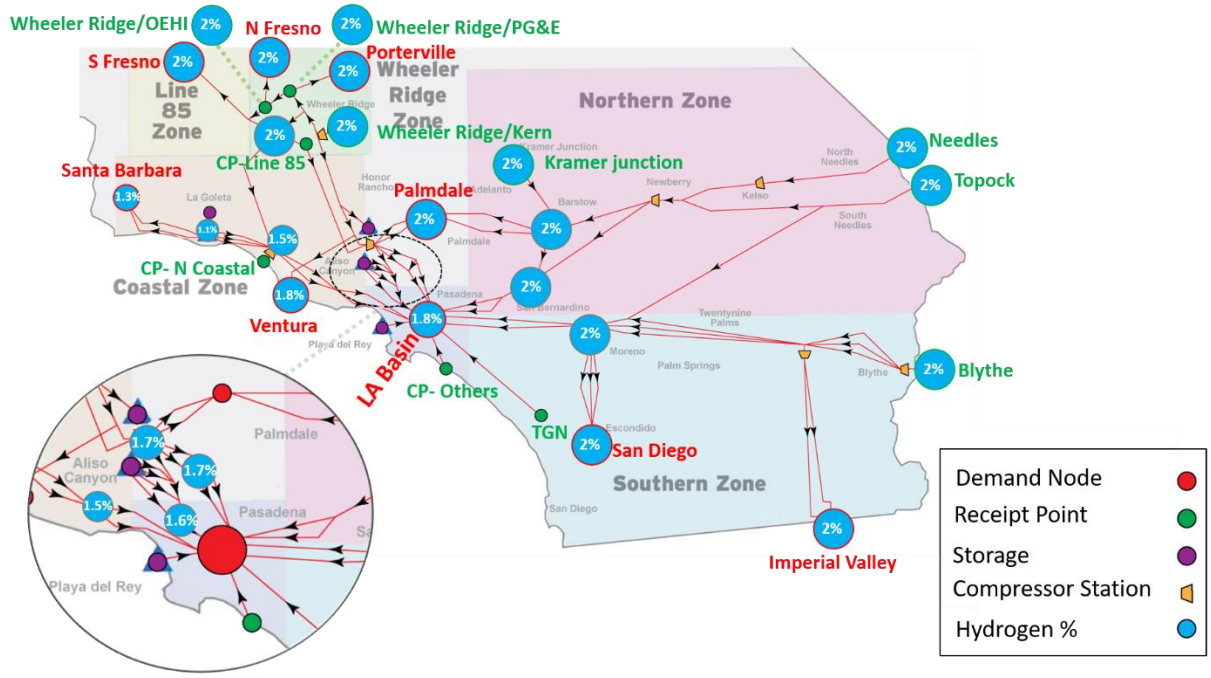

Figure 5.38. Hydrogen percentage distribution in the SoCalGas pipeline network – scenario 1

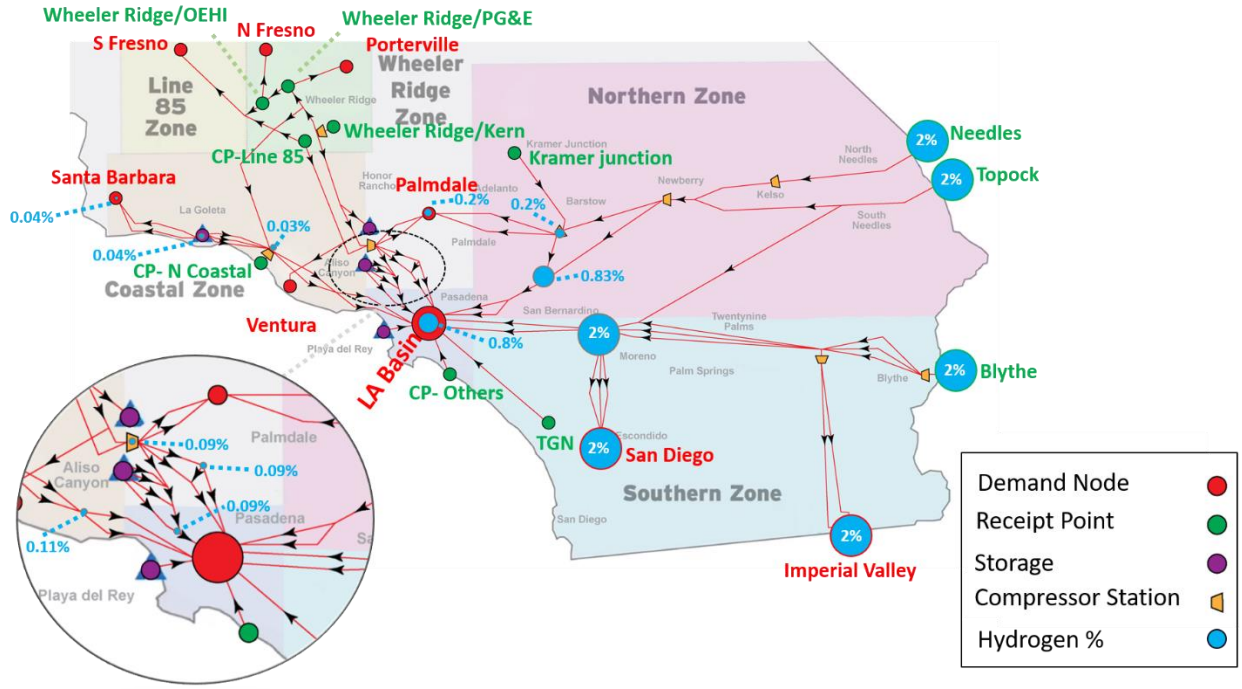

Figure 5.39. Hydrogen percentage distribution in the SoCalGas pipeline network – scenario 2

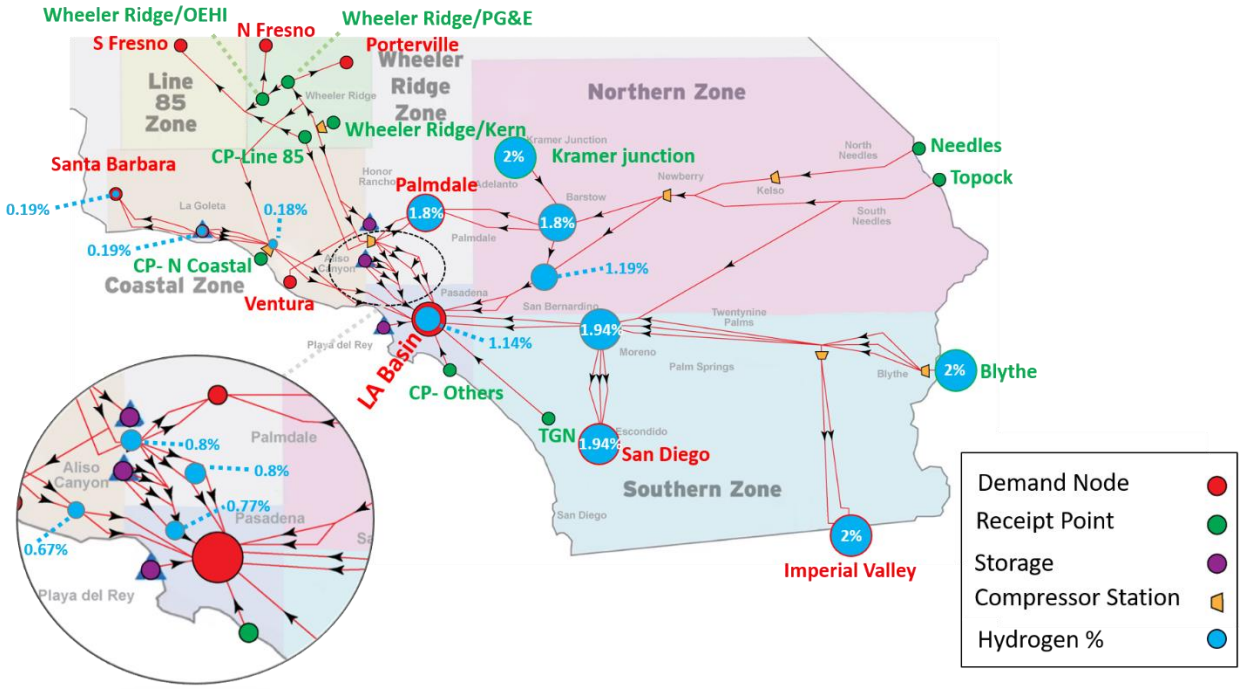

Figure 5.40. Hydrogen percentage distribution in the SoCalGas pipeline network – scenario 3

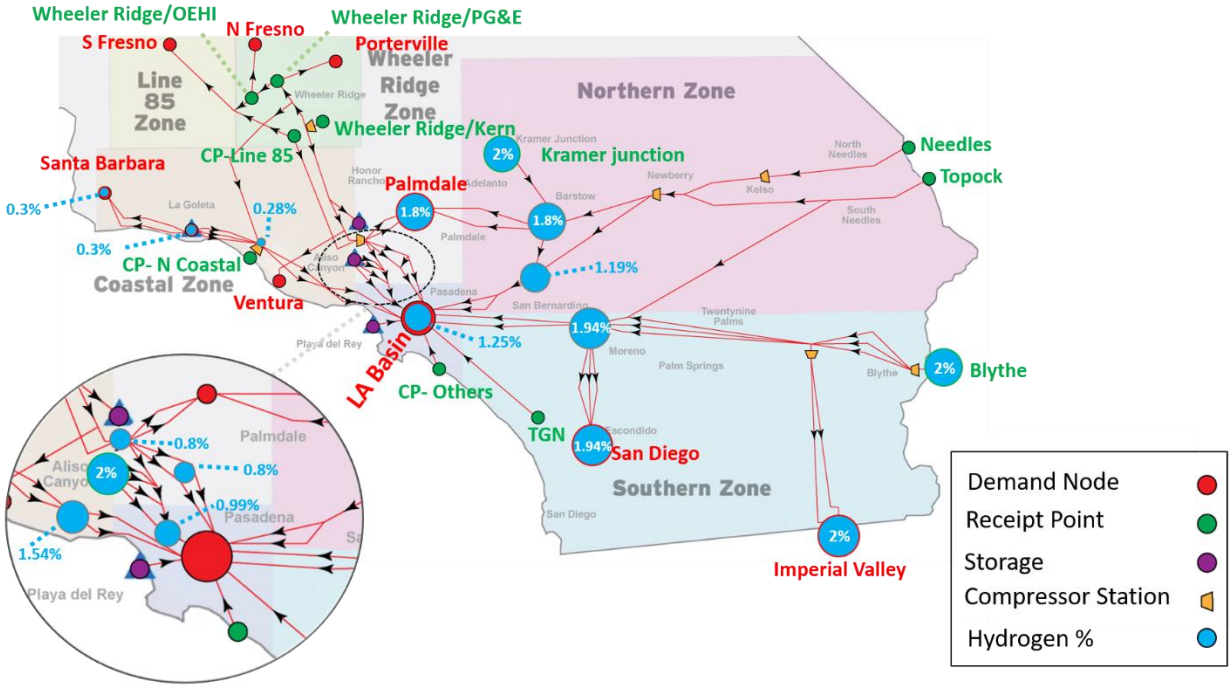

Figure 5.41. Hydrogen percentage distribution in the SoCalGas pipeline network – scenario 4

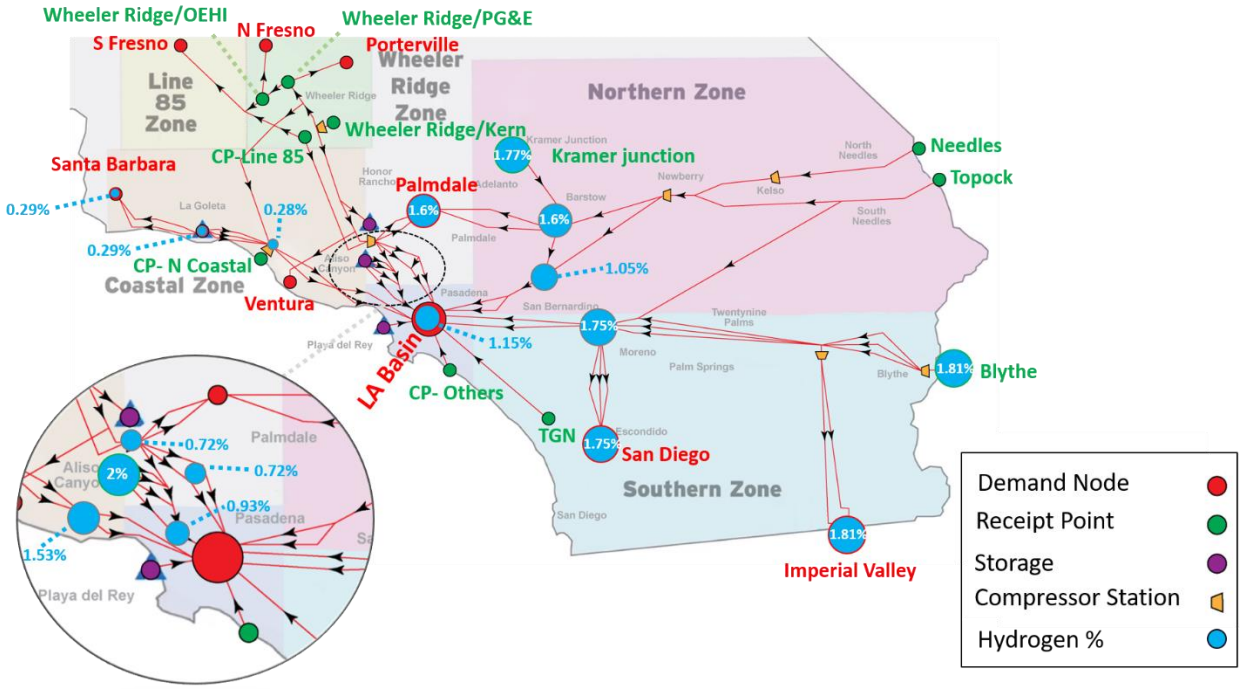

Figure 5.42. Hydrogen percentage distribution in the SoCalGas pipeline network – scenario 4M

- **Scenario 5: Hydrogen is injected into five receipt points at 20% vol.**

As previously stated, several projects by other groups that studies the impact of injecting hydrogen in the natural gas pipeline networks concluded that blending hydrogen up to 20% by volume into the natural gas network typically does not require a lot of modifications in the natural gas infrastructure systems.

In this scenario 5, 20% vol. hydrogen is injected in the SoCalGas pipeline network at the same receipt points used in scenario 1, representing 96% of the total gas supplied. To ensure the same amount of energy is supplied to the SoCalGas network, volumetric flow rate at the recipe points needs to increase by 15.91%. The network is analyzed to examine whether the SoCalGas network can handle the increase in flow rates without violating any of the network constraints.

Figure 5.43 shows the total amount of hydrogen received at each demand node by the end of year. Santa Barbara, Ventura, S Fresno, and LA Basin demand points receive less than 20% hydrogen while the rest of demand nodes receive 20% hydrogen. LA Basin which is the biggest demand node in the network receives gas from all receipt points, as well as the storage fields and as a result its hydrogen concentration is less than 20%. Figure 5.44 shows that hydrogen carrying capacity for this scenario reaches 19.4% at the end of year. As expected, Figure 5.44 also shows that the net injection/withdraw (inj/wdr) is higher compared to the 100% natural gas network.

Figure 5.45 shows how the inventory of each storage facility changes compared with the 100% natural gas network. Playa del Rey capacity is decreased due to higher hydrogen concentration in the storage and is filled sooner (day 111 compared to day 183 for NG network) and cannot be filled out until day 335 when the demand is higher than supply. The same issue is seen in La Goleta and Honor Rancho. They both reach their max capacity on day 290 and 273, respectively. After day 290, the network can only rely on Aliso Canyon to store gas. This can pose risk to the network, considering the prior issues with Aliso Canyon and the capacity limit mandated by CPUC for Aliso Canyon (the inventory not permitted to go above 34 BCF). As it is shown in Figure 5.45, Aliso Canyon passed this limit on day 273 and it goes up 38.8 (BCF) in day 328. It should be noted that, this capacity limitation set by CPUC is monitored every year to make sure there is no leakage related problem with this facility. Assuming no new leakage occurs, Aliso Canyon could in theory accommodate the needed storage by 2030.

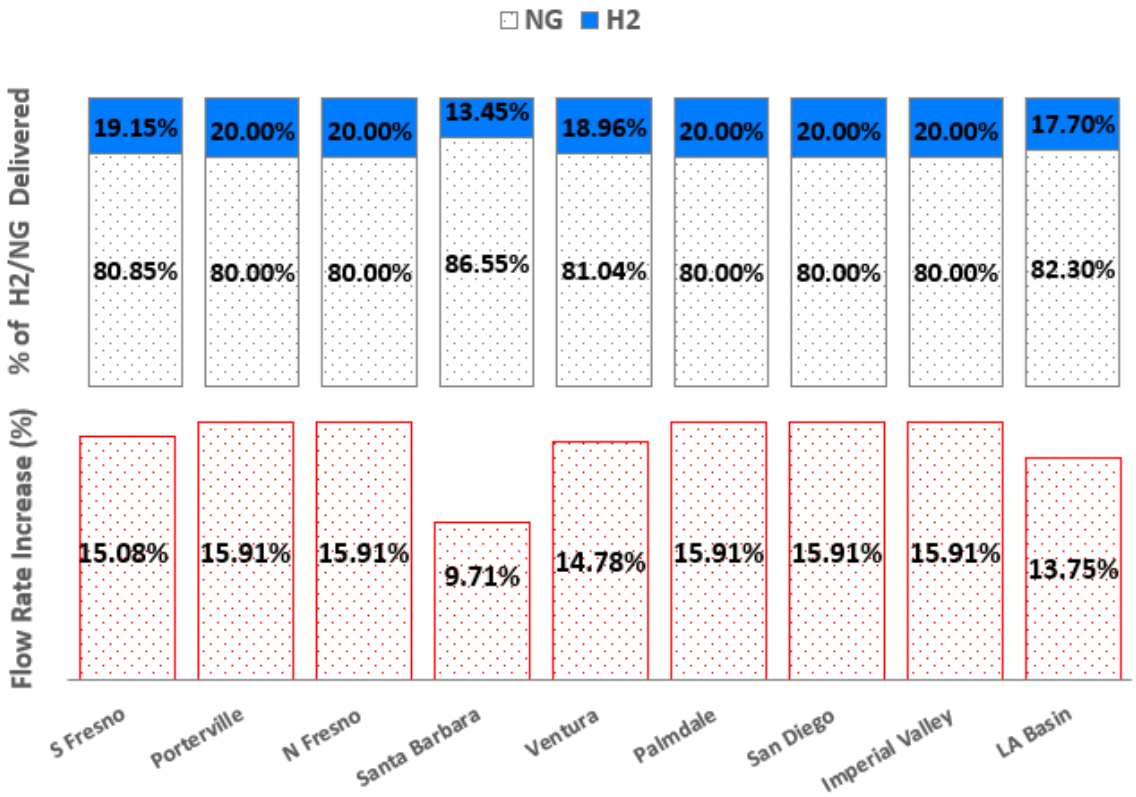

Figure 5.43. Hydrogen to natural gas percentage (top) and percent increase of flow rate (bottom) at the demand nodes – 20% hydrogen injection scenario

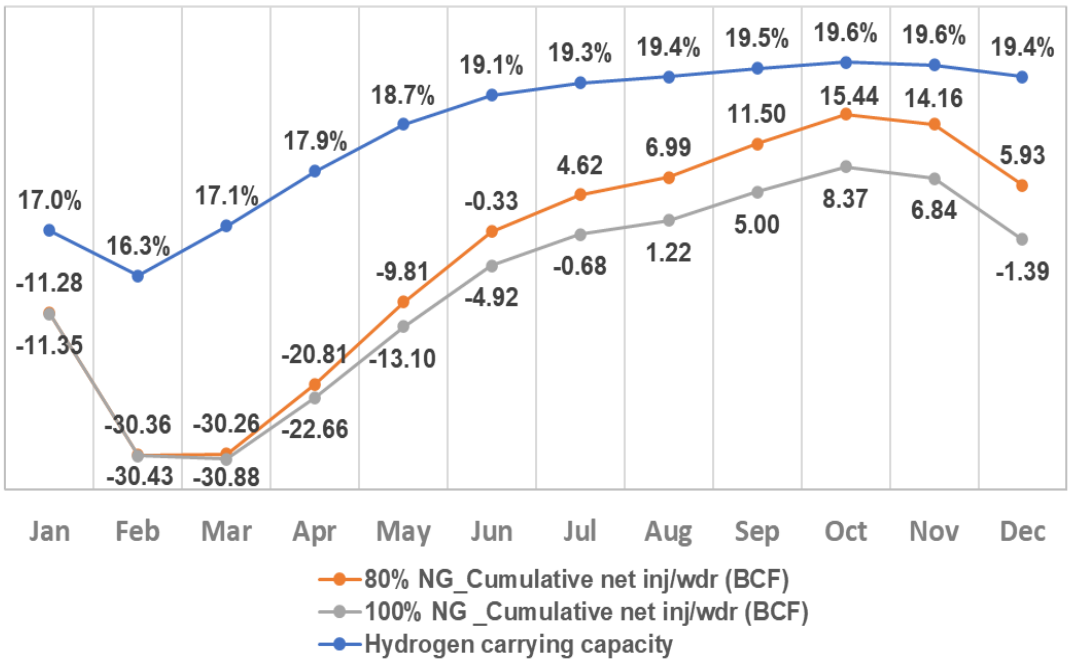

Figure 5.44. Total hydrogen carrying capacity and cumulative net injection/withdraw - 20% hydrogen injection scenario

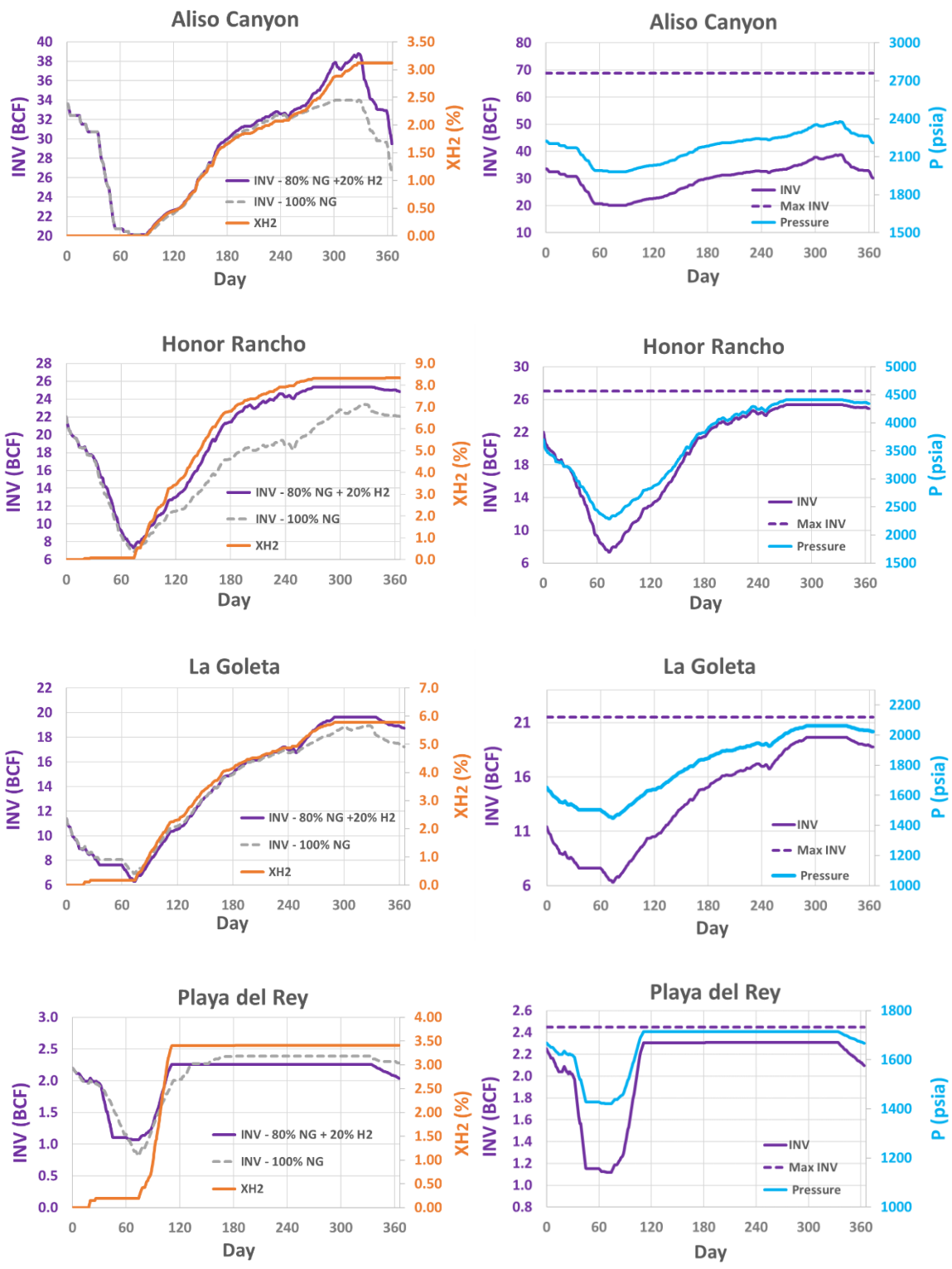

Figure 5.45. Storage field's inventory, pressure, and hydrogen concentration - 20% hydrogen injection scenario

To determine whether any of the network constraints are violated when 20% vol. hydrogen is injected at the five receipt points, pressure limits for the network pipelines and power capacity limits for compressor stations were examined. The analysis identified two violations. The pipeline maximum allowable operating pressure at the Kramer junction receipt point and the maximum discharge flow rate for Wheeler compressor station were violated. Figure 5.46 shows these two points in the network (highlighted in blue). The first problem was at Kramer junction receipt point located in the northern zone (see Figure 5.47), where the maximum allowable pressure goes above the pipeline limit (950 psi-g). As it was depicted in Figure 5.14, Kramer point was operating at its capacity for most of the year for the original case of 100% NG network and therefore this violation was expected to occur at 15.9% higher flow rate. The second violation occurred at Wheeler compressor station, where the required capacity exceeded the maximum compressor capacity of 765 (MMCFD) during the first five months of the year (see Figure 5.48). Therefore, the capacity of the Wheeler compressor station needs to be increased to allow the station to handle higher volumetric flow rate.

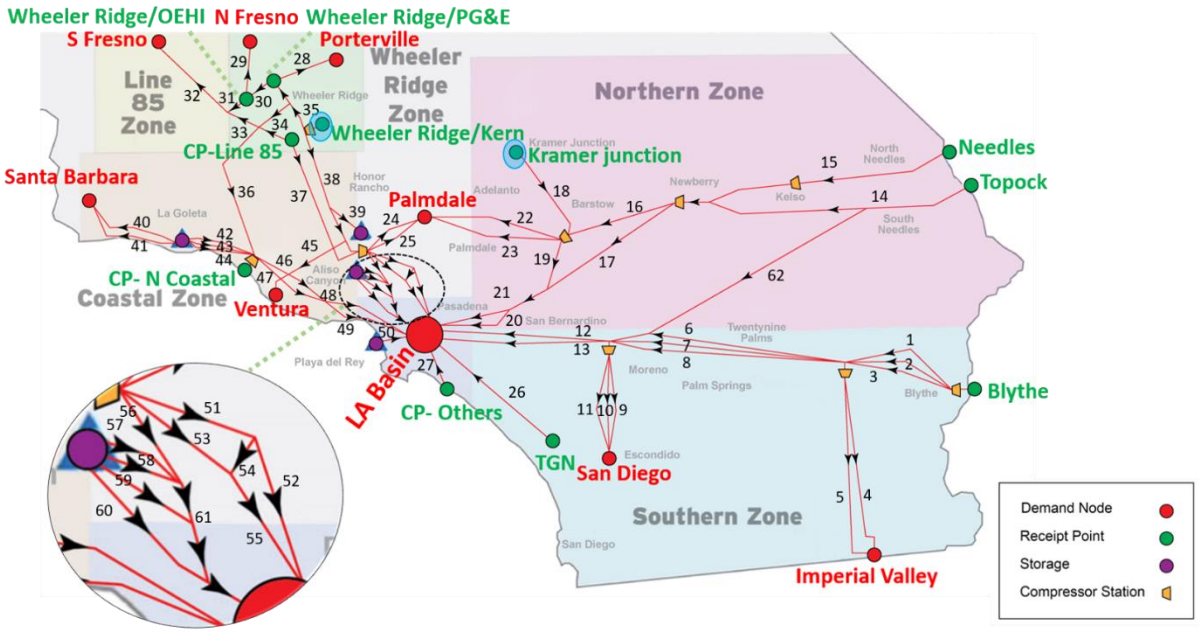

Figure 5.46. Two identified points facing problem (highlighted in blue) - for 20% hydrogen injection scenario

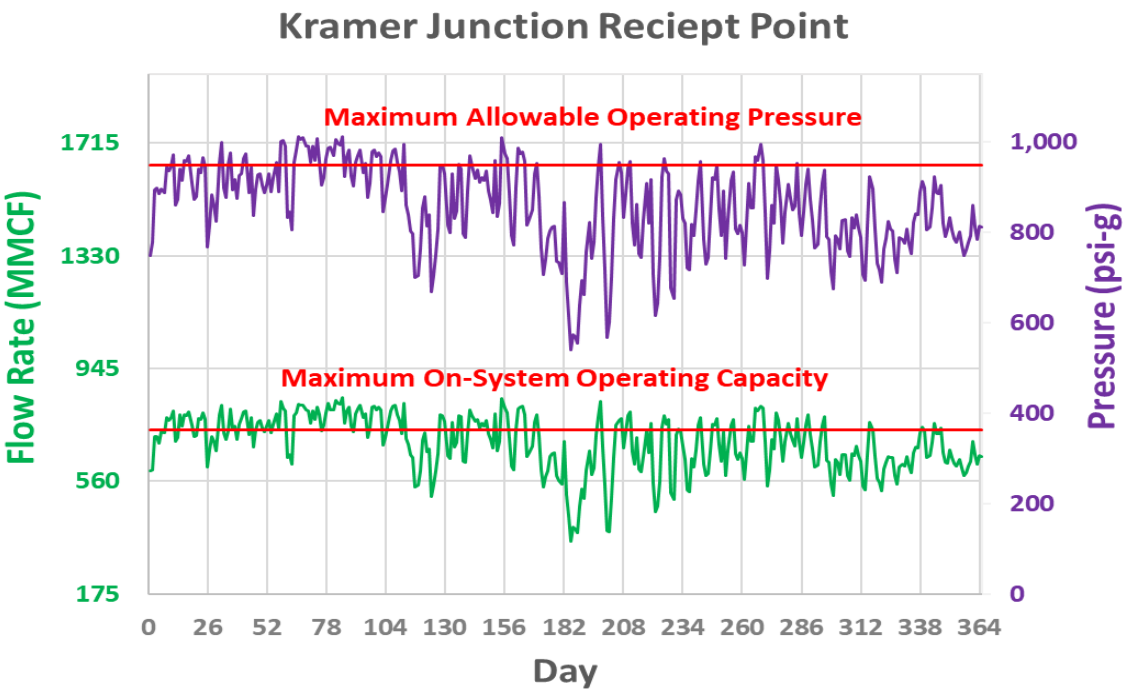

Figure 5.47. Pressure and flow rate of Kramer receipt point - 20% hydrogen injection scenario

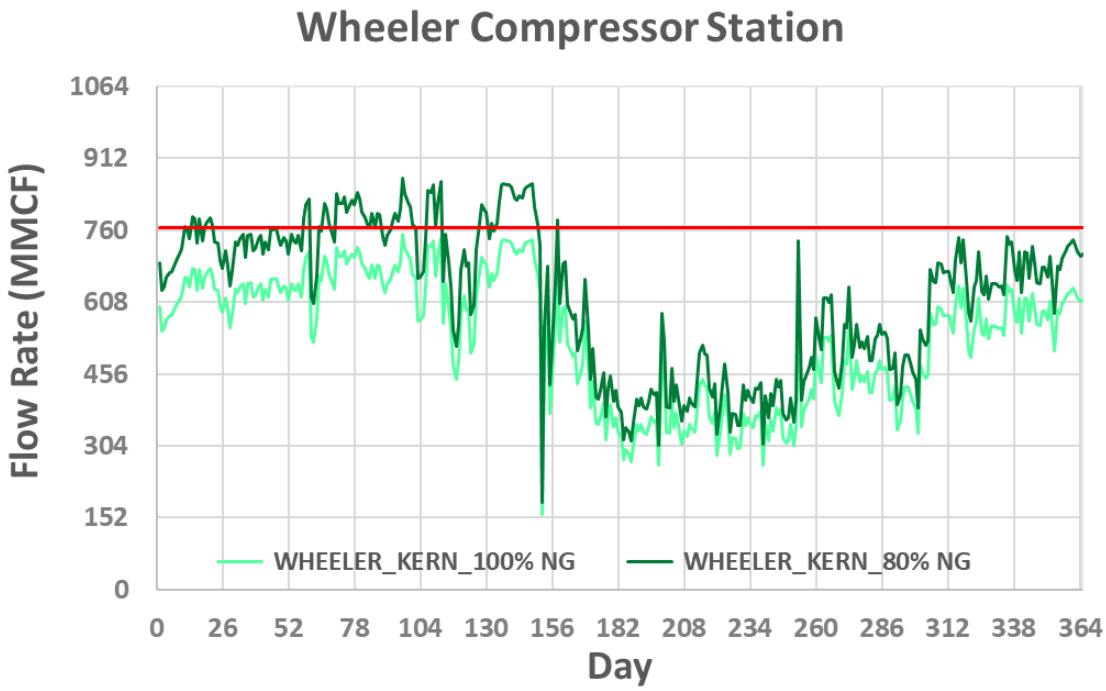

Figure 5.48. Flow rate of Wheeler compressor station - 20% hydrogen injection scenario

Table 5.6 summarized the amount of hydrogen that is produced in each injection point for 2% and 20% cases. It also shows the capacity of electrolyzer with efficiency of 65% that is needed and the amount of land that is required to produce the required hydrogen. The size of the land is calculated using the same methodology that was explained in chapter 4.

Table 5.6. Solar farm and electrolyzer required to achieve 2% & 20% hydrogen injection

Hydrogen Injection Point	Size of Solar Farm (sq. mi)		Electrolyzer Capacity (MW)		Total hydrogen Produced (kt/year)	
	2%	20%	2%	20%	2%	20%
Blythe	1.3	14.9	111	1273	13.76	157.27
Topock	0.4	4.8	36	408	2.45	28.06
Needles	0.5	5.3	40	454	2.8	31.99
Kramer	1	11.9	89	1015	11.53	131.84
Wheerler_Kern	1.1	12.2	91	1043	10.32	118.02
Wheeler_OEHI	0.1	1.2	9	99	0.54	6.17
Wheeler_PG&E	0.7	7.6	57	652	3.19	36.52
Aliso Canyon	1.1	-	98	-	2.6	-

5.5 Summary

In this chapter, the impact of injecting hydrogen in the natural gas infrastructure were analyzed using a detailed gas network of Southern California. As stated earlier, prior research on injecting hydrogen into natural gas network of other regions generally showed that the network can transport and consume the blended gas if the hydrogen percentage is under 20%. The network was solved for three scenarios, when hydrogen mix was 0%, 2%, and 20% vol. to investigate whether the network can satisfy the pipeline pressure constraints in the network while meeting the energy demand of Southern California. While it was observed that the pipelines in the network can meet their pressure constraints when the gas mix has 2% vol. of hydrogen, some of the pipeline pressure constraints in the network cannot be met when the mix percentage is increased to 20% vol. The analysis indicates that increasing the hydrogen percentage to 20% vol. requires the installation of additional pipelines to meet the energy demand of Southern California.

For the scenario where blended hydrogen at select injection points were 2%, various locations were analyzed to study the impact of location on the hydrogen carrying capacity of the network at the demand points. It was shown that a well-blended network results in a higher hydrogen carrying capacity. For the case when 2% vol. hydrogen is injected in all the receipt points, the hydrogen carrying capacity reaches 1.92% at the end of the year.

6 Conclusions & Future Work

6.1 Conclusions

The goals of this dissertation were to evaluate various stages of transitioning the current energy portfolio of Southern California to a zero-emission portfolio. The transition path starts with moderating emissions from the current natural gas infrastructure, and ends with a 100% renewable portfolio, where hydrogen replaces natural gas. In between, hydrogen is mixed with natural gas and is injected in the natural gas infrastructure to facilitate the transition.

In the work presented in this dissertation, three main questions were answered: 1- How change in throughput in a natural gas infrastructure impacts methane emissions, 2- What additional resources are required to transition the current natural gas infrastructure of Southern California to achieve 100% renewable energy penetration, and 3- What impact blending of hydrogen and natural gas has on the current Southern California natural gas infrastructure. The primary findings of this dissertation are outlined in four chapters as follows:

- **Chapter 2:** Identified the major methane emissions sources from the upstream of natural gas system. The marginal emissions coefficients (time, event, throughput) for those sources were determined based on their physical mechanism and characteristics. It was found that:
    - Ten major emissions sources in all sectors of the natural gas system contribute to 50.68% of the total methane emissions, namely: 1) Pneumatic controllers, 2) gas engines, 3) compressors, 4) liquid unloading, 5) blowdown, 6) storage wellhead and wellbore, 7) storage tank, 8) equipment leaks, 9) dehydrated, 10) chemical injection pumps.
    - Some of these ten major emissions sources have zero dependency to the system throughput and some have complete or partial dependency to the throughput.
    - Pneumatic controllers (intermittent bleed) that contribute to 13% of the total emissions have 20% dependency to the throughput.
    - Engines that contributes to 11% of total emissions, have 80% dependency to the throughput.

- Reciprocating compressors that contribute to 7% of total emission, have 10% dependency to the throughput.

- **Chapter 3:** developed a new cause-based model using the marginal methodology to estimate the change in methane emissions with the change in throughput. The marginal coefficients from chapter 2 were applied to the model to study the effect of the marginal change in methane emissions. Two different scenarios were defined using the EPA/GHGI data to analyze the impact of the marginal change in methane emissions when the total throughput increases or decreases by 5%, 15%, 30%, and 50%. Scenario 1 considered the natural gas system as is without any technological modifications and scenario 2 took into account the effect of system expansion and reduction as well as the technological improvements. The main takeaways from this chapter are:

  - Marginal methane emissions estimate shows that the simple average method for estimation of the change in methane emissions overestimates change in methane emissions when throughput increases and underestimates it when throughput decreases.

  - In scenario 1, the marginal method shows a 32% increase in methane emissions with 50% increase in throughput and 34% reduction with 50% decrease in system throughput. The contribution of marginal components to the total change in methane emissions were found to be 7.5% out of 32% for the case when throughput increases. The contribution of the marginal components to the total methane emissions reduction were estimated to be 9.5% out of 34% total emissions.

  - In scenario 2, marginal method shows a 28% increase in methane emissions when throughput increases by 50% and 36% reduction in methane emissions when throughput decreases by 50%. The contribution of marginal components to the total change in methane emissions were 4% out of 28% when throughput increases. The contribution of the marginal components to the total methane emissions reduction were estimated to be 7% out of 36% total emissions.

- **Chapter 4:** evaluated the capacity of Southern California natural gas infrastructure and calculated the additional resources required to transition to 100% renewable energy penetration for the entire year. The analysis determined the amount of additional solar farms, pipeline network capacity, and underground storage facilities that are required. A transient model was developed to analyze the power-to-power system. The model captured the hourly excess power from renewable generation resources and the deficit power when the demand was higher than generation. When the generation was greater than the electric demand, hydrogen was produced in the electrolyzer. The produced hydrogen then was injected in the high pressure SoCalGas transmission pipelines to transport hydrogen to the underground storage facilities located near the demand nodes. When the demand was greater than generation, hydrogen was dispatched from underground storage facilities to generate electricity in the fuel cell. Three scenarios were investigated with different mix of resources to achieve the 100% renewable energy goal in Southern California. The scenarios were compared, and the best option was suggested.
    - In scenario 1, the model was solved to find the lowest solar scaling factor required for 100% renewable energy penetration in Sothern California, resulting in a solar scaling factor of 13. For this scenario, the model estimated that the total underground storage facilities in Southern California needs to be expanded by 120% to ensure stored hydrogen can be balanced at the beginning and at the end of the year. The preliminary cost analysis for this scenario suggested that an extra $131B is needed to cover the cost of additional solar farms, fuel cells, electrolyzers, and underground storage facilities. The analysis also showed that the current pipeline network can support 80% of peak hydrogen mass flow rate. Two pipeline expansions were suggested to increase the network capacity to 100%.
    - In scenario 2, it is assumed that the underground storage facilities cannot be extended. To ensure the beginning and end of year level of hydrogen inventories at the underground storage facilities are balanced, the model increased the solar scaling factor. It was shown that in this scenario, a solar scaling factor of 17.5 is required to achieve 100% renewable energy penetration in Sothern California. The cost of this scenario was estimated at $172B, which is $41B higher than scenario 1. Moreover, it was estimated that the pipeline network can only support 60% of peak hydrogen mass flow rate for this scenario.

- In scenario 3, a compromise between scenarios 1 and 2 were analyzed. It was assumed that underground storage facilities in Southern California was expanded by only 60%. For this scenario, the solar scaling factor required to achieve 100% renewable energy penetration in Sothern California was estimated at 15, with an approximate cost of $149B. For this scenario, the pipeline network can support 70% of peak hydrogen mass flow rate.

- **Chapter 5:** analyzed the impact of injecting hydrogen in the natural gas infrastructure of Southern California. Different scenarios with various hydrogen mixes were studied, including when 0%, 2%, and 20% vol. hydrogen mix is injected at select injection points.
  - It was shown that natural gas network developed in this model meet all of the network requirements and none of the constraints were violated.
  - It was found that with hydrogen mix of 2% vol., the pipelines in the network can meet all their pressure constraints.
  - The analysis indicated that a well-blended network has a higher hydrogen carrying capacity. For the case when 2% vol. hydrogen is injected in all the receipt points, the hydrogen carrying capacity reaches 1.92% at the end of the year.
  - When the hydrogen mix is increased to 20% vol., it was observed that some of the pipeline pressure constraints in the network cannot be met, requiring the installation of additional pipelines to meet the energy demand of Southern California.

6.2 Future Work

There are several areas where the current research work can be expanded to gain a deeper understanding of the problems outlined in this dissertation.

First, the marginal estimated coefficients for the major sources of methane emissions should be experimentally verified to more accurately identify other drivers of change in emissions including pressure, age, and geographic area. This is in addition to the time, event, and throughput dependency that was studied in this work. To further improve the accuracy of the model, primary research is needed to collect methane emissions data at the component level, considering 35% of methane emissions was not marginally assessed due to the lack of available component-based data.

Second, underground storage model used in this dissertation assumes the injected gas is mixed homogenously, and instantly. The storage model used in chapter 5 play a key role in analyzing the

energy infrastructure and balancing the stored gas. Therefore, a more realistic model of the storage facility where the impact of time and location of the injection and withdrawing wells are taken into accounts are important to achieve a more accurate analysis of the network.

Third, the model developed in chapter 5 can be expanded for the distribution network in SoCalGas service territory to investigate the impact of hydrogen injection locations on the total hydrogen carrying capacity.

REFERENCES

[1] California Energy Commission. 2019 Total System Electric Generation. Calif Energy Comm n.d. https://www.energy.ca.gov/data-reports/energy-almanac/california-electricity-data/2019-total-system-electric-generation (accessed October 2, 2020).

[2] A Brief History of Natural Gas - APGA n.d. https://www.apga.org/apgamainsite/aboutus/facts/history-of-natural-gas (accessed October 22, 2020).

[3] Ancient Chinese Drilling | CSEG RECORDER n.d. https://csegrecorder.com/articles/view/ancient-chinese-drilling (accessed October 28, 2020).

[4] Dodds PE, Demoullin S. Conversion of the UK gas system to transport hydrogen. Int J Hydrogen Energy 2013;38:7189–200. https://doi.org/10.1016/j.ijhydene.2013.03.070.

[5] Overview of Greenhouse Gases | Greenhouse Gas (GHG) Emissions | US EPA n.d. https://www.epa.gov/ghgemissions/overview-greenhouse-gases (accessed September 29, 2020).

[6] Bill Text - SB-1505 Fuel: hydrogen alternative fuel. n.d. https://leginfo.legislature.ca.gov/faces/billTextClient.xhtml?bill_id=200520060SB1505 (accessed October 17, 2020).

[7] Department of Energy- Office of Energy Efficiency and Renewable Energy. Hydrogen Delivery n.d. https://www.energy.gov/eere/fuelcells/hydrogen-delivery (accessed October 2, 2020).

[8] Melaina MW, Antonia O, Penev M. Blending Hydrogen into Natural Gas Pipeline Networks: A Review of Key Issues. 2013.

[9] American Gas Association. Transitioning the Transportation Sector: Exploring the Intersection of Hydrogen Fuel Cell and Natural Gas Vehicles. 400 N. Capitol St., NW, Washington, DC 20001: 2014.

[10] Myers A, Rosa Dominguez-Faus J, Ogden J, Parker NC, Scheitrum D, Mcdonald Z, et al. The potential to build current natural gas infrastructure to accommodate the future conversion to near-zero transportation technology. Report 2017:106.

[11] Djukic MB, Sijacki Zeravcic V, Bakic GM, Sedmak A, Rajicic B. Hydrogen damage of steels: A case study and hydrogen embrittlement model. Eng Fail Anal 2015;58:485–98. https://doi.org/10.1016/j.engfailanal.2015.05.017.

[12] Wasim M, Li CQ, Mahmoodian M, Robert D. Mechanical and microstructural evaluation of corrosion and hydrogen-induced degradation of steel. J Mater Civ Eng 2019;31:1–11. https://doi.org/10.1061/(ASCE)MT.1943-5533.0002560.

[13] Steen M. Workshop Putting Science into Standards: Power-to-Hydrogen and HCNG Concluding remarks Head of Unit Energy Conversion and Storage Technologies. n.d.

[14] Stansberry JM, Brouwer J. Experimental dynamic dispatch of a 60 kW proton exchange membrane electrolyzer in power-to-gas application. Int J Hydrogen Energy 2020;45:9305–16. https://doi.org/10.1016/j.ijhydene.2020.01.228.

[15] Hydrogenics Selected References Grid Balancing, Power to Gas (PtG). 2016.

[16] Projects - Australian Renewable Energy Agency (ARENA) n.d. https://arena.gov.au/projects/?project-value-start=0&project-value-end=200000000&technology=hydrogen (accessed October 22, 2020).

[17] Iskov H, Rasmussen NB. Global screening of projects and technologies for Power-to-Gas and Bio-SNG A reference report. n.d.

[18] The GRHYD demonstration project | Gas | ENGIE n.d. https://www.engie.com/en/businesses/gas/hydrogen/power-to-gas/the-grhyd-demonstration-project (accessed October 22, 2020).

[19] Hydrogen is vital to tackling climate change - HyDeploy n.d. https://hydeploy.co.uk/ (accessed October 22, 2020).

[20] Energiepark Mainz: Energiepark n.d. https://www.energiepark-mainz.de/en/project/energiepark/ (accessed October 22, 2020).

[21] Quarton CJ, Samsatli S. Power-to-gas for injection into the gas grid: What can we learn from real-life projects, economic assessments and systems modelling? Renew Sustain Energy Rev 2018;98:302–16. https://doi.org/10.1016/j.rser.2018.09.007.

[22] Limits on hydrogen blending in natural gas networks, 2018 – Charts – Data & Statistics - IEA n.d. https://www.iea.org/data-and-statistics/charts/limits-on-hydrogen-blending-in-natural-gas-networks-2018 (accessed October 22, 2020).

[23] International Energy Agency. International Energy Agency, “Technology Roadmap: Hydrogen and Fuel Cells,” OECD/IEA, 75739 Paris Cedex 15, France, 2015. n.d. http://ieahydrogen.org/pdfs/TechnologyRoadmapHydrogenandFuelCells-(1).aspx (accessed October 2, 2020).

[24] Haeseldonckx D, D’haeseleer W. The use of the natural-gas pipeline infrastructure for hydrogen transport in a changing market structure. Int J Hydrogen Energy 2007;32:1381–6. https://doi.org/10.1016/j.ijhydene.2006.10.018.

[25] Barnoush A. Hydrogen embrittlement, revisited by in situ electrochemical nanoindentation 2007:288.

[26] van der Zwaan BCC, Schoots K, Rivera-Tinoco R, Verbong GPJ. The cost of pipelining climate change mitigation: An overview of the economics of CH4, CO2 and H2 transportation. Appl Energy 2011;88:3821–31. https://doi.org/10.1016/j.apenergy.2011.05.019.

[27] Castello P, Tzimas E, Moretto P. Techno-economic assessment of hydrogen transmission & distribution systems in Europe in the medium and long term. Eur Comm Jt 2005.

[28] NATURALHY European Project (FP6). Preparing for the hydrogen economy by using the

existing natural gas system as a catalyst - Final Report 2010:68.

[29] Iskov H, Jensen J. Field test of hydrogen in the natural gas grid. vol. 3. 2006.

[30] Mac Kinnon M, Heydarzadeh Z, Doan Q, Ngo C, Reed J, Brouwer J. Need for a marginal methodology in assessing natural gas system methane emissions in response to incremental consumption. J Air Waste Manag Assoc 2018;68:1139–47. https://doi.org/10.1080/10962247.2018.1476274.

[31] Natural Gas and Petroleum Systems in the GHG Inventory: Additional Information on the 1990-2015 GHG Inventory (published April 2017) | Greenhouse Gas (GHG) Emissions | US EPA n.d. https://www.epa.gov/ghgemissions/natural-gas-and-petroleum-systems-ghg-inventory-additional-information-1990-2015-ghg (accessed September 29, 2020).

[32] Harrison MR, Shires TM, Wessels JK, Cowgill RM. Methane Emissions from the Natural Gas Industry, Volume 1: Executive Summary. EPA 1996:1–24.

[33] Greenhouse Gas Reporting Program (GHGRP) | US EPA n.d. https://www.epa.gov/ghgreporting (accessed September 29, 2020).

[34] Frey HC. Quantification of Uncertainty in Emissions Factors and Inventories. 16th Annu Int Emiss Invent Conf Emiss Invent "Integration, Anal Commun Raleigh,NCUS EPA 2007:1–16.

[35] Pouliot G, Wisner E, Mobley D, Hunt W. Quantification of emission factor uncertainty. J Air Waste Manag Assoc 2012;62:287–98. https://doi.org/10.1080/10473289.2011.649155.

[36] Nicholson KW. A critique of empirical emission factor models: A case study of the AP-42 model for estimating PM10 emissions from paved roads (Venkatram, A., Atmospheric Environment 34, 1-11). Atmos Environ 2001;35:185–6. https://doi.org/10.1016/S1352-2310(00)00294-6.

[37] AP-42: Compilation of Air Emissions Factors | Air Emissions Factors and Quantification | US EPA n.d. https://www.epa.gov/air-emissions-factors-and-quantification/ap-42-compilation-air-emissions-factors (accessed September 29, 2020).

[38] Brandt AR, Heath GA, Kort EA, O'Sullivan F, Pétron G, Jordaan SM, et al. Methane leaks from North American natural gas systems. Science (80-) 2014;343:733–5. https://doi.org/10.1126/science.1247045.

[39] Subramanian R, Williams LL, Vaughn TL, Zimmerle D, Roscioli JR, Herndon SC, et al. Methane emissions from natural gas compressor stations in the transmission and storage sector: Measurements and comparisons with the EPA greenhouse gas reporting program protocol. Environ Sci Technol 2015;49:3252–61. https://doi.org/10.1021/es5060258.

[40] AP-42: Compilation of Air Emissions Factors | Air Emissions Factors and Quantification | CH 3:2 Natural Gas-fired Reciprocating Engines | US EPA n.d. https://www.epa.gov/air-emissions-factors-and-quantification/ap-42-compilation-air-emissions-factors (accessed September 29, 2020).

[41] Karion A, Sweeney C, Pétron G, Frost G, Michael Hardesty R, Kofler J, et al. Methane

emissions estimate from airborne measurements over a western United States natural gas field. Geophys Res Lett 2013;40:4393–7. https://doi.org/10.1002/grl.50811.

[42] Clark NN, McKain DL, Johnson DR, Wayne WS, Li H, Akkerman V, et al. Pump-to-wheels methane emissions from the heavy-duty transportation sector. Environ Sci Technol 2017;51:968–76. https://doi.org/10.1021/acs.est.5b06059.

[43] Lyon DR, Zavala-Araiza D, Alvarez RA, Harriss R, Palacios V, Lan X, et al. Constructing a Spatially Resolved Methane Emission Inventory for the Barnett Shale Region. Environ Sci Technol 2015;49:8147–57. https://doi.org/10.1021/es506359c.

[44] Smith ML, Kort EA, Karion A, Sweeney C, Herndon SC, Yacovitch TI. Airborne Ethane Observations in the Barnett Shale: Quantification of Ethane Flux and Attribution of Methane Emissions. Environ Sci Technol 2015;49:8158–66. https://doi.org/10.1021/acs.est.5b00219.

[45] Lavoie TN, Shepson PB, Cambaliza MOL, Stirm BH, Karion A, Sweeney C, et al. Aircraft-Based Measurements of Point Source Methane Emissions in the Barnett Shale Basin. Environ Sci Technol 2015;49:7904–13. https://doi.org/10.1021/acs.est.5b00410.

[46] Nathan BJ, Golston LM, O'Brien AS, Ross K, Harrison WA, Tao L, et al. Near-Field Characterization of Methane Emission Variability from a Compressor Station Using a Model Aircraft. Environ Sci Technol 2015;49:7896–903. https://doi.org/10.1021/acs.est.5b00705.

[47] Johnson DR, Covington AN, Clark NN. Methane Emissions from Leak and Loss Audits of Natural Gas Compressor Stations and Storage Facilities. Environ Sci Technol 2015;49:8132–8. https://doi.org/10.1021/es506163m.

[48] Roscioli JR, Yacovitch TI, Floerchinger C, Mitchell AL, Tkacik DS, Subramanian R, et al. Measurements of methane emissions from natural gas gathering facilities and processing plants: Measurement methods. Atmos Meas Tech 2015;8:2017–35. https://doi.org/10.5194/amt-8-2017-2015.

[49] Rella CW, Tsai TR, Botkin CG, Crosson ER, Steele D. Measuring emissions from oil and natural gas well pads using the mobile flux plane technique. Environ Sci Technol 2015;49:4742–8. https://doi.org/10.1021/acs.est.5b00099.

[50] Lan X, Talbot R, Laine P, Torres A. Characterizing Fugitive Methane Emissions in the Barnett Shale Area Using a Mobile Laboratory. Environ Sci Technol 2015;49:8139–46. https://doi.org/10.1021/es5063055.

[51] Yacovitch TI, Herndon SC, Pétron G, Kofler J, Lyon D, Zahniser MS, et al. Mobile Laboratory Observations of Methane Emissions in the Barnett Shale Region. Environ Sci Technol 2015;49:7889–95. https://doi.org/10.1021/es506352j.

[52] Zimmerle DJ, Williams LL, Vaughn TL, Quinn C, Subramanian R, Duggan GP, et al. Methane Emissions from the Natural Gas Transmission and Storage System in the United States. Environ Sci Technol 2015;49:9374–83. https://doi.org/10.1021/acs.est.5b01669.

[53] Shires T, Matthew H. Methane Emissions from the Natural Gas Industry Volume 6: Vented

and combustion sources. EPA 1996.

[54] Argonne GREET Model n.d. https://greet.es.anl.gov/ (accessed September 30, 2020).

[55] Simpson D. Pneumatic Controllers in Upstream Oil and Gas. Oil Gas Facil 2014;3:083–96. https://doi.org/10.2118/172505-pa.

[56] EPA. Lessons learned from Natural Gas STAR Partners: options for reducing methane emissions from pneumatic devices in the natural gas industry. 2006:2013JD021272. https://doi.org/10.1002/2013JD021272.

[57] Allen DT, Pacsi AP, Sullivan DW, Zavala-Araiza D, Harrison M, Keen K, et al. methane emissions from process equipment at natural gas production sites in the united states: Pneumatic Controllers". Environ Sci Technol 2015;49:633–40. https://doi.org/10.1021/acs.est.5b00507.

[58] Allen DT, Torres VM, Thomas J, Sullivan DW, Harrison M, Hendler A, et al. Measurements of methane emissions at natural gas production sites in the United States. Proc Natl Acad Sci U S A 2013;110:17768–73. https://doi.org/10.1073/pnas.1304880110.

[59] Harrison MR, Galloway KE, Hendler A, Shires TM, Allen D, Foss M, et al. Natural Gas Industry Methane Emission Factor Improvement Study Final Report Cooperative Agreement No. XA-83376101. 2011.

[60] EPA. Lessons learned from Natural Gas STAR Partners: REDUCING METHANE EMISSIONS FROM COMPRESSOR ROD PACKING SYSTEMS. 2003.

[61] EPA. Lessons learned from Natural Gas STAR Partners: Replacing Wet Seals with Dry Seals in Centrifugal Compressors 2006:1–8.

[62] Climate & Clean Air Coalition. CCAC OGMP – Technical Guidance Document Number 3: Centrifugal Compressors with “Wet” (Oil) Seals_SG17.1.3. 2017.

[63] Methane Emissions from Process Equipment at Natural Gas Production Sites in the United States: Liquid Unloadings - FAQs. Univ Texas Austin, Cent Energy Environ Resour n.d. http://dept.ceer.utexas.edu/methane2/study/faqs_unl.cfm (accessed September 30, 2020).

[64] Climate & Clean Air Coalition. CCAC OGMP-Technical Guidance Document Number 7: Well Venting for Liquids Unloading TECHNICAL GUIDANCE DOCUMENT NUMBER 7: WELL VENTING FOR LIQUIDS_SG.17.17 UNLOADING. 2017.

[65] U.S. EPA Office of Air Quality Planning and standards (OQPS). Oil and Natural Gas Sector Liquid Unloading Processes. 2014.

[66] Allen DT, Pacsi AP, Sullivan DW, Zavala-Araiza D, Harrison M, Keen K, et al. Methane emissions from process equipment at natural gas production sites in the United States: Liquid Unloading. Environ Sci Technol 2015;49:641–8. https://doi.org/10.1021/es5040156.

[67] Shires TM, Matthew H. Methane Emissions from the Natural Gas Industry, Volume 7:_Blow and Purge Activities. EPA; 1996.

[68] EPA. Lessons learned from Natural Gas STAR Partners: Reducing Emissions When Taking Compressors Off-Line. 2006.

[69] Underground Natural Gas Storage Integrity and Safe Operations 2016. http://www.energyinfrastructure.org/energy-101/natural-gas-storage (accessed September 30, 2020).

[70] Climate & Clean Air Coalition. CCAC O&G Methane Partnership – Technical Guidance Document Number 6: Unstabilized Hydrocarbon Liquid Storage Tanks_SG.17.1.6. 2017.

[71] Robinson D. US EPA's Natural Gas STAR International: An Overview of Emission Reduction Best Practices 1 st Asia Pacific Global Methane Initiative Oil & Gas Sector Workshop. 2011.

[72] Climate & Clean Air Coalition. CCAC O&G Methane Partnership – Technical Guidance Document Number 2: Fugitive Component and Equipment Leaks_SG.17.1.2. 2017.

[73] The Canadian Association of Petroleum Producers (CAPP). Management of Fugitive Emissions at Upstream Oil and Gas Facilities n.d. https://www.capp.ca/wp-content/uploads/2019/11/Best_Management_Practice_for_Fugitive_Emissions_Management-116116.pdf (accessed September 30, 2020).

[74] EPA. Lessons Learned From Natural Gas STAR Partners: REPLACING GAS-ASSISTED GLYCOL PUMPS WITH ELECTRIC PUMPS. 2004.

[75] Myers DB, Harrison MR. Methane Emissions from the Natural Gas Industry-Volume 15-Gas-assisted Glycol Pumps. EPA. 1996.

[76] Myers DB. Methane Emissions from the Natural Gas Industry-Volume 14-Glycol Dehydrators. EPA 1996.

[77] EPA. Lessons Learned From Natural Gas STAR Partners: Optimize Glycol Circulation And Install Flash Tank Separators In Glycol Dehydrators Glycol Dehydrators. 2006.

[78] Shires TM. Methane Emissions from the Natural Gas Industry-Volume 13-Chemical injection pumps. EPA 1996.

[79] US EPA. Partner Reported Opportunities (PROs) for Reducing Methane Emissions_Convert Natural Gas-Driven Chemical Pumps_PRO Fact Sheet No. 202. 2011.

[80] Foley A, Tyther B, Calnan P, Ó Gallachóir B. Impacts of Electric Vehicle charging under electricity market operations. Appl Energy 2013;101:93–102. https://doi.org/10.1016/j.apenergy.2012.06.052.

[81] Hawkes AD. Long-run marginal CO2 emissions factors in national electricity systems. Appl Energy 2014;125:197–205. https://doi.org/10.1016/j.apenergy.2014.03.060.

[82] Khan I, Jack MW, Stephenson J. Analysis of greenhouse gas emissions in electricity systems using time-varying carbon intensity. J Clean Prod 2018;184:1091–101. https://doi.org/10.1016/j.jclepro.2018.02.309.

[83] Rogers MM, Wang Y, Wang C, McElmurry SP, Miller CJ. Evaluation of a rapid LMP-

based approach for calculating marginal unit emissions. Appl Energy 2013;111:812–20. https://doi.org/10.1016/j.apenergy.2013.05.057.

[84] Bigazzi A. Comparison of marginal and average emission factors for passenger transportation modes. Appl Energy 2019;242:1460–6. https://doi.org/10.1016/j.apenergy.2019.03.172.

[85] Innovative Environmental Solutions and Gas Technology Institute. Field Measurement Program to Improve Uncertainties for Key Greenhouse Gas Emission Factors for Distribution Sources. Des Plaines, IL: 2009.

[86] Eberle AC. An Engineering Estimate of the incremental change in methane emissions with increasing throughput in a model natural gas system. American Gas Association and the Gas Research institute 1993.

[87] Stapper CJ. Methane Emissions from the Natural Gas Industry-Volume 2: Compressor Driver Exhaust. EPA 1996.

[88] Omara M, Zimmerman N, Sullivan MR, Li X, Ellis A, Cesa R, et al. Methane Emissions from Natural Gas Production Sites in the United States: Data Synthesis and National Estimate. Environ Sci Technol 2018;52:12915–25. https://doi.org/10.1021/acs.est.8b03535.

[89] Brantley HL, Thoma ED, Squier WC, Guven BB, Lyon D. Assessment of methane emissions from oil and gas production pads using mobile measurements. Environ Sci Technol 2014;48:14508–15. https://doi.org/10.1021/es503070q.

[90] Eastern Research Group Inc. (ERG). Natural Gas Air Quality Study (Final Report) 2011. http://fortworthtexas.gov/gaswells/air-quality-study/final/ (accessed October 1, 2020).

[91] Mitchell AL, Tkacik DS, Roscioli JR, Herndon SC, Yacovitch TI, Martinez DM, et al. Measurements of methane emissions from natural gas gathering facilities and processing plants: Measurement results. Environ Sci Technol 2015;49:3219–27. https://doi.org/10.1021/es5052809.

[92] Natural Gas STAR Program. Recommended Technologies to Reduce Methane Emissions | EPA's Voluntary Methane Programs for the Oil and Natural Gas Industry | US EPA n.d. https://www.epa.gov/natural-gas-star-program/recommended-technologies-reduce-methane-emissions (accessed October 1, 2020).

[93] Assembly Bill No. 32, Air pollution: greenhouse gases: California Global Warming Solutions Act of 2006. n.d. https://leginfo.legislature.ca.gov/faces/billNavClient.xhtml?bill_id=200520060AB32 (accessed September 29, 2020).

[94] Beaudin M, Zareipour H, Schellenberglabe A, Rosehart W. Energy storage for mitigating the variability of renewable electricity sources: An updated review. Energy Sustain Dev 2010;14:302–14. https://doi.org/10.1016/j.esd.2010.09.007.

[95] Maton JP, Zhao L, Brouwer J. Dynamic modeling of compressed gas energy storage to complement renewable wind power intermittency. Int J Hydrogen Energy 2013;38:7867–

80. https://doi.org/10.1016/j.ijhydene.2013.04.030.

[96] Gahleitner G. Hydrogen from renewable electricity: An international review of power-to-gas pilot plants for stationary applications. Int J Hydrogen Energy 2013;38:2039–61. https://doi.org/10.1016/j.ijhydene.2012.12.010.

[97] Götz M, Lefebvre J, Mörs F, McDaniel Koch A, Graf F, Bajohr S, et al. Renewable Power-to-Gas: A technological and economic review. Renew Energy 2016;85:1371–90. https://doi.org/10.1016/j.renene.2015.07.066.

[98] Jentsch M, Trost T, Sterner M. Optimal use of Power-to-Gas energy storage systems in an 85% renewable energy scenario. Energy Procedia 2014;46:254–61. https://doi.org/10.1016/j.egypro.2014.01.180.

[99] Schiebahn S, Grube T, Robinius M, Tietze V, Kumar B, Stolten D. Power to gas: Technological overview, systems analysis and economic assessment for a case study in Germany. Int J Hydrogen Energy 2015;40:4285–94. https://doi.org/10.1016/j.ijhydene.2015.01.123.

[100] ADVANCED POWER & ENERGY PROGRAM. Engineering Science to Practical Application 2017. http://www.apep.uci.edu/PDF_Bridging/Bridging_2017_APEP_082417.pdf (accessed October 2, 2020).

[101] González A, McKeogh E, Gallachóir BÓ. The role of hydrogen in high wind energy penetration electricity systems: The Irish case. Renew Energy 2004;29:471–89. https://doi.org/10.1016/j.renene.2003.07.006.

[102] California Fuel Cell Partnership. Medium-and Heavy-Duty Fuel Electric Cell Truck Action Plan for California. 2016.

[103] E4Tech-Strategic thinking in sustainable energy. The Fuel Cell Industry Review 2015 2015. http://www.fuelcellindustryreview.com/archive/TheFuelCellIndustryReview2015.pdf (accessed October 2, 2020).

[104] Panfilov M. Underground and pipeline hydrogen storage. Compend Hydrog Energy 2016:91–115. https://doi.org/10.1016/b978-1-78242-362-1.00004-3.

[105] Reports — Fuel Cell & Hydrogen Energy Association n.d. http://www.fchea.org/reports/ (accessed October 28, 2020).

[106] Colella W, James B, Moron J, Saur G, Ramsden T. Techno-economic Analysis of PEM Electrolysis for Hydrogen Production. Electrolytic Hydrog Prod Work 2014:38.

[107] Szoplik J. The Gas Transportation in a Pipeline Network. Adv Nat Gas Technol 2012. https://doi.org/10.5772/36902.

[108] Woldeyohannes AD, Majid MAA. Simulation model for natural gas transmission pipeline network system. Simul Model Pract Theory 2011;19:196–212. https://doi.org/10.1016/j.simpat.2010.06.006.

[109] Herrán-González A, De La Cruz JM, De Andrés-Toro B, Risco-Martín JL. Modeling and

simulation of a gas distribution pipeline network. Appl Math Model 2009;33:1584–600. https://doi.org/10.1016/j.apm.2008.02.012.

[110] Ebrahimzadeh E, Shahrak MN, Bazooyar B. Simulation of transient gas flow using the orthogonal collocation method. Chem Eng Res Des 2012;90:1701–10. https://doi.org/10.1016/j.cherd.2012.02.018.

[111] Reddy HP, Narasimhan S, Bhallamudi SM. Simulation and state estimation of transient flow in gas pipeline networks using a transfer function model. Ind Eng Chem Res 2006;45:3853–63. https://doi.org/10.1021/ie050755k.

[112] Wang H, Liu X, Zhou W. Transient flow simulation of municipal gas pipelines and networks using semi implicit finite volume method. Procedia Eng 2011;12:217–23. https://doi.org/10.1016/j.proeng.2011.05.034.

[113] Gato LMC, Henriques JCC. Dynamic behaviour of high-pressure natural-gas flow in pipelines. Int J Heat Fluid Flow 2005;26:817–25. https://doi.org/10.1016/j.ijheatfluidflow.2005.03.011.

[114] Alamian R, Behbahani-Nejad M, Ghanbarzadeh A. A state space model for transient flow simulation in natural gas pipelines. J Nat Gas Sci Eng 2012;9:51–9. https://doi.org/10.1016/j.jngse.2012.05.013.

[115] Behbahani-Nejad M, Shekari Y. Reduced order modelling of natural gas transient flow in pipelines. Int J Eng Appl Sci 2008;5:148–52.

[116] Chaczykowski M. Transient flow in natural gas pipeline - The effect of pipeline thermal model. Appl Math Model 2010;34:1051–67. https://doi.org/10.1016/j.apm.2009.07.017.

[117] Chaczykowski M. Sensitivity of pipeline gas flow model to the selection of the equation of state. Chem Eng Res Des 2009;87:1596–603. https://doi.org/10.1016/j.cherd.2009.06.008.

[118] Ke SL, Ti HC. Transient analysis of isothermal gas flow in pipeline network. Chem Eng J 2000;76:169–77. https://doi.org/10.1016/S1385-8947(99)00122-9.

[119] Kwabena Addo Pambour. Modelling, simulation and analysis of security of supply scenarios in integrated gas and electricity transmission networks. 2018.

[120] Helgaker JF, Müller B, Ytrehus T. Transient flow in natural gas pipelines using implicit finite difference schemes. J Offshore Mech Arct Eng 2014;136:1–11. https://doi.org/10.1115/1.4026848.

[121] Helgaker JF, Ytrehus T. Coupling between Continuity/Momentum and Energy Equation in 1D Gas Flow Jan. Energy Procedia 2012;26:82–9. https://doi.org/10.1016/j.egypro.2012.06.005.

[122] Kiuchi T. An implicit method for transient gas flows in pipe networks. Int J Heat Fluid Flow 1994;15:378–83. https://doi.org/10.1016/0142-727X(94)90051-5.

[123] Abbaspour M, Chapman KS. Nonisothermal transient flow in natural gas pipeline. J Appl Mech Trans ASME 2008;75:0310181–8. https://doi.org/10.1115/1.2840046.

[124] U.S. Energy Information Administration (EIA) n.d. https://www.eia.gov/naturalgas/ngqs/#?report=RP7&year1=2012&year2=2012&company=Name&sortby=ACI&items= (accessed October 9, 2020).

[125] NIST Standard Reference Database 4 | NIST n.d. https://www.nist.gov/srd/nist-standard-reference-database-4 (accessed October 12, 2020).

[126] California Independent System Operator (CAISO), "Hourly renewable and production data" 2017. http://oasis.caiso.com/mrioasis/logon.do (accessed October 2, 2020).

[127] Reed J. DOE Hydrogen and Fuel Cell Technical Advisory Committee Hydrogen Energy Storage Activities. 2015.

[128] Sempra - SoCalGas ENVOY n.d. https://scgenvoy.sempra.com/ (accessed October 13, 2020).

[129] Natural Gas Interstate and Intrastate Pipelines | ArcGIS Hub n.d. https://hub.arcgis.com/datasets/cc3813401e0849c193213d5793959dc7 (accessed October 2, 2020).

[130] Southern California Gas Company. SOUTHERN CALIFORNIA GAS COMPANY NORTH-SOUTH PROJECT Updated Report Adelanto Compressor Station Adelanto to Moreno Pipeline 2014.

[131] Steward D, Saur G, Penev M, Ramsden T. Lifecycle cost analysis of hydrogen versus other technologies for electrical energy storage. Tech Rep NREL/TP-560-46719 2009:59–120. https://doi.org/10.2172/968186.

[132] Fu R, Feldman D, Margolis R. U.S. Solar Photovoltaic System Cost Benchmark: Q1 2018, NREL/TP-6A20-72399. Tech Rep NREL/TP-6A20-72399 2018.

[133] Ong S, Campbell C, Denholm P, Margolis R, Heath G. Land-Use Requirements for Solar Power Plants in the United States- the National Renewable Energy Laboratory (NREL). 2013. https://doi.org/10.1016/j.rapm.2006.08.004.

[134] IEA's World Energy Outlook 2014 - IER n.d. https://www.instituteforenergyresearch.org/fossil-fuels/coal/ieas-world-energy-outlook-2014/ (accessed October 17, 2020).

[135] Dickinson RR, Battye DL, Linton VM, Ashman PJ, Nathan G (Gus) J. Alternative carriers for remote renewable energy sources using existing CNG infrastructure. Int J Hydrogen Energy 2010;35:1321–9. https://doi.org/10.1016/j.ijhydene.2009.11.052.

[136] ENEA Consulting. The Potential of Power-To-Gas 2016;33:51.

[137] Staffell I, Scamman D, Velazquez Abad A, Balcombe P, Dodds PE, Ekins P, et al. The role of hydrogen and fuel cells in the global energy system. Energy Environ Sci 2019;12:463–91. https://doi.org/10.1039/c8ee01157e.

[138] Guandalini G, Campanari S, Romano MC. Power-to-gas plants and gas turbines for improved wind energy dispatchability: Energy and economic assessment. Appl Energy 2015;147:117–30. https://doi.org/10.1016/j.apenergy.2015.02.055.

[139] Pellegrino S, Lanzini A, Leone P. Greening the gas network – The need for modelling the distributed injection of alternative fuels. Renew Sustain Energy Rev 2017;70:266–86. https://doi.org/10.1016/j.rser.2016.11.243.

[140] Abeysekera M, Wu J, Jenkins N, Rees M. Steady state analysis of gas networks with distributed injection of alternative gas. Appl Energy 2016;164:991–1002. https://doi.org/10.1016/j.apenergy.2015.05.099.

[141] Zeng Q, Fang J, Li J, Chen Z. Steady-state analysis of the integrated natural gas and electric power system with bi-directional energy conversion. Appl Energy 2016;184:1483–92. https://doi.org/10.1016/j.apenergy.2016.05.060.

[142] Hafsi Z, Elaoud S, Akrout M, Hadj-Taïeb E. Numerical Approach for Steady State Analysis of Hydrogen–Natural Gas Mixtures Flows in Looped Network. Arab J Sci Eng 2017;42:1941–50. https://doi.org/10.1007/s13369-016-2393-y.

[143] Tabkhi F, Azzaro-Pantel C, Pibouleau L, Domenech S. A mathematical framework for modelling and evaluating natural gas pipeline networks under hydrogen injection. Int J Hydrogen Energy 2008;33:6222–31. https://doi.org/10.1016/j.ijhydene.2008.07.103.

[144] Vandewalle J, Bruninx K, D'Haeseleer W. Effects of large-scale power to gas conversion on the power, gas and carbon sectors and their interactions. Energy Convers Manag 2015;94:28–39. https://doi.org/10.1016/j.enconman.2015.01.038.

[145] Sveinbjörnsson D, Ben Amer-Allam S, Hansen AB, Algren L, Pedersen AS. Energy supply modelling of a low-CO2 emitting energy system: Case study of a Danish municipality. Appl Energy 2017;195:922–41. https://doi.org/10.1016/j.apenergy.2017.03.086.

[146] Qadrdan M, Ameli H, Strbac G, Jenkins N. Efficacy of options to address balancing challenges: Integrated gas and electricity perspectives. Appl Energy 2017;190:181–90. https://doi.org/10.1016/j.apenergy.2016.11.119.

[147] Pambour KA, Cakir Erdener B, Bolado-Lavin R, Dijkema GPJ. SAInt – A novel quasi-dynamic model for assessing security of supply in coupled gas and electricity transmission networks. Appl Energy 2017;203:829–57. https://doi.org/10.1016/j.apenergy.2017.05.142.

[148] Kunz O, Wagner W. The GERG-2008 wide-range equation of state for natural gases and other mixtures: An expansion of GERG-2004. J Chem Eng Data 2012;57:3032–91. https://doi.org/10.1021/je300655b.

[149] Varzandeh F, Stenby EH, Yan W. Comparison of GERG-2008 and simpler EoS models in calculation of phase equilibrium and physical properties of natural gas related systems. Fluid Phase Equilib 2017;434:21–43. https://doi.org/10.1016/j.fluid.2016.11.016.

[150] Ellison JF, Corbet TF, Brooks RE. Natural Gas Network Resiliency to a "ShakeOut Scenario" Earthquake. Sandia Natl Labortories 2013.

[151] United States - Maps - U.S. Energy Information Administration (EIA) n.d. https://www.eia.gov/state/maps.php (accessed October 2, 2020).

[152] Aliso Canyon Well Failure n.d. https://www.cpuc.ca.gov/aliso/ (accessed October 13,

2020).

[153] BY STAFF OF THE CALIFORNIA PUBLIC UTILITIES COMMISSION. Winter 2018-19 SoCalGas Conditions and Operations Report 2020.

[154] BY CALIFORNIA PUBLIC UTILITIES COMMISSION STAFF. Winter 2019-20 Southern California Reliability Assessment 2019.